



**TURUN  
YLIOPISTO**  
UNIVERSITY  
OF TURKU

# PROSTATE-SPECIFIC MEMBRANE ANTIGEN AS A TARGET FOR PROSTATE CANCER PET IMAGING

---

Simona Malaspina





**TURUN  
YLIOPISTO**  
UNIVERSITY  
OF TURKU

# **PROSTATE-SPECIFIC MEMBRANE ANTIGEN AS A TARGET FOR PROSTATE CANCER PET IMAGING**

---

Simona Malaspina

## University of Turku

---

Faculty of Medicine  
Clinical Physiology and Nuclear Medicine  
Doctoral Programme in Clinical Research  
Turku PET Centre  
Turku, Finland

## Supervised by

---

Professor Jukka Kempainen  
Turku PET Centre and Department of  
Clinical Physiology and Nuclear Medicine  
University of Turku and  
Turku University Hospital  
Turku, Finland

Adjunct Professor Otto Ettala  
Department of Urology  
University of Turku and  
Turku University Hospital  
Turku, Finland

## Reviewed by

---

Associate Professor Laura Evangelista  
Nuclear Medicine Unit,  
Department of Medicine – DIMED  
Padova University Hospital  
Padova, Italy

Adjunct Professor Mika Raitanen  
Department of Urology, The Hospital  
district of South Ostrobothnia  
Seinäjoki, Finland  
Faculty of Medicine and Health  
Technology, Tampere University  
Tampere, Finland

## Opponent

---

Associate Professor Matthias Eiber  
Department of Nuclear Medicine  
Technical University Munich  
Munich, Germany

The originality of this publication has been checked in accordance with the University of Turku quality assurance system using the Turnitin OriginalityCheck service.

ISBN 978-951-29-9184-6 (PRINT)  
ISBN 978-951-29-9185-3 (PDF)  
ISSN 0355-9483 (Print)  
ISSN 2343-3213 (Online)  
Painosalama, Turku, Finland 2023

*To my loved ones*

UNIVERSITY OF TURKU

Faculty of Medicine

Clinical Physiology and Nuclear Medicine

SIMONA MALASPINA: Prostate-specific membrane antigen as a target for prostate cancer PET imaging

Doctoral Dissertation, 177 pp.

Doctoral Programme in Clinical Research

March 2023

## ABSTRACT

Prostate-specific membrane antigen (PSMA) is a transmembrane protein overexpressed in prostate cancer (PCa) cells. In the last decade, PSMA-targeting positron emission tomography (PET) has gained increasing acceptance for PCa imaging. Among the different available PSMA ligands, theranostic agents that can be labelled with both diagnostic and therapeutic radioisotopes have raised particular interest. Androgen deprivation therapy (ADT) is known to upregulate PSMA expression. However, studies investigating this phenomenon in humans are limited. In the clinical context, while the use of PSMA PET has been established in detecting recurrence after radical treatment, the role of PSMA PET in primary staging was only recently affirmed.

The aim of this doctoral thesis was to investigate novel aspects of PSMA PET imaging, from the kinetics of a novel theranostic radiotracer, through the physiology of PSMA expression, to its use for primary staging in the clinical practice. The uptake kinetics of radiohybrid [ $^{18}\text{F}$ ]-rhPSMA-7.3 in PCa lesions and reference tissues were assessed in a prospective Phase I trial and demonstrated dominant irreversible components. The uptake in PCa lesions and lesion-to-reference ratios increased over time, with the optimal visual detection starting from 60 minutes post-injection. Two prospective studies demonstrated a heterogeneous increase in PSMA uptake after short-term ADT (PSMA flare) in treatment-naïve PCa patient, most evidently seen in bone metastases. This phenomenon was negatively correlated with glucose metabolism, which suggests that lesions with low or absent flare might be more aggressive. Finally, [ $^{18}\text{F}$ ]-PSMA-1007 PET/computed tomography (CT) was prospectively compared to whole body magnetic resonance imaging (WBMRI) and CT in the primary nodal staging of patients with unfavourable intermediate or high-risk PCa. The study demonstrated improved sensitivity and accuracy while maintaining high specificity.

**KEYWORDS:** prostate cancer, prostate-specific membrane antigen, positron emission tomography, androgen deprivation therapy

TURUN YLIOPISTO

Lääketieteellinen tiedekunta

Kliininen fysiologia ja isotooppilääketiede

SIMONA MALASPINA: Prostataspesifinen membraaniantigeeni

eturauhassyövän PET-kuvantamisessa

Väitöskirja, 177 s.

Turun kliininen tohtoriohjelma

Maaliskuu 2023

## TIIVISTELMÄ

Prostataspesifisen membraaniantigeenin (PSMA) ilmentyminen on voimakkaasti lisääntynyt eturauhassyövän solukalvoilla. Tämän takia PSMA on erinomainen kohde eturauhassyövän positroniemissiotomografia(PET)-kuvaukselle. PSMA PET:n käyttö eturauhassyövän kuvantamisessa on lisääntynyt selvästi viime vuosikymmenen aikana ja PSMA:han sitoutuvia merkkiaineita on kehitetty useita. Erityistä kiinnostusta ovat herättäneet ns. teranostiset merkkiaineet, jossa sama PSMA-ligandi voidaan leimata sekä PET-kuvantamiseen että kehonsisäiseen sädehoitoon tarkoitetuilla isotoopeilla. Androgeenideprivaatioterapia (ADT) tiedetään lisäävän PSMA:n ilmenemistä, mutta tätä ilmiötä on tutkittu hyvin niukasti. Yleisin, kliinisesti vahvistettu PSMA-PET:n käyttöindikaatio on eturauhassyövän hoidon jälkeisen taudin uusiutumisen havaitseminen, mutta myös PSMA-PET:n rooli taudin levinneisyyden selvittämisessä on tarkentumassa.

Tämän väitöskirjan tarkoituksena oli tutkia PSMA-PET-kuvauksen uusia näkökohtia, kuten uuden teranostisen merkkiaineen kinetiikkaa, hormonihoidon vaikutusta PSMA-PET:n löydöksiin sekä PSMA-PET:n suorituskyky eturauhassyövän levinneisyyden selvittämisessä. [<sup>18</sup>F]-rhPSMA-7.3:n kinettisen analyysin tulokset osoittivat, että tautipesäkkeiden aktiivisuudet sekä pesäke/vertailukudos-aktiivisuussuhteet voimistuivat ajan myötä ja optimaalinen pesäkkeiden visuaalinen paikallistaminen alkoi 60 minuuttia injektioista. Kahdessa muussa tutkimuksessa osoitettiin, että PSMA:n ilmentymisen lisääntyminen lyhytaikaisen ADT:n jälkeen (PSMA-flare) on heterogeenista ja voimakkainta luustoetäpesäkkeissä levinnyttä eturauhassyöpää sairastuvilla potilailla. PSMA-flare-ilmiö korreloi negatiivisesti glukoosin aineenvaihduntaan, mikä viittaa siihen, että matala PSMA-flare tai sen puuttuminen on yhteydessä etäpesäkkeiden aggressiivisuuteen. Lisäksi [<sup>18</sup>F]-PSMA-1007 PET/tietokonetomografia (TT) verrattiin koko kehon magneettiin ja TT:hen korkean riskin eturauhassyöpäpotilailla. Tutkimus osoitti PSMA-PET/TT:n korkeamman herkkyuden ja tarkkuuden.

AVAINSANAT: eturauhassyöpä, positroniemissiotomografia, prostataspesifinen membraaniantigeeni, androgeenideprivaatioterapia

# Table of Contents

<b>Abbreviations .....</b>	<b>8</b>
<b>List of Original Publications .....</b>	<b>10</b>
<b>1 Introduction .....</b>	<b>11</b>
<b>2 Review of the Literature .....</b>	<b>12</b>
2.1 Characteristics, diagnosis and staging of prostate cancer .....	12
2.1.1 Epidemiology, aetiology and risk factors .....	12
2.1.2 Grading and tumour, node, metastasis (TNM) classification.....	13
2.1.3 Diagnostic evaluation .....	15
2.1.4 Clinical staging .....	16
2.2 Principles of the treatment of prostate cancer .....	19
2.2.1 Local treatments.....	19
2.2.2 Hormone-sensitive disease .....	20
2.2.3 Castration-resistant disease .....	22
2.3 Principles of positron emission tomography (PET) imaging ....	23
2.3.1 Physical principles of PET .....	23
2.3.2 Hybrid imaging .....	25
2.4 Evolution of PET radiotracers for prostate cancer .....	26
2.4.1 Fluorodeoxyglucose (FDG) .....	26
2.4.2 Sodium fluoride (NaF) .....	27
2.4.3 Choline, acetate and fluciclovine .....	27
2.4.4 Bombesin .....	29
2.5 Prostate specific membrane antigen (PSMA) and PSMA PET.....	31
2.5.1 Prostate specific membrane antigen (PSMA).....	31
2.5.2 Main PSMA ligands for prostate cancer imaging .....	32
2.5.2.1 Evolution of the PSMA ligands for imaging ...	32
2.5.2.2 <sup>68</sup> Ga-labelled ligands .....	33
2.5.2.3 <sup>18</sup> F-labelled ligands .....	35
2.5.2.4 <sup>99m</sup> Tc-labelled ligands .....	38
2.5.2.5 <sup>64</sup> Cu-labelled ligands.....	38
2.5.3 PSMA PET imaging .....	39
2.5.3.1 PSMA PET in biochemical recurrence .....	39
2.5.3.2 PSMA PET in primary staging .....	40
2.5.3.3 PSMA PET in therapy response assessment .....	41
2.5.3.4 PSMA theranostics .....	43



2.5.3.5	PSMA PET structured reporting.....	45
2.5.3.6	PSMA PET in non-prostatic tumours.....	47
<b>3</b>	<b>Aims .....</b>	<b>50</b>
<b>4</b>	<b>Materials and Methods.....</b>	<b>51</b>
4.1	Study population and eligibility .....	51
4.2	Study design .....	52
4.2.1	Study I.....	52
4.2.2	Study II.....	53
4.2.3	Study III.....	53
4.2.4	Study IV .....	54
4.3	Imaging protocols.....	54
4.3.1	Dynamic PET scans and blood sampling (Study I) .....	54
4.3.2	PET/MRI and PET/CT scans.....	55
4.3.3	CT and WBMRI (Study IV) .....	56
4.4	Radiopharmaceutical preparation.....	57
4.5	Histopathological analysis .....	57
4.6	Imaging interpretation and analysis .....	58
4.6.1	Study I.....	58
4.6.2	Study II.....	61
4.6.3	Study III.....	61
4.6.4	Study IV .....	62
4.7	Software for imaging analysis.....	62
4.8	Statistical analysis .....	63
4.9	Ethics .....	63
<b>5</b>	<b>Results .....</b>	<b>64</b>
5.1	Study I.....	64
5.2	Study II.....	70
5.3	Study III.....	74
5.4	Study IV .....	80
<b>6</b>	<b>Discussion .....</b>	<b>88</b>
6.1	Biodistribution and kinetics of novel rh-PSMA-3.7 tracer .....	88
6.2	Physiology of PSMA expression in relation to ADT.....	90
6.3	Clinical utility of PSMA PET in primary nodal staging .....	94
6.4	Strengths and Limitations.....	97
6.5	Implications and future perspectives .....	98
<b>7</b>	<b>Conclusions.....</b>	<b>101</b>
	<b>Acknowledgements .....</b>	<b>102</b>
	<b>References .....</b>	<b>105</b>
	<b>Original Publications.....</b>	<b>131</b>

# Abbreviations

$^{18}\text{F}$	$^{18}\text{Fluorine}$
$^{68}\text{Ga}$	$^{68}\text{Gallium}$
$^{99\text{m}}\text{Tc}$	$^{99\text{m}}\text{Tecnetium}$
ADT	Androgen deprivation therapy
BCR	Biochemical recurrence
BS	Bone scintigraphy
Ce	Contrast-enhanced
CRPC	Castration resistant prostate cancer
CT	Computed tomography
DWI	Diffusion weighted imaging
EAU	European Association of Urology
FAPI	Fibroblast activation protein inhibitor
FDG	Fluoro-deoxy-glucose
FSH	Follicle stimulating hormone
GGG	Gleason grade group
GnRH	Gonadotropin releasing hormone
GS	Gleason score
H&E	Haematoxylin and eosin
HCC	Hepatocellular carcinoma
ISUP	International Society of Urological Pathology
Ki	Net influx rate
LH	Luteinising hormone
Mp	Multiparametric
MRI	Magnetic resonance imaging
MTGA	Multiple-time graphical analysis
PCa	Prostate cancer
PET	Positron emission tomography
PI-RADS	Prostate Imaging Reporting and Data System
PLND	Pelvic lymph node dissection
PSA	Prostate specific antigen
PSMA	Prostate-specific membrane antigen

RALP	Robot-assisted laparoscopic prostatectomy
RCC	Renal cell carcinoma
Rh	Radiohybrid
RLT	Radioligand therapy
RT	Radiation therapy
SPECT	Single photon emission tomography
SUV	Standardised uptake value
TAC	Time-activity curve
TNM	Tumour node metastases
TRUS	Transrectal ultrasound
WB	Whole body

# List of Original Publications

This dissertation is based on the following original publications, which are referred to in the text by their Roman numerals:

- I Simona Malaspina, Vesa Oikonen, Anna Kuisma, Otto Ettala, Kalle Mattila, Peter J Boström, Heikki Minn, Kari Kalliokoski, Ernst J. Postema, Matthew P. Miller, Mika Scheinin. Kinetic analysis and optimisation of [<sup>18</sup>F]-rhPSMA-7.3 PET imaging of prostate cancer. *European Journal of Nuclear Medicine and Molecular Imaging (EJNMMI)*, 2021; 48(11); 3723–3731.
- II Otto Ettala, Simona Malaspina, Terhi Tuokkola, Pauliina Luoto, Eliisa Löyttyniemi, Peter J. Boström, Jukka Kempainen. Prospective study on the effect of short-term androgen deprivation therapy on PSMA uptake evaluated with [<sup>68</sup>Ga]-PSMA-11 PET/MRI in men with treatment-naïve prostate cancer. *European Journal of Nuclear Medicine and Molecular Imaging (EJNMMI)*, 2020; 47(3): 665-673
- III Simona Malaspina, Otto Ettala, Tuula Tolvanen, Johan Rajander, Olli Eskola, Peter J. Boström, Jukka Kempainen. Flare on [<sup>18</sup>F]-PSMA-1007 PET/CT after short-term androgen deprivation therapy and its correlation to FDG uptake: possible marker of tumour aggressiveness in treatment-naïve metastatic prostate cancer patients. *European Journal of Nuclear Medicine and Molecular Imaging (EJNMMI)*, 2023; 50(2): 613-621
- IV Simona Malaspina, Mikael Anttinen, Pekka Taimen, Ivan Jambor, Minna Sandell, Irina Rinta-Kiikka, Sami Kajander, Jukka Schildt, Ekaterina Saukko, Tommi Noponen, Jani Saunavaara, Peter B. Dean, Roberto Blanco Sequeiros, Hannu J. Aronen, Jukka Kempainen, Marko Seppänen, Peter J. Boström, Otto Ettala. Prospective comparison of [<sup>18</sup>F]-PSMA-1007 PET/CT, whole-body MRI and CT in primary nodal staging of unfavourable intermediate- and high-risk prostate cancer. *European Journal of Nuclear Medicine and Molecular Imaging (EJNMMI)*, 2021; 48(9); 2951-2959.

The original publications have been reproduced with the permission of the copyright holders.

# 1 Introduction

Prostate-specific membrane antigen (PSMA) positron emission tomography (PET) has been a game changer in prostate cancer (PCa) imaging in the last five to ten years. Several PSMA ligands have been developed for PET imaging. The first PSMA ligands used in clinical practice were  $^{68}\text{Ga}$ -labelled. Recently,  $^{18}\text{F}$ -labelled ligands have been increasingly used in preference to their  $^{68}\text{Ga}$ -labelled counterparts due to their longer half-life and lower positron range and therefore, higher spatial and contrast image resolution. In the current era of theranostics, the use of ligands that can be labelled with both diagnostic ( $^{68}\text{Ga}$  and  $^{18}\text{F}$ ) and therapeutic ( $^{177}\text{Lu}$  and  $^{225}\text{Ac}$ ) radioisotopes is a very appealing option. Novel radiohybrid (rh)PSMA-7 ligands were recently developed for this purpose; and, among different diastereoisomers, [ $^{18}\text{F}$ ]-rhPSMA-7.3 has been chosen as the lead compound for further assessment.

Although PSMA and its mechanisms of expression in prostatic and non-prostatic tissue have been known through *in vitro* studies, the physiology of this protein and particularly, the effects of PCa treatments on PSMA expression need further clarification. Preclinical and a few human studies have demonstrated that androgen deprivation therapy (ADT) upregulates PSMA expression, which can be visualised as a transitory increase in PSMA uptake in PET scans. This phenomenon, known as PSMA flare, has been poorly studied so far, and its possible clinical significance remains still unknown.

PSMA PET has an established role in patients with biochemical recurrence (BRC) of PCa. However, the role of PSMA PET and its influence on patient outcomes in the context of primary staging have not yet been assessed. Bone scintigraphy (BS) and computed tomography (CT) are the conventional imaging modalities recommended in the primary staging of PCa, although their sensitivity is known to be poor. In particular, the dimensional and morphological evaluation of lymph nodes used in CT is not sufficient for detecting lymph node metastases, as the majority of PCa lymph node metastases are normally sized. Advanced imaging modalities, such as magnetic resonance imaging (MRI) with diffusion-weighted imaging (DWI) and PSMA PET have been shown to increase the imaging accuracy, allowing a better and earlier localisation of the extent of the regional disease. However, prospective comparative studies of the conventional and advanced imaging modalities in the primary staging of PCa are still limited.

## 2 Review of the Literature

### 2.1 Characteristics, diagnosis and staging of prostate cancer

#### 2.1.1 Epidemiology, aetiology and risk factors

Prostate cancer (PCa) indicates a variety of malignant neoplasms of the prostate gland. The vast majority (> 95%) of PCAs are adenocarcinomas, which arise from the glandular epithelium. Minor variants of PCa include neuroendocrine PCa, squamous cell carcinoma, transitional cell carcinoma, sarcomas and lymphomas. Two-thirds of cases of prostate adenocarcinoma originates from the peripheral zone of the prostate, and the remaining originate from the transitional zone (McNeal et al. 1988). PCa can spread locally, typically to the adjacent organs or to the pelvic lymph nodes, through lymphatic spread. Typical sites of distant metastases are the bone and extra-pelvic lymph nodes, followed by the visceral organs, particularly, the lung and liver (Gandaglia et al. 2014).

PCa is the second most frequent malignancy diagnosed in men worldwide (Rawla 2019). The frequency of autopsy-detected PCa is approximately the same worldwide (Haas et al. 2008). However, the incidence of clinically diagnosed PCa varies according to different geographic areas, being the highest in Australia, Northern America and Europe, and the lowest in Asia and Northern Africa (Culp et al. 2020). The prevalence of PCa is mostly dependent on age, with a prevalence of 59% (95% confidence interval [CI] 48-71%) at > 79 years of age (Haas et al. 2008).

Family history and ethnical background are associated with increased risk of PCa, which suggest a genetic predisposition (Hemminki 2012). However, a true hereditary PCa is rare. Several genetic mutations are considered to be involved in the increased risk of PCa. The most common pathogenetic variants have been identified in the BRCA2, CHECK2, ATM and BRCA1 genes (Giri et al. 2019). In particular, BRCA1/2 mutations are associated with more aggressive PCa and risk of metastasis at diagnosis (Castro et al. 2013; Nyberg et al. 2020; Page et al. 2019).

Moreover, many exogenous, environmental or dietary risk factors are involved in the development of PCa. These factors include single components of metabolic syndrome, such as hypertension and waist circumference, obesity and alcohol

consumption ( Dickerman et al. 2017;Esposito et al. 2013; Vidal et al. 2014). Nevertheless, the association of these factors with the increased risk of PCa is still controversial, and currently no specific preventive or dietary measures have been introduced in the clinical guidelines.

### 2.1.2 Grading and tumour, node, metastasis (TNM) classification

Histological grading of biopsy-detected PCa and prostatectomy specimens follows the Gleason grading system. The Gleason score (GS) is represented as the sum of the most extensive Gleason grade pattern (primary) and the second most common pattern (secondary). According to the modifications of the 2014 International Society of Urological Pathology (ISUP), GSs have also been represented through the ISUP grading system, which ranges from 1 to 5. This allows to distinguish between two different ISUP grades in patients with GS=7 (**Table 1**).

**Table 1.** Classification of Gleason Scores and corresponding ISUP grades. ISUP: International Society of Urological Pathology. Modified from Mottet et al., 2022.

Gleason score	ISUP grade
2-6	1
7 (3+4)	2
7 (4+3)	3
8 (4+4, 3+5 or 5+3)	4
9-10	5

The staging of PCa follows the Tumour, Node, Metastasis (TNM) classification (**Table 2**). It has three components; T: the extent of the primary tumour; N: the presence or absence of regional (pelvic) lymph node metastases; and M: the presence or absence of distant metastases. Clinical T-staging is traditionally based on digital rectal examinations (DREs). Pathological T-staging (pT) refers to the histopathological findings, and it parallels the clinical T-staging except for the absence of the T1 and T2 substages. Clinical N- and M-staging are based on imaging findings (traditionally, BS and CT).

**Table 2.** Clinical Tumour Node Metastasis (TNM) classification. PSA: prostate specific antigen. Modified from: Mottet et al., 2022.

<b>T- Primary tumour (clinical)</b>
TX Primary tumour cannot be assessed
T0 No evidence of primary tumour
T1 Clinically inapparent tumour that is not palpable
T1a Tumour incidental histological finding in 5% or less of tissue resected
T1b Tumour incidental histological finding in more than 5% of tissue resected
T1c Tumour identified by needle biopsy (e.g. because of elevated PSA)
T2 Tumour that is palpable and confined within the prostate
T2a Tumour involves one half of one lobe or less
T2b Tumour involves more than half of one lobe, but not both lobes
T2c Tumour involves both lobes
T3 Tumour extends through the prostatic capsule
T3a Extracapsular extension (unilateral or bilateral)
T3b Tumour invades the seminal vesicles
T4 Tumour is fixed or invades adjacent structures other than the seminal vesicles: external sphincter, rectum, levator muscles, and/or pelvic wall.
<b>N- Regional lymph nodes</b>
NX Regional lymph nodes cannot be assessed
N0 No regional lymph node metastases
N1 Regional lymph node metastases
<b>M- Distant metastases</b>
M0 No distant metastases
M1 Distant metastases
M1a Non-regional lymph nodes
M1b Bone
M1c Other site(s)
When more than one site of metastases is present the most advanced category is used
(p)M1c is the most advanced category

According to the European Association of Urology (EAU) guidelines, PCa patients can be stratified into three risk groups according to their T-stage, GS and prostate-specific antigen (PSA) value, which guide management and treatment options (**Table 3**). The National Cancer Network (NCCN) further classifies the intermediate risk group into two subcategories: favourable and unfavourable intermediate, where the unfavourable includes ISUP grade 3, and/or  $\geq 50\%$  positive biopsy cores and/or at least two intermediate risk factors (**Table 3**).



**Table 3.** Risk group classification. ISUP: International Society of Urological Pathology. IRF: intermediate risk factors. PSA: prostate specific antigen. GG: Gleason grade. Modified from: Schaeffer et al., 2021.

Low-risk	Intermediate risk		High-risk	
PSA < 10 ng/ml and ISUP GG 1 and cT1-2a	One or more IRFs: PSA 10-20 ng/ml ISUP GG 2/3 cT2b-cT2c	Favourable	ISUP GG 2 1 IRFs < 50% positive biopsy core	PSA >20 ng/ml or ISUP GG 4/5 or cT2c or cT3-4 or cN+ with any PSA and any GS *
		Unfavourable	ISUP GG 3 two OR 3 IRFs ≥ 50% positive biopsy core	

### 2.1.3 Diagnostic evaluation

The first diagnostic tests performed when PCa is suspected are serum PSA measurement and digital rectal examination (DRE).

PSA is a serum marker that indicates greater likelihood of PCa at higher levels and its value is a predictor of more aggressive PCa (Stamey et al. 1987;Thompson et al. 2004). Being organ-specific rather than cancer-specific, PSA might also be elevated in benign conditions, such as in benign prostatic hypertrophy (BPH) or prostatitis. For this reason, an elevated PSA in a single measurement is not sufficient to proceed with a prostate biopsy. In particular, when the initial PSA is 3-10 ng/mL, the test should be repeated to confirm the increase.

For a more accurate diagnosis of PCa, other PSA-based parameters have been introduced. PSA density is the level of serum PSA divided by the prostate volume. A PSA density > 0.10-0.15 ng/ml<sup>2</sup> is correlated with higher risk of clinically significant PCa (Nordström et al. 2018; Omri et al. 2020). Other parameters are PSA velocity and PSA doubling time, which express the absolute annual increase in the serum PSA and the exponential increase in the serum PSA over time, respectively (Carter et al. 1995; Schmid et al. 1993). A PSA velocity > 0.35 ng/ml/year and a PSA doubling time < 10 months can indicate a higher risk of clinically significant PCa, and can predict the likelihood of subsequent development of metastatic disease (Pound et al. 1999; Carroll et al. 2015). However, the diagnostic use of PSA velocity and PSA doubling time is limited due to different variables (e.g., different methods of calculation, different time intervals in PSA determinations and acceleration or decelerations over time). Serum PSA exists in a free form (5-40% of the total) as well as complexed to protease inhibitors. It has been shown that PCa patients have a higher percentage of PSA bound to proteins compared to negative controls (Hoffman et al. 2000). The free to total PSA ratio might be used in cases of 4-10 ng/mL PSA and a negative DRE result. However, there is no recommendation for its use in PSA > 10 ng/ml or during follow-up of known PCa.

Definite diagnosis of PCa depends on histopathological verification of adenocarcinoma on prostate biopsy specimens. Transrectal ultrasound (TRUS) has traditionally been the cornerstone of the diagnosis of PCa, as it represents a feasible imaging modality for the evaluation of the posterolateral area of the prostate, where most of PCas are diagnosed. Nevertheless, standard TRUS alone has been demonstrated to be unreliable in detecting PCa and should be used only to guide systematic biopsies (Rouvière et al. 2019). TRUS-guided biopsies can be performed either with the transrectal or transperineal approach. At least 8 systematic needle biopsies (10-12 in cases of a larger prostate) are recommended.

New diagnostic pathways that emerged during the last decade have incorporated magnetic resonance imaging (MRI) in the diagnosis and local staging of PCa (Johnson et al. 2019). Multiparametric MRI (mpMRI) consists of different anatomical and functional sequences including T2-weighted and T1-weighted imaging, diffusion-weighted imaging (DWI) with apparent diffusion coefficient (ADC) maps, contrast-enhanced sequences and proton magnetic resonance spectroscopy. The reporting and interpretation of MRI findings on the prostate have been structured and standardised using the Prostate Imaging-Reporting And Data System (PI-RADS) score. Each suspect lesion is assigned a score from 1 to 5 according to the findings in the T2 and DWI sequences as well as the presence of contrast enhancement. The score represents the likelihood of significant PCa (Puryrsko et al. 2020). Biparametric MRI, which includes only T2 and DWI sequences and not contrast-enhanced sequences, has gained increasing interest as it has shown results comparable to those of mpMRI (Jambor et al. 2019; Knaapila et al. 2021).

MRI has been demonstrated to be a very sensitive imaging method for the detection of PCa according to its grade and size (ISUP grade  $\geq 2$  or with diameter  $> 10$  mm) (Bratan et al. 2013; Johnson et al. 2019). MRI is also considered the most useful method for local T-staging (de Rooij et al. 2016). Moreover, MRI-guided targeted biopsies have been shown to increase the detection of clinically significant PCa and to simultaneously reduce the detection of insignificant PCa compared to template biopsies (Kasivisvanathan et al. 2018; van der Leest et al. 2019).

#### 2.1.4 Clinical staging

Although PCa can be treated radically in most of the cases, many men, after radical treatment, are diagnosed with metastatic recurrence (Welch et al., 2015). This might suggest that the disease had already spread at the time of the initial diagnosis. Therefore, accurate staging is paramount to assess the correct treatment planning. Current guidelines traditionally recommend BS and CT for the primary staging of PCa (**Figure 1**).

BS has been the cornerstone of skeletal nuclear medicine imaging for decades. It uses  $^{99m}\text{Tc}$ -labelled phosphate analogues to evaluate the distribution of active bone formation in malignant and benign diseases. The uptake of the radiotracer indicates the number of radiolabelled phosphonates that are being absorbed to the surface of hydroxyapatite crystals and is correlated with the local blood flow and the osteoblastic activity. The clearance from soft tissue is very fast, providing an optimal bone tissue to background ratio. BS is a sensitive method compared to anatomical imaging methods, as it can detect bone metastases at a stage in which they would not be visible on radiological images. However, many other non-neoplastic conditions might cause tracer uptake, such as trauma, infections and arthrosis. Conventionally, BS is performed as a planar scintigraphy, even though single photon emission computed tomography (SPECT)/CT can significantly increase the sensitivity and improve the correlation of the uptakes with the anatomical reference (Horger et al. 2004).

CT is used as a complementary imaging method to BS in the staging of PCa to evaluate lymph nodes, as well as the bone tissue and visceral organs. The guidelines recommend CT of the abdomen and pelvis, even though whole-body CT, including the thorax, is usually performed. For lymph nodes, morphological and dimensional criteria are used to assess suspicious malignant findings (a round shape and a short axis  $> 8$  mm in the pelvis and  $> 10$  mm outside the pelvis). However, the diagnostic accuracy of CT in assessing lymph node metastases has been demonstrated to be limited (Hövels et al. 2008). Moreover, both BS and CT have demonstrated poor sensitivity and accuracy in the detection of bone metastases compared to advanced imaging modalities (Anttinen et al. 2020; Hofman et al. 2020; Suh et al. 2018).

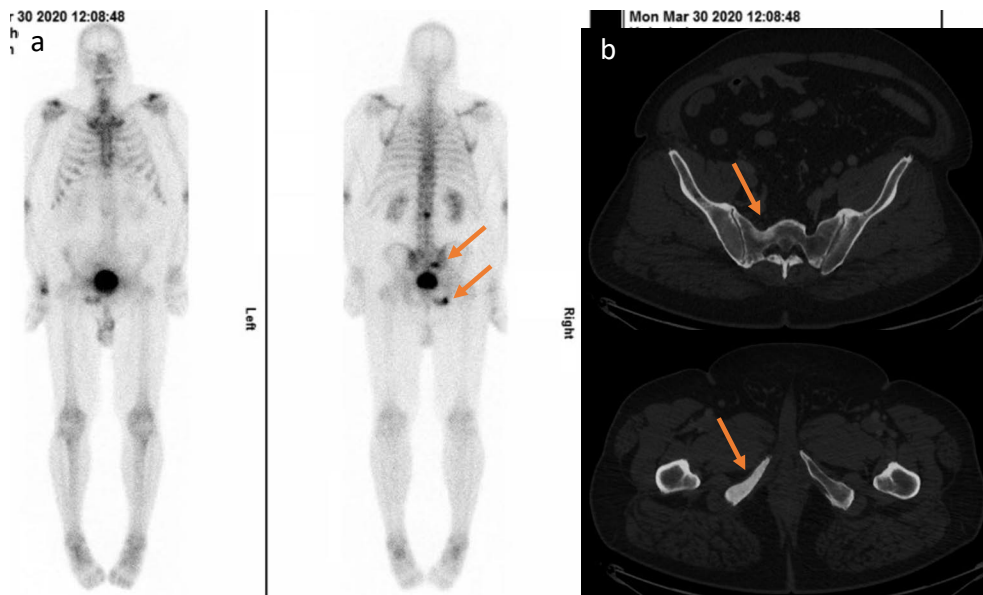


**Figure 1.** Planar bone scintigraphy (BS) and computed tomography (CT) images of a representative patient from Study III. The BS shows focal uptakes in the sacrum and right ischium bone (a, orange arrows) that correspond to the sclerotic lesions on the CT images (b, orange arrows).

An overview of the performance of CT and BS in primary N- and M-staging of PCa according to systematic reviews and meta-analysis is presented in **Table 4**.

**Table 4.** Sensitivity and Specificity of CT and BS in primary N- and M-staging of PCa.

Modality	Sensitivity		Specificity	
	N-staging	M-staging	N-staging	M-staging
CT	0.42 <sup>a</sup>	0.56 <sup>b</sup>	0.82 <sup>a</sup>	0.74 <sup>b</sup>
BS	-	0.79-0.86 <sup>c</sup>	-	0.68-0.95 <sup>c</sup>

<sup>a</sup> Hövels et al. 2008; <sup>b</sup> Talbot et al. 2011

<sup>c</sup> Shen et al. 2014; Zhou et al. 2019; Zhao et al. 2021; Zhao and Ji 2022

Due to the limited accuracy of BS and CT in the staging of PCa, more advanced imaging techniques have gained increasing acceptance in the work-up of PCa.

Whole-body MRI (WBMRI) is an accurate diagnostic tool that allows the evaluation of possible bone and soft tissue metastases in one session (Pasoglou et al. 2014). This imaging method has been demonstrated to be superior to the combination of conventional imaging methods in patients with high-risk PCa (Lecouvet et al. 2007). Among the MRI sequences used, DWI can provide an added value to the anatomical evaluation and help in characterising metastases in normally sized lymph

nodes as well as early intramedullary bone metastases (Komori et al. 2007; Luboldt et al., 2008; Thoeny et al. 2014).

Hybrid positron emission tomography (PET) imaging, including PET/CT and PET/MRI, has been successfully used in PCa imaging. PET is a functional imaging modality that uses short-lived positron-emitting radioisotopes labelled to a biological molecule of interest. Radiotracers that targeted lipid or amino acid metabolism as well as glucose metabolism in aggressive disease have been available for PCa imaging before the advent of prostate-specific membrane antigen (PSMA), which has become a game changer over the past 10 years. Sections 2.4 and 2.5 of this doctoral thesis describe the evolution of PET radiotracers for PCa imaging and a give a detailed overview of PSMA PET.

## 2.2 Principles of the treatment of prostate cancer

### 2.2.1 Local treatments

Low-risk PCa, which will most likely remain indolent and has a low risk of progression, can be treated with active surveillance to reduce the risk of overtreatment or post-treatment morbidity. Active surveillance consists of a deferred treatment strategy, wherein definitive treatment is administered in case disease progression is detected during regular follow-ups. Although no formal randomised controlled trial on active surveillance has been conducted, many single-arm observational studies on active surveillance and active treatment demonstrated similar rates of overall survival (OS) at 10 years (85-100%) in patients with low-risk PCa (Mottet et al. 2021). However, active treatment seems to be associated with less incidence of disease progression or metastases (Hamdy et al. 2016).

In localised intermediate- to high-risk PCa radical treatment options include surgery and radiotherapy (RT). Surgery consists of radical prostatectomy, where the entire prostate, its capsule and the seminal vesicles are removed, followed by vesico-urethral anastomosis. The preferred surgical approach, when available, is robotic-assisted laparoscopic prostatectomy (RALP), which is minimally invasive and has a lower recovery time, blood loss and complication rates than open surgery (Coughlin et al. 2018). 3D laparoscopy has been proposed in few studies as a potentially cost-effective option to RALP, with comparable oncological and functional outcomes (Andras et al. 2017; Haapiainen et al. 2022).

During the prostatectomy procedure, it is also possible to perform bilateral pelvic lymph node dissection (PLND). At present, the gold standard procedure is extended PLND, which include the removal of the lymphatic tissue around the external and internal iliac vessels and the obturator nerve. This approach provides a more accurate staging than a limited PLND (removal of only the lymph nodes in the obturator

fossa) (Lestingi et al. 2021). PLND provides important information for staging and prognosis and is usually reserved for patients with a high risk of metastases according to EAU risk groups (Fossati et al. 2017). The individual risk for lymph node metastases and, therefore, the decision of performing PLND is based on validated nomograms, such as the Briganti nomogram, the Memorial Sloan Kettering Cancer Center (MSKCC) nomograms and the Roach formula, which have shown similar diagnostic accuracy (Briganti et al. 2012; Roach et al. 1994; Cimino et al. 2017).

RT is an established alternative to surgical treatment of localised PCa. External beam RT (EBRT) with intensity modulated RT (IMRT) with or without image-guided RT (IGRT) is considered the best available RT approach (Mottet et al. 2021). These techniques more efficiently modulate the dose to the tumour and reduce toxicity to the surrounding tissues (Yu et al. 2016). Several trials have shown that the dose escalation (usually with a range of 74-80 Gy) has a significant impact on 10-years biochemical relapse, disease-specific mortality, and OS, especially in intermediate- and high-risk PCa (Beckendorf et al. 2011; Heemsbergen et al. 2014; Kalbasi et al. 2015; Pasalic et al. 2019). ADT has been demonstrated to be beneficial as neoadjuvant or adjuvant therapy to RT compared to RT alone (Bolla et al. 2010; D'Amico et al. 2008; Denham et al. 2011). Brachytherapy, where radioactive seeds are implanted directly into the prostate gland, can also be used to treat localised PCa with or without EBRT. High-dose-rate brachytherapy is a promising technique, where seeds are implanted only temporarily and can be delivered in a single or multiple fractions, in combination with EBRT (Mottet et al. 2021).

In addition to surgery and RT, new ablative techniques have attracted interest in the past few years for the treatment of localised PCa. These treatments aim to direct a tissue-destroying energy to the tumour using natural channels, such as the rectum or urethra. These ablative treatments include high-intensity focused ultrasound (HIFU), cryotherapy, photodynamic therapy or MRI-guided transurethral ultrasound ablation (TULSA) (Anttinen et al. 2019; Gill et al. 2019; Stabile et al. 2019; Shah et al. 2019).

## 2.2.2 Hormone-sensitive disease

Most of early-stage PCas are hormone-sensitive, which means that they are responsive to hormonal treatment. Hormone-sensitive PCa can be non-metastatic, when it is localised to the prostate or locally advanced, or metastatic. Metastatic hormone-sensitive PCa is usually categorized into high-volume ( $\geq 4$  bone metastases including  $\geq 1$  outside vertebral column and pelvis or visceral metastasis) and low-volume (not high) disease (Sweeney et al. 2015).

The first-line treatment in metastatic hormone-sensitive PCa is ADT, the aim of which is to suppress the secretion of testicular androgens. Testosterone is produced in men by the Leyding cells of the testes under the stimulation of luteinising hormone (LH) and follicle-stimulating hormone (FSH) secreted by the anterior pituitary gland. LH and FSH secretions are regulated by the gonadotropin-releasing hormone (GnRH) secreted by the hypothalamus. The simplest and fastest way to achieve the castration levels of testosterone (serum testosterone < 1.7 nmol/L) is surgical castration through bilateral orchiectomy. However, this procedure is irreversible. Thus, in most cases, pharmacological treatment with ADT is preferred (Chodak 2008).

The main forms of ADT used in clinical practice are LH-releasing hormone (LHRH) agonists and antagonists, and anti-androgens. These are administered as subcutaneous injections, usually on a 1, 3 or 6-monthly, or yearly basis. LHRH agonists (also called GnRH agonists) downregulate the gonadal luteinising receptors in the pituitary gland and therefore, suppress the secretion of LH and the production of testosterone. However, after the first injections, LHRH agonists typically induce a release of LH, which leads to a transitory rise in testosterone (known as testosterone flare). LHRH agonists can be administered concurrently with anti-androgens to reduce the incidence of this flare phenomenon. LHRH antagonists (also known as GnRH antagonists) directly block the LH receptors of the pituitary gland, inducing a rapid decrease in the LH and testosterone levels. The advantage of LHRH antagonists is that no testosterone flare occurs, and no concomitant anti-androgen therapy is needed. Moreover, LHRH antagonists typically induce a very rapid decrease in testosterone within the first two to three weeks of treatment. Degarelix (LHRH antagonist) has been demonstrated to be more effective in terms of PSA progression free survival than leuprolide (LHRH agonist) (Shore 2013). However, the superiority of LHRH antagonists to LHRH agonists still needs to be proven. Anti-androgens, the most used of which is bicalutamide, compete with circulating androgens to the binding site of the androgen receptor (AR) in the testes. This leads to an unchanged or slightly elevated serum testosterone levels.

In the case of oligometastatic disease (usually defined as four or fewer metastases not including visceral metastases), long-term ADT can be combined with RT of the primary tumour to increase its efficacy and improve the patient outcomes, as demonstrated by two prospective randomised trials (Boevé et al. 2019; Parker et al. 2018). Because of the increasing use of advanced imaging modalities, oligometastatic disease in particular, is detected more often. In this context, metastases-directed stereotactic RT (SRT) has gained particular scientific interest. Although these treatments, especially of metastases detected only with advanced imaging, are experimental, a recent randomised Phase II trial showed improved outcomes in oligometastatic patients treated with stereotactic ablative radiation compared to observation (Phillips et al. 2020).

In the case of more extended or high-volume metastatic diseases, ADT is combined with chemotherapy to improve outcomes and OS, provided that patients are fit enough to receive the treatment. In this context, docetaxel, a cytotoxic agent that disrupts the normal function of microtubules, is used. Prospective randomised trials have demonstrated survival benefits using docetaxel + ADT versus ADT alone (Clarke et al. 2019; Gravis et al. 2013; James et al. 2016). Moreover, in both oligometastatic and high-volume metastatic PCa next generation hormonal agents can be used, such as abiraterone, enzalutamide, apalutamide or darolutamide. Abiraterone inhibits the cytochrome P450 17 $\alpha$ -hydroxylase/17,20-lyase (CYP17) enzyme, which is responsible for the synthesis of testosterone precursors in the adrenal glands and inside cancer cells. This compound should be used together with prednisone in order to prevent drug-induced hyperaldosteronism. In prospective randomised trials abiraterone in combination with ADT demonstrated improved OS and radiographic progression-free survival (PFS) in patients with metastatic hormone-sensitive PCa. (Fizazi et al. 2017; James et al. 2017). Enzalutamide, apalutamide and darolutamide are novel non-steroidal anti-androgens with higher affinity to the AR receptor compared to bicalutamide. These agents have also been investigated in combination with ADT in a prospective randomised setting and showed reduced risk of metastatic progression or death over the standard of care (Armstrong et al. 2019; Chi et al. 2019; Davis et al. 2019).

### 2.2.3 Castration-resistant disease

Hormone-sensitive disease will gradually and naturally shift to castration-resistant PCa (CRPC). CRPC is defined as a level of testosterone < 1,7 nmol/L + disease progression despite ADT, which can be either biochemical progression (with three consecutive rises in PSA at least one week apart and a PSA > 2 ng/ml) or radiological progression (with the appearance of new lesions on BS or CT). In the CRPC state, treatment options depend on previously received treatment, known drug interactions and the patient's status. First-line hormonal treatments of CRPC include abiraterone and enzalutamide (Beer et al. 2014; Ryan et al. 2015). Other systemic treatments consist of chemotherapy with docetaxel if not given in a hormone-sensitive state and subsequent cabazitaxel (Tannock et al. 2004; de Wit et al. 2019). Novel systemic treatments include immunotherapy with Sipuleucel-T or protein kinase B (Akt) inhibitors. [<sup>223</sup>Ra]-dichloride is a bone-specific alpha-emitting treatment for patients with metastases confined to the bone. It is usually administered in later stages in patients who experienced chemotherapy failure or were unfit for it (Parker et al. 2013).

Despite the treatments available, the outcome of metastatic CRPC (mCRPC) patients is usually poor. With the increasing use of PSMA PET imaging and the advent of theranostics, <sup>177</sup>Lu-labelled and <sup>225</sup>Ac-labelled PSMA radioligand therapy



(RLT) have been under keen scientific interest as a valuable options in mCRPC. The Food and Drug Administration (FDA) has very recently approved the use of [ $^{177}\text{Lu}$ ]-PSMA-617 for the treatment of patients with CRPC, based on the results of randomised trials that showed that [ $^{177}\text{Lu}$ ]-PSMA treatment is safe and efficient in terms of survival benefit (Hofman et al. 2021; Sartor et al. 2021).

In this context, radiohybrid (rh)PSMA ligands, one of which is under investigation in this doctoral thesis, could represent an interesting novelty, as these ligands can be labelled with both diagnostic ( $^{18}\text{F}$ ) and therapeutic radioisotopes ( $^{177}\text{Lu}$ ). A more detailed overview of PSMA theranostics is provided in Section 2.5.3.4 of this thesis.

## 2.3 Principles of positron emission tomography (PET) imaging

### 2.3.1 Physical principles of PET

Positron emission tomography (PET) is a functional method of measuring the biodistribution of positron-emitting radiotracers in vivo. Radiotracers consist of short half-lived radioisotopes that are mostly produced with a cyclotron or extracted from a decaying source by a generator, labelled to a biological molecule of interest. Radiotracers are usually administered intravenously in a bolus, after which the radioligand behaves according to the molecule's natural biological process. Positrons emitted by PET radiotracers travel a short distance in tissue. This distance varies according to the radioisotope (e.g.  $^{68}\text{Ga}$ 's positron range is  $> 1\text{mm}$ , and  $^{18}\text{F}$ 's positrons range is  $< 1\text{mm}$ ). Then, the positron interacts with a nearby electron and is annihilated to form two 511 keV photons directed in opposite directions (**Figure 2**). These photon pairs are then detected by a ring of detectors, and from the detection of such coincidence counts reconstructed tomographic images are produced (Turkington, 2001).

Most annihilation photons are typically absorbed in the body depending on the density and volume of the tissues. This phenomenon, called attenuation, prevents the photons from being detected appropriately. Traditional methods of correcting attenuation consisted of transmission scans using orbiting radionuclide sources. Currently, attenuation correction is performed using anatomic CT or MRI images. In conventional PET imaging, a positron annihilation is recognised along a 180-degree line of response, which does not represent the actual location of the event. Currently, PET scanners with time-of-flight (TOF) technology not only measures the distance and attenuation of photons, but also adds to the algorithm the actual time difference between the detection of the photons released during coincident events to more accurately identify the distance from the annihilation event to the detector.

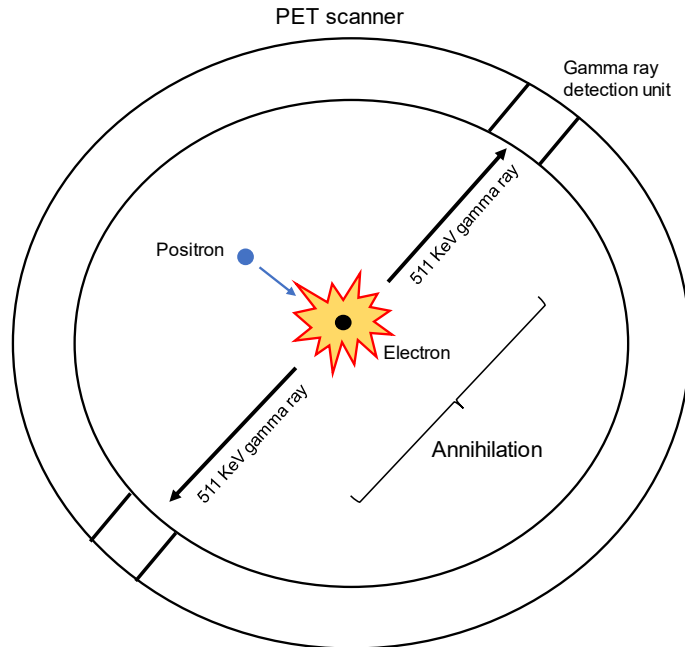


**Figure 2.** Positron emission, annihilation, and coincidence event detection.

The PET raw data collected during scanning is processed by the scanner computing unit and stored as a sinogram file (count averages during each time frame) or in list mode data (counts without predefined time frames). The sinogram data are then reconstructed using mathematical algorithms and converted into a three-dimensional (3D) PET image.

PET images have the advantage of providing quantitative and semi-quantitative measures of radiotracer concentration in vivo. Diagnostic PET images are typically static images acquired at a specific time after injection depending on the radiotracer, e.g. usually after 50 min for [ $^{18}\text{F}$ ]-FDG or after 60 min for most of [ $^{68}\text{Ga}$ ]/ [ $^{18}\text{F}$ ]-PSMA tracers. In static scans, the standardised uptake value (SUV) is widely used as a semi-quantitative method of measuring the radiotracer uptake. The SUV represents the ratio of the tissue radioactivity concentration at a single time point (KBq/ml) to the injected dose of radioactivity adjusted per kilogram of the patient's body weight or lean body mass (MBq/Kg) (Thie 2004). However, as the SUV is a relative value, dynamic imaging is needed to obtain quantitative measurements.

Dynamic data allow the creation of a tissue specific time-activity curve (TAC) using the frames of the dynamic scan and the blood input function obtained either from image-derived blood pool or, more accurately, from blood samples. These data, can be then transformed using multiple-time graphical analysis (MTGA). MTGA is a method wherein the radiotracer concentration curves of the region-of-

interest and arterial plasma are combined into a single curve that approaches linearity when dynamic equilibrium is reached. The data plotted for MTGA approaches linearity if the data support irreversible uptake in the case of a Patlak plot, or if the data support reversible uptake in the case of a Logan plot (Logan et al. 2003; Patlak and Blasberg 1985). The data can be plotted on a graph, and the line can be fitted to the linear phase. The slope of the fitted line represents the net uptake rate of the radiopharmaceutical or the volume of distribution. A line is fitted to the linearly increasing phase of the plot, and the slope of the line represents either the net influx rate ( $K_i$  in the case of a Patlak plot) or the volume of distribution (VT in the case of a Logan plot). The greater the slope is, the larger the respective uptake parameter is.

### 2.3.2 Hybrid imaging

Hybrid imaging is the fusion of two (or more) modalities to form a new and more powerful imaging technique (**Figure 3**). Relatively early in the development of clinical PET in oncology, the need to correlate functional and anatomical information was addressed (Wahl et al. 1993). Soon after the concept of imaging fusion was introduced, hybrid scanners that combine PET and CT (PET/CT) were developed. The initial combination of PET and CT into a single device used in clinical oncology was reported in 2000 (Beyer et al. 2000). The advantages of adding anatomical images to PET are multiple, including the use of CT for attenuation correction, providing anatomical information to help in the interpretation of PET findings (image fusion), and allowing two clinical examinations to be performed in one session. In the last two decades, the use of PET/CT has grown more rapidly than the use of any other hybrid imaging technique, particularly with the widespread of [ $^{18}\text{F}$ ]-FDG in clinical oncology. Moreover, imaging technology has been moving forward at an impressive pace. Among the most successful achievements, the implementation of silicon photomultipliers-based detectors allowed the move from analogical to digital PET/CT scanners. More recently, long axial field-of-view PET/CT, the so-called total-body PET, has been developed to cover the entire PET/CT's length in a single bed or position (Cherry et al. 2018).

In recent years, another powerful hybrid imaging modality, PET/MRI, was introduced. MRI imaging provides better soft tissue contrast than CT and can perform multiparametric evaluation including DWI and spectroscopy. Besides, PET/MRI reduces patients exposure to ionising radiation compared to PET/CT. PET/MRI has demonstrated good oncological applications, for example, in head and neck cancers and in pelvic malignancies (Ehman et al. 2017). Regarding PCa, PSMA PET/MRI might have promising applications in guiding prostate biopsies, in the characterisation and targeting of intraprostatic lesions in patients referred for focal

therapies or in monitoring tumour aggressiveness in patients in active surveillance (Evangelista et al. 2021; Ferraro et al. 2021). However, due to the higher costs and availability of the scanners, the clinical use of PET/MRI is still limited.

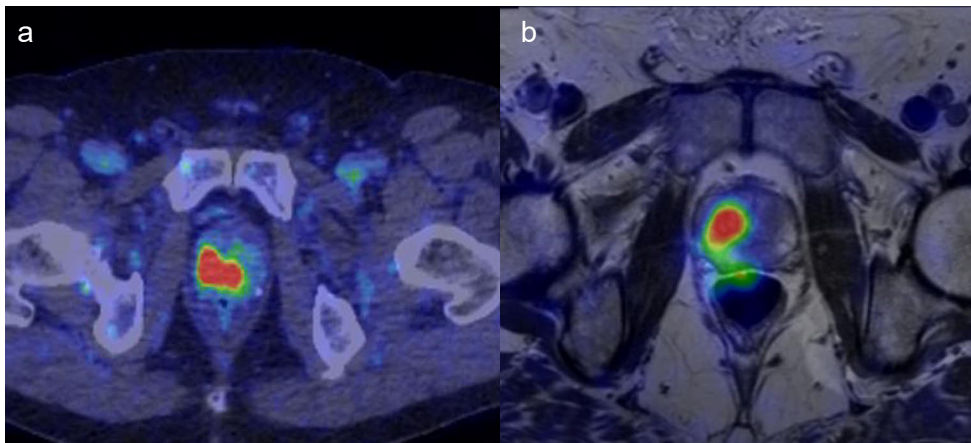


**Figure 3.** Examples of hybrid imaging. PSMA PET/CT (a) and PET/MRI (b) fused images of PCa. The image in panel a is from a representative patient in Study III. Image in panel b is from a representative patient in Study II.

## 2.4 Evolution of PET radiotracers for prostate cancer

### 2.4.1 Fluorodeoxyglucose (FDG)

[<sup>18</sup>F]-fluorodeoxyglucose (FDG) is an established radiotracer that is used to image a wide spectrum of malignant diseases. Cancer cells usually present higher glycolytic rates and higher expression of glucose transporters (GLUT) and hexokinase than normal cells. The increase in glucose metabolism in cancer tissues results in increased tracer uptake on [<sup>18</sup>F]-FDG PET images (Pauwels et al. 1998). [<sup>18</sup>F]-FDG is taken up in cells via different glucose transporters isoforms depending on the target tissue (GLUT-1-4) and, once inside, is phosphorylated typically by hexokinase to [<sup>18</sup>F]-FDG-6-phosphate. FGD-6-phosphate is not substantially further metabolised after this step and is retained in cancer cells (S. Zhao et al. 2005). The degree of FDG uptake is related to the cellular glycolytic metabolic rate, which has close relationships with histological characteristics and tumour differentiation.

Prostate adenocarcinoma is known to have a low glycolytic rate, which limits the use of [<sup>18</sup>F]-FDG PET (Jadvar 2013; Schöder et al. 2005). However, in vitro studies have demonstrated that GLUT-1 expression in PCa cells is directly related to the tumour grade, and that its expression is higher in poorly differentiated hormone-

sensitive LNCaP cell lines than in well-differentiated ones. GLUT-1 gene expression also seems correlated directly with the GS (Effert et al. 2004; Stewart et al. 2008). Clinical studies also demonstrated that FDG uptake increases in relation to the Gleason grade, clinical stage and serum PSA levels (Morris et al. 200; Oyama et al. 1999). Therefore, increased FDG uptake might be considered as a marker of tumour aggressiveness in PCa (Jadvar 2009; Jadvar 2013; Jadvar 2016). An example of the physiological biodistribution of [ $^{18}\text{F}$ ]-FDG in PCa patients is depicted in (**Figure 4**). FDG uptake has also been considered as an independent prognostic factor in PCa patients and has been associated with poorer outcomes and OS (Meirelles et al. 2010; Morris et al. 2005). Currently, [ $^{18}\text{F}$ ]-FDG PET is used to assess the eligibility for RLT with [ $^{177}\text{Lu}$ ]-PSMA. In this context, the presence of FDG positive PCa has shown to be a negative predictive and prognostic factor (Buteau et al. 2022; Hofman et al. 2018; Michalski et al. 2021).

#### 2.4.2 Sodium fluoride (NaF)

[ $^{18}\text{F}$ ]-sodiumfluoride (NaF) is a bone-specific PET radiotracer that is used to evaluate bone metastases in PCa patients. [ $^{18}\text{F}$ ]-NaF, similar to  $^{99\text{m}}\text{Tc}$ -labelled diphosphonates, targets increased bone turnover and osteoblastic activity (**Figure 4**). [ $^{18}\text{F}$ ]-NaF PET/CT has demonstrated a better sensitivity than  $^{99\text{m}}\text{Tc}$ -HDP planar scintigraphy and SPECT/CT (Fonager et al. 2017; Wondergem et al. 2018), as well as similar performance to WBMRI + DWI (Jambor et al. 2016). However, despite the higher sensitivity of this radiotracer, its specificity is limited because of its non-specific uptake in degenerative and inflammatory bone diseases (Evangelista et al. 2016). Studies on modest patient cohorts have demonstrated that the performance of [ $^{18}\text{F}$ ]-NaF in the detection of bone metastases is comparable to that of [ $^{68}\text{Ga}$ ]-PSMA (Dyrberg et al. 2019; Zacho et al. 2018). Interestingly, it has been suggested that the uptake of NaF and PSMA might vary according to the state of the disease, and that NaF might overcome PSMA PET in the early stages of hormone-sensitive disease (Harmon et al. 2018). However, further studies are needed to confirm this hypothesis. As [ $^{18}\text{F}$ ]-NaF PET cannot evaluate soft tissues and bone marrow metastases, it is of limited use by itself for staging or restaging PCa patients. However, given the possibility of PSMA-negative bone metastases, [ $^{18}\text{F}$ ]-NaF might have a complementary role to PSMA, particularly in restaging PCa patients prior to RLT initiation (Uprimny et al. 2018).

#### 2.4.3 Choline, acetate and fluciclovine

Choline, a component of the phosphatidylcholines, is an important substrate for the metabolism of phospholipids, which are an integral part of the cell membrane. The

use of choline-targeted radiotracers for imaging PCa is based on the increased phosphorylcholine levels and elevated phosphatidylcholine turnover in PCa cells (Ackerstaff et al, 2003). Choline can be labelled with either  $^{11}\text{C}$  ( $[^{11}\text{C}]$ -choline) or  $^{18}\text{F}$  ( $[^{18}\text{F}]$ -choline). The latter has the advantages of a longer half-life (120 min vs 20 min). Both radiotracers present physiological uptake in the liver, pancreas, spleen, salivary glands and bowel, but  $[^{18}\text{F}]$ -choline has higher bladder activity than its  $[^{11}\text{C}]$ -labelled counterpart. No significant differences between the two tracers have been reported in the setting of primary staging (Nitsch et al. 2016). Before the PSMA-era, choline PET was one of the main ligands used in PCa imaging, to the point that FDA approved it in 2012. Choline PET has demonstrated a pooled sensitivity of 86% and specificity of 93% for the detection of local PCa recurrence and metastases, according to a meta-analysis of a total of 1555 patients (Evangelista et al. 2013). In another meta-analysis, the pooled detection rate was 62%. However, the rates were significantly lower at low PSA values (<1-2 ng/ml) (Fanti et al. 2016). In primary staging, despite choline PET's high specificity, low sensitivity (pooled sensitivity of 49%) for the detection of lymph node metastases has been reported (Evangelista et al. 2013). Moreover, the evaluation of the primary tumour is limited by the presence of uptake in benign prostatic hyperplasia (Souvatzoglou et al. 2011).

$[^{11}\text{C}]$ -acetate was proposed as an alternative PET radiotracer for PCa imaging. Acetate is an important substrate that is involved in different metabolic pathways, including in the tricarboxylic cycle, and in fatty acid, phospholipid and cholesterol synthesis.  $[^{11}\text{C}]$ -acetate is transported across cell membranes and converted to acetyl CoA, and its retention into PCa cells is most likely due to increased fatty acid synthesis (Baron et al. 2004). In this regard, acetate's cell retention mechanism is similar to that of choline, as both are incorporated into the phospholipids of the cancer cell membrane. The physiological biodistribution of  $[^{11}\text{C}]$ -acetate includes uptake in the myocardium, kidneys, pancreas, spleen and bone marrow, with minimal urinary excretion due to the active reabsorption of  $[^{11}\text{C}]$ -acetate in the proximal convoluted tubule (**Figure 4**). One of the first studies on  $[^{11}\text{C}]$ -acetate in PCa demonstrated good uptake in PCa lesions and its higher performance than that of FDG (Oyama et al. 2002). Several successive studies have assessed the performance of  $[^{11}\text{C}]$ -acetate in the evaluation of primary tumour and nodal staging, with promising results (Haseebuddin et al. 2013; Jambor et al. 2012; Mena et al. 2012). However, similar to choline,  $[^{11}\text{C}]$ -acetate cannot reliably distinguish between benign prostatic hyperplasia and PCa (Kato et al. 2002).  $[^{11}\text{C}]$ -acetate has also been evaluated in BCR, and the results are comparable to those of  $[^{11}\text{C}]$ / $[^{18}\text{F}]$ -choline, showing limited performances at low PSA values (< 1-2 ng/ml) (Buchegger et al. 2014; Dusing et al. 2014).

$[^{18}\text{F}]$ -fluciclovine, also known as anti1-amino-3- $[^{18}\text{F}]$ -fluorocyclobutane-1-carboxylic acid (FACBC), is a PET radiotracer approved by the FDA in 2016 for

imaging of PCa recurrence. FACBC is an analogue of leucine, an essential amino acid that is transported inside the cells by amino acid transporters. These transporters are upregulated in many carcinomas, including in PCa (Sakata et al. 2009). The physiological biodistribution of this radiotracer includes high uptake in the pancreas and liver, with moderate uptake in the salivary glands, pituitary gland and bowel. This agent has minimal activity in the excreted urine, which is an advantage in the evaluation of the prostatic area. Due to the rapid influx and efflux of amino acids (and therefore, of [ $^{18}\text{F}$ ]-fluciclovine) in PCa cells, PET images are usually acquired earlier than other radiotracers for PCa, usually 3-5 min after the radiotracer injection. In a prospective comparative study on 50 patients with BCR, [ $^{18}\text{F}$ ]-fluciclovine PET/CT has demonstrated a higher lesion detection rate than [ $^{11}\text{C}$ ]-choline (Nanni et al. 2015). Later, larger prospective multicentre trials have assessed the role of [ $^{18}\text{F}$ ]-fluciclovine PET/CT in BCR (Andriole et al. 2020; Ashesh et al. 2021; Scarsbrook et al. 2020). The results of the Phase III FALCON trial, which included 104 patients with BCR, demonstrated that the detection rate of [ $^{18}\text{F}$ ]-fluciclovine PET/CT increased according to the PSA levels, with a detection rate of 93% in the presence of PSA > 2 ng/ml. Moreover, 64% of the patients had major change in management after scanning (Scarsbrook et al. 2020). Similar results were presented from the LOCATE trial on 213 patients with BCR, where change in management was observed in 59% of the patients (Andriole et al. 2020). The EMPIRE trial was a Phase III randomised trial on 165 patients, that demonstrated improved survival free from BCR with [ $^{18}\text{F}$ ]-flucilovine PET compared to conventional imaging (Ashesh B. et al. 2021). Finally, a recent systematic review of studies on a total of 850 patients showed good performance of [ $^{18}\text{F}$ ]-Fluciclovine PET/CT in patients with recurrent PCa, with detection rates of up to 53% in patients with PSA < 0.5 ng/ml (Rais-Bahrami et al. 2021).

#### 2.4.4 Bombesin

In the evolution of radiotracers for PCa imaging, gradually the use of metabolic agents (that targeted glucose, lipid or amino acid metabolism) shifted towards the development of more specific receptor-targeting radiotracers.

Bombesin is a protein with high affinity to the gastrin-releasing peptide receptors (GRPRs). GRPRs have various physiological functions in the gastrointestinal and nervous system and are overexpressed in several malignancies, including in PCa (Jensen et al. 2008; Mansi et al. 2013).  $^{68}\text{Ga}$  was the first radioisotope used to label bombesin-based ligands for PET imaging. Different [ $^{68}\text{Ga}$ ]-labelled radiotracers have been investigated preclinically and in preliminary clinical studies, such as [ $^{68}\text{Ga}$ ]-RM2 and [ $^{68}\text{Ga}$ ]-SB3 (Kahkonen et al. 2013; Maina et al. 2016; Roivainen et al. 2013). Bombesin-targeted radiotracers have shown main excretion through the

urinary tract, and their highest physiological uptake was documented in the bladder, kidneys and pancreas, followed by the liver, spleen and bowel (**Figure 4**). [<sup>68</sup>Ga]-RM2 PET/CT in a cohort of 14 patients revealed sensitivity of 88% and 70% in detecting primary tumour and lymph node metastases, respectively (Kahkonen et al. 2013). One study also directly compared [<sup>68</sup>Ga]-RM2 and [<sup>68</sup>Ga]-PSMA-11 in seven patients with biochemically recurrent PCa, and showed that the detection of malignant lesions on [<sup>68</sup>Ga]-PSMA-11 did not statistically differ from that on [<sup>68</sup>Ga]-RM2 (Minamimoto et al. 2016). <sup>18</sup>F- and <sup>64</sup>Cu-labelled radiotracers that target GRPR have also been assessed in a few studies (Sah et al. 2015; Wieser et al. 2014).

Although bombesin-based radiotracers have shown promising results, the introduction and wide use of PSMA as a target for PCa imaging limited its clinical use. However, very recently a bombesin-based theranostic radiotracer, <sup>64</sup>Cu-SAR-bombesin, is being investigated as a promising application in patients with PSMA-negative PCa (NCT05407311).

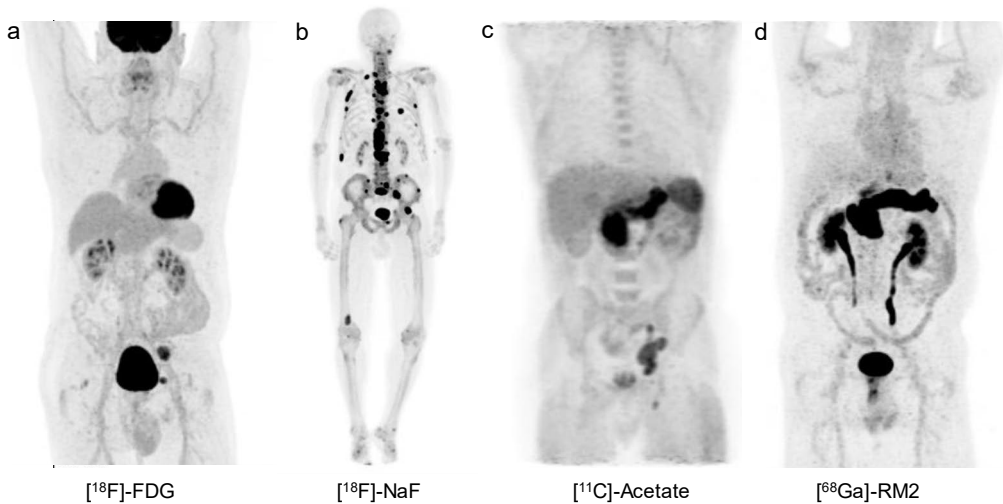


**Figure 4.** Maximum intensity projection (MIP) images of different PET tracers used for PCa imaging. **a)** [<sup>18</sup>F]-FDG image from a representative patient of Study III with pelvic lymph node metastases **b)** [<sup>18</sup>F]-NaF image of a patient with bone metastases **c)** [<sup>11</sup>C]-Acetate image of a patient with pelvic lymph node metastases **d)** [<sup>68</sup>Ga]-RM2 (bombesin) image of a patient with local recurrence on the prostate bed. Image b is courtesy of Jukka Kemppainen, Department of Clinical Physiology and Nuclear Medicine, University of Turku and Turku University Hospital, Turku, Finland. Images c and d are courtesy of Heikki Minn, Department of Oncology, University of Turku and Turku University Hospital, Turku, Finland.



## 2.5 Prostate specific membrane antigen (PSMA) and PSMA PET

### 2.5.1 Prostate specific membrane antigen (PSMA)

PSMA is a type II transmembrane protein discovered in 1983 while investigating metastatic PCa cell lines (LNCaP) (Horoszewicz et al. 1983). PSMA is encoded by the FOLH1 gene located in the short arm of chromosome 11 and its structure consists of three parts: an intracellular domain, also called cytoplasmic tail; a transmembrane domain; and an extracellular domain (Chang 2004) (**Figure 5**). The extracellular domain is the larger component of the protein and contains the target for the small-molecule PSMA inhibitors currently used in PET imaging (**Figure 5**).

PSMA has an internalisation capacity into an endosomal compartment, which makes this protein a particularly interesting target for imaging and therapeutic approaches (Liu et al. 1998). It has enzymatic peptidase activity, acting as a glutamate-carboxypeptidase, and it is also involved in the activation of signalling pathways. However, all the physiological functions of PSMA and its impact on tissues have yet to be clarified (O’Keefe et al. 2018).

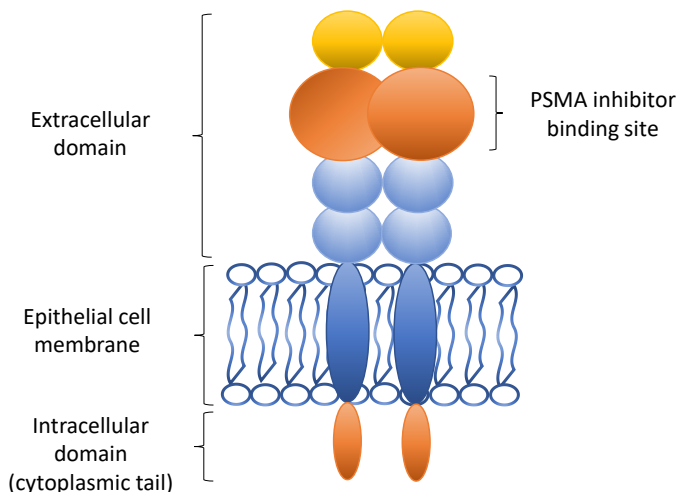


**Figure 5.** Structure of prostate-specific membrane antigen (PSMA). Modified from: Chang, 2004.

PSMA is expressed in the epithelial cells of normal prostate gland, but its expression is up to 10-fold higher in PCa cells and it is correlated with the tumour grade (Ghosh and Heston 2004). Moreover, PSMA expression is correlated with the GS and PSA, and progressively increases in metastatic disease and CRPC (Uprimny et al. 2017). ADT is also known to increase PSMA expression at the cellular level (Wright et al.

1996). Notably, about 10% of PCas do not exhibit PSMA expression in immunohistochemistry or PET images, independently from PSA values (Maurer et al. 2016; Minner et al. 2011; Yaxley et al. 2019).

PSMA is typically expressed in PCa cells in the apical membrane. This is the main mechanism responsible for PSMA uptake in PET imaging and positivity on PSMA immunohistochemistry, although the expression can be heterogeneous (**Figure 6**). However, unlike what its name says, PSMA expression is not prostate-specific but can occur in many other benign or malignant conditions, that should be considered when interpreting PSMA PET images. The expression in non-prostatic tumours is mainly due to the endothelial expression of PSMA. This mechanism is not present in normal endothelial cells, but it is typically associated with tumour neovasculture (De Galiza Barbosa et al. 2020). The potential role of PSMA PET in tumours other than PCa is presented in more detail in Section 2.5.3.6 of this thesis.

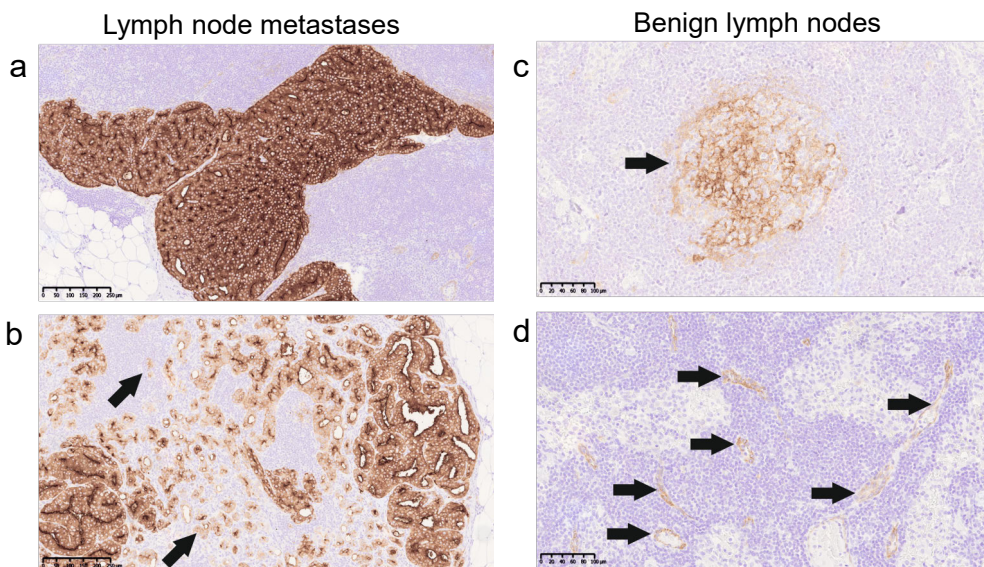


**Figure 6.** Heterogeneity of PSMA expression in lymph node metastases (**a-b**) and benign lymph nodes (**c-d**). **a)** homogeneous expression **b)** heterogeneous expression **c)** weak expression in the lymphoid germinal centres and **d)** weak expression in the endothelial cells of the medullary sinus within the lymph node. Modified from original publication IV.

## 2.5.2 Main PSMA ligands for prostate cancer imaging

### 2.5.2.1 Evolution of the PSMA ligands for imaging

One of the first imaging probes to target PSMA was anti-PSMA antibodies, which were developed for both the intracellular and extracellular domains of PSMA. The

first monoclonal antibody 7E11-CE was developed for the intracellular domain of PSMA. This monoclonal antibody was then labelled with  $^{111}\text{In}$  to develop the first PSMA tracer for SPECT imaging, [ $^{111}\text{In}$ ]-capromab pendetide, also known as ProstaScint®. The first studies demonstrated that [ $^{111}\text{In}$ ]-capromab pendetide could be safely administered, but the detection rates for viable tumour lesions were low (Plut and Hinkle 2000; Wynant et al. 1991). Although FDA approved the use of [ $^{111}\text{In}$ ]-capromab pendetide in 1999 for BRC of PCa, its clinical use was limited.

Subsequently, high-affinity antibodies that target the extracellular domain, one of the most promising of which was J591 labelled with  $^{89}\text{Zr}$ , showed cleared advantages over ligands that target the intracellular domain. However, the translation of  $^{89}\text{Zr}$  J591 into clinical imaging was also limited due to its long circulatory half-life and poor tumour penetrations (Liu et al. 1998; Lütje et al. 2015).

Small-molecule PSMA-inhibiting ligands started to be developed for human imaging because of their faster blood clearance, faster extravasation and therefore, higher tumour-to-background ratios. Small-molecule inhibitors have three main categories: urea-based, phosphorous-based and thiol-based compounds. The urea-based type gained the most interest because of its internalisation into the cell after binding to the active domain of PSMA. The first class of urea-based PSMA inhibitors was described in 2001 (Kozikowski et al. 2001), and the first preclinical imaging studies that used  $^{11}\text{C}$ -labelled PSMA ligands in a PSMA-positive tumour xenograft were reported a few years later (Foss et al. 2005; Pomper et al. 2002;). Other early tracers that use small-molecule PSMA inhibitors for imaging of PCa were [ $^{123}\text{I}$ ]-MIP-1072 and [ $^{123}\text{I}$ ]-MIP-1095 for SPECT imaging (Maresca et al. 2009). These agents demonstrated in clinical studies the ability to rapidly detect PCa lesions in soft tissues, bone, and prostate bed as early as 1 h after injection (Barrett et al. 2013). The first use of radioiodinated PSMA ligands on humans made the conceptual leap to radioligand therapy a short one, as the initial therapeutic studies were conducted with [ $^{131}\text{I}$ ]-MIP-1095 (Zechmann et al. 2014).

The significance of the first preclinical and clinical studies on PSMA-ligands lead to a period where PSMA ligands were explored, developed, and refined for application in imaging and therapy. In the next subchapters, the main and current PSMA ligands for PCa imaging are presented.

### 2.5.2.2 $^{68}\text{Ga}$ -labelled ligands

The largest amount of published data available on PSMA PET imaging is from studies conducted using [ $^{68}\text{Ga}$ ]-PSMA-HBED-CC, also known as [ $^{68}\text{Ga}$ ]-PSMA-11. This now well-established ligand was developed in Heidelberg, Germany, in 2011 and presented strong binding affinity to PSMA as well as highly efficient internalisation into PCa cells (Eder et al. 2012). The use of [ $^{68}\text{Ga}$ ]-PSMA-11 spread

worldwide during the past decade and contributed to the clinical breakthrough of PET imaging with PSMA. [<sup>68</sup>Ga]-PSMA-11 is also the first PSMA PET radiotracer to have received FDA approval in 2020 (**Table 5**). The first clinical study on [<sup>68</sup>Ga]-PSMA-11 demonstrated excellent tumour-to-background ratios and high detection rates in 37 patients with BCR (Afshar-Oromieh et al. 2013). Subsequently, sensitivity and specificity of [<sup>68</sup>Ga]-PSMA-11 PET imaging were evaluated in a large systematic review and meta-analysis (Perera et al. 2016). In a per-lesion analysis, the specificity and sensitivity were 97 % and 80 %, respectively. In a per-patient analysis, the specificity and sensitivity were both 86 %. Moreover, [<sup>68</sup>Ga]-PSMA-11 has demonstrated high sensitivity and high detection rates (70-85%) in BCR with a strong correlation to PSA values (Afshar-Oromieh et al. 2017; Cerci et al. 2022; Eiber et al. 2015; Fendler et al. 2019 ). A recent prospective randomised trial, the proPSMA study, demonstrated the superiority of [<sup>68</sup>Ga]-PSMA-11 in the primary staging of PCa compared to conventional imaging (Hofman et al. 2020).

As the PSMA-11 ligand cannot bind clinically relevant therapeutic radiometals, theranostic variants started to be developed and were radiolabelled with the therapeutically relevant trivalent radiometals, <sup>177</sup>Lu for beta therapy and <sup>225</sup>Ac for alpha therapy. Modifications of PSMA-11 resulted in the development of PSMA-617, a small-molecule theranostic agent that was firstly investigated preclinically in 2015 and showed high binding affinity to PSMA and highly efficient internalisation into PCa cells (Benešová et al. 2015). [<sup>68</sup>Ga]-PSMA-617 has demonstrated detection of PCa lesions with high contrast especially at later time points (2-3 hours post injection), with a biodistribution and radiation exposure comparable to those of [<sup>68</sup>Ga]-PSMA-11 (0,021 mSv/MBq) (Afshar-Oromieh et al. 2015). The PSMA-617 ligand was successfully used in in therapeutic application with the spread of [<sup>177</sup>Lu]-PSMA-617, which demonstrated prolonged PFS and OS in metastatic CRPC (Hofman et al. 2018; Sartor et al. 2021). The FDA approved [<sup>177</sup>Lu]-PSMA-617 very recently in March 2022.

In 2015, another theranostic small-molecule PSMA inhibitor for imaging and therapy, PSMA-I&T, was introduced (Weineisen et al. 2015) and had promising results for diagnostic application with <sup>68</sup>Ga and for therapeutic application with <sup>177</sup>Lu. Few studies have investigated the performance of [<sup>68</sup>Ga]-PSMA-I&T in BCR and primary staging, showing high detection rates that were comparable to those of [<sup>68</sup>Ga]-PSMA-11 (Berliner et al. 2017; Cytawa et al. 2020). However, the clinical use of this tracer is still limited.

<sup>68</sup>Ga-labelled PSMA tracers have a relatively straightforward radioisotope production, by a germanium-gallium generator, without the need for an on-site cyclotron. Strong physiological uptake is usually seen in the salivary glands, kidneys, small intestine and moderate uptake is observed in the liver and spleen (**Figure 7**). <sup>68</sup>Ga-labelled tracers are mainly excreted through the urinary tract, which represents a limitation in the evaluation of the prostatic area due to uptake in the

bladder. This limitation might be overcome with delayed imaging after forced diuresis, although this is usually not routinely performed. Physiological uptake of both [ $^{68}\text{Ga}$ ]-labelled and [ $^{18}\text{F}$ ]-labelled PSMA tracers generally occurs in the nervous ganglia, which should not be confused with active lymph nodes. The most common locations of the active nervous ganglia are the stellate ganglia in the upper thorax, the coeliac ganglia in the abdomen, and the presacral ganglia in the pelvis.

### 2.5.2.3 $^{18}\text{F}$ -labelled ligands

Compared to  $^{68}\text{Ga}$ ,  $^{18}\text{F}$  has some significant advantages, such as (1) a larger production capacity, since high activities can be produced with on-site cyclotrons; (2) a longer radiochemical half-life (110 min vs. 68 min), which allows the transport of the radiotracers to more distant centers; (3) a higher positron yield and a shorter positron range, which results in improved spatial and/or contrast resolution. With the increasing clinical demand for PSMA PET imaging, different  $^{18}\text{F}$ -labelled radiotracers have been developed and are currently available (Rowe et al. 2017; Werner et al. 2020). The first  $^{18}\text{F}$ -labelled radiotracer, [ $^{18}\text{F}$ ]-DCFBC, started to be developed approximately at about the same time as [ $^{68}\text{Ga}$ ]-labelled tracers (Mease et al. 2008). [ $^{18}\text{F}$ ]-DCFBC has demonstrated a promising ability to detect metastatic PCa (Cho et al. 2012; Robu et al. 2018), and discrete performance on primary tumour (Rowe et al. 2015). However, its major disadvantages are its slow clearance and high blood-pool radioactivity, which have limited its clinical use.

One of the most successful second-generation radiofluorinated PSMA PET agents and the first to have received FDA approval is 2-(3-(1-carboxy-5-((6- $^{18}\text{F}$ )fluoropyridine-3-carbonyl)-amino)-pentyl)-ureido)-pentanedioic acid, known as [ $^{18}\text{F}$ ]-DCFPyL (Szabo et al. 2015) (**Table 5**). [ $^{18}\text{F}$ ]-DCFPyL is mainly excreted via the urinary tract and, similarly to [ $^{68}\text{Ga}$ ]-PSMA-11, high physiological uptake is observed in the kidneys, salivary glands and duodenum, whereas moderate uptake is observed in the spleen and liver. Two large prospective Phase 2 and 3 trials have demonstrated good diagnostic accuracy of [ $^{18}\text{F}$ ]-DCFPyL PET/CT both in BCR and primary staging (Morris et al. 2021; Pienta et al. 2021). The OSPREY trial included a total of 345 patients divided into two cohorts: Cohort A with newly diagnosed PCa scheduled for prostatectomy and lymph node dissection, and Cohort B with patients with suspected recurrent or metastatic disease. [ $^{18}\text{F}$ ]-DCFPyL PET/CT demonstrated high specificity in primary staging and BCR (96% in Cohort A and 98% in Cohort B), despite low sensitivity values in nodal staging (40%) (Pienta et al. 2021). The CONDOR trial investigated the performance of [ $^{18}\text{F}$ ]-DCFPyL in 208 men with biochemically recurrent PCa and its primary end point was the correct localisation rate (CLR), defined as the positive predictive value with an additional requirement of anatomic lesion colocalisation between [ $^{18}\text{F}$ ]-DCFPyL PET/CT and a composite standard of truth

(SOT). The CLR was 84.8-87% among three readers, and 64% of the patients had a change in intended management after [ $^{18}\text{F}$ ]-DCFPyL PET/CT (Morris et al. 2021).

[ $^{18}\text{F}$ ]-PSMA-1007 was developed as a next generation PSMA-targeted imaging agent (Cardinale et al. 2017) that has recently gained increasing interest, particularly in Europe. [ $^{18}\text{F}$ ]-PSMA-1007's biodistribution differs from that of other PSMA ligands because of its predominant hepatobiliary excretion and the minimal urinary excretion, which are significant advantages in the evaluation of the prostate region. Therefore, [ $^{18}\text{F}$ ]-PSMA-1007 has high physiological uptake in the gallbladder and liver, followed by the pancreas and salivary glands, but low uptake in the kidneys and bladder (**Figure 7**). In preclinical evaluations, [ $^{18}\text{F}$ ]-PSMA-1007 has demonstrated favourable binding and internalisation properties in vitro and high and specific tumour uptake in vivo (Cardinale et al. 2017). In clinical studies carried out until recently, [ $^{18}\text{F}$ ]-PSMA-1007 has demonstrated diagnostic performances comparable to that of other PSMA-targeted imaging agents. In particular, [ $^{18}\text{F}$ ]-PSMA-1007 has demonstrated high detection rates in patients with biochemically recurrent PCa (Ferrari and Treglia 2021; Giesel et al. 2019; Sprute et al. 2020). Promising results in primary staging have also been reported in recent retrospective studies (Sprute et al. 2021; Ingvar et al. 2022). Currently, the tracer has entered multicentre Phase III clinical trials (e.g., NCT04742361).

However, compared to other  $^{18}\text{F}$ -labelled tracers, [ $^{18}\text{F}$ ]-PSMA-1007 has a higher incidence of non-specific uptakes in the bone, which might increase the risk of false positive interpretations (Anttinen et al. 2020; Hagens et al. 2022; Rauscher et al. 2020; Wondergem et al. 2021). The mechanisms related to its non-specific uptakes in the bone remains still unclear. The most plausible explanation is that [ $^{18}\text{F}$ ]-PSMA-1007 has higher affinity to PSMA receptors, which might result in higher uptake in benign bone lesions (Cardinale et al. 2017). These uptakes are unlikely to be explained by the presence of free  $^{18}\text{F}$ -fluorine due to radiolysis, given that quality control reports have shown a concentration of free  $^{18}\text{F}$ -fluorine  $< 2\%$  after synthesis of [ $^{18}\text{F}$ ]-PSMA-1007 (Wondergem et al. 2021). From a matched-pair comparison of [ $^{68}\text{Ga}$ ]-PSMA-11 with [ $^{18}\text{F}$ ]-PSMA-1007, it has been hypothesised that the higher incidence of non-specific bone uptakes might be related to the lower positron energy, longer half-life and higher injected activities of  $^{18}\text{F}$ -labelled tracers compared to  $^{68}\text{Ga}$ -labelled ones (Rauscher et al. 2020). However, this does not explain the difference in the incidence of such uptakes within different  $^{18}\text{F}$ -labelled tracers (Hagens et al. 2022; Wondergem et al. 2021).

Radiohybrid (rh)PSMA ligands constitute a new class of theranostic PSMA ligands, which can be efficiently labelled with  $^{18}\text{F}$  and with radiometals and, therefore, used for both diagnostic and therapeutic applications (Wurzer et al. 2020). Promising imaging data have been reported for [ $^{18}\text{F}$ ]-rhPSMA-7, which comprises four diastereoisomers (Oh et al. 2020). In retrospective studies, [ $^{18}\text{F}$ ]-rh-PSMA 7 has demonstrated a sensitivity of 72.2% and a specificity of 92.5% in N-staging and high

detection rates in patients with BCR (Eiber et al. 2020) (Kroenke et al. 2020) (Rauscher et al. 2021). [ $^{18}\text{F}$ ]-rh-PSMA-7 has demonstrated similar performances to [ $^{68}\text{Ga}$ ]-PSMA-11, despite an apparent higher incidence of nonspecific uptakes, including in the ganglia, bone and unspecific lymph nodes (Kroenke et al. 2020). One of the rhPSMA isomers, [ $^{18}\text{F}$ ]-rhPSMA-7.3, was selected as the lead rhPSMA compound for clinical development based on preclinical assessments (Wurzer et al. 2020). To date, the safety and radiation dosimetry of [ $^{18}\text{F}$ ]-rhPSMA-7.3 have been established in healthy volunteers (Tolvanen et al. 2021). Currently, [ $^{18}\text{F}$ ]-rh-PSMA 7.3 is under investigation in 2 multicentre Phase III trials for PET imaging, SPOTLIGHT (NCT04186845) and LIGHTHOUSE (NCT04186819). The preliminary results of the SPOTLIGHT trial on 366 men with BCR have demonstrated that [ $^{18}\text{F}$ ]-rh-PSMA 7.3 PET findings frequently resulted in post-scan upstaging of patients with negative baseline conventional imaging (European Association of Nuclear Medicine (EANM)22 Abstract Book, 2022).

Finally, [ $^{18}\text{F}$ ]-PSMA-11 is a radiotracer that has very recently attracted interest, as it consists of the same molecule as [ $^{68}\text{Ga}$ ]-PSMA-11 but with the advantages of [ $^{18}\text{F}$ ]-labelling. A recent prospective double-blind randomised trial on 85 patients with primary or recurrent PCa compared the two mentioned tracers and demonstrated that [ $^{18}\text{F}$ ]-PSMA-11 is not inferior to [ $^{68}\text{Ga}$ ]-PSMA-11 and could be used as a valid alternative (De Man et al. 2022).

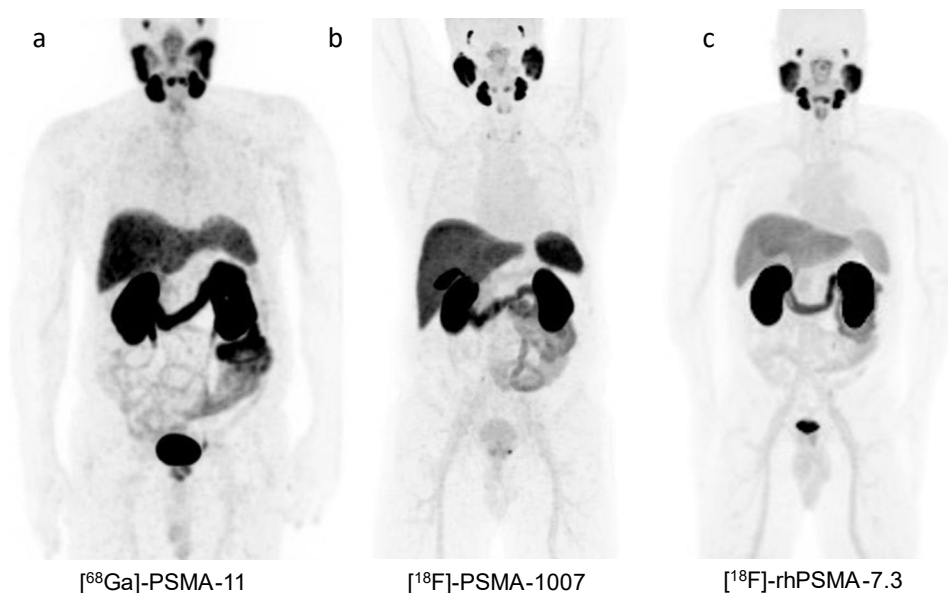


**Figure 7.** Maximum intensity projection (MIP) images of the three PSMA-ligands used in the studies in this doctoral thesis. **a)** [ $^{68}\text{Ga}$ ]-PSMA-11 from a representative patient of Study II **b)** [ $^{18}\text{F}$ ]-PSMA-1007 from a representative patient of Study IV **c)** [ $^{18}\text{F}$ ]-rhPSMA-7.3 from a representative patient of Study I.

#### 2.5.2.4 $^{99m}\text{Tc}$ -labelled ligands

The widespread use of  $^{99m}\text{Tc}$  in diagnostic nuclear medicine, together with the broad availability of SPECT scanners in nearly all hospitals, has made the development of  $^{99m}\text{Tc}$ -labelled PSMA tracers particularly appealing. MIP-1404 and MIP-1405 were the first high-affinity small-molecule PSMA inhibitors for SPECT imaging to be introduced into the clinical setting (Hillier et al. 2013). Between them, MIP-1404 was later chosen as the lead compound due its lower urinary excretion. In retrospective and prospective studies, [ $^{99m}\text{Tc}$ ]-MIP-1404 demonstrated high potential to detect PCa lesions, with superior performance compared to conventional imaging (Goffin et al. 2017; Schmidkonz et al. 2018). In primary nodal staging, Goffin et al. reported a sensitivity of 50% and specificity of 87% compared to histology (Goffin et al. 2017). Another study on 225 patients with BCR reported a detection rate of 90% at PSA values  $\geq 2$  ng/ml and 54% at PSA  $< 2$  ng/ml (Schmidkonz et al. 2018).

Along with [ $^{99m}\text{Tc}$ ]-MIP-1404, several other [ $^{99m}\text{Tc}$ ]-PSMA compounds are under investigation, such as PSMA-I&T and HYNIC-PSMA. [ $^{99m}\text{Tc}$ ]-PSMA-I&T has been investigated on 210 patients with recurrent PCa. At low PSA levels ( $< 4$  ng/ml), its detection rates were clearly inferior to those reported for PSMA PET-imaging. On the other hand, at higher PSA values ( $> 4$  ng/ml), its detection rates were high (83%) (P. Werner et al. 2020). In addition to diagnostic imaging,  $^{99m}\text{Tc}$ -labelled PSMA ligands might have interesting applications in radioguided surgery. Few studies have shown that this technique of identifying metastatic lesions in recurrent PCa intraoperatively using a gamma probe seems feasible and might successfully detect metastases in patients scheduled for salvage surgery (Maurer et al. 2019). However, the impact of radioguided surgery on patient outcomes needs to be evaluated.

#### 2.5.2.5 $^{64}\text{Cu}$ -labelled ligands

$^{64}\text{Cu}$ -labelled PSMA ligands for PET imaging have attracted interest in the imaging of PCa. PET imaging using  $^{64}\text{Cu}$  is promising and potentially preferable to  $^{68}\text{Ga}$  because of its longer half-life (12.7 h), economic production by cyclotron and higher imaging resolution due to its lower energy at emission (Obata et al. 2003). PSMA-617 and PSMA-I&T labelled with  $^{64}\text{Cu}$  have both been investigated in relatively small prospective studies. [ $^{64}\text{Cu}$ ]-PSMA-617 showed high diagnostic accuracy in primary nodal staging in 23 PCa patients (Cantiello et al. 2017). The same authors compared [ $^{64}\text{Cu}$ ]-PSMA-617 to [ $^{18}\text{F}$ ]-choline in 43 patients in restaging after BCR, and demonstrated higher performance of [ $^{64}\text{Cu}$ ]-PSMA, especially at low PSA values (Cantiello et al. 2018). [ $^{64}\text{Cu}$ ]-PSMA-I&T was very recently investigated to establish its feasibility and biodistribution, and it showed promising characteristics



as a candidate for future clinical trials (Lee et al. 2022). Larger studies that will assess the performance of  $^{64}\text{Cu}$ -labelled PSMA tracers and comparative studies with  $^{68}\text{Ga}$ - or  $^{18}\text{F}$ -labelled PSMA tracers are needed to confirm their potential role in clinical practice.

**Table 5.** Main small-molecule PSMA ligand used for PCa imaging and their current status in clinical trials.

Radioisotope	Imaging agent	Status in prospective clinical trials
$^{68}\text{Ga}$	$^{68}\text{Ga}$ -PSMA-11	FDA approved
	$^{68}\text{Ga}$ -PSMA-617	Early phase
	$^{68}\text{Ga}$ -PSMA-I&T	Early phase
$^{18}\text{F}$	$^{18}\text{F}$ -DCFBC	Early phase
	$^{18}\text{F}$ -DCFpyL	FDA approved
	$^{18}\text{F}$ -PSMA-1007	Undergoing Phase III
	$^{18}\text{F}$ -rhPSMA-7/7.3	Completed Phase III
	$^{18}\text{F}$ -PSMA-11	Early phase
$^{99\text{m}}\text{Tc}$	$^{99\text{m}}\text{Tc}$ -MIP-1404	Completed Phase III
	$^{99\text{m}}\text{Tc}$ -PSMA-I&T	Early phase
	$^{99\text{m}}\text{Tc}$ -HYNIC-PSMA	Early phase
$^{64}\text{Cu}$	$^{64}\text{Cu}$ -PSMA-617	Early phase
	$^{64}\text{Cu}$ -PSMA-I&T	Early phase

### 2.5.3 PSMA PET imaging

#### 2.5.3.1 PSMA PET in biochemical recurrence

Between 30% and 50% of the patients treated with RP or RT with curative intent will develop a rising PSA, the so-called biochemical recurrence (BCR) (Mottet et al. 2022). The definition of clinically relevant PSA relapse depends on the primary treatment: after RP the threshold used is  $> 0,2$  ng/ml; after RT, BCR is defined as any PSA increase  $> 2$  ng/ml higher than the PSA nadir, which is defined as the lowest PSA value prior to failure.

The role of PSMA PET/CT in patients with BCR is currently well established and its use is recommended in the current EAU guidelines when the PSA level is  $> 0,2$  ng/ml after RP and if the results will influence subsequent treatment decisions or when the PSA level rises after RT and the patient is fit for curative salvage treatment. A systematic review and meta-analysis that involved 1309 patients demonstrated that the positivity of  $^{68}\text{Ga}$ -PSMA PET/CT is correlated to the PSA level; that is, for PSA categories 0–0.2, 0.2–1, 1–2, and  $> 2$  ng/ml of 42%, 58%,

76%, and 95%, respectively (Perera et al. 2016). In particular, [ $^{68}\text{Ga}$ ]- and [ $^{18}\text{F}$ ]-PSMA PET/CT have been demonstrated to be superior to other PET tracers, such as Choline or Fluciclovine, as the sensitivity of PSMA PET/CT was significantly higher at low PSA values ( $< 1$  ng/ml) (Afshar-Oromieh et al. 2014; Morigi et al. 2015; Wang et al. 2021). Subsequently, several large prospective studies have evaluated the performance of  $^{68}\text{Ga}$ - and  $^{18}\text{F}$ -labelled PSMA in patients with BCR, and demonstrated high detection rates of local and metastatic diseases (Caroli et al. 2018; Ceci et al. 2019; Fendler et al. 2019; Morris et al. 2021; Pienta et al. 2021).

Studies have also demonstrated that PSMA PET/CT can guide salvage RT in patients with BCR. PSMA-based RT has shown significant PSA responses that might lead to a deferral of long-term ADT or other systemic therapies (Habl et al. 2017; Schmidt-Hegemann et al. 2018). A negative PSMA PET in patients with rising PSA after radical prostatectomy has demonstrated to be predictive of high response to SRT to the prostatic fossa (Emmett et al. 2017). This knowledge can have important implications for the clinical management of patients with BCR. Moreover, in a recent multicentre prospective study PSMA PET/CT results in men who were undergoing salvage RT for BCR after RP were highly predictive of freedom from progression at 3 years (Emmett et al. 2020).

### 2.5.3.2 PSMA PET in primary staging

PSMA PET/CT has only recently gained a place in the EAU guidelines for the diagnosis of prostate cancer. The latest summary of evidence from March 2022 stated that PSMA PET/CT is more sensitive and accurate than CT and BS for the primary staging of patients with high-risk PCa. However, there is still no outcome data that could inform subsequent management. The performance of PSMA PET/CT in the primary staging of patients with high-risk PCa was assessed in recent years in prospective studies on both N-staging and M-staging. Most of these studies were performed using  $^{68}\text{Ga}$ -labelled tracers, although there are also valid data from prospective studies with  $^{18}\text{F}$ -labelled ligands.

Regarding primary nodal staging, prospective multicentre trials performed with [ $^{68}\text{Ga}$ ]-PSMA-11 and [ $^{18}\text{F}$ ]-DCFPyl have reported high specificity (90-94%) but moderate sensitivity (40-41%) (Jansen et al. 2020; van Kalmthout et al. 2020; Pienta et al. 2021). A recent prospective multicentre Phase III trial assessed the performance of [ $^{68}\text{Ga}$ ]-PSMA-11 in primary nodal staging and its results are consistent with those of previous studies. In 277 patients whose histology confirmation was available, the sensitivity and specificity of PSMA PET/CT were 40% and 95%, respectively (Hope et al. 2021). Retrospective studies on quite large cohorts of patients have evaluated the performance of [ $^{18}\text{F}$ ]-PSMA-1007 and [ $^{18}\text{F}$ ]-rhPSMA-7.3 in primary N-staging, and presented variable sensitivity (from 30% to 80%), while maintaining high

specificity (> 95%) (Ingvar et al. 2022; Langbein et al. 2022; Sprute et al. 2021). Very limited sensitivity of PSMA PET/CT was found for lymph nodes < 3 mm (Ingvar et al. 2022). A systematic review and meta-analysis of studies including a total of 1597 patients compared the performance of PSMA PET/CT and MRI in the detection of lymph node metastases, and it was observed that [<sup>68</sup>Ga]-PSMA had higher sensitivity but comparable specificity to MRI in the nodal staging of intermediate- and high-risk PCa. Its reported pooled sensitivity was 65% compared to 41% of MRI. (Wu et al. 2020).

Regarding primary staging, including the detection of distant metastases, available data suggest that PSMA PET/CT is superior to conventional imaging (CT and BS). A systematic review reported variable sensitivity (median sensitivity range in the per-lesion analysis 33–92%, and in the per-patient analysis 66–91%), whereas the specificity was high (>90%) (Corfield et al. 2018).

A prospective multicentre randomized clinical trial (proPSMA) published in 2020 has provided important evidence on the role of PSMA PET/CT in the primary staging of patients with high-risk PCa (Hofman et al. 2020). The proPSMA trial included 302 patients who, before curative-intent surgery or RT, were randomly assigned to conventional imaging with CT and BS or [<sup>68</sup>Ga]-PSMA-11 PET/CT. The primary end point was the accuracy in the detection of regional lymph nodes or distant metastases, which was 92% for [<sup>68</sup>Ga]-PSMA-11 PET/CT and 65% for conventional imaging. Moreover, [<sup>68</sup>Ga]-PSMA-11 PET/CT demonstrated higher sensitivity and specificity than conventional imaging (85% vs 38% and 98% vs 91%, respectively) as well as more frequent changes in management (28% of the patients vs 15%). It was also noteworthy that [<sup>68</sup>Ga]-PSMA-11 PET/CT had less radiation exposure than conventional imaging (8.4 mSv vs 19.2 mSv). Data from the proPSMA trial demonstrated also that PSMA PET/CT, by providing a more accurate diagnosis, which leads to a more appropriate treatment, is more cost-effective than conventional imaging in the primary staging of patients with high-risk PCa (de Feria Cardet et al. 2021). Similar results regarding the cost-effectiveness of PSMA PET/CT have been shown in a few recent studies (Song et al. 2022; van der Sar et al. 2022).

The results of the proPSMA trial could possibly move forward the replacement of conventional imaging (abdominopelvic CT + BS) with PSMA PET/CT for the primary staging of patients with high-risk PCa. However, the outcome and survival benefit of patients with metastatic disease detected using more sensitive imaging modalities are still unknown (Cornford et al. 2020; Hicks et al. 2017).

### 2.5.3.3 PSMA PET in therapy response assessment

PSMA PET/CT is a potentially a useful tool for assessing response to therapy, particularly in patients with metastatic disease before and after systemic therapies or

PSMA-targeted RLT. However, there is still little evidence of the prognostic value of PSMA PET/CT in this setting (Grubmüller et al. 2020; Seitz et al. 2018). Moreover, while the role of PSMA PET/CT in the detection of recurrent disease is well established and its role in primary staging of selected patients was recently affirmed, the possible criteria to be used for therapy response assessment are still under debate. In a recent consensus statement it was agreed that PSMA PET/CT should be used to assess response to therapy only if the results would change the clinical management (Fanti et al. 2021). Given that PSMA PET/CT is the most sensitive imaging method for detecting metastases and, therefore, will most likely change the management of M+ patients, PSMA PET/CT could be used before and after any local or systemic treatment in patients with regional or distant metastases. Nevertheless, the prognosis of patients with metastases detected only by PSMA PET remains unclear. Regarding the timing for performing PSMA PET/CT, there are concerns regarding treatment-naïve patients starting ADT because of the possible increase of PSMA uptake. The relationship between short-term ADT and PSMA expression is the core topic of Studies II and III of this doctoral thesis and will be presented in detail in the Discussion sections. Nonetheless, for the sole purpose of assessing the response to ADT and avoiding the potential flare of PSMA uptake, performing PSMA PET/CT not earlier than three months after initiation of the treatment is recommended (Fanti et al. 2021).

In radiological examinations the Response Evaluation Criteria in Solid Tumours (RECIST) criteria is a well-established method for assessing response to therapy (Eisenhauer et al. 2009). Equivalent criteria for PET imaging, the PET Response Criteria in Solid Tumours (PERCIST), have been presented for several solid tumours imaged with FDG PET (Pinker et al. 2017). However, standardised criteria for treatment response assessment with PSMA PET/CT have not been developed yet, although a combination of molecular, morphological and locational criteria has been proposed (Eiber et al. 2018; Fanti et al. 2020; Gupta et al. 2020). The consensus statements of Fanti et al. suggested that the disappearance of any lesion with PET uptake would define a complete response, a  $> 30\%$  reduction in the uptake or tumour PET volume would define a partial response, and a  $> 30\%$  the increase in the uptake or tumour PET volume or the appearance of  $\geq 2$  new lesions would define progression (Fanti et al. 2021). In polymetastatic disease, the appearance of two or more new lesions alone does not indicate progressive disease if the total tumour PET volume or uptake does not increase by  $> 30\%$ , because in mCRPC a heterogeneous response could occur.

The SUV is the most commonly used semi-quantitative parameter for measuring the tracer uptake. However, SUV values (SUV<sub>max</sub>, SUV<sub>mean</sub> and SUV<sub>peak</sub>) are dependent on the type of scanner, reconstruction algorithm, injected activity and uptake time. Volumetric PET measurements based on available software packages

have better reproducibility and could accurately assess the tumour burden. However, volumetric measurements are technically demanding and are still not widely used in clinical practice. Moreover, to guarantee a correct assessment of the tumour volume further harmonisation and standardisation of the interpretation of the PSMA PET findings is recommended. This topic is presented more in more detail in Subsection 2.5.3.5. Very recently, a standardised framework for response evaluation criteria in PSMA PET/CT (RECIP 1.0) has been proposed for men with mCRPC who have been treated with [<sup>177</sup>Lu]-PSMA (Gafita et al. 2022). This multicentre retrospective study on 124 patients assessed the prognostic value of RECIP 1.0 for OS. The framework is based on the PSMA tumour volume and includes the following classifications: a complete response (RECIP-CR), the absence of any PSMA ligand uptake in the interim PET/CT; a partial response (RECIP-PR), a  $\geq 30\%$  decline in the tumour volume and no appearance of new lesions; progressive disease (RECIP-PD),  $\geq 20\%$  increase in the tumour volume and appearance of new lesions; and a stable disease (RECIP-SD): any condition other than RECIP-PR or RECIP-PD. The results showed that patients with progressive disease had a shorter OS than patients with stable disease or partial response (8 months vs 13 months and 21 months, respectively) and that the combination of RECIP and PSA response was a prognostic biomarker of the efficacy of [<sup>177</sup>Lu]-PSMA therapy (Gafita et al. 2022).

#### 2.5.3.4 PSMA theranostics

The term theranostic was firstly used by John Funkhouser in 2002 to indicate, as the name suggests, a combination of therapy and diagnostics (Funkhouser, 2002). With the increasing use of RLT for neuroendocrine tumours and, more recently, for PCa, theranostics are currently driving the growth and future of nuclear medicine, as they bring a great opportunity to improve patient care through personalised medicine. PSMA-targeting agents are perfect examples of theranostics, as they offer the possibility of diagnostic and therapeutic applications. The internalisation of the PSMA substrate after binding to its receptor allows enhanced uptake and retention in the tumour, which results in high image quality and a high local dose for treatment. In this context, PSMA PET has a crucial role in establishing the patient's eligibility for PSMA-targeted RLT and baseline PSMA PET can also provide important prognostic and predictive information (Buteau et al. 2022; Ferdinandus et al. 2020; Violet et al. 2020).

Among different medical isotopes, <sup>177</sup>Lu is the most commonly used for RLT. <sup>177</sup>Lu is a radioisotope that emits beta radiation to induce DNA damage in cancer cells. RLT with [<sup>177</sup>Lu]-PSMA was recently approved for the treatment of metastatic CRPC patients, who are ineligible for approved alternative treatment options and have adequate PSMA uptake on pre-therapy PET imaging. The efficacy of [<sup>177</sup>Lu]-

PSMA treatment was assessed in a single-centre phase II trial (Lu-PSMA) first in 2018 (Hofman et al. 2018). The Lu-PSMA trial included 30 patients with CRPC that progressed after standard treatment and the primary end point was to assess the PSA response defined as a greater than 50% PSA decline from the baseline. In this study, PSMA and FDG PET/CT were performed to confirm high PSMA expression and to exclude the presence of FDG-positive disease. The patients received four cycles of [ $^{177}\text{Lu}$ ]-PSMA-617 at six weeks intervals. The results showed high response rates (57% of the patients had a PSA response), and the treatment was well tolerated and resulted in improvement of pain symptoms (Hofman et al. 2018).

Three years later, a multicentre randomised Phase II trial (TheraP) compared the performance of [ $^{177}\text{Lu}$ ]-PSMA and cabazitaxel in 200 patients with mCRPC (Hofman et al. 2021). Similar methods (confirmation of a PSMA-positive disease with PSMA and FDG PET/CT and [ $^{177}\text{Lu}$ ]-PSMA-617 treatment every six weeks) and a similar primary end point (at least 50% PSA reduction from the baseline) were used. The group that was treated with  $^{177}\text{Lu}$ -PSMA-617 showed higher PSA responses than the cabazitaxel group (66% of the patients vs 44%) and fewer adverse events (33% vs 53%). The authors concluded that  $^{177}\text{Lu}$ -PSMA-617 could be a potential alternative to cabazitaxel in men with mCRPC, with greater activity but less severe side-effects and improvements in patient-reported outcomes.

Recently, the results of the Vision trial, a milestone in PSMA theranostics, were published. Vision was a Phase III multicentre randomised trial that compared  $^{177}\text{Lu}$ -PSMA-617 treatment plus standard of care (excluding chemotherapy) with standard of care alone in 831 mCRPC patients (Sartor et al. 2021). The Vision trial showed that combined treatment with [ $^{177}\text{Lu}$ ]-PSMA and standard of care prolonged imaging-based PFS (median: 8.7 months vs 3.4 months) and OS (median: 15.3 vs 11.3 months). Based on these results, the FDA approved [ $^{177}\text{Lu}$ ]-PSMA in March 2022.

Despite the promising results of [ $^{177}\text{Lu}$ ]-labelled PSMA RLT, beta-emitters radioisotopes have a relatively low linear energy transfer (LET) (maximum of 0.5 MeV) and a relatively wide soft tissue range of 1.7 mm (Hosono et al. 2018). A low LET might cause easy-to-repair single-stranded DNA breaks, which can lead to treatment failure or resistance. Valid alternatives for PSMA-targeted RLT are alpha-emitters, such as [ $^{225}\text{Ac}$ ]-PSMA-617. Alpha particles have a higher LET and a significantly shorter soft tissue range (< 100  $\mu\text{m}$ ) than beta particles, which increase the cytotoxicity by causing double-strand DNA breaks (Juzeniene et al. 2021). Data on the use of [ $^{225}\text{Ac}$ ]-PSMA RLT on PCa patients are still limited, and prospective randomised trials are being awaited. Nevertheless, recent systematic reviews and meta-analyses showed that [ $^{225}\text{Ac}$ ]-PSMA-617 is an effective and safe treatment for mCRPC patients, with 63-66% of the patients achieving PSA response (> 50% PSA

decline) and a pooled PFS and OS of 9 and 13 months, respectively (Ma et al. 2022; Satapathy et al. 2021).

### 2.5.3.5 PSMA PET structured reporting

With the wide use of PSMA PET in clinical practice and the development of different PSMA radiotracers with distinct characteristics and biodistributions, the need for a standardised imaging interpretation and structured report has been addressed. As a general statement, every PET report should provide clear, accurate and consistent content to support the clinicians in therapeutic decision-making. The traditional narrative report is still the main form of report used by most nuclear medicine physicians and radiologists. However, the variability in language, length and style can limit the assessment of the diagnostic performance of the imaging modality and hamper the comparison with other modalities. Although it is important for diagnostic imaging specialists to learn how to report imaging studies and to have the freedom to describe the findings according to their expertise, the presence of consistent templates for organising the data might improve clarity and guarantee a standardised and reproducible interpretation of the findings (Dhakshinamoorthy et al. 2018). Moreover, in the era of artificial intelligence (AI), consistent, precise and easy-to-extract data are increasingly needed to train the computer systems.

Currently, three criteria have been proposed to harmonise the interpretation of PSMA PET findings: the EANM criteria (Fanti et al. 2017), the Prostate Cancer Molecular Imaging Standardised Evaluation (PROMISE) criteria (Eiber et al. 2018) and the PSMA Reporting and Data System (PSMA-RADS) criteria (Werner et al. 2019). These criteria were recently partially merged and presented as part of the E-PSMA, the EANM's standardised reporting guidelines (Ceci et al. 2021). The use of a structured report implies a standardised nomenclature and imaging interpretation (Fanti et al. 2017). According to the PROMISE criteria, the visual interpretation of PSMA uptake should be performed according to four scores, using the blood pool, liver and salivary gland uptake as reference (**Table 6**). For [<sup>18</sup>F]-PSMA-1007 the use of spleen uptake instead of the liver uptake is recommended, given the hepatobiliary excretion.

**Table 6.** Visual score according to the intensity of PSMA uptake. Modified from: Ceci et al., 2021.

Visual score	Intensity of PSMA uptake
0	< blood pool (no uptake)
1	≥ blood pool and < liver/spleen (low)
2	≥ liver/spleen and < parotid gland (intermediate)
3	≥ parotid gland (high)

Then, the grade of PSMA uptake must be correlated with the presence of anatomical correspondence as well as with the site to provide a grade of confidence in the interpretation of the findings. In the E-PSMA guidelines, similar to the PSMA-RADS criteria, a 5-point score is proposed (**Table 7**).

**Table 7.** Interpretation of the PSMA PET findings according to the reader confidence on a 5-point scale. Modified from: Ceci et al., 2021.

Score	Definition	Description
1	Benign lesion	Lesion without abnormal uptake
2	Probably benign lesion	Lesion with faint PSMA uptake in a site atypical for prostate cancer
3	Equivocal finding	Lesion with faint uptake in a site typical for prostate cancer or intense uptake in a site atypical for prostate cancer
4	Probably prostate cancer	Lesion with intense uptake in a site typical for prostate cancer but without anatomical correspondence
5	Definitively prostate cancer	Lesion with intense uptake in a site typical for prostate cancer with definitive anatomical correspondence

Once the findings have been interpreted, the structured report might include a new TNM staging classification based on molecular imaging (miTNM), which was first proposed in the PROMISE criteria (**Table 8**). This would further help organise the findings into comprehensible categories to promote the exchange of information among physicians and institutions.

**Table 8.** Molecular imaging(mi) TNM staging for PCa. Modified from: Eiber et al, 2018.

<b>Local tumour (T)</b>	
miT0	No local tumour
miT2	Organ-confined tumour
miT3a	Extracapsular extension
miT3b	Invasion of the seminal vesicles
miT4	Invasion of adjacent structures other than the seminal vesicles
miTr	Local recurrence after radical prostatectomy
<b>Regional lymph nodes (N)</b>	
miN0	No positive regional lymph nodes
miN1a	Single regional lymph node
miN1b	Multiple (≥ 2) regional lymph nodes
<b>Distant metastases (M)</b>	
miM0	No distant metastasis
miM1a	Extrapelvic lymph nodes
miM1b	Bone metastases
miM1c	Visceral metastases



According to a recent study that evaluated the inter-reader agreement between the different PSMA PET interpretation criteria, it seems that these criteria have solid reproducibility with [ $^{68}\text{Ga}$ ]-PSMA-11 (Toriishara et al. 2020). Further work is needed to harmonise the criteria and take more into consideration currently used  $^{18}\text{F}$ -labelled radiotracers.

### 2.5.3.6 PSMA PET in non-prostatic tumours

In the analysis of a PSMA PET scan of a PCa patients, incidental detection of PSMA uptake in non-prostatic conditions is not uncommon (De Galiza Barbosa et al. 2020). PSMA uptake can be seen in several benign findings, such as in inflammatory and infectious processes, benign neoplasms (most commonly haemangiomas and adenomas) and bone-related conditions (e.g., fractures, osteodegenerative findings, Paget's disease and fibrous dysplasia). Several case reports have also been published regarding PSMA uptake in malignant tumours other than PCa (**Figure 8** and **Table 9**). This uptake is mostly related to the increased PSMA expression in the tumour-associated neovasculature (Chang et al. 1999).

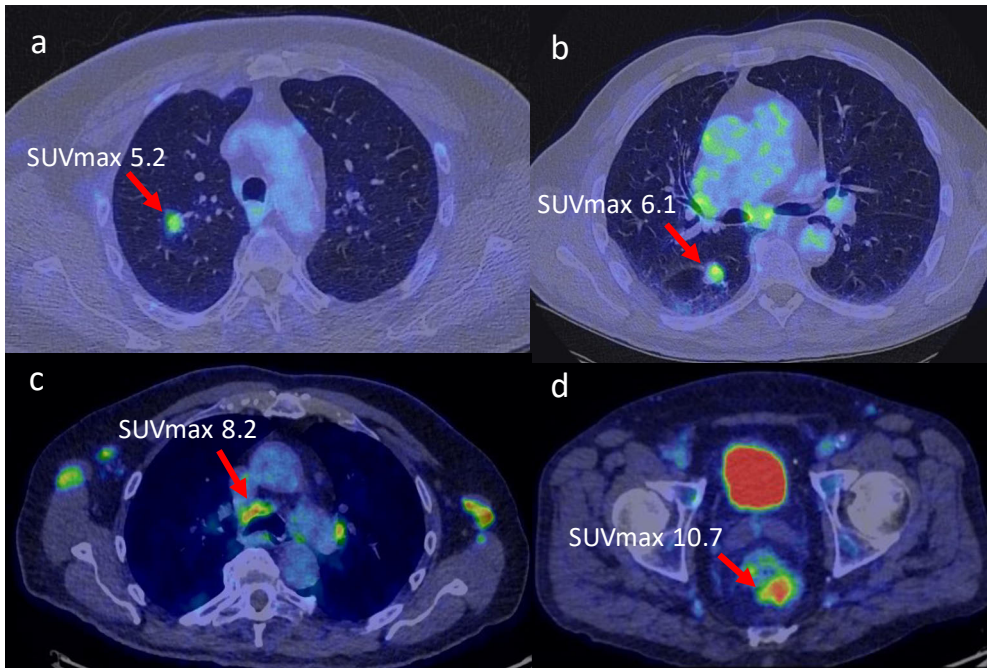


**Figure 8.** Examples of histologically confirmed malignant tumours other than prostate cancer detected on clinical [ $^{18}\text{F}$ ]-PSMA-1007 PET/CT scans. (a) Lung squamous cell carcinoma (b) Lung adenocarcinoma (c) Lymphoma (d) Rectum adenocarcinoma.

**Table 9.** Overview of the malignant tumours that have showed PSMA uptake on PET imaging. Modified from: de Galiza Barbosa et al. 2020.

Site	Tumour
Nervous system	Gliomas
Cervical	Head and neck SCC Salivary gland carcinoma Thyroid cancer
Thoracic	Lung cancer Breast cancer Mesothelioma Thymoma
Abdominal	Renal cell carcinoma Hepatocellular carcinoma Colorectal cancer Pancreatic carcinoma Transitional cell carcinoma Neuroendocrine tumours Ovarian cancer Cervical carcinoma Endometrium cancer Vulvar carcinoma
Skeletal and soft tissues	Melanoma Lymphoma Osteosarcoma Multiple myeloma

While the non-specificity of PSMA expression for PCa lesions might represent a limitation that makes it important to be aware of the potential pitfalls, new opportunities to use PSMA ligands in diagnostic or even therapeutic approaches for other malignant tumours could arise. The role of PSMA-ligands in non-prostatic tumours has been investigated in relatively small prospective studies (Uijen et al. 2021). These studies focused on tumours that present highly vascularisation, including renal cell carcinoma (RCC), high-grade gliomas, salivary gland cancer, iodine refractory thyroid cancer and hepatocellular carcinoma (HCC).

RCC is one of the tumours first and most assessed by PSMA PET imaging because of its high-grade of vascularisation. However, given the high physiological uptake in the kidneys, PSMA PET has demonstrated better performance in the detection of recurrences or metastases, with higher sensitivity than CT and changes in patient management (Raveenthiran et al. 2019; Rhee et al. 2016). High-grade gliomas have shown clear PSMA uptake on PET imaging together with optimal correlation with MRI imaging (Kumar et al. 2022; Verma et al. 2019). Among high-grade gliomas, glioblastoma multiforme is known to be an aggressive and particularly treatment resistant malignancy. In this scenario, PSMA RLT could

represent a valuable treatment option, and in a few case reports of patients with recurrent glioblastoma multiforme, [<sup>177</sup>Lu]-PSMA was safely administered and even resulted in tumour shrinkage (Kumar et al. 2022; Kunikowska et al. 2020). Adenocystic carcinoma of the salivary gland and differentiated thyroid cancer have also demonstrated considerable PSMA uptake, particularly in metastatic lesions (Lütje et al. 2017; Van Boxtel et al. 2020; Verma et al. 2018). Moreover, patients with radioiodine-refractory thyroid cancer might particularly benefit from PSMA theranostic applications (Vries et al. 2021). HCC is a highly vascularised tumour that might be difficult to diagnose, as low glucose metabolism and physiological uptake in the liver limit the use of FDG PET. HCC has demonstrated high PSMA expression, despite possible heterogeneity in the uptake (Kesler et al. 2019; Kuyumcu et al. 2019). In one study on 40 patients, change of management after PSMA PET was demonstrated in 50% of the patients (Hirmas et al. 2021).

Despite promising data on the diagnostic and therapeutic use of PSMA ligands in tumours other than PCa, larger prospective studies are needed, particularly focusing on advanced-stage diseases that would mostly benefit from theranostic approaches. Moreover, larger studies, including dosimetry, are needed to establish the efficacy of PSMA-targeted RLT and tracer kinetics in these tumours.

# 3 Aims

This doctoral thesis investigated PSMA as a target for PET imaging of PCa. The first study investigated the biodistribution and kinetics of a novel theranostic PSMA tracer. Studies II and III focused on investigating the physiology of PSMA expression in relation to short-term ADT. Study IV investigated the diagnostic performance of PSMA PET in the primary nodal staging of PCa.

The specific aims of the doctoral studies were as follows:

- I. To assess the biodistribution and kinetics of [<sup>18</sup>F]-rh-PSMA-7.3 in PET imaging of PCa.
- II. To investigate the time course effect of short-term ADT on PSMA uptake in treatment-naïve PCa using [<sup>68</sup>Ga]-PSMA-11 PET/MRI.
- III. To investigate the flare of PSMA uptake after short-term ADT and its correlation with FDG-uptake in metastatic treatment naïve PCa using [<sup>18</sup>F]-PSMA-1007 PET/CT.
- IV. To compare the diagnostic performance of [<sup>18</sup>F]-PSMA-1007 PET/CT to those of ceCT and WBMRI in primary nodal staging of men with newly diagnosed unfavourable intermediate- and high-risk PCa.

## 4 Materials and Methods

### 4.1 Study population and eligibility

The study population for the studies of this doctoral thesis was from four prospective registered clinical trials conducted at the Turku University Hospital (TYKS) between 2018 and 2022 (**Table 10**). The first trial (Study I) included three distinct patient cohorts: men with newly diagnosed treatment-naïve high risk PCa scheduled for prostatectomy (Cohort A); men with newly diagnosed treatment-naïve metastatic PCa (Cohort B); and men with castration-resistant metastatic PCa (Cohort C). The other three trials (Studies II-IV) had a similar source population that consisted of men with newly diagnosed treatment-naïve histologically confirmed PCa. Study II had as an additional inclusion criterion the presence of distant metastases (M1) confirmed on conventional imaging. The inclusion and exclusion criteria for the four studies are represented in **Table 10**. All the study patients were selected at TYKS by the investigating urologist, in collaboration with the investigating nuclear medicine physician (for Studies II and III). Patients who met the eligibility criteria were informed about the study at the Department of Urology of TYKS and signed an informed consent form.

**Table 10.** Inclusion and exclusion criteria of the studies.

Study	Clinicaltrials.gov identifier	Subjects (n)	Inclusion criteria	Exclusion criteria
I	NCT03995888	9	Histologically confirmed PCa - Newly diagnosed treatment-naïve high risk PCa scheduled for prostatectomy (Cohort A) -Newly diagnosed treatment-naïve metastatic PCa (Cohort B) -Castration-resistant metastatic PCa (Cohort C)	Any previous PCa treatment (Cohort A and B) Radiation treatment of lesions in the field of view of the dynamic images (Cohort C)
II	NCT03313726	9	Newly diagnosed treatment-naïve histologically confirmed PCa	Any previous PCa treatment Uncontrolled serious infection Contraindications for MRI
III	NCT03876912	25	Newly diagnosed treatment-naïve histologically confirmed PCa with distant metastases (M1) confirmed on conventional imaging	Any previous PCa treatment Uncontrolled serious infection Presence of malignances other than PCa
IV	NCT03537391	79	Newly diagnosed treatment-naïve histologically confirmed unfavourable intermediate or high risk PCa	Any previous PCa treatment Any previous imaging for PCa staging Contraindications for MRI

## 4.2 Study design

### 4.2.1 Study I

Study I (NCT03995888) was a prospective, Phase I, single centre study that included nine patients selected from three distinct patient populations (Cohorts A-C, as described in the previous paragraph). The study aimed to assess the biodistribution and kinetics of [<sup>18</sup>F]-rhPSMA-7.3 in the imaging of PCa.

All the patients underwent dynamic 45-min PET scanning of a target area immediately after injection of [<sup>18</sup>F]-rhPSMA-7.3, followed by two whole-body PET/CT scans acquired at 60 min and 90 min post-injection. Moreover, venous blood sampling up to 120 min after injection was performed. The imaging study is outlined in **Figure 9**.

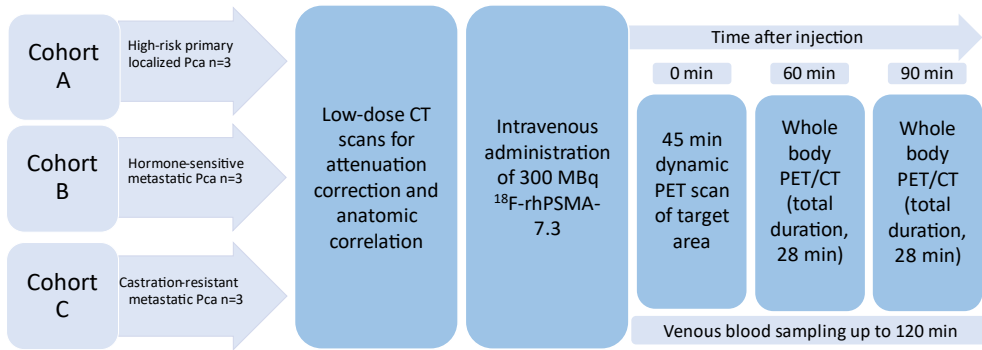


**Figure 9.** Outline of Study I.

#### 4.2.2 Study II

Study II (NCT03313726) was a prospective, single centre, pilot study that investigated the effect of short-term ADT on PSMA uptake at different time points using [ $^{68}\text{Ga}$ ]-PSMA-11 PET/MRI. Nine patients with newly diagnosed, histologically confirmed treatment-naïve PCa underwent a [ $^{68}\text{Ga}$ ]-PSMA-11 PET/MRI scan immediately before and at three time points after the administration of degarelix (240 mg): at the means (ranges) of 1.5 (0.8-2.5) weeks, 2.9 (1.9-4.5) weeks, and 6.2 (3.5-8.7) weeks, respectively. Serum PSA and testosterone samples were collected before each PET scan. The study outline is represented in **Figure 10**.

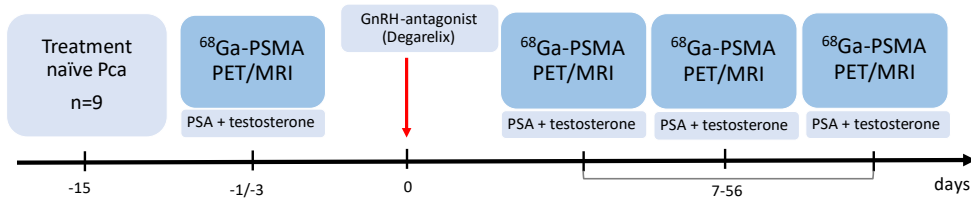


**Figure 10.** Outline of Study II.

#### 4.2.3 Study III

Study III (NCT03876912) was a prospective, single centre study that was designed as a continuation of Study II. The purpose of this trial was to investigate the increase of PSMA uptake (the PSMA flare) after short-term ADT as a possible marker of tumour aggressiveness. Twenty-five men with newly diagnosed treatment naïve metastatic PCa were enrolled. The metastatic status of the patients was confirmed by conventional imaging (CT and BS), performed within two weeks before their enrollment. All the patients underwent a [ $^{18}\text{F}$ ]-PSMA-1007 PET/CT and a [ $^{18}\text{F}$ ]-FDG PET/CT immediately before the administration of ADT (degarelix, 240 mg). [ $^{18}\text{F}$ ]-

FDG PET/CT was performed to assess the potential aggressiveness of the lesions. Subsequently, [<sup>18</sup>F]-PSMA-1007 PET/CT was performed three to four weeks after ADT initiation. This time point was chosen according to the results of Study II. Serum PSA and testosterone were collected before each PSMA PET scan. The study outline is represented in **Figure 11**.

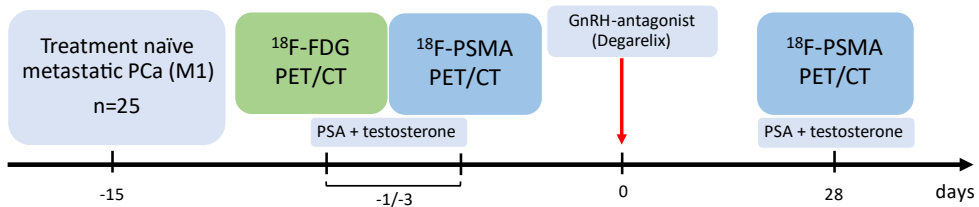


**Figure 11.** Outline of Study III.

#### 4.2.4 Study IV

Study IV (NCT03537391) was a prospective, single centre study that included 79 men with newly diagnosed histologically confirmed unfavourable intermediate- or high-risk PCa. All the patients underwent contrast-enhanced abdominopelvic and thoracic CT, [<sup>99m</sup>Tc]-HMDP planar BS, [<sup>99m</sup>Tc]-HMDP SPECT/CT, WBMRI with DWI and [<sup>18</sup>F]-PSMA-1007 PET/CT within a period of two weeks. The purpose of the study was to compare the diagnostic performance of the imaging modalities in the primary staging of PCa. Since this study focused on regional nodal staging, only CT, WBMRI and [<sup>18</sup>F]-PSMA-1007 PET/CT were evaluated. The results of the M-staging had been reported separately (Anttinen et al. 2020).

### 4.3 Imaging protocols

#### 4.3.1 Dynamic PET scans and blood sampling (Study I)

In Study I, dynamic PET imaging was performed. The patients underwent a 45-min dynamic scan (Scan 1) of a target region, starting at the time of the [<sup>18</sup>F]-rhPSMA-7.3 administration. The dynamic scan was performed in list mode, and the target region varied according to the patient’s cohort: for Cohort A, the prostate; and for Cohort B and C, the most relevant lesion identified on standard of care imaging (CT and BS). Care was taken to include at least one bone lesion and one lymph node metastasis, if present. Moreover, when possible, the area that included the thoracic or abdominal aorta was chosen. Two intravenous cannulae (IV) were positioned, one in each arm. The right arm was the preferred arm for the administration of the radiotracer, and the left arm was used for blood sampling. A vacuum mattress was



used to position the subjects on the PET imaging bed and to ensure the same positioning after the scan break.

Non-arterialised venous blood samples (2 mL) were collected starting after the administration of [ $^{18}\text{F}$ ]-rhPSMA-7.3 and according to the following approximate sampling schedule: 20 s, 40 s, 60 s, 80 s, 100 s, 120 s, 140 s, 160 s, 180 s, 4 min, 5 min, 7.5 min, 10 min, 15 min, 20 min, 30 min, 40 min, 50 min, 59 min, and 120 min post-injection. Blood samples were collected into heparinised tubes, mixed, and chilled on ice. Then, they were immediately divided into two aliquots, and one aliquot was centrifuged in a cooled (+4°C) centrifuge at 2118 g for 5 min. Next, 700  $\mu\text{l}$  of plasma was separated into another tube. Both the plasma and whole-blood radioactivity were measured. Haematocrit was measured at the screening, at the baseline (-120 min to -5 min, relative to injection), and at 45 min, 3 hours, 4 hours, and at 24 hours post-injection (as part of the study safety laboratory evaluations).

#### 4.3.2 PET/MRI and PET/CT scans

All the PET studies from the four studies were performed at the Turku PET Centre at TYKS. The CT and WBMRI scans of the Study IV were performed at the Radiology Department of TYKS. All the PET scans were carried out by the investigating nuclear medicine physician, who was responsible for the preparation of the patient and the administration of the radiopharmaceutical. In all the studies, the administration of the radiopharmaceutical was performed through a IV cannula, followed by a flush of saline.

In Study I, the PET scans were performed using a General Electric (GE) Discovery MI PET/CT scanner (GE Healthcare, Milwaukee, WI, USA). A dynamic 45-min PET scan of a target area was performed, followed by two static 28-min PET scans from the mid-thigh to the vertex (7 bed positions at 4 min/bed), starting at 60 min (Scan 2) and 90 min (Scan 3) post-injection. Low-dose CT scans (one of the target area and one from vertex to mid-thigh before the first static scan) were acquired for attenuation correction and anatomic correlation. The CT acquisition parameters were a tube potential of 120 kV, a tube current modulated 10–120 mA, and a noise index of 30.

In Study II, the [ $^{68}\text{Ga}$ ]-PSMA PET/MRI scans were performed using a sequential Philips Ingenuity PET/MRI scanner (Philips Healthcare, Cleveland, OH, USA). The MRI scanning sequences included axial, coronal and sagittal T2-weighted turbo-spin-eco (TSE) and DWI imaging of the prostate area (b-values 0, 50, 400 and 800  $\text{s}/\text{mm}^2$ ) using a dedicated external coil for the lower abdomen (Sense Torso XL). These sequences were followed by whole-body T2-weighted and MRI-based attenuation correction sequences. The PET scans were acquired from the mid-thighs to the base of the skull and started at 60 min post-injection. PET imaging

reconstructions were performed using the default reconstruction algorithm Blob-OSTF, a 3D ordered subset iterative TOF reconstruction technique. The reconstruction used 3 iterations and 33 subsets in a 144×144 matrix with an isotropic voxel size of 4 mm. All the reconstructions included the necessary corrections for image quantification: attenuation, random coincidences, scatter, dead-time, decay and detector normalization.

In Studies III and IV, the [<sup>18</sup>F]-PSMA-1007 PET/CT scans were carried out using a GE Discovery MI PET/CT scanner (GE Healthcare, Milwaukee, WI, USA). The patients underwent whole-body PET/CT scans from the mid-thigh to the vertex starting at 60 min post-injection. Low-dose CT scans were acquired for attenuation correction and anatomic correlation. The CT acquisition parameters were the same as those in Study I: a tube potential of 120 kV, a tube current modulated between 10-120 mA, and a noise index of 30. The PET scans were acquired in 3D mode with 2-min/bed positions. The sinogram data were corrected for deadtime, decay and photon attenuation and, then, reconstructed on a 256×256 matrix. For the image reconstruction, a Bayesian penalised-likelihood iterative reconstruction algorithm (Q.Clear) was utilised with a  $\beta$  value of 500 for [<sup>18</sup>F]-PSMA-1007, incorporating random and scatter corrections. The [<sup>18</sup>F]-FDG PET/CT scans in Study III were performed using the same PET/CT camera and following the same imaging protocol. The PET scan started 50 min post-injection. The same algorithm (Q.Clear) was utilised for image reconstruction using a  $\beta$  value of 350.

#### 4.3.3 CT and WBMRI (Study IV)

In Study IV, ceCT and WBMRI were performed. Abdominopelvic and thoracic ceCT was carried out with a Discovery NM/CT 670 CZT, a digital SPECT/CT imaging system, including an Optima CT540 subsystem (GE Healthcare, Tirat, Hacarmel, Israel). A helical CT tomogram with a modulated mAs, a noise index ~ 30, a rotation time of 0.5 s, a tube potential of 120 kV, a pitch of 0.938 and a 1.25-mm slice thickness was acquired. Soft tissue, bone and lung kernels were used with a 40 % dose reduction in the Adaptive Statistical Iterative Reconstruction (ASIR, GE Healthcare, USA) algorithm. A biphasic contrast-enhanced CT protocol (arterial phase at 10 s, followed by venous phase at 30 s) was performed. Contrast agent (Omnipaque (iohexol)<sup>TM</sup> GE Healthcare, iodine concentration of 350 mg/ml) was used, unless clinical contraindications were present.

The WBMRI imaging was performed using a Siemens Magnetom Avanto fit 1.5 T MR system (Siemens Healthcare GmbH, Erlangen, Germany). The WBMRI acquisition protocol consisted of axial T2-weighted fat suppressed (FS) half-Fourier single shot turbo spin-echo (HASTE) images, axial short-tau inversion recovery (STIR) DWI, b-values 0, 50 and 900 s/mm<sup>2</sup> and coronal 3D T1-weighted volumetric

interpolated breath-hold examination (VIBE) Dixon sequences. In addition, whole spine sagittal T1- and T2-weighted STIR turbo spin-echo (TSE) sequences and axial STIR DWI images from the level of the pelvis, with b values 0 and 1500 s/mm<sup>2</sup>, were acquired.

## 4.4 Radiopharmaceutical preparation

[<sup>68</sup>Ga]-PSMA-11, [<sup>18</sup>F]-PSMA-1007, [<sup>18</sup>F]-rhPSMA-7.3 and [<sup>18</sup>F]FDG solutions for injection were produced on site at the Radiochemistry Laboratory of Turku PET Centre. During Study IV, [<sup>18</sup>F]-PSMA-1007 was still not produced at the Turku PET Centre. Therefore, the radiopharmaceutical was produced by MAP Medical Technologies Oy, Curium Pharma (Helsinki, Finland).

[<sup>18</sup>F]-rhPSMA-7.3 was produced using a single-use cassette-based proprietary automated synthesis platform for radiolabelling, purification and formulation (Scintomics GRP, Scintomics GmbH, Fürstfeldbruck, Germany), and using an in-house remotely operated sterile filtration device for aseptic filling.

The [<sup>68</sup>Ga]-PSMA-11 synthesis was performed in a Class C clean room by a fully automated cassette-based synthesis device (Modular Lab, PharmTracer, Eckert & Ziegler Eurotope GmbH, Berlin, Germany). <sup>68</sup>Ga was obtained from a <sup>68</sup>Ge/<sup>68</sup>Ga generator (GalliaPharm, 50 mCi, Eckert & Ziegler Radiopharma GmbH, Berlin, Germany).

For Study IV, [<sup>18</sup>F]-PSMA-1007 was manufactured by MAP Medical Technologies Oy, Curium Pharma (Helsinki, Finland) using an automated cassette-based synthesis unit (GE TRACERlab Mx or ORA Neptis). The synthesis of [<sup>18</sup>F]PSMA-1007 at the Turku PET Centre was performed with TRASIS AllInOne synthesiser (TRASIS Radiopharma, Ans, Belgium) using the single-use cassettes supplied by TRASIS and reagents supplied by ABX (ABX advanced biochemical compounds GmbH, Radeberg, Germany). [<sup>18</sup>F]-FDG was synthesised using a FASTLab® synthesiser (GE Healthcare, Waukesha, WI, USA) and FDG-phosphate cassettes.

In all the <sup>18</sup>F-labelled radiopharmaceuticals, Fluorine-18 was produced with the GE PETtrace cyclotron. For all the radiopharmaceuticals, the radiochemical and chemical purities were evaluated by radio high-performance liquid chromatography (HPLC) and the pH was measured from the final product.

## 4.5 Histopathological analysis

In Study IV, histopathological analysis of the lymph nodes was performed in patients who had undergone lymphadenectomy. Surgical tissue specimens from PLND were fixed in 10% buffered formalin for at least 24 h. The number of palpable lymph

nodes identified on each side was determined, and the lymph nodes were cut into 3-4 mm sections before routine tissue processing. Consecutive 4- $\mu$ m thick histological sections were used for haematoxylin and eosin (H&E) staining and for immunohistochemistry. Epitope unmasking was done by microwaving the slides in a Tris-EDTA buffer. PSMA staining was carried out with a Lab Vision autostainer (Thermo Fisher Scientific) using a mouse monoclonal PSMA antibody (Dako, clone M3620, 1:100) and an Envision detection kit (EP192). Pan-cytokeratin staining was carried out using a BenchMark ULTRA automated slide stainer (Ventana Medical Systems, Tucson, Arizona, USA) and an anti-pan-cytokeratin antibody (clone AE1/AE3/PCK26, 46.3  $\mu$ g/ml).

## 4.6 Imaging interpretation and analysis

In all the studies, PSMA positivity was interpreted visually and semi-quantitatively taking into account the current suggested procedure guidelines on PSMA PET imaging, considering normal distribution and possible pitfalls (Ceci et al. 2021). More specifically, PSMA uptake was considered malignant in the following conditions:

- focal uptake above the local background in the prostate for the primary tumour (for Study II with anatomical correspondence on MRI images).
- uptake above the blood pool with a corresponding CT/MRI finding (also normally sized lymph nodes) in a site typical for PCa for lymph node metastases.
- uptake above the blood pool with a corresponding CT/MRI finding in a site typical for PCa for bone and visceral metastases.

### 4.6.1 Study I

In Study I, two experienced PET researchers (S.M. and K.K.) manually drew volume-of-interest (VoI) regions on as many PCa lesions and healthy reference tissues as were identified in the images of the target area. For primary prostate tumours, the blood pool or skeletal muscle was used as the reference. For lymph node metastases, the blood pool was used as the reference. For bone metastases, healthy bone marrow or the blood pool from the same image was used as the reference. Blood pool VoI regions were drawn on large arteries, usually the abdominal aorta. If allowed by the size of the reference tissue, VoIs were drawn over at least four mid-tissue PET planes with the help of the correlating anatomic CT image. Care was taken to avoid the surfaces of the reference tissues to prevent partial volume effects in the measurement of radioactivity. The positions of the VoIs were

checked against all three PET scan sets and if any movement was observed, the VoI position was adjusted accordingly.

The mean VoI radioactivity values of each lesion and its reference tissue, each scan set, and each subject were extracted and individual time–activity concentration curves (TACs) for each lesion and reference tissue were generated for each subject (**Figure 12**).

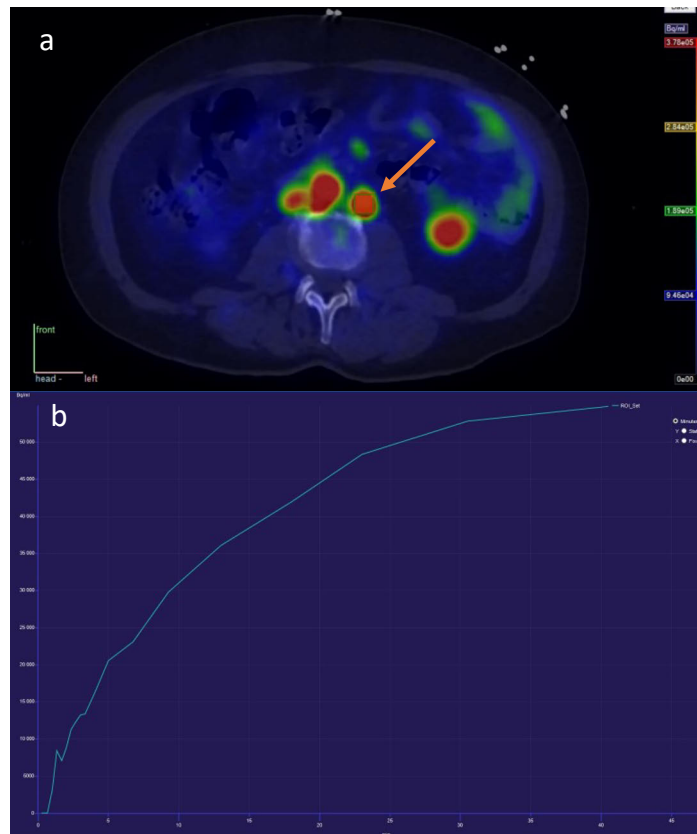


**Figure 12.** Representative image of the analysis of the dynamic PET data using Carimas Software. (a) Delineation of the VOI in a para-aortic lymph node metastasis. (b) Time-activity curve (TAC).

The VoI radioactivity concentrations from the two static PET scans were corrected for the decay of  $^{18}\text{F}$  to the administration time, and the corrected radioactivity concentrations were added to the TACs of the dynamic scan to construct full 0–118 min regional TACs. The regional TACs and the venous plasma and blood TACs were converted from radioactivity concentration units (Bq/mL and kBq/mL,

respectively) into standardised uptake value (SUV) units (g/mL) to enable direct comparisons of TACs between subjects.

The plasma-to-blood ratio as a function of time was calculated from the blood and plasma sample data. As shown in the Results section, the plasma-to-blood ratio remained constant and at a level that implied that [<sup>18</sup>F]-rhPSMA-7.3 remains in blood plasma and does not enter the red cells of the blood during the relevant time period from injection. In this case, the blood TAC can be converted to plasma TAC using the following Equation:

$$Plasma = \frac{Blood}{1 - Haematocrit}$$

where *Blood* is the radioactivity concentration in blood (g/mL); *Plasma* is the radioactivity concentration in plasma (g/mL) and *Haematocrit* (HCT) is the average HCT. The average HCT from the baseline, 45 minutes and 3 hour samples was used to convert the PET-image-based blood TAC to the plasma TAC. The over-time averaged plasma-to-blood ratios were calculated for each subject, excluding the first 2 minutes, and these individual ratios were compared to the plasma-to-blood ratios based on the HCT values. While the concentrations in the arterial plasma are independent of blood sampling site, the venous plasma concentrations are dependent on the clearance of the compound in the vascular bed and thus, the sampling site. Depending on the radioligand, transient equilibrium between the arterial and venous plasma may be reached sometime after administration of a radiotracer (Eary and Mankoff 1998; Zanotti-Fregonara et al. 2011), and therefore, the initial phase of a venous plasma TAC is distorted, unlike that of a simultaneous arterial plasma TAC. On the other hand, image-derived blood TACs may be distorted by spill-out into adjacent tissues at early timepoints and by spill-in from adjacent tissues at late time points. At very early time points, the image-derived blood TACs were markedly higher than the manually sampled blood TACs, and at later timepoints, they were generally lower. Therefore, for all the subject scans, the plasma and blood TACs were constructed as combinations of image-derived arterial TACs and manually sampled venous blood TACs. The image-derived arterial TACs were utilised from the administration time to the peak of each TAC, and manually sampled venous TACs were utilised starting from their peak value.

The lesion-to-reference ratios were calculated at different timepoints, and the ratios were plotted as a function of time. During the dynamic scan, the reference tissue was measured at the same timepoints as the lesions. In the late static scans with multiple bed positions, the measurement time points might have been somewhat different, but insignificantly so because of the relatively slow observed changes in the radioactivity uptake, especially in the reference tissues. The blood pool from the

image was used as the reference tissue to mimic the visual image analysis. For comparison, the blood TACs based on venous blood sampling were used to calculate the ratios.

Multiple-time graphical analysis (MTGA) (i.e., Patlak and Logan plots) was performed for the lesion and reference tissue data, using the plasma TAC as the input function. A compartmental model for the radioligand and tissues of interest is not known at this stage of development. MTGAs are instead independent of the number of tissue compartments, and the only assumptions of the approach are that the radioactivity concentration in the plasma and the non-bound radioactivity concentration in the tissue reach a dynamic equilibrium during the PET scan, and that tissue either contains an irreversible uptake component or components (Patlak plot), or does not contain any irreversible uptake components (Logan plot). In addition, inaccuracies in the initial plasma TAC affect MTGAs less than compartmental model analyses.

#### 4.6.2 Study II

In Study II, two experienced nuclear medicine physicians (S.M. and J.K.) analysed the images while blinded to the results of the other reader. In the case of equivocal findings, a consensus between the two readers was reached in a multidisciplinary board meeting. The SUVmax values were calculated for PSMA-positive prostate and metastatic lesions. Moreover, the SUVmax values were obtained from the salivary glands, liver, spleen and kidneys. The changes in the SUVmax at different time points after ADT were represented as  $\Delta$ SUVmax. The lesions were divided and analysed into two groups: the 'decrease' group of lesions in which the change in SUVmax was constantly negative in every time point compared to the baseline; and the 'increase' group of all other lesions. The two groups were further analysed by evaluating the maximum increase and the maximum decrease in the SUVmax from each type of lesion or normal organ. These changes in the SUVmax were reported as mean proportions (ranges) and the time points when the changes occurred were reported as mean weeks (ranges).

#### 4.6.3 Study III

In Study III, an experienced nuclear medicine physician (S.M.) reviewed the PSMA and FDG PET/CT scans. All the metastases documented in conventional imaging (CT and BS) that showed PSMA uptake at the baseline [ $^{18}\text{F}$ ]-PSMA-1007 PET/CT were included in the analysis. Then, all the PSMA-positive lesions were then carefully matched with [ $^{18}\text{F}$ ]-FDG PET/CT. Lesions with tracer uptake above the blood pool were considered FDG-positive. The SUVmax values were calculated for

all prostate and metastatic lesions. The changes in the PSMA uptake after ADT were represented as  $\Delta$ SUVmax. Then, the PSMA-positive lesions were divided into two groups. The first group included all the lesions with a  $\Delta$ SUVmax  $\geq +20\%$  (PSMA flare), and the second group consisted of the remaining lesions that exhibited either a decrease or no change ( $<20\%$ ) in the SUVmax. The FDG SUVmax was further divided into three categories:  $\leq$  the blood pool (FDG-negative),  $>$  the blood pool up to 10 (mild to moderate uptake), and  $> 10$  (strong uptake).

#### 4.6.4 Study IV

In Study IV, there was a total of six readers (four radiologists and two nuclear medicine physicians, I.J., M.S., I.K., S.K., S.M. and J.S.), two for each of the three imaging modalities. Each imaging modality was independently reviewed by the same pair of experienced modality-based experts who were blinded for the other modalities. The pelvic lymph nodes were reported as malignant, equivocal or benign. Both optimistic (equivocal lesions interpreted as benign) and pessimistic (equivocal lesions interpreted as malignant) analyses were performed to resolve the equivocal lesion status. In the CT and WBMRI, the lymph node diameter (short diameter  $> 8$  mm) and morphology (rounded) were used to determine malignancy. In the MRI, diffusion restriction was also used to assess nodal invasion, especially in normalized lymph nodes.

The reference standard diagnosis was used to validate the reported lesions. It included histopathological data (when available) or alternatively lymph nodes were considered malignant if at least three of the following criteria were met: (1) concordance between the primary imaging modalities; (2) increase in the size or number of lymph nodes during the follow-up imaging; (3) decrease in the size or number of lymph nodes during the follow-up imaging in response to treatment; (4) increase in the serum PSA suggesting progression; (5) decrease in the serum PSA in response to treatment; (6) increase in the PSMA uptake during follow-up imaging (when available); (7) decrease in the PSMA-uptake during the follow-up imaging (when available) in response to treatment.

### 4.7 Software for imaging analysis

In Study I, the Carimas image analysis tool (version 2.10, Turku PET Centre, Turku, Finland) was used to measure the radioactivity concentrations in the target lesions and reference tissues in both the dynamic and static PET images.

The analysis of the PET/CT or PET/MRI scans in Studies II-IV was performed using an AW 4.5 or 4.7 workstation (General Electrics (GE) Healthcare). In Study IV, the WBMRI and CT images were analysed using Weasis Medical Viewer



(version 3.5.3, University Hospital of Geneva, Switzerland) and Vue PACS (version 12.2.0.1007, Carestream Health Inc, Rochester, USA).

In Studies I and II, data were collected using an Excel data sheet; and in Studies III and IV data were collected using a Research Electronic Data Capture (REDCap) database (Harris et al. 2019).

## 4.8 Statistical analysis

In all the studies descriptive data were presented as mean or median values and their standard deviations or ranges, including interquartile intervals in Studies III and IV. In Studies II and IV, Cohen's Kappa (95%CI) was calculated to evaluate the inter-reader agreement. In Study III, Pearson's correlation coefficient was used to assess the correlation between the PSMA SUVmax and the FDG SUVmax as well as the correlation between the PSMA  $\Delta$ SUVmax, FDG SUVmax and  $\Delta$ PSA. Welch's analysis of variance (ANOVA) was used to compare the PSMA  $\Delta$ SUVmax to the different classes of FDG SUVmax.

In Study IV, the sensitivity, specificity and accuracy were reported with a 95% CI and compared between modalities with Fisher's exact test. For both the patient- and lesion-based statistical analyses, the correct side of the pelvis (right or left) was considered to achieve correct agreement with the reference standard diagnosis. Pearson's correlation coefficient was used to study the correlation between the PSMA SUVmax and the lesion size.

In all the studies, P values < 0,05 were considered statistically significant. Statistical analysis was carried out using JMP® software.

## 4.9 Ethics

All the studies were conducted in compliance with the current revision of the Declaration of Helsinki, which guides physicians and medical research involving human subjects (64<sup>th</sup> World Medical Association General Assembly, Fortaleza, Brasil, 2013). All the studies were approved by the local ethics committee of the Hospital District of Southwest Finland.

# 5 Results

## 5.1 Study I

The primary objective of Study I was to assess the kinetics of [<sup>18</sup>F]rhPSMA-7.3 radiotracer. Nine patients (three for each Cohort) completed the dynamic and total body scans. Their mean age was 66 years (range: 55 to 80 years). The mean administered radioactivity was 301 MBq (range: 284 to 322 MBq). The magnitude of the administered activity (300 MBq) was chosen following the results in healthy volunteers (Tolvanen et al. 2021). The healthy volunteer dosimetry data demonstrated that a 300 MBq administered activity would result in a total effective dose of 4.2 mSv which was considered acceptable, considering the objectives and endpoints of the study. The patient's characteristics are presented in **Table 11**.

**Table 11.** Patient's characteristics of Study I. Modified from Malaspina et al., 2021.

Patient	Gleason grade (biopsy or surgery) at diagnosis	ISUP Grade Group at diagnosis	PSA (ng/mL) before the PET/CT scan (screening visit)	T-stage <sup>a</sup>	Time from diagnosis to PET/CT scan (months)
A-001 (Cohort A)	4+3	3	21	pT3a	3
A-002 (Cohort A)	4+3	3	76	pT3a	1
A-003 (Cohort A)	4+5	5	6.1	pT2c	2
B-001 (Cohort B)	3+5	4	20	cT3	1
B-002 (Cohort B)	4+5	5	35	cT3	2
B-003 (Cohort B)	4+5	5	3.9	pT1b	1
C-001 <sup>b</sup> (Cohort C)	4+4	4	170	pT2b*	177
C-002 <sup>b</sup> (Cohort C)	3+3	1	17	pT3*	195
C-003 <sup>b</sup> (Cohort C)	3+5	4	64	pT2*	70

<sup>a</sup> The pathological T-stage of the patients in Cohort A (newly diagnosed localised PCa) and Cohort B patient B-003 (newly diagnosed hormone-sensitive metastatic PCa) was determined from the results of radical prostatectomy performed after the [<sup>18</sup>F]-rhPSMA-7.3 PET/CT scan. The pathological T-stage of the patients in Cohort C (castration-resistant metastatic PCa) was determined from the results of the radical prostatectomy performed at diagnosis.

<sup>b</sup> For Cohort C patients the PSA at diagnosis was 9,4 ng/ml, 9,1 ng/ml and 6,2 ng/ml for patient C-001, C-002 and C-003, respectively. Metastases occurred after 14, 12 and 5 years from the diagnosis for patient C-001, C-002 and C-003, respectively.

An overview of the PET images of the nine patients is presented in **Figure 13**. The patients in Cohort A had pathological PSMA uptake that was confined in the prostate gland. Among the patients in Cohort B and C, one had locally advanced disease with lymph node metastases in the pelvis, and the remaining five patients had distant metastases (two in the bone, one in the extraregional lymph nodes and two in the bone + extraregional lymph nodes).

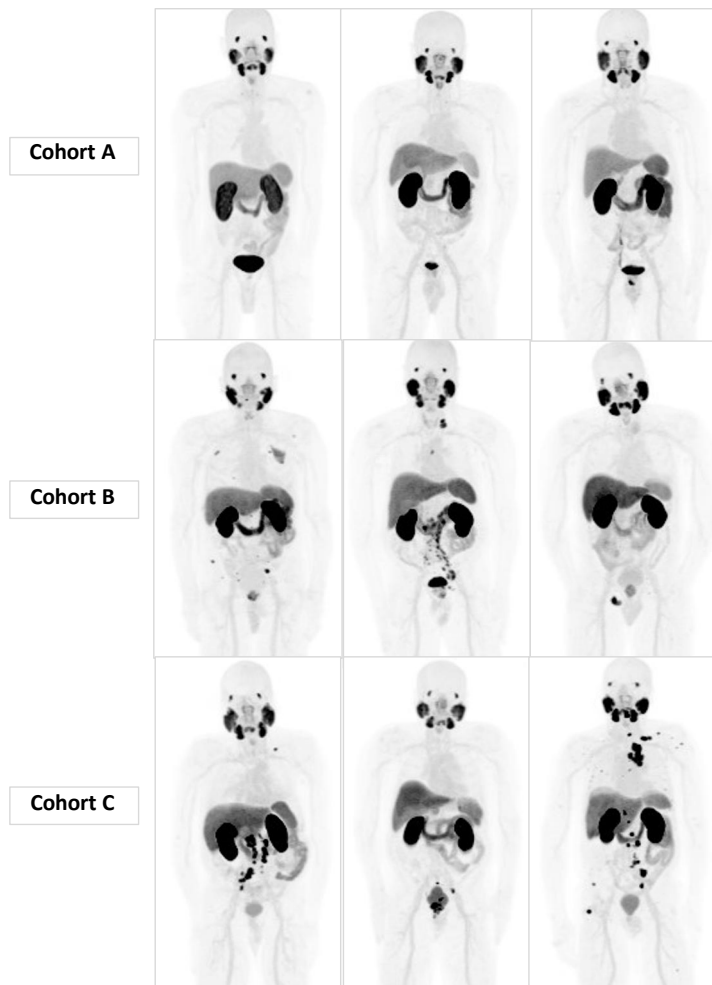


**Figure 13.** Maximum intensity projection (MIP) images of the nine patients of the study.

A total of 44 lesions were identified and analysed in the selected target regions: 6 prostate or prostate bed lesions (4 primary and 2 recurrent tumours), 26 lymph node metastases, and 12 bone metastases. The tissue radioactivity concentrations (SUV) and lesion-to-reference ratios as a function of time increased at least up to the end of

the second scanning session (**Figure 14** and **Figure 15**), suggesting a significant irreversible uptake component. The increases were not substantial after the first whole-body scan, and optimal visual detection of primary tumours and/or metastases was achieved at 60 minutes post-injection.

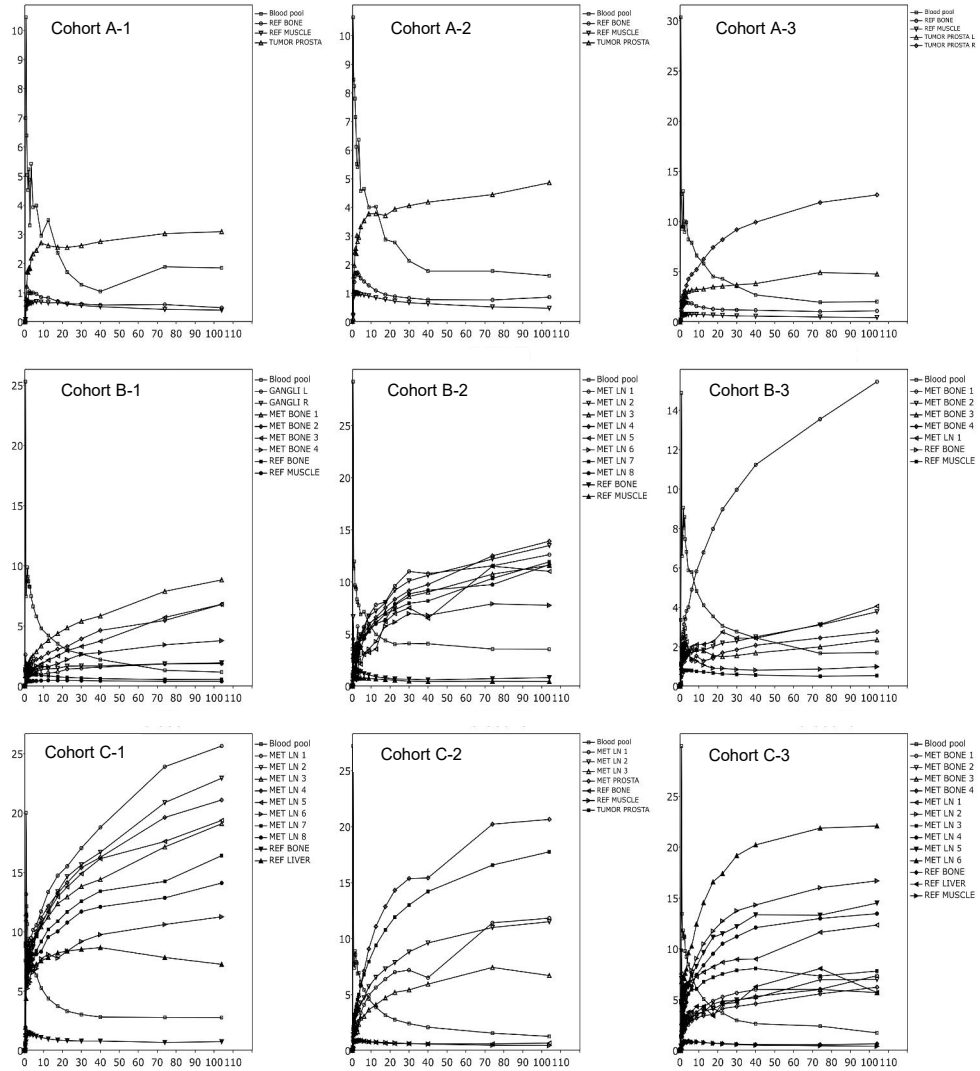


**Figure 14.** SUV (g/ml) as a function of time (min) using both dynamic and static data. Modified from original publication 1.

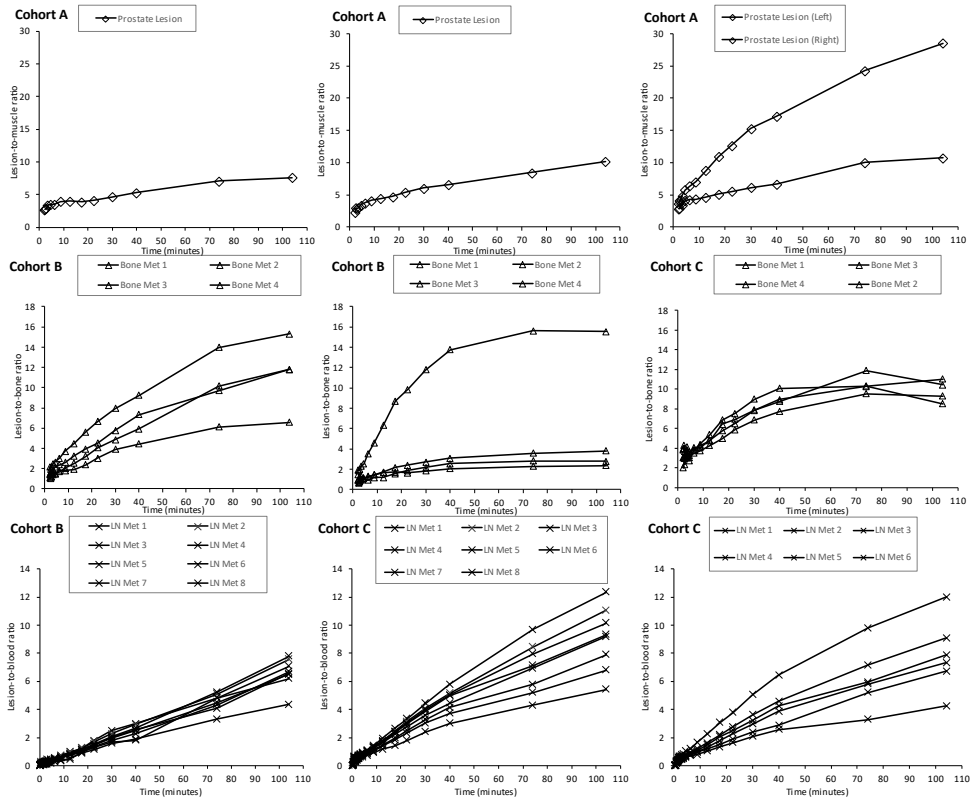


**Figure 15.** Lesion-to-reference ratios as function of time (min) using both dynamic and static data. Modified from original publication I.

In detail, the mean (SD) SUVs at 35–45, 60–88 and 90–118 min were 8.4 (5.6), 10.1 (7) and 10.6 (7.5) g/ml, respectively, for prostate lesions, 11.2 (4.3), 13 (4.8) and 14 (5.2) g/ml for lymph node metastases and 4.6 (2.6), 5.7 (3.1) and 6.4 (3.5) g/ml, for bone metastases. The mean (SD) percentage of the SUV increases from the earliest (35–45 min) to the later (60–88 and 90–118 min) scan time frames were 17% (8) and 23% (7), respectively for the prostate, 19% (17) and 29% (20) for the lymph node metastases, and 23% (12) and 40% (18), respectively for the bone lesions. Between the two later scans the mean (SD) SUV increases in the prostate, lymph node and bone lesions were 5% (3), 8% (7) and 14% (8), respectively. The mean (SD) lesion-to-reference ratios at 35–45 min, 60–88 min and 90–118 min were 14.5 (9.6), 20.8 (14.6) and 23.6 (16.4) for the prostate, 7 (3.5), 8.7 (4.2) and 9.1 (4.5) for the lymph node metastases, 3.4 (1.4), 5.4 (2) and 7.3 (2.5) for the bone lesions, respectively.

The mean (SD) lesion-to-reference ratio percentages of the increases from the earliest (35–45 min) to the later (60–88 min and 90–118 min) time frames were 40% (10) and 59% (9) for the prostate, 65% (27) and 125% (47) for the lymph node

metastases, and 25% (19) and 32% (30) for the bone lesions. Between the later scans, the ratios increased by a mean (SD) of 14% (5), 35% (12) and 5% (10) for the prostate, lymph node and bone lesions, respectively.

The blood radioactivity concentrations decreased rapidly after radiopharmaceutical administration, as [<sup>18</sup>F]-rhPSMA-7.3 was distributed in the blood pool and in the tissues of the body. The average (SD) haematocrit during the PET investigations was 0.41 (0.04). The plasma-to-blood ratio was stable during the scans, with an average of 1.66 when calculated from the samples collected starting at 2 min after the radiopharmaceutical administration (**Figure 16**). Assuming that all the radioactivity present in the blood remains in the plasma compartment (Equation), plasma-to-blood ratio amounts to a haematocrit level of 0.40.

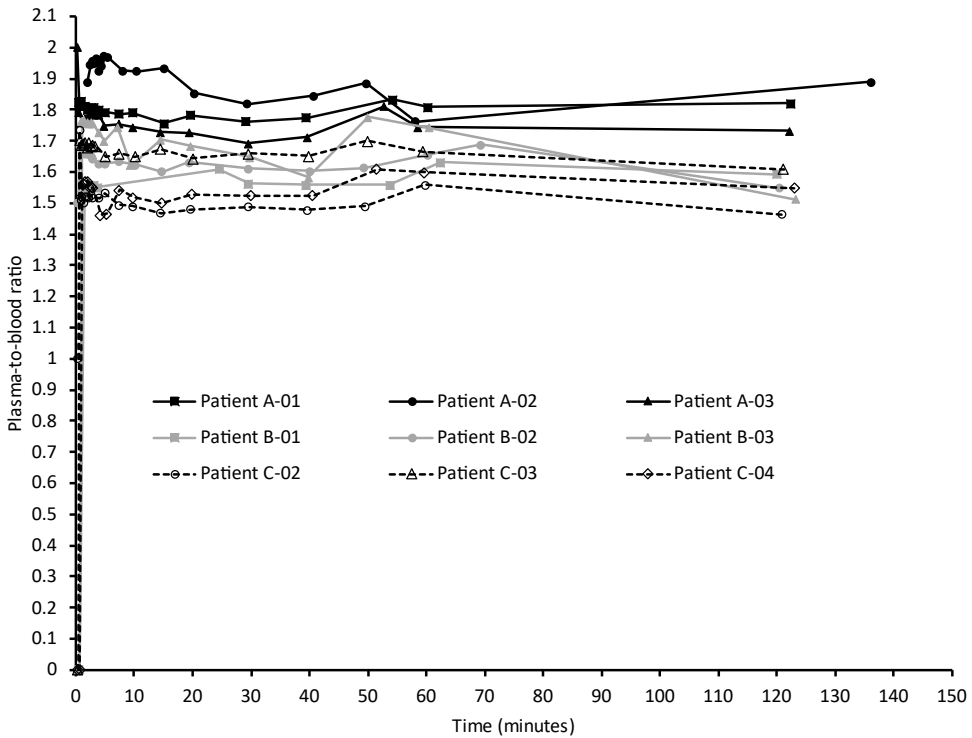


**Figure 16.** Plasma-to-blood ratio of each patient (from original publication I).

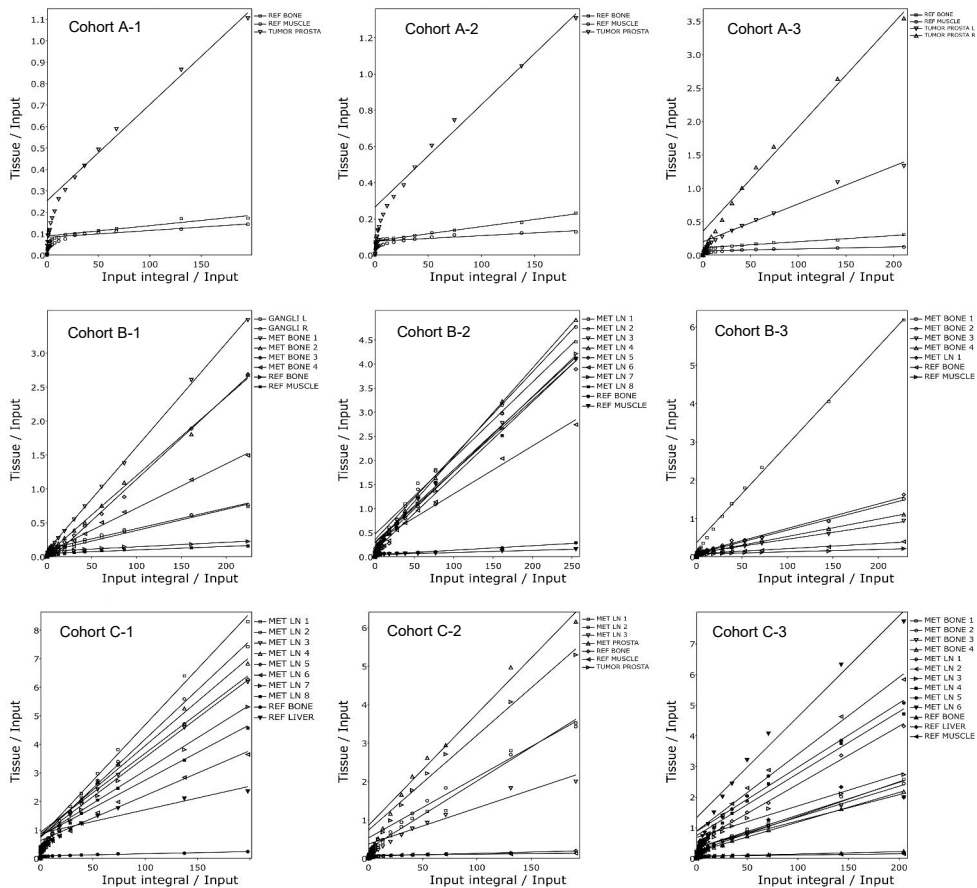


**Figure 17.** Patlak plots from data collected from dynamic and static imaging (118 minutes). Modified from original publication I.

The MTGA for irreversible uptake kinetics (Patlak plot) reached linearity about 10 min post-injection (**Figure 17**). The net influx rate ( $K_i$ ) of the radioligand (calculated as the slope of the linear part of the plot) was clearly higher in the suspected disease lesions than in the reference tissues. The linearity and positive slopes indicate a strong irreversible uptake component. However, downward curvature was also seen in most subjects, especially when the static late scans were included in the plot, which suggests that some reversible component were present at later time points. This will lead to a time-dependent underestimation of the  $K_i$  with the Patlak plot. The MTGA for reversible uptake kinetics (Logan plot) led to almost vertical curves for the suspected disease lesions, with a strong upward curvature. The slopes could not be reliably determined from the high-uptake regions, as data noise leads to even negative slopes in some cases. Therefore, scans could not be reliably analysed using Logan plots. The Patlak plot  $K_i$  was used as a surrogate standard measure to compare

the other results with. The SUVs showed a good correlation with the Patlak Ki values, and the tissue-to-blood ratios also appeared to be well correlated with the Patlak Ki results (**Figure 18**).

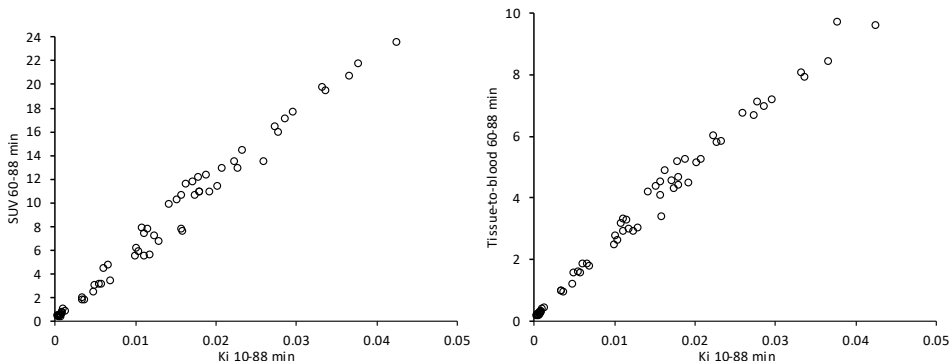


**Figure 18.** Comparison of the Patlak  $K_i$  results with the SUV and tissue-to-blood ratios. Modified from original publication I.

## 5.2 Study II

The primary objective of Study II was to investigate the time-course trend of PSMA uptake in PSMA avid PCa lesions in response to short-term ADT treatment. Nine patients were included in the study. Eight completed all the four [ $^{68}\text{Ga}$ ]PSMA-11 PET/MRI scans, and one patient was scanned only three times due to withdrawal from the study. The patient’s characteristics are presented in **Table 12**. The median age of the patients was 70 years (range: 64-78), and their median serum PSA and serum testosterone at the baseline scan were 25 ng/ml (range: 7-280) and 13 nmol/L (range: 7-26), respectively.

**Table 12.** Patient’s characteristics of Study II (from original publication II).

Patient	Age (years)	PSA, ng/ml	S-Testo, nmol/L	Gleason score	cTNM
1	64	21	26	4+5	T2cN1M1
2	69	25	13	4+5	T3aN0M0
3	69	7	19	5+5	T3aN0M0
4	77	7	7	4+5	T1bN1M1
5	66	280	10	4+5	T2aN0M1
6	71	52	9	5+4	T3aN1M1
7	78	54	23	5+4	T4N1M0
8	70	26	18	5+4	T1bN1M1
9	70	9	12	5+3	T2aN0M0



The median administered activity of [ $^{68}\text{Ga}$ ]PSMA-11 was 154 MBq (range: 124-168) and the PET scans were performed at median of 63 min (range: 58-68) post injection.

At the baseline, before the administration of ADT (degarelix 240 mg), three patients had disease localised in the prostate gland with or without involvement of the seminal vesicles, one had metastases in the regional lymph nodes, and five had distant metastases, two in the extra-regional lymph nodes and three in the bone. After the administration of ADT, all the patients reached castration levels of serum testosterone ( $< 1,7$  nmol/L) within two weeks (**Figure 19**). During the observational period, a continuous decrease of the PSA values occurred, with a mean decrease of 55% (range: 13-90) at two weeks (**Figure 19**).

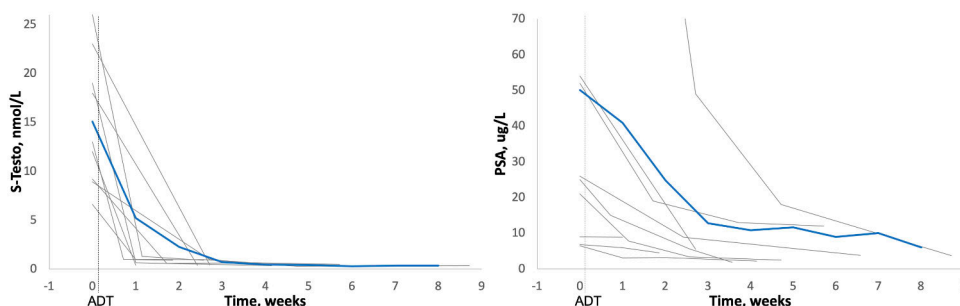


**Figure 19.** Time course trends of serum testosterone and PSA. Grey line, single patient; blue line, mean trend; and dotted line, initiation of androgen deprivation therapy (ADT). Modified from original publication II.

A patient-based overview of the lesions and the time-course trend of the SUVmax at different scanning time points is shown in **Figure 20**. In seven patients, a heterogenous upregulation of the PSMA uptake was observed in the metastatic and/or prostate lesions. In the two remaining patients, the SUVmax had a decreasing trend in all the lesions after ADT. A lesion-based analysis is represented in **Table 13**. In total 16 prostate/seminal vesicles lesions, 16 lymph nodes and 23 bone lesions were included in the analysis. An increase in the SUVmax after ADT was observed in 31%, 44% and 57% of the prostate, lymph node and bone lesions, respectively. The highest increase in the PSMA uptake was observed in the bone lesions, with a mean SUVmax increase of 76% (range 8-238) at a mean time-point of 4 weeks (range 3-9). The respective mean SUVmax increase in the lymph nodes and prostate were 29% and 19%, respectively. Despite the decrease in the SUVmax none of the lesions disappeared during the observational period. Upregulation of the PSMA uptake was also observed in normal organs (**Table 13**), but less evidently than in the PCa lesions. The salivary glands were the organs that showed the highest

upregulation of PSMA uptake with a mean SUVmax increase of 23% (range 5-45) in the parotid gland at a mean time point of 3 weeks (range: 1-6). In the other organs (liver, spleen and kidney) the mean percentage of the SUVmax changes was less than 20%.

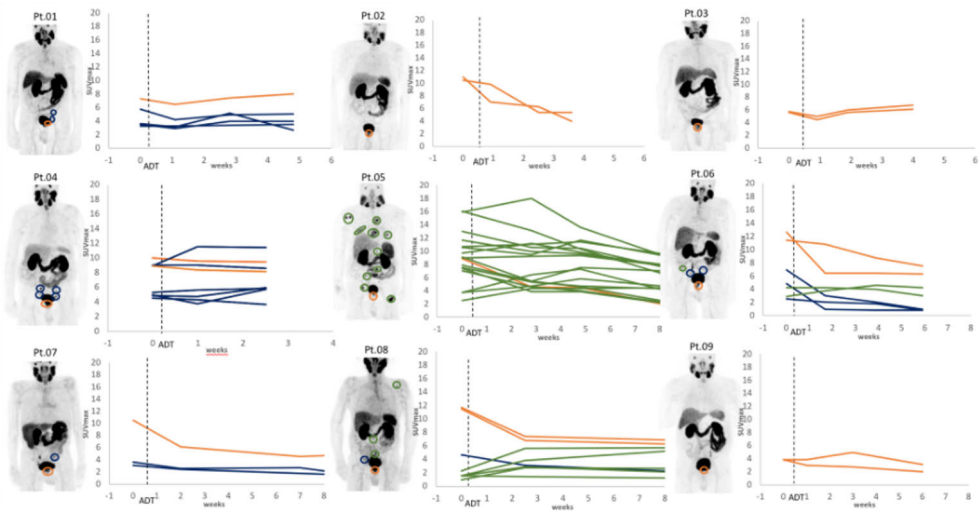


**Figure 20.** Patient-based changes in the SUVmax after the administration of ADT (from original publication II). Orange line, prostate lesions; blue line, lymph node metastases; green lines, bone metastases; dotted vertical line, initiation of androgen deprivation therapy (ADT).

**Table 13.** Maximum increase and maximum decrease in the SUVmax in the prostate, lymph node, bone lesions, and normal PSMA-avid organs (from original publication II).

Lesion/Normal organ	Maximum increase			Maximum decrease		
	n	SUVmax, %; mean (range)	Time point, weeks; mean (range)	n	SUVmax, %; mean (range)	Time point, weeks; mean (range)
Prostate tumour	5	29 (6-84)	4.3 (3.0-4.8)	11	-46 (-64-[-4])	5.8 (1.0-8.6)
Lymph node metastases	7	19 (11-41)	2.7 (1.0-4.8)	9	-48 (-86-[-4])	5.2 (1.1-8.7)
Bone lesions	13	76 (8-238)	4.3 (2.5-8.7)	10	-50 (-77-[-20])	7.7 (2.5-8.7)
Parotid glands	8	23 (5-45)	3.3 (1.1-5.9)	1	-8	3.5
Submandibular glands	8	22 (5-49)	4.1 (1.7-8.5)	1	-14	2.5
Sublingual glands	9	15 (8-22)	2.7 (1.7-4.0)	-	-	-
Liver	9	7 (2-13)	2.8 (0.9-5.9)	-	-	-
Spleen	6	16 (2-36)	4.0 (1.9-8.0)	3	-19 (-6-[-14])	1.6 (0.8-3.0)
Kidneys	8	10 (7-18)	3.6 (0.8-7.0)	1	-19	8.7

In one patient with already known bone metastases new bone uptakes appeared at the second PSMA PET scan with anatomical correspondence detected already at the baseline PSMA PET/CT (**Figure 21**).

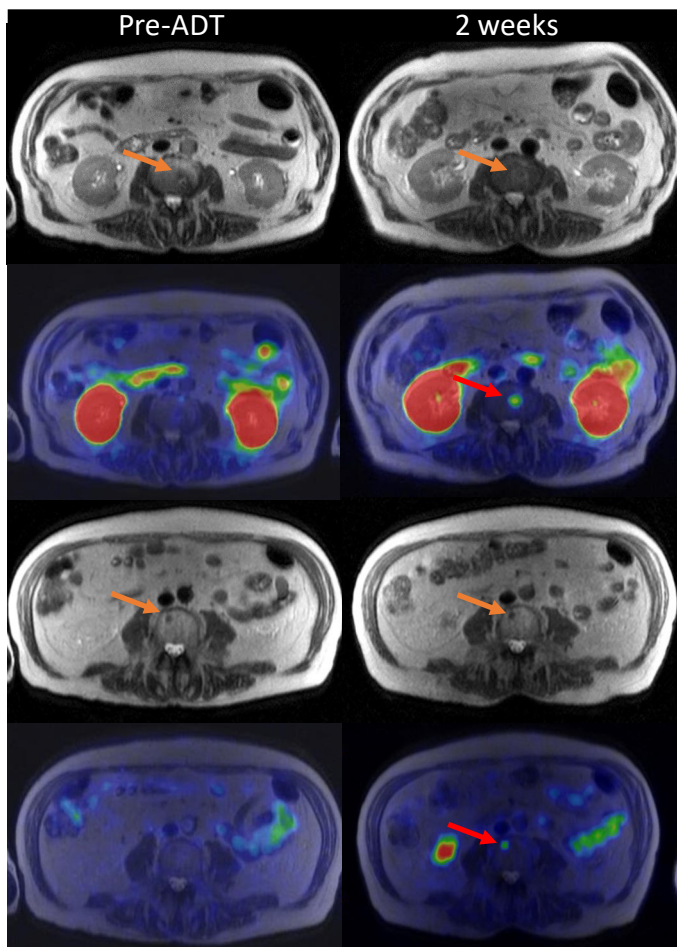


**Figure 21.** MRI and fused PET/MRI images of patient n.ro 8. Two new bone uptakes detected at two weeks post-ADT (red arrows) that presented anatomical correspondence on MRI images (orange arrows).

### 5.3 Study III

The primary objective of Study III was to assess the flare of the PSMA uptake in PCa lesions after the administration of ADT and its correlation with glucose metabolism. The study included 25 patients, all of whom completed all the PET scans. The patients' demographics are presented in **Table 14**.

**Table 14.** Patient's characteristics of Study III (from original publication III).

<b>Age</b>	<b>Median (IQR; range)</b>
Years	74 (70–78; 63–84)
<b>PSA at baseline</b>	<b>Median (IQR; range)</b>
ng/ml	49 (33–140; 15–5000)
<b>S-testo at baseline</b>	<b>Median (IQR; range)</b>
nmol/L	12 (7–17; 2–27)
<b>Biopsy GGG<sup>a</sup></b>	<b>n (%)</b>
1	0 (0)
2	0 (0)
3	3 (12)
4	4 (16)
5	18 (72)
<b>Clinical T-category</b>	<b>n (%)</b>
cT1	0 (0)
cT2	2 (8)
cT3	19 (76)
cT4	4 (16)

The median age was 74 (IQR 70-78; range: 63-84), the median serum PSA at the time of the baseline PSMA PET/CT scan was 49 ng/ml (IQR 33-140; range: 15-5000) and the median serum testosterone levels was 12 nmol/L (IQR 7-17; range 2-27). All the patients reached castration testosterone levels (< 1.7 nmol/L) within the time of the second PSMA PET/CT scan, which was performed at a median of 27 days (IQR 21-30; range: 20-33) after the administration of ADT (degarelix 240 mg). The median administered activity of [<sup>18</sup>F]-PSMA-1007 was 255 MBq (IQR 251-259; range: 241-278), and the respective median activity of [<sup>18</sup>F]-FDG was 368 MBq (IQR 333-381; range: 278-398). The serum PSA decreased in all the patients at three to four weeks after ADT administration, with a median decrease of 87% (IQR 81-92; range 32-99).

All the patients had pathological uptake in the prostate, and 10 patients had PSMA uptake in the seminal vesicles. All the patients had pathologically PSMA-positive lymph nodes in the pelvis. Among the distant metastases, nine patients had bone + extraregional lymph node metastases (retroperitoneal and mediastinal), two had bone, lymph nodes and lung metastases, one patient had only extraregional lymph node metastases and the remaining 13 patients had metastases only in the bone. An overview of the PCa lesions and the respective SUVmax value at the baseline [<sup>18</sup>F]-PSMA-1007 PET/CT is shown in **Figure 22**. In all the men, a heterogeneous upregulation of the PSMA uptake was observed, in either the prostate, lymph nodes or bone metastases, with considerable intra-patient variability (**Figure 23**).

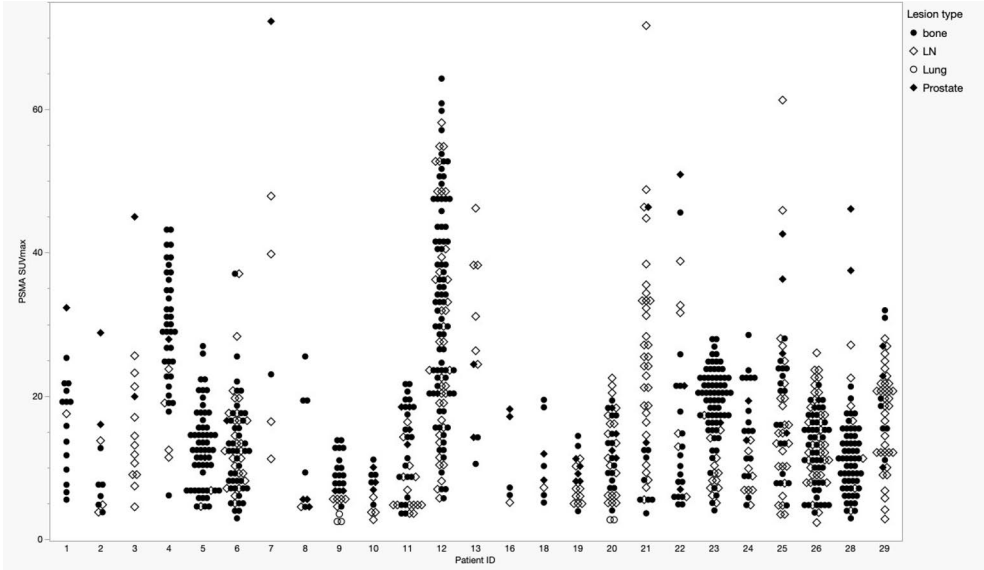


Figure 22. Baseline PSMA SUVmax of the PCa lesions at the patient level (from original publication III).

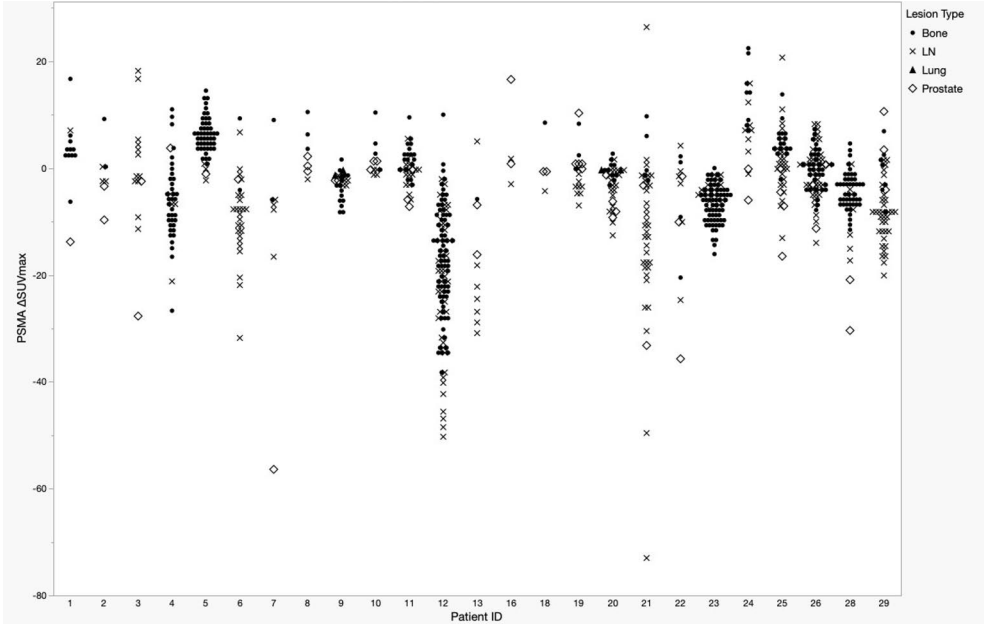


Figure 23. Changes in the PSMA uptake after ADT administration ( $\Delta$ SUVmax) in the PCa lesions at the patient level (from original publication III).

In total, 57 prostate, 314 LN and 406 bone lesions were analysed. The results of the lesion-based analysis are presented in **Table 15**. A flare in the PSMA uptake was observed in 26% of the bone metastases ( $\Delta$ SUVmax of +50%, IQR 32-72; range 20-161), and the respective percentages for the lymph node metastases and the prostate lesions were 11% ( $\Delta$ SUVmax +60%, IQR 32-114; range: 20-222) and 11% ( $\Delta$ SUVmax 45%, IQR 20-106; range: 23-134), respectively. All the remaining lesions showed either no change ( $\pm$  20%) or decrease in the PSMA uptake. Nevertheless, none of the lesions disappeared (uptake below the blood pool) in the second PSMA PET scan.

At the baseline, among the PSMA-positive lesions, 27 (47%) prostate, 144 (46%) lymph node, 254 (63%) bone and 3 (60%) lung lesions were positive on the [ $^{18}$ F]FDG PET/CT. In the lymph node metastases and, more evidently, in the bone metastases, a significant positive correlation was observed between the intensity of the baseline PSMA SUVmax and the FDG SUVmax (**Figure 24**). This correlation suggests that the intensity of the PSMA uptake is linked to the aggressiveness of the metastases. Moreover, a negative correlation was observed between the intensity of the FDG uptake (SUVmax) and the changes in the PSMA uptake after ADT ( $\Delta$ SUVmax) (**Figure 25**), which suggests that the PSMA flare is linked to less aggressive metastases. The prostate lesions did not show significant correlations with the FDG uptake.

The correlation between the PSMA  $\Delta$ SUVmax and the changes in the serum PSA ( $\Delta$ PSA) is shown in **Figure 26**. The results showed a negative correlation among metastatic lesions ( $p < 0.001$ ), which indicates that the PSMA flare phenomenon was less evident in the patients who experienced a rapid decrease in their serum PSA. In 10 patients, who already had bone metastases at the baseline, new uptakes (that were not included in the analysis) appeared in the second PSMA PET/CT scan in response to the ADT treatment (median SUVmax 5; IQR 5-10; range 4-18). An example is illustrated in **Figure 27**.

**Table 15.** Changes in the PSMA uptake after ADT administration (from original publication III).

Lesion type	Lesions (n) at baseline PSMA PET	Increase ( $\geq 20\%$ ) of PSMA uptake, n (%)	$\Delta$ SUVmax%, median (IQR; range)	No change/Decrease ( $< 20\%$ ) of PSMA uptake, n (%)	$\Delta$ SUVmax% median (IQR; range)
Prostate	57	6 (11%)	+45% (20–106; 23–134)	49 (89%)	-28% (-45–7; -78–14)
Lymph nodes	314	33 (11%)	+60% (32–114; 20–222)	281 (89%)	-51% (-74–21; -99–9)
Bone	406	104 (26%)	+50% (32–72; 20–161)	302 (74%)	-33% (-53–15; -90–14)
Visceral (Lung)	5	-	-	5 (100%)	-40% (-49–22; -53–16)

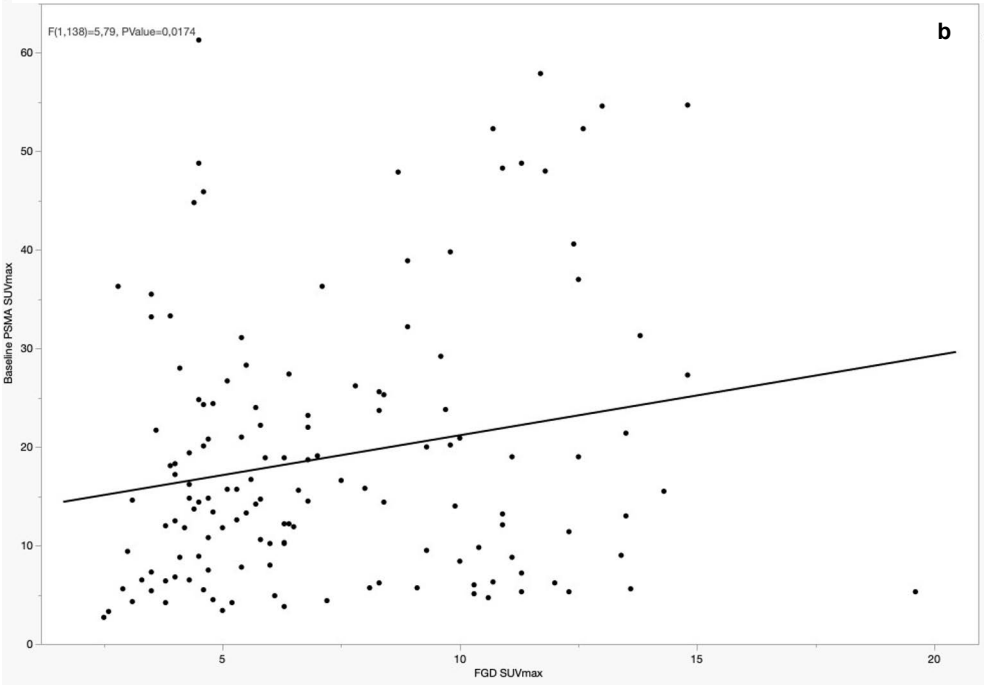
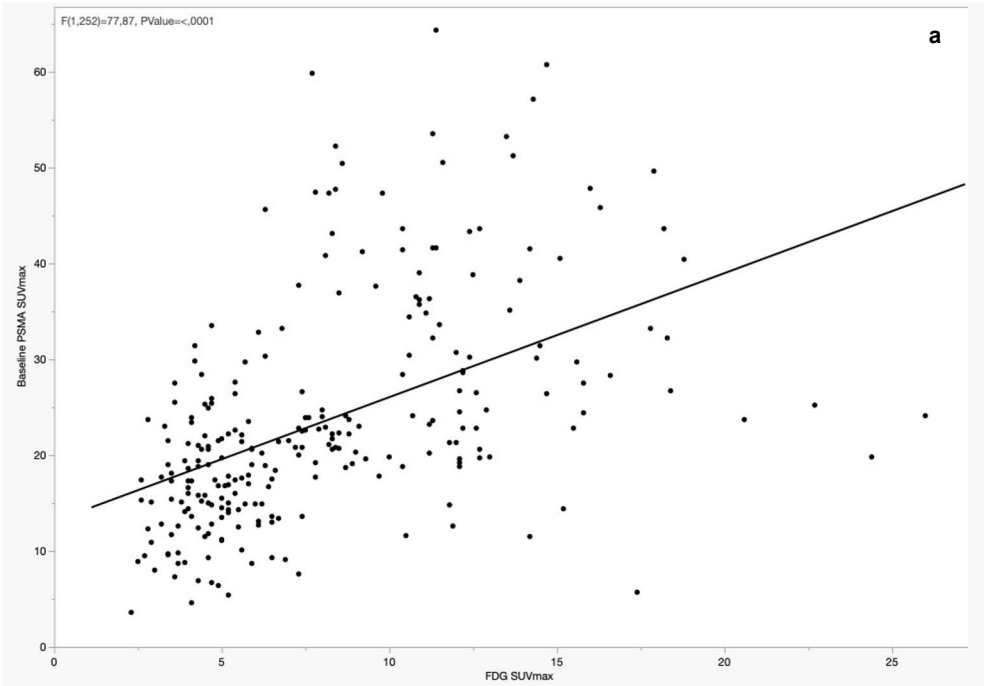


**Figure 24.** Correlation between the baseline PSMA SUVmax and the FDG SUVmax in the bone lesions (a) and the lymph node metastases (b). Modified from original publication III.



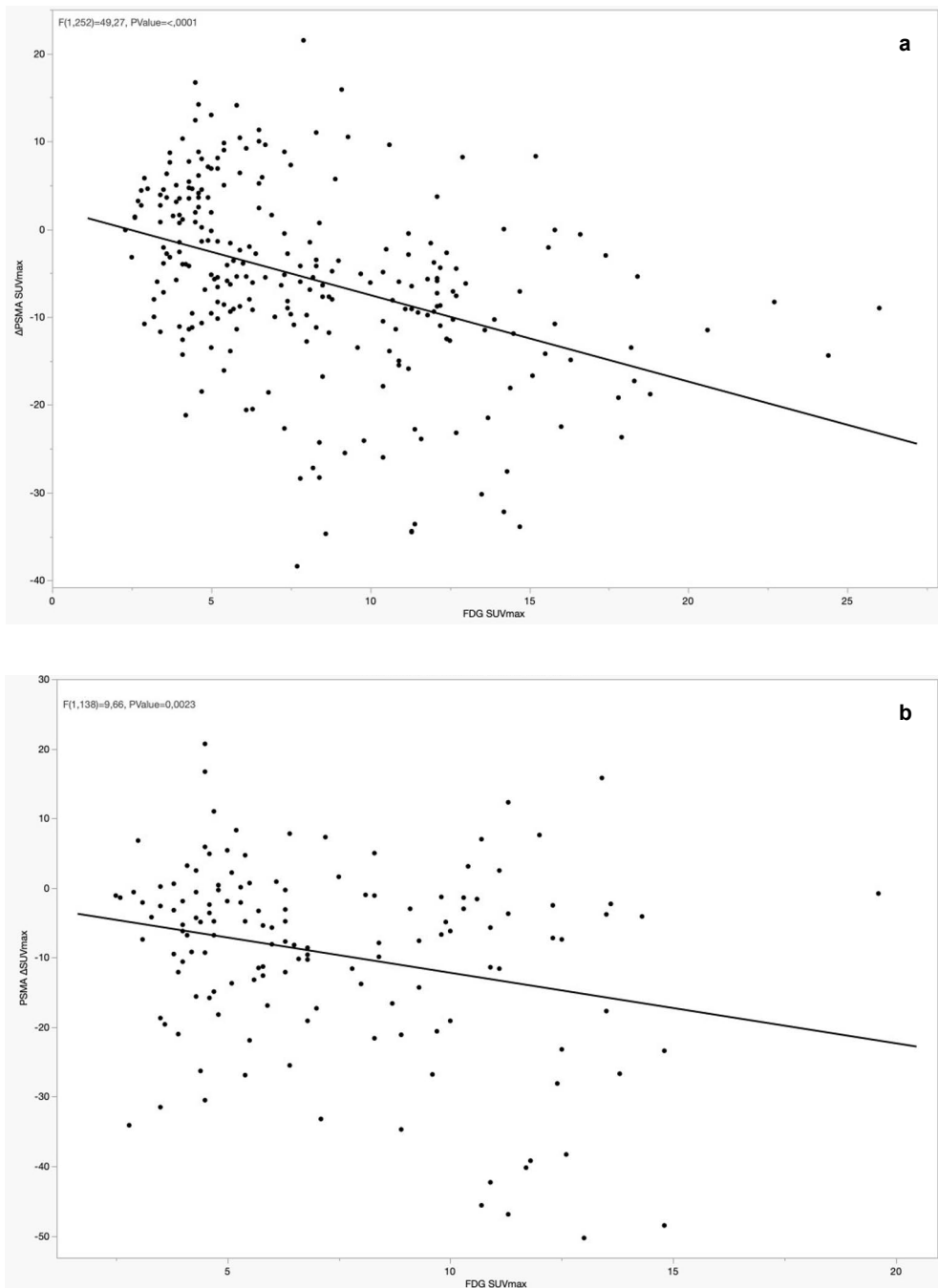


**Figure 25.** Correlation between the PSMA  $\Delta$ SUVmax and the FDG SUVmax in the bone lesions (a) and the lymph node metastases (b). Modified from original publication III.

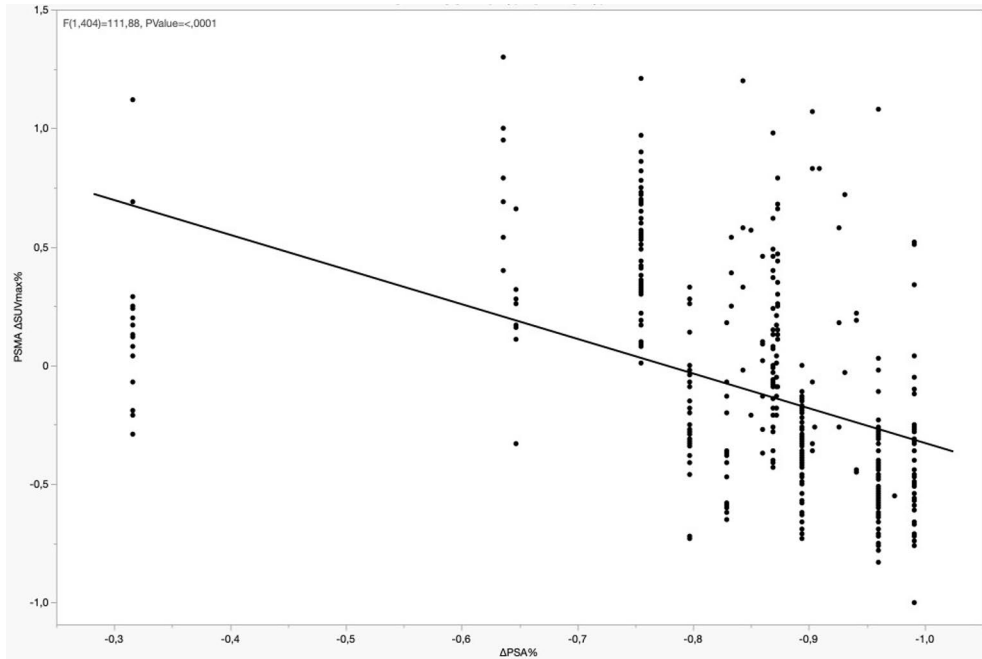


**Figure 26.** Correlation between the PSMA  $\Delta$ SUVmax and  $\Delta$ PSA in the bone lesions (from original publication III).

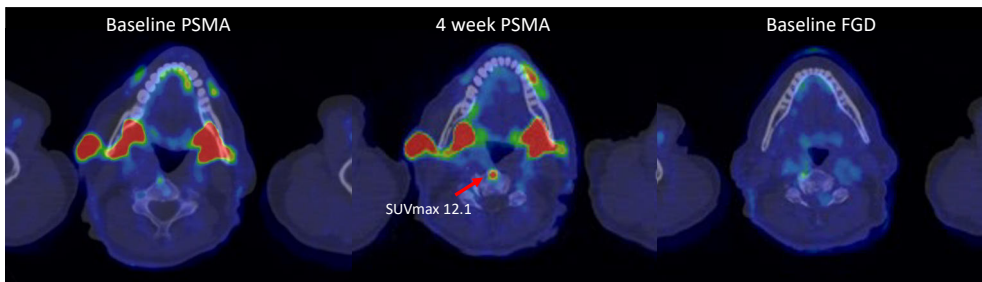


**Figure 27.** New bone uptake on the C3 vertebra detected in the [ $^{18}\text{F}$ ]PSMA-1007 PSMA PET/CT four weeks after ADT administration. The uptake was not seen in the baseline [ $^{18}\text{F}$ ]PSMA and [ $^{18}\text{F}$ ]FDG PET/CT scans.

## 5.4 Study IV

The primary objective of Study IV was to compare the diagnostic performance of [ $^{18}\text{F}$ ]-PSMA-1007 PET/CT, WBMRI and CT in the primary nodal staging of patients with unfavourable intermediate- or high-risk PCa. Seventy-nine patients were included in the study. The patient's characteristics are shown in **Table 16**.

**Table 16.** Patient's characteristics of Study IV (from original publication IV).

<b>Age</b>	<b>median ([IQR] range)</b>
years	72 ([66-77] 52-87)
<b>PSA</b>	<b>median ([IQR] range)</b>
ng/ml	12 ([7-23] 3-2000)
<b>Clinical T-category<sup>a</sup></b>	<b>n (%)</b>
cT1	7 (11)
cT2	37 (46)
cT3	27 (33)
cT4	8 (10)
<b>Biopsy GGG</b>	<b>n (%)</b>
1 <sup>b</sup>	3 (4)
2	1 (1)
3	29 (37)
4	13 (16)
5	33 (42)

<sup>a</sup> Clinical T-category was determined based on transrectal ultrasound and digital rectal examination before any imaging.

<sup>b</sup> All patients with GGG 1 had PSA >20 ng/ml.

GGG: Gleason Grade Group

All the patients completed all the imaging modalities, except for one patient who, due to claustrophobia, did not complete the WBMRI scan. Seventeen patients (22%) were treated surgically with RALP and PLND. For those who were not treated with surgery (n=62), pelvic follow-up imaging was performed in 56/62 (90%) patients: CT in 15 patients, MRI with DWI in 31 patients and [<sup>18</sup>F]-PSMA-1007 PET/CT in 10 patients. The median follow-up period was 21 months (IQR 19-25; range: 16-29). The median age was 72 years (IQR 66-77; range: 52-87) and the median PSA was 12 (IQR 7-23; range: 3-2000). The median interval between the first and last imaging was 8 days (IQR 6-12; range: 1-44). The median administered activity of [<sup>18</sup>F]-PSMA-1007 was 250 MBq (IQR 246-256; range 206-279), and the PET/CT scans were acquired at a median of 60 min (IQR 60-60; range 59-63) from tracer injection. According to the EAU risk group classification, 17/79 (22%) patients belonged to the unfavourable intermediate group and the rest (62/79, 78%) to the high-risk group. According to the ground truth, 41 patients had a localised disease, 18 had pelvic lymph node metastases and 20 had distant metastatic disease, of which 13/20 also had metastases in the regional lymph nodes. Overall, 31 patients (39%) had metastases in the pelvic lymph nodes. In 8/31 (26%) patients, pelvic lymph node metastases were detected only by [<sup>18</sup>F]-PSMA-1007 PET/CT, while both CT and WBMRI were reported as negative. The sensitivity, specificity, accuracy, positive and negative predictive values (PPV and NPV) in the optimistic and pessimistic analysis at the patient level are reported in **Table 17**.

**Table 17.** Sensitivity, specificity, accuracy, PPV and NPV of both readers of each imaging modality in pessimistic and optimistic analysis at the patient level (modified from original publication IV). (a) statistically significant difference ( $p < 0.05$ ) compared to [ $^{18}\text{F}$ ]-PSMA-1007 PET/CT reader 1 (b) statistically significant difference ( $p < 0.05$ ) compared to [ $^{18}\text{F}$ ]-PSMA-1007 PET/CT reader 2.

Imaging modality	Reader	Pessimistic analysis					Optimistic analysis				
		Sensitivity (95%CI)	Specificity (95%CI)	Accuracy (95%CI)	PPV	NPV	Sensitivity (95%CI)	Specificity (95%CI)	Accuracy (95%CI)	PPV	NPV
CT	1	0.39 (0.24-0.56) <sup>a,b</sup>	0.94 (0.83-0.98)	0.72 (0.61-0.80) <sup>a,b</sup>	0.80 (0.51-0.95)	0.70 (0.57-0.80) <sup>a,b</sup>	0.16 (0.07-0.32) <sup>a,b</sup>	1.00 (0.93-1.00)	0.67 (0.56-0.76) <sup>a,b</sup>	1 (0.46-1)	0.64 (0.53-0.75) <sup>a,b</sup>
	2	0.32 (0.19-0.50) <sup>a,b</sup>	0.94 (0.83-0.98)	0.70 (0.59-0.79) <sup>a,b</sup>	0.77 (0.46-0.94)	0.68 (0.55-0.79) <sup>a,b</sup>	0.26 (0.14-0.43) <sup>a,b</sup>	0.98 (0.89-0.99)	0.70 (0.59-0.79) <sup>a,b</sup>	0.89 (0.50-0.99)	0.67 (0.50-0.78) <sup>a,b</sup>
WBMRI with DWI	1	0.40 (0.25-0.58) <sup>a,b</sup>	0.96 (0.86-0.99)	0.74 (0.63-0.83) <sup>a,b</sup>	0.68 (0.56-0.97)	0.71 (0.58-0.82) <sup>a,b</sup>	0.37 (0.22-0.55) <sup>a,b</sup>	0.98 (0.89-1.00)	0.74 (0.63-0.83) <sup>a,b</sup>	0.92 (0.60-0.99)	0.70 (0.58-0.81) <sup>a,b</sup>
	2	0.50 (0.33-0.67) <sup>a,b</sup>	0.91 (0.80-0.97)	0.75 (0.65-0.84) <sup>a,b</sup>	0.79 (0.54-0.93)	0.74 (0.60-0.84) <sup>a,b</sup>	0.37 (0.22-0.55) <sup>a,b</sup>	0.98 (0.89-1.00)	0.74 (0.63-0.83) <sup>a,b</sup>	0.92 (0.60-0.99)	0.70 (0.58-0.81) <sup>a,b</sup>
[ $^{18}\text{F}$ ]-PSMA-1007 PET/CT	1	0.84 (0.67-0.93)	0.96 (0.86-0.99)	0.91 (0.83-0.96)	0.93 (0.75-0.99)	0.90 (0.78-0.96)	0.77 (0.60-0.89)	0.98 (0.89-1.00)	0.90 (0.81-0.95)	0.96 (0.78-0.99)	0.87 (0.74-0.94)
	2	0.90 (0.75-0.97)	0.94 (0.83-0.98)	0.93 (0.85-0.96)	0.90 (0.73-0.97)	0.94 (0.82-0.98)	0.87 (0.71-0.95)	0.96 (0.86-0.99)	0.92 (0.84-0.96)	0.93 (0.76-0.99)	0.92 (0.80-0.97)

CT, computed tomography; WBMRI, whole-body magnetic resonance imaging; DWI, diffusion-weighted imaging; [ $^{18}\text{F}$ ]-PSMA-1007 PET/CT, prostate specific membrane antigen positron emission tomography-CT.

[<sup>18</sup>F]-PSMA-1007 PET/CT was significantly superior to WBMRI with DWI and CT in sensitivity, accuracy and NPV, while maintaining high specificity and PPV. The inter-reader agreement for [<sup>18</sup>F]-PSMA-1007 PET/CT at the patient-level was superior to that for the other imaging modalities (**Table 18**)

**Table 18.** Inter-reader agreement in optimistic and pessimistic analysis at the patient level (from original publication IV).

	<b>Kappa (95%CI) optimistic</b>	<b>Kappa (95%CI) pessimistic</b>
<b>CT</b>	0.69 (0.41-0.97)	0.51 (0.27-0.75)
<b>WBMRI with DWI</b>	0.47 (0.21-0.74)	0.40 (0.17-0.63)
<b>[<sup>18</sup>F]-PSMA-1007 PET/CT</b>	0.89 (0.78-0.99)	0.86 (0.75-0.98)

CT, computed tomography; WBMRI, whole-body magnetic resonance imaging; DWI, diffusion-weighted imaging; <sup>18</sup>F-PSMA-1007 PET/CT, prostate specific membrane antigen positron emission tomography-CT.

At the lesion-level, 206 lymph nodes were interpreted as malignant (the reference standard diagnosis). The number of true positive, false positive and false negative lesions for each imaging modality and reader are shown in **Table 19**. The detection rate of lymph node metastases by [<sup>18</sup>F]-PSMA-1007 PET/CT was 83%, compared to 58% by WBMRI with DWI and 52% by CT. The detection rates for each imaging modality and reader in the group of patients that underwent PLND is shown in **Table 20**.

**Table 19.** The total number of reported lesions by both readers of each imaging modality and their concordance with the reference standard diagnosis at the lesion level in all the patients (from original publication IV).

Imaging modality	Reader	Number of positive lesions reported	Number of true positive lesions	Detection rate of true positive lesions	Number of false positive lesions	Number of false negative lesions	Number of equivocal lesions reported
CT	1	52	52	25%	0	154	36
	2	146	107	52%	39	99	12
WBMRI with DWI	1	93	91	44%	2	110	1
	2	179	120	58%	59	81	9
<sup>18</sup> F-PSMA-1007 PET/CT	1	178	170	83%	8	36	4
	2	156	144	70%	12	62	1

CT, computed tomography; WBMRI, whole-body magnetic resonance imaging; DWI, diffusion-weighted imaging; <sup>18</sup>F-PSMA-1007 PET/CT, prostate specific membrane antigen positron emission tomography-CT.

**Table 20.** The total number of reported lesions by both readers of each imaging modality and their concordance with the reference standard diagnosis at lesion level in patients (n=17) that underwent PLND (from original publication IV).

Imaging modality	Reader	Number of positive lesions reported	Number of true positive lesions	Detection rate of true positive lesions	Number of false positive lesions	Number of false negative lesions	Number of equivocal lesions reported
CT	1	0	0	0%	0	15	1
	2	0	0	0%	0	15	0
WBMRI with DWI	1	0	0	0%	0	15	1
	2	2	1	7%	1	14	0
<sup>18</sup> F-PSMA-1007 PET/CT	1	4	3	20%	1	12	2
	2	7	5	27%	2	10	0

CT, computed tomography; WBMRI, whole-body magnetic resonance imaging; DWI, diffusion-weighted imaging; <sup>18</sup>F-PSMA-1007 PET/CT, prostate specific membrane antigen positron emission tomography-CT.

Out of all the metastatic lesions detected by [<sup>18</sup>F]-PSMA 1007 PET/CT, 126/170 (74%) were smaller than the anatomical cut-off value of 8 mm, of which 90 lymph nodes had a short diameter between 5 and 8 mm and 36 lymph nodes had a short diameter < 5 mm (**Figure 28**). Of those 17 patients who were treated surgically with RALP and PLND, five had pelvic lymph node metastases. [<sup>18</sup>F]-PSMA-1007 PET/CT was concordant with the histopathology in 14/17 (82%) patients, and the corresponding numbers for WBMRI with DWI and CT were 12/17 (71%) and 11/17 (65%), respectively. Out of the five patients with histologically confirmed metastases, the metastases of three patients were detected by [<sup>18</sup>F]-PSMA PET/CT (an example is illustrated in **Figure 29**) but it failed to detect lymph node metastases in two patients (an example is shown in **Figure 30**).

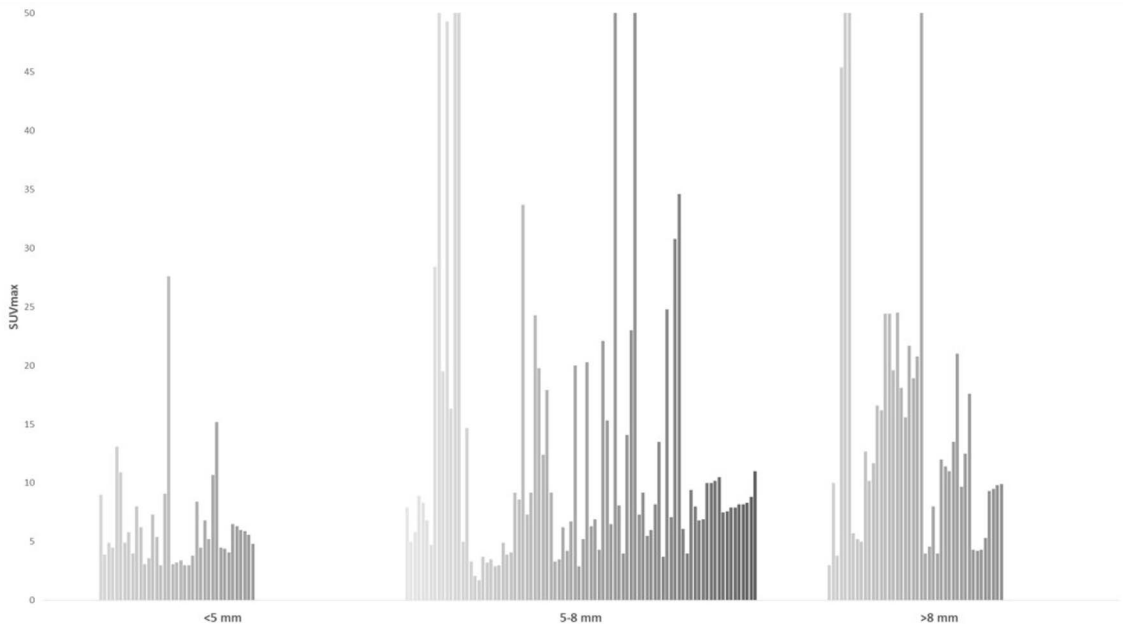


**Figure 28.** SUVmax values of metastatic lymph nodes (reference standard) divided according to lymph node short diameter (from original publication VI). The analysis of Reader 1 (with a higher detection rate) is presented.

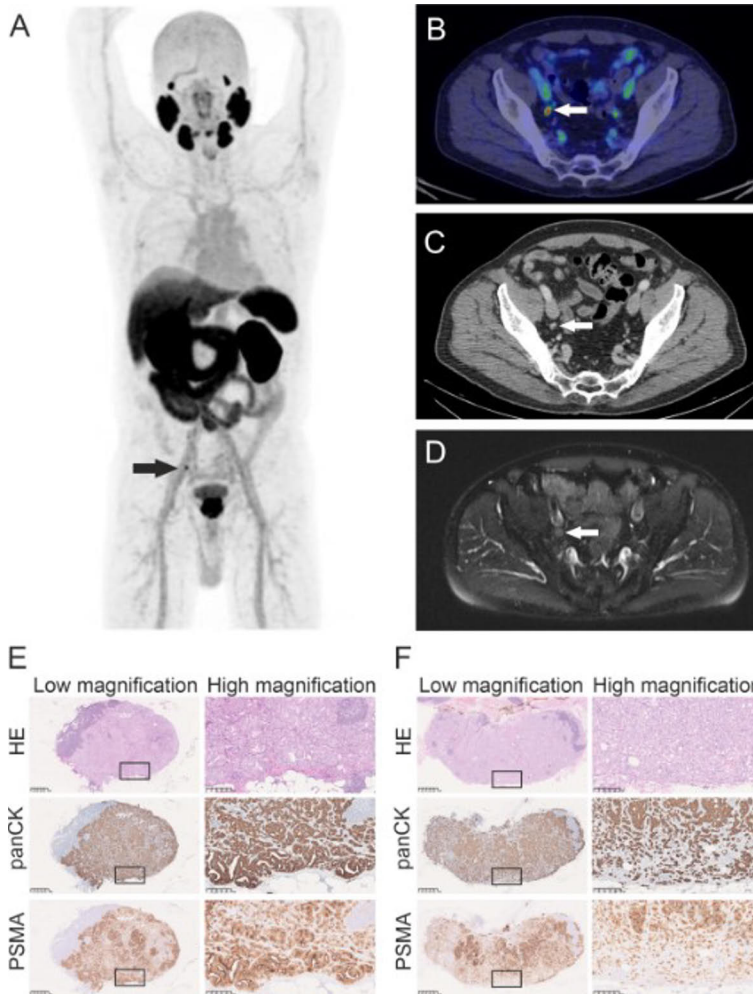


**Figure 29.** Imaging and histopathological findings of patient n. 48 (from original publication IV). [ $^{18}\text{F}$ ]-PSMA-1007 PET/CT clearly identified one pelvic lymph node metastasis (short diameter: 6 mm) on the right (**a-b**) which was retrospectively identified by CT (**c**) and WBMRI (**d**). The histopathological examination confirmed one lymph node metastasis on the right (maximum diameter 7 mm) with intense PSMA and pan-cytokeratin staining in the immunohistochemistry (**e**). On the other hand, [ $^{18}\text{F}$ ]-PSMA-1007 PET/CT did not detect another lymph node metastasis found in the histopathological examination on the left (maximum diameter 8,5 mm, **f**). This lymph node showed less intense immunohistochemical PSMA staining when that than on the right.



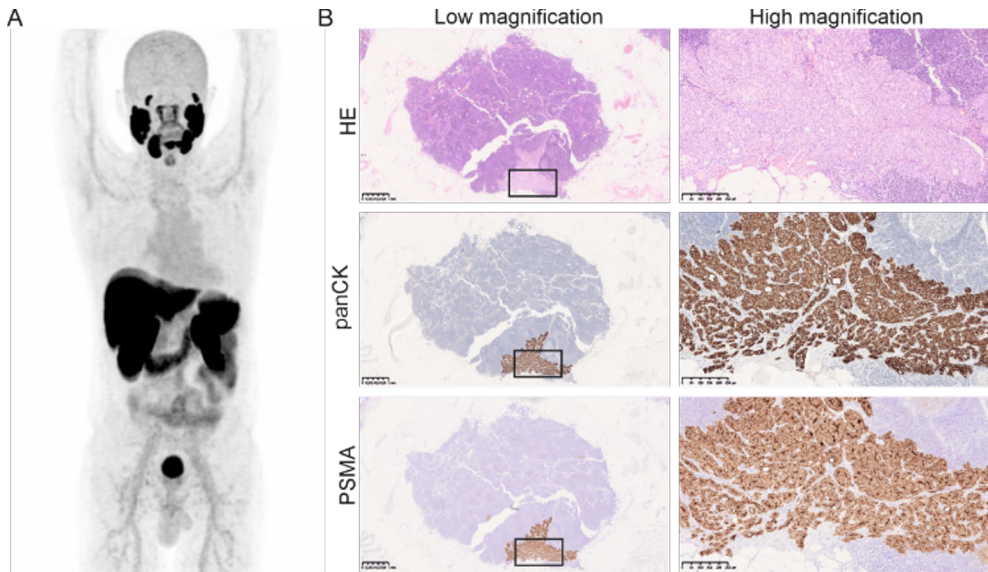


**Figure 30.** Imaging and histopathological findings of patient n. 44 (from original publication VI). [ $^{18}\text{F}$ ]-PSMA-1007 PET/CT (**a**) failed to detect one lymph node metastasis with maximum diameter of 2,5 mm in the histopathological specimens (**b**), although the lymph node showed intense PSMA staining in the immunohistochemistry.

## 6 Discussion

### 6.1 Biodistribution and kinetics of novel rh-PSMA-3.7 tracer

Study I was a prospective Phase I study that assessed the uptake kinetics of [ $^{18}\text{F}$ ]-rhPSMA-7.3 in nine patients with PCa in order to optimise its use for PET/CT imaging. [ $^{18}\text{F}$ ]-rhPSMA-7.3 has been investigated as part of this same trial in healthy volunteers, in which it demonstrated favourable safety, biodistribution and radiation dosimetry (Tolvanen et al. 2021).

We observed high uptake in PCa lesions within the first hour and increases in the tissue radioactivity concentration and the lesion-to-reference ratios at least until the end of the scanning sessions (118 min post-injection). This might suggest that later time points could provide more optimal imaging, as it has been previously demonstrated for other PSMA tracers (Afshar-Oromieh et al. 2013, 2015; Giesel et al. 2017; Rahbar et al. 2018). However, according to the results of our study, the increases were not substantial after the first whole-body scan. Therefore, considering logistical reasons for the diagnostic use of [ $^{18}\text{F}$ ]-rhPSMA-7.3 PET in clinical practice, the optimal time for the assessment of both prostate tumours and metastatic lesions is between 60 min and 90 min post-injection, and 60 min can be considered the optimal time for commencing the PET scan. In contrast with the aforementioned studies with other PSMA tracers, we did not evaluate later time points ( $> 2$  h post injection) in this study. This might be a limitation, as this information could be useful in a radiometabolic treatment setting. However, this study was designed primarily to investigate the uptake kinetics of rhPSMA 7.3 specifically to optimise its diagnostic use.

The radioactivity concentrations in the blood decreased rapidly after [ $^{18}\text{F}$ ]-rhPSMA-7.3 administration as [ $^{18}\text{F}$ ]-rhPSMA-7.3 was distributed in the blood pool and in the reference tissues. Our data showed that the plasma-to-blood ratio remained constant over the scanning period and at a level that implied that [ $^{18}\text{F}$ ]-rhPSMA-7.3 remains in blood plasma and does not enter the red blood cells during the relevant time period after injection. As demonstrated by our previous studies with [ $^{18}\text{F}$ ]-FDG (Eskelinen et al. 2015; Minn et al. 1995), combining venous sampling and image-based arterial or venous estimates as input functions for the TACs is a useful technique in kinetic studies. In this study, combining venous blood sampling data

with initial arterial data from a blood pool in the PET images we improved the otherwise underestimated initial phase of the plasma TACs. Generally, if a blood pool of sufficiently high quality can be identified from PET images, then venous sampling can be replaced with a blood pool-derived estimation from the PET image, thus eliminating the need for blood sampling for radioactivity analyses.

The general increase in the tissue-to-blood ratios with time suggests a significant irreversible uptake component. The MTGA data further confirmed this; the Patlak plots suggested that [ $^{18}\text{F}$ ]-rhPSMA-7.3 uptake kinetics in lesions and relevant reference tissues are dominated by irreversible components, but some reversible components were also present. This is as expected for a radiotracer that can bind reversibly to its specific target molecule on cell membranes but can also be internalised into cells, and possibly slowly recirculated back to the cell surface. The downward curvature of the Patlak plot leads to  $K_i$  estimates that are dependent on the scan duration and on the selection of the time range used for the slope estimation from the plot. If the uptake kinetics were fully irreversible during the PET scan, the Patlak slope would have been time-independent after an initial equilibration period. This would be a considerable advantage over the SUV and ratio methods, which can provide only time-dependent measures. Therefore, the curvature of the plots prevents a bias-free, scan duration-independent assessment of the slope (the net influx rate  $K_i$  in the case of Patlak plots). Thus, a longer and more laborious dynamic PET protocol with blood sampling may not offer such quantitative advantages over the simpler SUV and ratio methods.

Since Patlak  $K_i$  estimates are dependent on the selected line fit time range, the results are reported from different time frames. The decreases over time suggest that extending the PET scan duration beyond 90 min may not improve the detectability of lesions, and may even do the opposite, if Patlak analyses are used. Taken all together, the different analyses presented here provided concordant results. The findings indicate that simplified measures of [ $^{18}\text{F}$ ]-rhPSMA-7.3 PET uptake are sufficient, thereby eliminating the need for dynamic PET scans and/or blood sampling.

The static PET scans at 60 min were further analysed to assess lesion detectability and the results were presented in a different publication (Malaspina et al. 2022). Despite the presentation of mainly descriptive results, [ $^{18}\text{F}$ ]-rhPSMA-7.3 showed a good detection of both primary and metastatic PCa lesions with no significant interference from bladder activity. In particular, the [ $^{18}\text{F}$ ]-rhPSMA-7.3 findings on the patients referred for radical prostatectomy (Cohort A) were correlated with the histopathology including PSMA staining, and showed good accuracy in detecting intraprostatic lesions with ISUP grade  $\geq 3$  (Malaspina et al. 2022).

Based on our results and the data in the literature, rhPSMA-7.3 appears to be a promising ligand for diagnosis and potentially treatment of PCa, with its possible strengths and limitations over other PSMA agents (**Table 21**).

**Table 21.** Advantages and disadvantages of rhPSMA over other PSMA agents.

Advantages
rhPSMA can be labelled to both diagnostic ( $^{18}\text{F}$ ) and therapeutic (alfa- and beta-emitters) isotopes (true theranostic pair)
$^{18}\text{F}$ -rhPSMA has longer half-life than $^{68}\text{Ga}$ -PSMA, which can allow a central production
$^{18}\text{F}$ -rhPSMA has lower positron range than $^{68}\text{Ga}$ -PSMA, which results in higher image contrast and resolution
$^{18}\text{F}$ -rhPSMA has lower uptake in the urinary bladder than $^{68}\text{Ga}$ -PSMA
$^{177}\text{Lu}$ -rhPSMA has favourable dosimetry and tumour retention compared to $^{177}\text{Lu}$ PSM I&T <sup>a</sup>
Disadvantages
$^{18}\text{F}$ -rhPSMA has possibly a higher incidence of non-specific uptakes compared to $^{68}\text{Ga}$ -PSMA <sup>b</sup>
$^{18}\text{F}$ -rhPSMA has higher uptake in the urinary bladder than $^{18}\text{F}$ -PSMA-1007

<sup>a</sup> Feurecker et al. 2022 <sup>b</sup> Kroenke et al. 2020

## 6.2 Physiology of PSMA expression in relation to ADT

Studies II and III prospectively investigated the changes in PSMA uptake after short-term ADT. Our pilot study on nine treatment-naïve PCa patients demonstrated a heterogeneous transient increase in the PSMA expression using [ $^{68}\text{Ga}$ ]-PSMA PET/MRI. This was most evidently seen at three to four weeks after the initiation of the treatment, especially in the bone metastases. This phenomenon was confirmed in our larger cohort of treatment-naïve metastatic PCa patients (Study III) and, interestingly, it was negatively correlated with the FDG uptake, which suggests that the PSMA flare phenomenon in patients with hormone-sensitive PCa seems to be linked to less aggressive disease.

The upregulation of the PSMA expression by short-term ADT has been already demonstrated by preclinical studies on cell lines or animal models (Bakht et al. 2017; Meller et al. 2015; Wright et al. 1996). The PSMA flare phenomenon was successively confirmed in a few clinical studies on small patient cohorts (Aggarwal et al. 2018; Emmett et al. 2019). Aggarwal et al. demonstrated a heterogeneous increase in the SUVmax in eight patients, scanned with [ $^{68}\text{Ga}$ ]-PSMA-11 PET before and after the initiation of ADT within a variable period of two to four weeks. The SUVmax increased in 68% and in 41% of the lesions in hormone-sensitive men (n=4) and in castration-resistant men (n=4), respectively. The other study, conducted by Emmet et al., also included both hormone-sensitive (n=8) and castration-resistant men (n=7). Although in that study the increase was more evidently seen in castration-resistant men, our data and the study by Aggarwal et al. showed that the increase

also occurs in hormone-sensitive men. In fact, in the study by Emmet et al., of those eight men with hormone-sensitive disease, four had GS 7 PCa. It might well be, that the upregulation is more evidently seen in poorly differentiated tumours.

It is known that long-term ADT ( $\geq$  three months) can significantly reduce the PSMA uptake in PCa lesions (Afshar-Oromieh et al. 2018; Tseng et al. 2022). Therefore, a relevant clinical question is whether the initiation of ADT could also interfere with PSMA PET results. In both of our studies (Studies II and III), none of the lesions disappeared after four weeks of treatment, which suggests that ongoing short-term ADT (at least up to one month) does not represent a contraindication for performing a PSMA PET scan. On the other hand, it has been hypothesised that the increased PSMA expression at three to four weeks might improve the detection rate of primary staging PSMA PET scans. However, no change in staging results was observed in any of our patients in both studies. Yet Study III included patients who already had distant metastases, thus this aspect could not be reliably assessed. One might speculate that short-term ADT could increase the diagnostic accuracy of PSMA PET also in patients with BCR. Given the higher incidence of the flare in the bone, the benefit would be most likely minor. However, no studies about the PSMA flare in BCR patients have been published yet.

The upregulation of PSMA expression might have interesting applications in theranostics. Although [ $^{177}\text{Lu}$ ]-PSMA RLT is currently used in CRPC, a pilot study on the safety and feasibility of PSMA RLT in hormone-sensitive patients was recently published (Privé et al. 2021) and the first randomized trial on RLT in hormone-sensitive oligometastatic patients is ongoing (NCT04443062). If RLT is proven to be effective in hormone-sensitive disease, it would be reasonable to hypothesise that the timing between the administration of ADT and [ $^{177}\text{Lu}$ ]-PSMA RLT is crucial. ADT could increase the tumour targeting and therefore increase the efficacy of [ $^{177}\text{Lu}$ ]-PSMA treatment during the time window of the maximum PSMA uptake. There are ongoing trials already investigating the possible synergistic effect of PSMA RLT and enzalutamide in patients with CRPC (NCT04419402). In the future, the same phenomenon could be investigated in a hormone-sensitive setting as well.

The possible association between the flare in PSMA uptake and glucose metabolism had not been investigated so far. It is well known that FDG uptake and its intensity are associated with more aggressive PCa (Jadvar 2013; Oyama et al. 1999). Given the metastatic status of our patient cohort, the presence of FDG-positive lesions was expected. Interestingly, we observed a negative correlation between the flare in the PSMA uptake and the intensity of the FDG uptake in the bone metastases and, to a lesser degree, in the lymph node metastases. This suggests that lesions presenting with the flare and milder FDG uptake might be less aggressive

than lesions without the flare and with a stronger FDG uptake. Therefore, this flare phenomenon might be able to identify more aggressive metastases, and potentially predict the response to ADT and the progression to CRPC.

Bone flare is a phenomenon that has already been observed in BS as either an increase in metabolic activity or the presence of new lesions within a few weeks to a few months of oncological treatments in PCa and other malignancies. This phenomenon is considered as a sign of a favourable response to treatment (Conteduca et al., 2021). In our study, 22/23 patients with bone metastases presented with flare of PSMA uptake after ADT in the bone. Moreover, 10 of them exhibited new PSMA bone uptakes without anatomical correspondence at the second PSMA PET scan. Whether these new PSMA uptakes are true metastases remains to be confirmed by a longer follow-up. Nevertheless, these uptakes were also negative in the baseline FDG PET scan, which corroborates our observation of the presence of PSMA flare in lesions with mild or no FDG-uptake, suggesting a less aggressive behaviour. In view of this, the PSMA flare might resemble the flare observed in BS. Although it has been hypothesised that the PSMA flare in the bone might be caused by an increased osteoblastic reaction or T-cell mediated immune response (Conteduca et al., 2021), we demonstrated that the flare is not bone-specific, as it is also seen in lymph node metastases, prostatic lesions and normal organs.

It is possible that a similar immune response might also occur in those tissues. Nevertheless, it is unlikely that this would be the only mechanism involved in the increase in the PSMA uptake and, ultimately, the exact physiology of the PSMA flare phenomenon is still not completely understood. A recent study on genomically characterized patient-derived xenografts (PDX) observed increases in the PSMA and androgen receptor (AR) mRNA as well as in the tumour microdensity after ADT in castration-sensitive models (Roy et al. 2021). Moreover, this study observed that the model that exhibited increased PSMA and AR mRNA had an intact phosphatase and tensin homolog (PTEN) gene, whereas the model with PTEN loss exhibited repressed AR transcriptional signaling. Given that the loss of the PTEN gene is usually associated with more aggressive disease, these findings might corroborate our hypothesis that the PSMA flare is a marker of less aggressive disease. In view of this, understanding the possible molecular mechanisms and genetic phenotypes that modulate the heterogeneous PSMA responses to ADT might help to better understand the flare phenomenon.

Moreover, the possible clinical significance of the flare phenomenon requires further clarifications. Although the increase in sensitivity is most likely limited, identifying patients at risk of rapid progression would allow for the implementation of appropriate follow-up strategies or further therapies. This would be particularly beneficial in patients with oligometastatic disease as we could selectively treat

metastases that are prone to progress with SRT. Results from a recent randomized trial demonstrated that SRT improved the outcomes of patients with oligometastatic PCa (Phillips et al. 2020). However, SRT on metastases that are visible only in PSMA PET imaging is still experimental.

In this study, FDG PET was used to select potentially aggressive PCa lesions and, through that, to investigate the possible correlation between FDG uptake and the PSMA flare phenomenon. Based on the results of our study, we do not recommend the use of FDG PET in the clinical practice for the primary staging of PCa. However, it would be scientifically interesting to observe whether FDG-positivity could have a predictive value in the development of castration resistance. Moreover, as we hypothesise about the PSMA-flare, FDG-positivity could also have a potential role in selecting aggressive lesions for metastases-targeted therapies. Longer follow-up will hopefully provide insight into these aspects. Very recently, the results of a prospective randomised trial on [<sup>177</sup>Lu]-PSMA-617 in metastatic CRPC demonstrated that a high FDG-positive tumour volume is a predictive and prognostic biomarker of a lower response to treatment (Buteau et al. 2022).

In Study III, we observed that the decrease in the serum PSA was negatively correlated with the presence of the PSMA flare. In other words, the PSA decreased more rapidly in patients most of whose lesions did not present with the PSMA flare. One might expect that a rapid decrease in serum PSA after ADT would be the result of rapid PCa cell death and therefore would predict better response to therapy (Arai Y, Yoshiki T 1990; Facchini et al. 2016). Interestingly, however, studies have observed that a slower decrease in serum PSA, particularly a longer time to nadir, is associated with better response and longer survival (Choueiri et al. 2010; Ji et al. 2017; Sasaki et al. 2011; Tomioka et al. 2014). The mechanisms responsible for the association between a rapid decline in PSA and a worse prognosis are still not clear. One explanation might be that a rapid fall in PSA is related to a transcriptional effect on PSA production rather than cell death. Another possibility is that the rapid removal of hormone-sensitive cells can stimulate the growth of castration-resistant cells (Sasaki et al. 2011; Tomioka et al. 2014). Our results seem to be consistent with this concept, since the serum PSA decreased more rapidly in the patients with potentially more aggressive lesions according to the lower incidence of the PSMA flare. However, the follow-up time for serum PSA in our cohort was too short to draw reliable conclusions, and longer follow-up is needed to confirm our hypothesis.

### 6.3 Clinical utility of PSMA PET in primary nodal staging

Study IV prospectively compared standard (CT) and next generation imaging modalities ( $^{18}\text{F}$ -PSMA-1007 PET/CT and WBMRI with DWI) in the primary nodal staging of men with unfavourable intermediate- and high-risk prostate cancer.  $^{18}\text{F}$ -PSMA-1007 PET/CT outperformed the other imaging modalities in terms of sensitivity, accuracy, NPV and inter-reader agreement, while maintaining high specificity and PPV. In our cohort, 31 patients had metastases in pelvic lymph nodes, 87% of which were detected by  $^{18}\text{F}$ -PSMA-1007 PET/CT, while the detection rates of WBMRI and CT were 45% and 26%, respectively.

The performance of  $^{68}\text{Ga}$ -PSMA-11 PET/CT in primary nodal staging has been assessed in prospective and retrospective studies that used histopathology as a reference and demonstrated sensitivity of around 60% and a high specificity ( $\geq 95\%$ ) (**Table 22**) (van Leeuwen et al. 2017; Maurer et al. 2016). Subsequently, prospective multicentre studies performed both with  $^{68}\text{Ga}$ - and  $^{18}\text{F}$ -labelled tracers have confirmed the good diagnostic accuracy of PSMA PET/CT in detecting lymph node metastases (Hope et al. 2021; Jansen et al. 2020; van Kalmthout et al. 2020; Pienta et al. 2021). These studies demonstrated consistently high specificity ( $>95\%$ ). However, the sensitivity was modest (40%) (**Table 22**). The reasons why sensitivity in large trials remained modest and below that of single centre studies are not obvious, although they may be related to the inhomogeneity of different scanners, reconstruction algorithms, and local reading paradigms.

Recent retrospective studies have evaluated the performance of  $^{18}\text{F}$ -PSMA-1007 and  $^{18}\text{F}$ -rhPSMA-7/7.3 in primary N-staging using histopathology confirmation. These studies reported variable sensitivity that was only partially in concordance with our studies (from 30% to 80%), while maintaining high specificity ( $> 95\%$ ) (**Table 22**) (Ingvar et al. 2022; Kroenke et al. 2020; Langbein et al. 2022; Sprute et al. 2021). This could again be explained, to some extent, by differences in the patient population or in the study methodology. Our results are in line with the recent data from the proPSMA trial, the first prospective randomized multicentre study that compared  $^{68}\text{Ga}$ -PSMA PET/CT and conventional imaging in the primary staging of PCa. In this study the sensitivity and specificity of  $^{68}\text{Ga}$ -PSMA PET/CT and conventional imaging in a subanalysis for nodal staging were 83% versus 23% and 99% versus 96%, respectively (Hofman et al. 2020). Two non-randomized prospective comparative studies on smaller patient cohorts also showed higher performance of  $^{68}\text{Ga}$ -PSMA PET/CT compared to MRI and/or CT (Petersen et al. 2019; Tulsyan et al. 2017).

Our data showed that that 74% of all lymph node metastases detected by  $^{18}\text{F}$ -PSMA-1007 PET/CT were smaller than the anatomical cut-off value of 8 mm (short diameter) used in CT and MRI, which explained the superior sensitivity of PSMA



PET. This result was partially expected, as it is known that in PCa the lymph node size is not necessarily correlated with the presence of metastases (Heesakkers et al. 2008; Tiguert et al. 1999). In 82% of the cases, [<sup>18</sup>F]-PSMA-1007 PET/CT was concordant with histology. However, there were histologically confirmed nodal metastases (n=9) with the longest diameter of  $\leq 4$  mm that [<sup>18</sup>F]-PSMA-1007 PET/CT did not detect. This finding was also confirmed in recent studies on [<sup>18</sup>F]-PSMA-1007, which showed very limited sensitivity in small lymph nodes (< 3 mm) detected by histopathology (Ingvar et al. 2022; Langbein et al. 2022). However, given the limited resolution of PET/CT scanners for lesion < 5 mm, the limited detection of very small metastases or micrometastases was expected. The varying detectability of lesions in PSMA PET might also be due to the heterogeneity in PSMA expression, as we observed variable intensity in the immunohistochemical PSMA staining between positive metastatic lymph nodes (**Figure 6**, **Figure 29** and **Figure 30**). Nevertheless, none of the lymph node metastases detected by H&E were negative in the PSMA-immunostaining, in line with recently published data (Petersen et al. 2019).

**Table 22.** Overview of PSMA PET/CT patient-based sensitivity and specificity in primary pelvic nodal staging from prospective and retrospective studies that used histopathology as a reference standard. \* Lesion-based sensitivity and specificity.

First author and year	Study design	Radiotracer	Study subjects (patients with histological verification)	Patients with histologically confirmed LN metastases	Sensitivity Patient-based	Specificity Patient-based
Maurer et al. 2016	retrospective	[ <sup>68</sup> Ga]-PSMA-11	130 (130)	41	0.66	0.99
van Leeuwen et al. 2017	prospective	[ <sup>68</sup> Ga]-PSMA-11	30 (30)	11	0.64	0.95
Öbek et al. 2017	retrospective	[ <sup>68</sup> Ga]-PSMA-11	51(51)	15	0.53	0.86
Van Leeuwen et al. 2017	retrospective	[ <sup>68</sup> Ga]-PSMA-11	30 (30)	11	0.64	0.95
Petersen et al. 2020	prospective	[ <sup>68</sup> Ga]-PSMA-11	20 (20)	5	0.39	1
van Kalmthout et al. 2020	prospective	[ <sup>68</sup> Ga]-PSMA-11	103 (97)	41	0.42	0.91
Jansen et al. 2020	prospective	[ <sup>18</sup> F]-DCFPyL	117 (117)	17	0.41	0.94
Kroenke et al. 2020	retrospective	[ <sup>18</sup> F]-rhPSMA-7	58 (58)	18	0.72	0.93
Hofman et al. 2020	prospective	[ <sup>68</sup> Ga]-PSMA-11	148 (7)	na	0.83*	0.99*
Hope et al. 2021	prospective	[ <sup>68</sup> Ga]-PSMA-11	764 (277)	75	0.40	0.95
Pienta et al. 2021	prospective	[ <sup>18</sup> F]-DCFPyL	268 (252)	62	0.40	0.98
Sprute et al. 2021	retrospective	[ <sup>18</sup> F]-PSMA-1007	96 (96)	31	0.74	0.99
Langbein et al. 2022	retrospective	[ <sup>18</sup> F]-rhPSMA-7.3	279 (83)	24	0.67	0.97
Ingvar et al. 2022	retrospective	[ <sup>18</sup> F]-PSMA-1007	104 (104)	26	0.27	0.96

## 6.4 Strengths and Limitations

Overall, the main strength of this doctoral thesis is its investigation of PSMA, an advanced target for PCa PET imaging, in a translational way, encompassing the kinetics of a novel radiopharmaceutical for imaging and possibly therapy of PCa, the physiology of PSMA expression, up to the use of this target in the clinical practice. Another strength is that all the studies are distinct single-centre prospective registered clinical trials. Study I, a prospective Phase I trial, laid the basis for the design of two Phase III trials (NCT04186819 and NCT04186845), whose soon-to-be published results will determine the role of [<sup>18</sup>F]-rhPSMA-7.3 in the diagnosis of PCa. Moreover, the effect of short-term ADT on PSMA expression and the performance of PSMA PET/CT in primary staging compared to other imaging modalities are two topics of great interest for the nuclear and clinical uro-oncology community, which we only very recently started to address and understand better. To our knowledge, the correlation between the PSMA flare and FDG uptake has not been investigated yet. Moreover, in Study IV, a clear strength was that all the patients prospectively underwent three different imaging modalities ([<sup>18</sup>F]-PSMA-1007 PET/CT, WBMRI with DWI and CT) in a very short time window and that a long follow-up was available to validate the reference standard diagnosis in lesions that lacked histological confirmation.

The studies are not without limitations. One limitation of Studies I and II was the small cohort of patients (n=9), which limited the drawing of firm conclusions. However, a small number of study participants is not uncommon for Phase I or proof-of-concept studies. Moreover, in the same way that the results of Study I were used to determine the optimal time window for PET imaging with [<sup>18</sup>F]-rhPSMA-7.3 in the aforementioned Phase III trials, the results of Study II were used to design the optimal time point in Study III for investigating the PSMA flare phenomenon in a larger cohort of patients. Another limitation of Study II is that the small patient cohort was not homogeneous, and the intervals of the scans varied. Nevertheless, by including a more heterogeneous cohort we were able to demonstrate that the PSMA flare is not exclusively seen in metastatic patients and, despite some variations in the scans' time interval, eight out of nine patients completed the study by undergoing four sequential [<sup>68</sup>Ga]-PSMA PET/MRI scans.

The use of SUVmax as the only parameter to describe PSMA uptake can also be considered as a limitation. However, in each of the four studies, all the patients were scanned with the same camera in order to minimise possible technical variation and no significant difference in the injected activities and scanning times was observed. Moreover, in Study III a 20% SUVmax cut-off to define the increase in the PSMA uptake was used to avoid any possible variation due to aspects of technical reproducibility. In addition, tumour volume measurements are predominantly used in therapy response assessment, which was not the case in any of the studies. The

absence of histopathological verification of potential metastases, except for the patients in Study II who underwent PLND, was another limitation. In particular, with the use of [<sup>18</sup>F]-PSMA-1007, there was a higher risk of non-specific bone uptakes. However, in Studies I-III the presence of bone metastases was confirmed by conventional imaging prior to PSMA PET scans and only lesions with correspondence on anatomical imaging (CT/MRI) were included in the analysis. In Study IV, long follow-up was available to support the standard reference diagnosis.

Regarding Studies II and III, which investigated the PSMA flare, follow-up data are still needed to assess the potential clinical role of this phenomenon in predicting the aggressiveness of metastatic lesions. All the patients in Study III are currently receiving follow-up, which consists of [<sup>18</sup>F]-PSMA-1007 PET/CT once a year until the onset of CRPC. Hopefully, these future results will provide further insights into the matter. Finally, a limitation of the comparative study on primary nodal staging (Study IV) was that the effect of PSMA PET/CT in patients management or treatment decision-making was not prospectively investigated. However, outcome data showing the survival benefit of detecting metastatic disease at the initial diagnosis by PSMA PET/CT are still lacking.

## 6.5 Implications and future perspectives

This thesis work deepens our knowledge of the role of PSMA as a target for PCa imaging, and concomitantly raises important clinical questions to be addressed in future studies. The introduction of PSMA PET has revolutionised the work-up of PCa patients, providing excellent opportunities for diagnostic and treatment applications.

PSMA PET/CT has very recently this year gained a place in the EAU guidelines as an accurate and potentially cost-effective imaging method for the primary staging of high-risk PCa, based on valid results from different prospective studies, in particular the proPSMA trial (Hofman et al. 2020). With the increasing use of PSMA PET, pelvic nodal metastases are diagnosed at an earlier stage, postponing the need for salvage treatments. Moreover, more and more often we are able to detect oligometastatic disease that would have been missed by conventional imaging. The improved sensitivity of PSMA PET compared to conventional imaging is driving the adoption of metastasis-directed therapy in men with limited volume metastatic disease. The treatment of PSMA-avid disease with stereotactic ablative body radiation has shown to improve progression-free and distant-metastasis-free survival (Phillips et al. 2020). However, these treatments are still experimental and further studies are needed to confirm whether the diagnosis of metastases at an earlier stage would have a survival benefit.

Understanding the complex physiology of PSMA is paramount to better define the role of PSMA PET in the clinical practice. We have demonstrated, in line with other studies, that short-term ADT is not a contraindication to performing a PSMA PET scan, rather it could improve the detection of PCa lesions by increasing PSMA uptake. More interestingly, it seems that the upregulation of PSMA expression by hormonal treatment could be an important predictive biomarker and it could be related to tumour aggressiveness. Authors hypothesized that the upregulation in a castration-resistant state might identify a more aggressive phenotype (Emmett et al. 2019; Zukotynski et al. 2021). According to our results, based on the correlation with FDG uptake, the PSMA flare in hormone-sensitive disease might instead be linked to less aggressive disease. It is well possible that PCa cells react differently to androgen deprivation according to the state of the disease. Future research and in particular longer follow-up will provide more insight into this matter.

Theranostics are currently driving the future of nuclear medicine. In recent years, the development and use of PSMA RLT with  $^{177}\text{Lu}$  have strongly increased. RLT with  $^{225}\text{Ac}$  is a valid alternative to  $^{177}\text{Lu}$ , although the development of alpha therapies still limits the availability of the treatments. Development of valid theranostic PSMA ligands, that can be easily labelled with both diagnostic and therapeutic radioisotopes, is needed. Although the FDA recently approved the theranostic ligand PSMA-617 for use in therapeutic applications ( $^{177}\text{Lu}$ -PSMA-617), this ligand in the form of  $^{68}\text{Ga}$ -PSMA-617 is not used for diagnostic imaging. Therefore, no true theranostic pair is currently available. Moreover,  $^{18}\text{F}$ -labelled ligands have progressively replaced their  $^{68}\text{Ga}$ -labelled counterparts for their favourable technical properties that will potentially allow the availability of PSMA-targeted imaging in all localities with an existing PET infrastructure. In this context, rhPSMA7.3 could be a promising theranostic agent. We have demonstrated that  $^{18}\text{F}$ -rhPSMA-7.3 is an accurate tracer for the diagnosis of PCa. The results of the recently completed Phase III trials (NCT04186845 and NCT04186819) will hopefully confirm this.

The role of PSMA RLT has been established in patients with CRPC. However, we still face challenges in determining the suitable dose for treatment as well as in predicting outcomes in terms of responders and non-responders. PSMA and FDG PET (and their combination) could be important predictive biomarkers in PSMA RLT, as it has recently been shown (Buteau et al. 2022). Evidence has recently suggested that PSMA RLT can be safely administered in a hormone-sensitive state (Privé et al. 2021). In this context, the combination of PSMA RLT with other systemic therapies to create a synergistic effect and improve treatment efficacy is of great scientific interest. For example, ongoing trials are investigating the combination of enzalutamide and  $^{177}\text{Lu}$ -PSMA, in the attempt to exploit the upregulation caused by hormonal treatment (NCT04419402). There are other trials

that are investigating combination of [<sup>177</sup>Lu]-PSMA with PARP inhibitors or immunotherapy (NCT03874884 and NCT03658447).

The increasing use of PSMA-ligands in imaging and therapy together with the development of several distinct PSMA-targeted radiotracers, highlight the need to standardise the interpretation of PSMA findings. The PROMISE criteria and the EANM's E-PSMA criteria suggest the adoption of a standardised visual score for grading PSMA uptake as well as a five-point scale for assessing reader's confidence about a finding on PSMA PET (Ceci et al. 2021; Eiber et al. 2018). Ultimately, nuclear medicine physicians and radiologists could provide a structured report of the PSMA PET scan, including a molecular imaging (mi) TNM classification (Eiber et al. 2018). A structured report, apart from improving the clarity and consistency of the report, would facilitate data mining for future research studies. Moreover, with the rapid advancement of artificial intelligence (AI), a standardised and structured report would provide discrete data for AI system training. In this context, standardisation of PSMA activity measurements on PET imaging is also needed, particularly for theranostic applications. Volumetric measurements of tumour burden are currently used to assess eligibility and response to treatment (Gafita et al. 2022). With the increasing datasets regarding PSMA imaging, AI algorithms are gradually improving their performance (Johnsson et al. 2022). Possibly in the future AI-based methods will be introduced in clinical practice for staging or response assessment of patients with PCa.

The knowledge that PSMA is not a 'prostate-specific' ligand is creating interesting opportunities for a new theranostic wave. In particular, tumours other than PCa that have demonstrated high uptake on PSMA PET imaging and that have limited treatment options available, such as recurrent glioblastoma multiforme, iodine-refractory metastatic thyroid cancer and metastatic or recurrent RCC, might benefit from PSMA RLT. The results of future prospective trials on both PSMA imaging and therapy in non-prostatic tumours, including studies on dosimetry and tracer kinetics, are being awaited.

Recently a new PET ligand, fibroblast activation protein inhibitor (FAPI) has attracted significant interest due to its demonstration of performance and tumour uptake that are comparable to those of FDG in many types of cancers (Giesel et al. 2021; Kratochwil et al. 2019). FAP is a type II transmembrane serine protease that is overexpressed by stromal fibroblasts in most epithelial carcinomas. There is preliminary evidence FAPI expression is elevated in patients with advanced CRPC and that PSMA negative PCa lesions have shown intermediate to high uptake of FAPI, usually matching FDG uptake (Khreish et al. 2020; Kratochwil et al. 2019). If this would prove correct, FAPI would become a promising theranostic agent in advanced PCa and would be particularly useful in the case of PSMA-negative disease.

## 7 Conclusions

This thesis investigated PSMA as a target for PET imaging of PCa. It evaluated aspects related to novel tracer kinetics, the physiology of PSMA expression in relation to ADT and the diagnostic performance of PSMA PET in primary nodal staging.

The main conclusions are as follows:

1. Study I have showed that a novel theranostic agent, [ $^{18}\text{F}$ ]-rhPSMA 7.3, has favourable kinetics and is a promising radiotracer for diagnostic and potentially therapeutic applications in PCa.
2. Studies II and III demonstrated that short-term ADT upregulates PSMA expression in treatment-naïve PCa patients, causing a flare of PSMA uptake, most evidently seen in bone metastases at four weeks after initiation of treatment. This phenomenon does not seem to significantly increase the sensitivity of PSMA PET/CT in primary staging; on the other hand, short-term ADT (up to one month) does not interfere with the interpretation of PET results. It seems that in hormone-sensitive disease low or absent PSMA flare could be associated with more aggressive disease, as we demonstrated a negative correlation between the PSMA flare and the intensity of FDG uptake.
3. In Study IV, [ $^{18}\text{F}$ ]-PSMA-1007 PET/CT demonstrated to be an effective imaging method in the primary nodal staging of patients with unfavourable intermediate- and high-risk PCa, showing superior accuracy and sensitivity compared to WBMRI and CT while maintaining high specificity.

# Acknowledgements

The research work for this thesis was conducted at the Turku PET centre, University of Turku and Turku University Hospital, during the years 2018-2022. The studies were financially supported by the Finnish Government Research and Development Funds for Medical Research, University of Turku, Turku University Hospital, Finnish Cancer Foundation, Sigrid Jusélius Foundation and Blue Earth Diagnostics Ltd. I wish to express my warmest thanks to Professor Juhani Knuuti, director of the Turku PET centre, for providing excellent facilities and for always promoting an atmosphere of enthusiasm to conduct research.

I wish to express my sincere gratitude to Professor Jukka Kemppainen and Adjunct Professor Otto Ettala for the opportunity to conduct my doctoral thesis under their supervision. Jukka, I remember how you kindly welcomed me when I first came to Turku in 2017 for an exchange period during my residency training. From the beginning you encouraged me to speak Finnish and made me feel part of the research team. Your deep knowledge and bright perspectives have inspired me, and your positive guidance has given me motivation during these years. Otto, your trust, brilliant advices and skills as a clinician have been fundamental during this work, and your kindness has cheered me up in many moments. Jukka and Otto, thank you for being such great mentors, for believing in me and for allowing me to grow professionally through this project.

I sincerely thank Associate Professor Mika Raitanen and Associate Professor Laura Evangelista for reviewing my thesis. Your feedback and valuable comments really improved my thesis and gave me precious insights from both the point of view of the clinician and the diagnostic imaging expert. I am very grateful to Associate Professor Matthias Eiber for having accepted to act as my opponent and I look forward to our discussion. I thank the members of the follow-up Committee, Professor Peter J. Böstrom and Adjunct Professor Saila Kauhanen for their support throughout this process. The director of the Doctoral Programme in Clinical Research, Professor Antti Saraste, is also warmly thanked.

The research projects could have not been a success without a solid teamwork. I thank Vesa Oikonen for his astounding expertise in PET kinetic analysis. Adjunct Professor Kari Kalliokoski is warmly thanked for his constant presence and valuable



help. I express my gratitude to Adjunct Professor Marko Seppänen for his precious assistance and kind encouragement. I also wish to sincerely thank Dr. Ernst J. Ponema for his excellent ideas and inspiring attitude towards research.

I wish to express my warmest gratitude to all the other members of the BED, ADTPSMA and PROSTAGE research group. I sincerely thank Mikael Anttinen, Peter J. Boström, Peter B. Dean, Roberto Blanco Sequeiros, Hannu J. Aronen, Mika Scheinin, Matthew P. Miller and Heikki Minn for their precious input during the design, implementation and realisation of the studies. I sincerely thank Jukka Schildt, Ivan Jambor, Minna Sandell, Irina Rinta-Kiikka, Sami Kajander and Terhi Tuokkola for their effort in reading the imaging scans. I wish to thank Pekka Taimen for his precious expertise as a skilled and experienced pathologist. I thank Pauliina Luoto, Johan Rajander and Olli Eskola for their contribution in the production of the radiotracers. Tuula Tolvanen, Tommi Noponen and Jani Saunavaara are thanked for their expertise as physicists regarding the scanning devices and image transfers. I thank Kalle Mattila for contributing to the recruitment of the study patients. I thank Anna Kuisma and Ekaterina Saukko for their help in performing the study scans. Eliisa Löyttyniemi is acknowledged for the statistical assistance.

I would like to thank the excellent personnel of the Turku PET centre, including all radiographers, nurses, radiochemists, physicists, laboratory technicians, IT-experts and secretaries. Your expertise and commitment to imaging studies made this work possible. Special thanks go to Minna Aatsinki for being such a kind point of reference during the organisational aspects of the study scans. Moreover, warm thanks go to the study nurses of the Department of Urology, Sara Karnell, Kaisa Reunanen, Minna Lyytinen and Anna Takatupa for doing an excellent job during the patient recruitment and follow up.

My research work has been deeply driven by my clinical work as a nuclear medicine specialist. I would like to express my gratitude to the late Professor Giovanni Lucignani, former Director of the residency training program in Nuclear Medicine at the University of Milan. He was one of the first person to see potential in me and he inspired me to pursue a career in research. I will always be grateful to him for encouraging me to move to Finland. I would also like to thank my former senior colleagues at the San Paolo Hospital in Milan, Angelo Del Sole, Stefano Vassallo and Luca Tagliabue. Thank you for introducing me to this beautiful speciality and for training me during my years as a resident.

I wish to sincerely thank Adjunct Professor Tuula Janatuinen. Tuula, you offered me a kind and safe space to learn and improve my skills as a nuclear medicine specialist. Your knowledge of clinical PET imaging and your work ethics are inspiring, and I am grateful to have you as a mentor and friend. Warm thanks go also to all my fellow colleagues of the Department of Clinical Physiology and Nuclear Medicine in TYKS for welcoming me and always being willing to help.

I would like to thank my friends and research colleagues Mia Sthåle, Eleni Rebelos, Minna Lahesmaa, Sanna Laurila, Miikka Honka, Muez U-Din, Prince Dadson, Luis Eduardo Juarez-Orozco, Riikka Viitanen, Kerttu Seppälä and Milena Pires. Thank you for the inspiring conversations and the many nice moments spent together at work and outside work. I would like to particularly thank Mia for having made the transition to the Finnish life easier, and for supporting me every step of the way with your energy and positivity.

Outside work dancing has brought much joy, friendship and love in my life. I would like to thank my beautiful friends Anu, Kaisa, Emilia, Anni, Sara, Annika, Aryan, Marita, Arash and Janina for the countless moments of happiness, fun and laughter in and outside the dancefloor. Moreover, I owe my gratitude to my lifelong friends Laura, Carolina and Federica: you have been my cornerstones since high school and no distance will ever change that.

I would like to thank my boyfriend Shahoo for his support and love, expressed with generosity, honesty and clarity. Finally, I wish to heartily thank my family. I thank my parents Corrado and Sinikka for their constant and loving presence, for believing in me and encouraging me to create my own path. I am also grateful to my brother Roberto for his support and for inspiring me with his elegance, culture and ambition.

Turku, March 2023  
*Simona Malaspina*

# References

- Ackerstaff, Ellen, Kristine Glunde, and Zaver M. Bhujwalla. 2003. 'Choline Phospholipid Metabolism: A Target in Cancer Cells?' *Journal of Cellular Biochemistry* 90 (3): 525–33. <https://doi.org/10.1002/jcb.10659>.
- Afshar-Oromieh, A., A. Malcher, M. Eder, M. Eisenhut, H. G. Linhart, B. A. Hadaschik, T. Holland-Letz, et al. 2013. 'Pet Imaging with a [68ga]Gallium-Labelled Psma Ligand for the Diagnosis of Prostate Cancer: Biodistribution in Humans and First Evaluation of Tumour Lesions'. *European Journal of Nuclear Medicine and Molecular Imaging* 40 (4): 486–95. <https://doi.org/10.1007/s00259-012-2298-2>.
- Afshar-Oromieh, Ali, Nils Debus, Monika Uhrig, Thomas A. Hope, Michael J. Evans, Tim Holland-Letz, Frederik L. Giesel, et al. 2018. 'Impact of Long-Term Androgen Deprivation Therapy on PSMA Ligand PET/CT in Patients with Castration-Sensitive Prostate Cancer'. *European Journal of Nuclear Medicine and Molecular Imaging* 45 (12): 2045–54. <https://doi.org/10.1007/s00259-018-4079-z>.
- Afshar-Oromieh, Ali, Henrik Hetzheim, Clemens Kratochwil, Martina Benesova, Matthias Eder, Oliver C. Neels, Michael Eisenhut, et al. 2015. 'The Theranostic PSMA Ligand PSMA-617 in the Diagnosis of Prostate Cancer by PET/CT: Biodistribution in Humans, Radiation Dosimetry, and First Evaluation of Tumor Lesions'. *Journal of Nuclear Medicine* 56 (11): 1697–1705. <https://doi.org/10.2967/jnumed.115.161299>.
- Afshar-Oromieh, Ali, Tim Holland-Letz, Frederik L. Giesel, Clemens Kratochwil, Walter Mier, Sabine Haufe, Nils Debus, et al. 2017. 'Diagnostic Performance of 68Ga-PSMA-11 (HBED-CC) PET/CT in Patients with Recurrent Prostate Cancer: Evaluation in 1007 Patients'. *European Journal of Nuclear Medicine and Molecular Imaging* 44 (8): 1258–68. <https://doi.org/10.1007/s00259-017-3711-7>.
- Aggarwal, Rahul, Xiao Wei, Won Kim, Eric J. Small, Charles J. Ryan, Peter Carroll, Matthew Cooperberg, Michael J. Evans, and Thomas Hope. 2018. 'Heterogeneous Flare in Prostate-Specific Membrane Antigen Positron Emission Tomography Tracer Uptake with Initiation of Androgen Pathway Blockade in Metastatic Prostate Cancer'. *European Urology Oncology* 1 (1): 78–82. <https://doi.org/10.1016/j.euo.2018.03.010>.
- Andras, Iulia, Nicolae Crisan, Maxim Gavrilita, Radu Tudor Coman, Viktoria Nvberer, and Ioan Coman. 2017. 'Every Setback Is a Setup for a Comeback: 3D Laparoscopic Radical Prostatectomy after Robotic Radical Prostatectomy'. *Journal of B.U.ON.* 22 (1): 87–93.
- Andriole, Gerald L, Alvin J Siteman, Lale Kostakoglu, Mount Sinai, Albert Chau, Blue Earth Diagnostics, United Kingdom, et al. 2020. 'The Impact of Positron Emission Tomography with 18Ffluciclovine on the Treatment of Biochemical Recurrence of Prostate Cancer: Results from the LOCATE Trial' 201 (2): 322–31. <https://doi.org/10.1016/j.juro.2018.08.050>.The.
- Anttinen, Mikael, Otto Ettala, Simona Malaspina, Ivan Jambor, Minna Sandell, Sami Kajander, Irina Rinta-Kiikka, et al. 2020. 'A Prospective Comparison of 18F-Prostate-Specific Membrane Antigen-1007 Positron Emission Tomography Computed Tomography, Whole-Body 1.5 T Magnetic Resonance Imaging with Diffusion-Weighted Imaging, and Single-Photon Emission Computed Tomography/Computed'. *European Urology Oncology*, 1–10. <https://doi.org/10.1016/j.euo.2020.06.012>.

- Arai Y, Yoshiki T, Yoshida O. 1990. 'Prognostic Significance of Prostate Specific Antigen in Endocrine Treatment for Prostatic Cancer'.
- Armstrong, Andrew J., Russell Z. Szmulewitz, Daniel P. Petrylak, Jeffrey Holzbeierlein, Arnaud Villers, Arun Azad, Antonio Alcaraz, et al. 2019. 'Arches: A Randomized, Phase III Study of Androgen Deprivation Therapy with Enzalutamide or Placebo in Men with Metastatic Hormone-Sensitive Prostate Cancer'. *Journal of Clinical Oncology* 37 (32): 2974–86. <https://doi.org/10.1200/JCO.19.00799>.
- Ashesh B., Jani, Eduard Schreibmann, Subir Goyal, Raghuvveer Halkar, Bruce Hershatler, Peter J. Rossi, Joseph W. Shelton, et al. 2021. '18F-Fluciclovine-PET/CT Imaging versus Conventional Imaging Alone to Guide Postprostatectomy Salvage Radiotherapy for Prostate Cancer (EMPIRE-1): A Single Centre, Open-Label, Phase 2/3 Randomised Controlled Trial'. *The Lancet* 397 (10288): 1895–1904. [https://doi.org/10.1016/S0140-6736\(21\)00581-X](https://doi.org/10.1016/S0140-6736(21)00581-X).
- Bakht, Martin K., So Won Oh, Hyewon Youn, Gi Jeong Cheon, Cheol Kwak, and Keon Wook Kang. 2017. 'Influence of Androgen Deprivation Therapy on the Uptake of PSMA-Targeted Agents: Emerging Opportunities and Challenges'. *Nuclear Medicine and Molecular Imaging* 51 (3): 202–11. <https://doi.org/10.1007/s13139-016-0439-4>.
- Baron, Antonella, Toshiro Migita, Dan Tang, and Massimo Loda. 2004. 'Fatty Acid Synthase: A Metabolic Oncogene in Prostate Cancer?' *Journal of Cellular Biochemistry* 91 (1): 47–53. <https://doi.org/10.1002/jcb.10708>.
- Barrett, John A., R. Edward Coleman, Stanley J. Goldsmith, Shankar Vallabhajosula, Neil A. Petry, Steve Cho, Thomas Armor, et al. 2013. 'First-in-Man Evaluation of 2 High-Affinity PSMA-Avid Small Molecules for Imaging Prostate Cancer'. *Journal of Nuclear Medicine* 54 (3): 380–87. <https://doi.org/10.2967/jnumed.112.111203>.
- Beckendorf, Véronique, Stéphane Guerif, Elisabeth Le Pris , Jean Marc Cosset, Agnes Bournoux, Bruno Chauvet, Naji Salem, et al. 2011. '70 Gy versus 80 Gy in Localized Prostate Cancer: 5-Year Results of GETUG 06 Randomized Trial'. *International Journal of Radiation Oncology Biology Physics* 80 (4): 1056–63. <https://doi.org/10.1016/j.ijrobp.2010.03.049>.
- Beer, Tomasz M., Andrew J. Armstrong, Dana E. Rathkopf, Yohann Loriot, Cora N. Sternberg, Celestia S. Higano, Peter Iversen, et al. 2014. 'Enzalutamide in Metastatic Prostate Cancer before Chemotherapy'. *New England Journal of Medicine* 371 (5): 424–33. <https://doi.org/10.1056/nejmoa1405095>.
- Benešová, Martina, Martin Schäfer, Ulrike Bauder-Wüst, Ali Afshar-Oromieh, Clemens Kratochwil, Walter Mier, Uwe Haberkorn, Klaus Kopka, and Matthias Eder. 2015. 'Preclinical Evaluation of a Tailor-Made DOTA-Conjugated PSMA Inhibitor with Optimized Linker Moiety for Imaging and Endoradiotherapy of Prostate Cancer.' *Journal of Nuclear Medicine : Official Publication, Society of Nuclear Medicine* 56 (6): 914–20. <https://doi.org/10.2967/jnumed.114.147413>.
- Berliner, Christoph, Milena Tienken, Thorsten Frenzel, Yuske Kobayashi, Annabelle Helberg, Uve Kirchner, Susanne Klutmann, et al. 2017. 'Detection Rate of PET/CT in Patients with Biochemical Relapse of Prostate Cancer Using [68Ga]PSMA I&T and Comparison with Published Data of [68Ga]PSMA HBED-CC'. *European Journal of Nuclear Medicine and Molecular Imaging* 44 (4): 670–77. <https://doi.org/10.1007/s00259-016-3572-5>.
- Beyer, T., D. W. Townsend, T. Brun, P. E. Kinahan, M. Charron, R. Roddy, J. Jerin, J. Young, L. Byars, and R. Nutt. 2000. 'A Combined PET/CT Scanner for Clinical Oncology'. *Journal of Nuclear Medicine* 41 (8): 1369–79.
- Boev , Liselotte M.S., Maarten C.C.M. Hulshof, Andr  N. Vis, Aeilko H. Zwinderman, Jos W.R. Twisk, Wim P.J. Witjes, Karl P.J. Delaere, R. Jeroen A. van Moorselaar, Paul C.M.S. Verhagen, and George van Andel. 2019. 'Effect on Survival of Androgen Deprivation Therapy Alone Compared to Androgen Deprivation Therapy Combined with Concurrent Radiation Therapy to the Prostate in Patients with Primary Bone Metastatic Prostate Cancer in a Prospective Randomised Clinical Trial'. *European Urology* 75 (3): 410–18. <https://doi.org/10.1016/j.eururo.2018.09.008>.

- Bolla, Michel, Geertjan Van Tienhoven, Padraig Warde, Jean Bernard Dubois, René Olivier Mirimanoff, Guy Storme, Jacques Bernier, et al. 2010. 'External Irradiation with or without Long-Term Androgen Suppression for Prostate Cancer with High Metastatic Risk: 10-Year Results of an EORTC Randomised Study'. *The Lancet Oncology* 11 (11): 1066–73. [https://doi.org/10.1016/S1470-2045\(10\)70223-0](https://doi.org/10.1016/S1470-2045(10)70223-0).
- Boxtel, Wim Van, Susanne Lütje, Ilse C.H. Van Engen-Van Grunsven, Gerald W. Verhaegh, Jack A. Schalken, Marianne A. Jonker, James Nagarajah, Martin Gotthardt, and Carla M.L. Van Herpen. 2020. '68Ga-PSMA-HBED-CC PET/CT Imaging for Adenoid Cystic Carcinoma and Salivary Duct Carcinoma: A Phase 2 Imaging Study'. *Theranostics* 10 (5): 2273–83. <https://doi.org/10.7150/thno.38501>.
- Bratan, Flavie, Emilie Niaf, Christelle Melodelima, Anne Laure Chesnais, Rémi Souchon, Florence Mège-Lechevallier, Marc Colombel, and Olivier Rouvière. 2013. 'Influence of Imaging and Histological Factors on Prostate Cancer Detection and Localisation on Multiparametric MRI: A Prospective Study'. *European Radiology* 23 (7): 2019–29. <https://doi.org/10.1007/s00330-013-2795-0>.
- Briganti, Alberto, Alessandro Larcher, Firas Abdollah, Umberto Capitanio, Andrea Gallina, Nazareno Suardi, Marco Bianchi, et al. 2012. 'Updated Nomogram Predicting Lymph Node Invasion in Patients with Prostate Cancer Undergoing Extended Pelvic Lymph Node Dissection: The Essential Importance of Percentage of Positive Cores'. *European Urology* 61 (3): 480–87. <https://doi.org/10.1016/j.eururo.2011.10.044>.
- Buchegger, Franz, Valentina Garibotto, Thomas Zilli, Laurent Allainmat, Sandra Jorcano, Hansjörg Vees, Olivier Rager, et al. 2014. 'First Imaging Results of an Intraindividual Comparison of 11C-Acetate and 18F-Fluorocholine PET/CT in Patients with Prostate Cancer at Early Biochemical First or Second Relapse after Prostatectomy or Radiotherapy'. *European Journal of Nuclear Medicine and Molecular Imaging* 41 (1): 68–78. <https://doi.org/10.1007/s00259-013-2540-6>.
- Buteau, James P, Andrew J Martin, Louise Emmett, Amir Iravani, Shahneen Sandhu, Anthony M Joshua, Roslyn J Francis, et al. 2022. 'PSMA and FDG-PET as Predictive and Prognostic Biomarkers in Patients given [<sup>177</sup>Lu] Lu-PSMA-617 versus Cabazitaxel for Metastatic Castration-Resistant Prostate Cancer (TheraP): A Biomarker Analysis from a Randomised, Open-Label, Phase 2 Trial'. *Lancet Oncology*, 1389–97. [https://doi.org/10.1016/S1470-2045\(22\)00605-2](https://doi.org/10.1016/S1470-2045(22)00605-2).
- Cantiello, Francesco, Fabio Crocerossa, Giorgio Ivan Russo, Vincenzo Gangemi, Matteo Ferro, Mihai Dorin Vartolomei, Giuseppe Lucarelli, et al. 2018. 'Comparison Between 64Cu-PSMA-617 PET/CT and 18F-Choline PET/CT Imaging in Early Diagnosis of Prostate Cancer Biochemical Recurrence'. *Clinical Genitourinary Cancer* 16 (5): 385–91. <https://doi.org/10.1016/j.clgc.2018.05.014>.
- Cantiello, Francesco, Vincenzo Gangemi, Giuseppe Lucio Cascini, Ferdinando Calabria, Marco Moschini, Matteo Ferro, Gennaro Musi, et al. 2017. 'Diagnostic Accuracy of 64Copper Prostate-Specific Membrane Antigen Positron Emission Tomography/Computed Tomography for Primary Lymph Node Staging of Intermediate- to High-Risk Prostate Cancer: Our Preliminary Experience'. *Urology* 106: 139–45. <https://doi.org/10.1016/j.urology.2017.04.019>.
- Cardinale, Jens, Martin Schäfer, Martina Benesova, Ulrike Bauder-Wüst, Karin Leotta, Matthias Eder, Oliver C. Neels, Uwe Haberkorn, Frederik L. Giesel, and Klaus Kopka. 2017a. 'Preclinical Evaluation of 18F-PSMA-1007, a New Prostate-Specific Membrane Antigen Ligand for Prostate Cancer Imaging'. *Journal of Nuclear Medicine* 58 (3): 425–31. <https://doi.org/10.2967/jnumed.116.181768>.
- Caroli, Paola, Israel Sandler, Federica Matteucci, Ugo De Giorgi, Licia Uccelli, Monica Celli, Flavia Foca, et al. 2018. '68 Ga-PSMA PET/CT in Patients with Recurrent Prostate Cancer after Radical Treatment: Prospective Results in 314 Patients'. *European Journal of Nuclear Medicine and Molecular Imaging* 45 (12): 2035–44. <https://doi.org/10.1007/s00259-018-4067-3>.
- Carroll, Peter R., J. Kellogg Parsons, Gerald Andriole, Robert R. Bahnson, Daniel A. Barocas, Erik P. Castle, William J. Catalona, et al. 2015. 'Prostate Cancer Early Detection, Version 2.2015: Clinical

- Practice Guidelines in Oncology'. *JNCCN Journal of the National Comprehensive Cancer Network* 13 (12): 1534–61. <https://doi.org/10.6004/jnccn.2015.0181>.
- Carter, H. Ballentine, Jay D. Pearson, E. Jeffrey Metter, Daniel W. Chan, Reubin Andres, James L. Fozard, William Rosner, and Patrick C. Walsh. 1995. 'Longitudinal Evaluation of Serum Androgen Levels in Men with and without Prostate Cancer'. *The Prostate* 27 (1): 25–31. <https://doi.org/10.1002/pros.2990270106>.
- Castro, Elena, Chee Goh, David Olmos, Ed Saunders, Daniel Leongamornlert, Malgorzata Tymrakiewicz, Nadiya Mahmud, et al. 2013. 'Germline BRCA Mutations Are Associated with Higher Risk of Nodal Involvement, Distant Metastasis, and Poor Survival Outcomes in Prostate Cancer'. *Journal of Clinical Oncology* 31 (14): 1748–57. <https://doi.org/10.1200/JCO.2012.43.1882>.
- Ceci, Francesco, Paolo Castellucci, Tiziano Graziani, Andrea Farolfi, Cristina Fonti, Filippo Lodi, and Stefano Fanti. 2019. '68Ga-PSMA-11 PET/CT in Recurrent Prostate Cancer: Efficacy in Different Clinical Stages of PSA Failure after Radical Therapy'. *European Journal of Nuclear Medicine and Molecular Imaging* 46 (1): 31–39. <https://doi.org/10.1007/s00259-018-4189-7>.
- Ceci, Francesco, Daniela E. Oprea-Lager, Louise Emmett, Judit A. Adam, Jamshed Bomanji, Johannes Czernin, Matthias Eiber, et al. 2021. 'E-PSMA: The EANM Standardized Reporting Guidelines v1.0 for PSMA-PET'. *European Journal of Nuclear Medicine and Molecular Imaging*. <https://doi.org/10.1007/s00259-021-05245-y>.
- Cerci, Juliano J., Stefano Fanti, Enrique E. Lobato, Jolanta Kunikowska, Omar Alonso, Sevastian Medina, Fuad Novruzov, et al. 2022. 'Diagnostic Performance and Clinical Impact of 68Ga-PSMA-11 PET/CT Imaging in Early Relapsed Prostate Cancer after Radical Therapy: A Prospective Multicenter Study (IAEA-PSMA Study)'. *Journal of Nuclear Medicine* 63 (2): 240–47. <https://doi.org/10.2967/JNUMED.120.261886>.
- Chang, Sam S., Victor E. Reuter, W. D.W. Heston, Neil H. Bander, Lana S. Grauer, and Paul B. Gaudin. 1999. 'Five Different Anti-Prostate-Specific Membrane Antigen (PSMA) Antibodies Confirm PSMA Expression in Tumor-Associated Neovasculature'. *Cancer Research* 59 (13): 3192–98.
- Chang, Sam S. 2004. 'Overview of Prostate-Specific Membrane Antigen.' *Reviews in Urology* 6 Suppl 10 (Figure 1): S13-8. <http://www.ncbi.nlm.nih.gov/pubmed/16985927> <http://www.pubmedcentral.nih.gov/articlerender.fcgi?artid=PMC1472940>.
- Cherry, Simon R., Terry Jones, Joel S. Karp, Jinyi Qi, William W. Moses, and Ramsey D. Badawi. 2018. 'Total-Body PET: Maximizing Sensitivity to Create New Opportunities for Clinical Research and Patient Care'. *Journal of Nuclear Medicine* 59 (1): 3–12. <https://doi.org/10.2967/jnumed.116.184028>.
- Chi, K. N., N. Agarwal, A. Bjartell, B. H. Chung, A. J. Pereira de Santana Gomes, R. Given, Juárez Soto, et al. 2019. 'Apalutamide for Metastatic, Castration-Sensitive Prostate Cancer'. *The New England Journal of Medicine* 202 (4): 661. <https://doi.org/10.1056/NEJMoa1903307>.
- Cho, Steve Y., Kenneth L. Gage, Ronnie C. Mease, Srinivasan Senthamizhchelvan, Daniel P. Holt, Akimosa Jeffrey-Kwanisai, Christopher J. Endres, et al. 2012. 'Biodistribution, Tumor Detection, and Radiation Dosimetry of 18F-DCFBC, a Low-Molecular-Weight Inhibitor of Prostate-Specific Membrane Antigen, in Patients with Metastatic Prostate Cancer'. *Journal of Nuclear Medicine* 53 (12): 1883–91. <https://doi.org/10.2967/jnumed.112.104661>.
- Chodak, Gerald W. 2008. 'Is the Increase in Orchiectomy for Prostate Cancer Patients Appropriate?' *Cancer* 112 (10): 2106–7. <https://doi.org/10.1002/cncr.23417>.
- Choueiri, Toni K, Wanling Xie, Anthony V D Amico, Robert W Ross, Jim C Hu, Meredith M Regan, Mary-ellen Taplin, Philip W Kantoff, Oliver Sartor, and William K Oh. 2010. 'Time to PSA Nadir Independently Predicts Overall Survival in Metastatic Hormone Sensitive Prostate Cancer Patients Treated with Androgen Deprivation Therapy' 115 (5): 981–87. <https://doi.org/10.1002/cncr.24064>.Time.
- Clarke, N. W., A. Ali, F. C. Ingleby, A. Hoyle, C. L. Amos, G. Attard, C. D. Brawley, et al. 2019. 'Addition of Docetaxel to Hormonal Therapy in Low- And High-Burden Metastatic Hormone

- Sensitive Prostate Cancer: Long-Term Survival Results from the STAMPEDE Trial'. *Annals of Oncology* 30 (12): 1992–2003. <https://doi.org/10.1093/annonc/mdz396>.
- Congress, Annual, and Nuclear Medicine October. 2022. 'Annual Congress of the European Association of Nuclear Medicine October 15-19, 2022 Barcelona, Spain'. *European Journal of Nuclear Medicine and Molecular Imaging* 49 (S1): 1–751. <https://doi.org/10.1007/s00259-022-05924-4>.
- Corfield, Julia, Marlon Perera, Damien Bolton, and Nathan Lawrentschuk. 2018. '68Ga-Prostate Specific Membrane Antigen (PSMA) Positron Emission Tomography (PET) for Primary Staging of High-Risk Prostate Cancer: A Systematic Review'. *World Journal of Urology* 36 (4): 519–27. <https://doi.org/10.1007/s00345-018-2182-1>.
- Coughlin, Geoffrey D., John W. Yaxley, Suzanne K. Chambers, Stefano Occhipinti, Hema Samaratunga, Leah Zajdlewicz, Patrick Teloken, et al. 2018. 'Robot-Assisted Laparoscopic Prostatectomy versus Open Radical Retropubic Prostatectomy: 24-Month Outcomes from a Randomised Controlled Study'. *The Lancet Oncology* 19 (8): 1051–60. [https://doi.org/10.1016/S1470-2045\(18\)30357-7](https://doi.org/10.1016/S1470-2045(18)30357-7).
- Culp, Mary Beth B., Isabelle Soerjomataram, Jason A. Efstathiou, Freddie Bray, and Ahmedin Jemal. 2020. 'Recent Global Patterns in Prostate Cancer Incidence and Mortality Rates'. *European Urology* 77 (1): 38–52. <https://doi.org/10.1016/j.eururo.2019.08.005>.
- Cytawa, Wojciech, Anna Katharina Seitz, Stefan Kircher, Kazuhito Fukushima, Johannes Tran-Gia, Andreas Schirbel, Tomasz Bandurski, et al. 2020. '68Ga-PSMA I&T PET/CT for Primary Staging of Prostate Cancer'. *European Journal of Nuclear Medicine and Molecular Imaging* 47 (1): 168–77. <https://doi.org/10.1007/s00259-019-04524-z>.
- D'Amico, Anthony V., Ming Hui Chen, Andrew A. Renshaw, Marian Loffredo, and Philip W. Kantoff. 2008. 'Androgen Suppression and Radiation vs Radiation Alone for Prostate Cancer: A Randomized Trial'. *Jama* 299 (3): 289–95. <https://doi.org/10.1001/jama.299.3.289>.
- Davis, Ian D., Andrew J. Martin, Martin R. Stockler, Stephen Begbie, Kim N. Chi, Simon Chowdhury, Xanthi Coskinas, et al. 2019. 'Enzalutamide with Standard First-Line Therapy in Metastatic Prostate Cancer'. *New England Journal of Medicine* 381 (2): 121–31. <https://doi.org/10.1056/nejmoa1903835>.
- Denham, James W., Allison Steigler, David S. Lamb, David Joseph, Sandra Turner, John Matthews, Chris Atkinson, et al. 2011. 'Short-Term Neoadjuvant Androgen Deprivation and Radiotherapy for Locally Advanced Prostate Cancer: 10-Year Data from the TROG 96.01 Randomised Trial'. *The Lancet Oncology* 12 (5): 451–59. [https://doi.org/10.1016/S1470-2045\(11\)70063-8](https://doi.org/10.1016/S1470-2045(11)70063-8).
- Dickerman, Barbra A, Sarah Coseo Markt, Markku Koskenvuo, Eero Pukkala, A Mucci, Jaakko Kaprio, and Finnish Cancer Registry. 2017. 'Alcohol Intake, Drinking Patterns, and Prostate Cancer Risk and Mortality : A 30-Year Prospective Cohort Study of Finnish Twins' 27 (9): 1049–58. <https://doi.org/10.1007/s10552-016-0778-6>.Alcohol.
- Dusing, Reginald W., Warner Peng, Sue Min Lai, Gordon L. Grado, Jeffrey M. Holzbeierlein, J. Brantley Thrasher, Jacqueline Hill, and Peter J. Van Veldhuizen. 2014. 'Prostate-Specific Antigen and Prostate-Specific Antigen Velocity as Threshold Indicators in 11C-Acetate PET/CTAC Scanning for Prostate Cancer Recurrence'. *Clinical Nuclear Medicine* 39 (9): 777–83. <https://doi.org/10.1097/RLU.0000000000000516>.
- Dyrberg, Eva, Helle W Hendel, Tri Hien Viet Huynh, Tobias Wrenfeldt Klausen, Vibeke B Løgager, Claus Madsen, Erik M Pedersen, Maria Pedersen, and Henrik S Thomsen. 2019. '(68)Ga-PSMA-PET/CT in Comparison with (18)F-Fluoride-PET/CT and Whole-Body MRI for the Detection of Bone Metastases in Patients with Prostate Cancer: A Prospective Diagnostic Accuracy Study.' *European Radiology* 29 (3): 1221–30. <https://doi.org/10.1007/s00330-018-5682-x>.
- Eary, Janet F., and David A. Mankoff. 1998. 'Tumor Metabolic Rates in Sarcoma Using FDG PET'. *Journal of Nuclear Medicine* 39 (2): 250–54.
- Eder, Matthias, Martin Schäfer, Ulrike Bauder-Wüst, William-Edmund Hull, Carmen Wängler, Walter Mier, Uwe Haberkorn, and Michael Eisenhut. 2012. '68Ga-Complex Lipophilicity and the

- Targeting Property of a Urea-Based PSMA Inhibitor for PET Imaging.’ *Bioconjugate Chemistry* 23 (4): 688–97. <https://doi.org/10.1021/bc200279b>.
- Ehfert, Peter, A. J. Beniers, Y. Tamimi, S. Handt, and G. Jakse. 2004. ‘Expression of Glucose Transporter 1 (Glut-1) in Cell Lines and Clinical Specimens from Human Prostate Adenocarcinoma’. *Anticancer Research* 24 (5 A): 3057–63.
- Ehman, Eric C., Geoffrey B. Johnson, Javier E. Villanueva-Meyer, Soonmee Cha, Andrew Palmera Leynes, Peder Eric Zufall Larson, and Thomas A. Hope. 2017. ‘PET/MRI: Where Might It Replace PET/CT?’ *Journal of Magnetic Resonance Imaging* 46 (5): spcone-spcone. <https://doi.org/10.1002/jmri.25872>.
- Eiber, M., T. Maurer, M. Souvatzoglou, A. J. Beer, A. Ruffani, B. Haller, F.-P. Graner, et al. 2015. ‘Evaluation of Hybrid 68Ga-PSMA Ligand PET/CT in 248 Patients with Biochemical Recurrence After Radical Prostatectomy’. *Journal of Nuclear Medicine* 56 (5): 668–74. <https://doi.org/10.2967/jnumed.115.154153>.
- Eiber, Matthias, Ken Herrmann, Jeremie Calais, Boris Hadaschik, Frederik L. Giesel, Markus Hartenbach, Thomas Hope, et al. 2018. ‘Prostate Cancer Molecular Imaging Standardized Evaluation (PROMISE): Proposed MiTNM Classification for the Interpretation of PSMA-Ligand PET/CT’. *Journal of Nuclear Medicine* 59 (3): 469–78. <https://doi.org/10.2967/jnumed.117.198119>.
- Eiber, Matthias, Markus Kroenke, Alexander Wurzer, Lena Ulbrich, Lena Jooß, Tobias Maurer, Thomas Horn, et al. 2020. ‘18F-RhPSMA-7 PET for the Detection of Biochemical Recurrence of Prostate Cancer After Radical Prostatectomy’. *Journal of Nuclear Medicine : Official Publication, Society of Nuclear Medicine* 61 (5): 696–701. <https://doi.org/10.2967/jnumed.119.234914>.
- Eisenhauer, E. A., P. Therasse, J. Bogaerts, L. H. Schwartz, D. Sargent, R. Ford, J. Dancey, et al. 2009. ‘New Response Evaluation Criteria in Solid Tumours: Revised RECIST Guideline (Version 1.1)’. *European Journal of Cancer* 45 (2): 228–47. <https://doi.org/10.1016/j.ejca.2008.10.026>.
- Emmett, Louise, Pim J. van Leeuwen, Rohan Nandurkar, Matthijs J. Scheltema, Thomas Cusick, George Hruby, Andrew Kneebone, et al. 2017. ‘Treatment Outcomes from 68 Ga-PSMA PET/CT–Informed Salvage Radiation Treatment in Men with Rising PSA After Radical Prostatectomy: Prognostic Value of a Negative PSMA PET’. *Journal of Nuclear Medicine* 58 (12): 1972–76. <https://doi.org/10.2967/jnumed.117.196683>.
- Emmett, Louise, Reuben Tang, Rohan Nandurkar, George Hruby, Paul Roach, Jo Anne Watts, Thomas Cusick, et al. 2020. ‘3-Year Freedom from Progression after 68Ga-PSMA PET/CT-Triaged Management in Men with Biochemical Recurrence after Radical Prostatectomy: Results of a Prospective Multicenter Trial’. *Journal of Nuclear Medicine* 61 (6): 866–72. <https://doi.org/10.2967/jnumed.119.235028>.
- Emmett, Louise, Charlotte Yin, Megan Crumbaker, George Hruby, Andrew Kneebone, Richard Epstein, Quoc Nguyen, et al. 2019. ‘Rapid Modulation of PSMA Expression by Androgen Deprivation: Serial 68Ga-PSMA-11 PET in Men with Hormone-Sensitive and Castrate-Resistant Prostate Cancer Commencing Androgen Blockade’. *Journal of Nuclear Medicine* 60 (7): 950–54. <https://doi.org/10.2967/jnumed.118.223099>.
- Eskelinen, Jari Joonas, Ilkka Heinonen, Eliisa Löyttyniemi, Virva Saunavaara, Anna Kirjavainen, Kirsi A. Virtanen, Jarna C. Hannukainen, and Kari K. Kalliokoski. 2015. ‘Muscle-Specific Glucose and Free Fatty Acid Uptake after Sprint Interval and Moderate-Intensity Training in Healthy Middle-Aged Men’. *Journal of Applied Physiology* 118 (9): 1172–80. <https://doi.org/10.1152/jappphysiol.01122.2014>.
- Esposito, K., P. Chiodini, A. Capuano, G. Bellastella, M. I. Maiorino, E. Parretta, A. Lenzi, and D. Giugliano. 2013. ‘Effect Ofmetabolic Syndrome and Its Components on Prostate Cancer Risk:Meta-Analysis’. *Journal of Endocrinological Investigation* 36 (2): 132–39. <https://doi.org/10.1007/BF03346748>.
- Evangelista, Laura, Francesco Bertoldo, Francesco Boccardo, Giario Conti, Ilario Menchi, Francesco Mungai, Umberto Ricardi, and Emilio Bombardieri. 2016. ‘Diagnostic Imaging to Detect and Evaluate Response to Therapy in Bone Metastases from Prostate Cancer: Current Modalities and New Horizons’. *European Journal of Nuclear Medicine and Molecular Imaging* 43 (8): 1546–62. <https://doi.org/10.1007/s00259-016-3350-4>.



- Evangelista, Laura, Andrea Guttilla, Fabio Zattoni, Pier Carlo Muzzio, and Filiberto Zattoni. 2013. 'Utility of Choline Positron Emission Tomography/Computed Tomography for Lymph Node Involvement Identification in Intermediate- to High-Risk Prostate Cancer: A Systematic Literature Review and Meta-Analysis'. *European Urology* 63 (6): 1040–48. <https://doi.org/10.1016/j.eururo.2012.09.039>.
- Evangelista, Laura, Fabio Zattoni, Gianluca Cassarino, Paolo Artioli, Diego Cecchin, Fabrizio dal Moro, and Pietro Zucchetta. 2021. 'PET/MRI in Prostate Cancer: A Systematic Review and Meta-Analysis'. *European Journal of Nuclear Medicine and Molecular Imaging* 48 (3): 859–73. <https://doi.org/10.1007/s00259-020-05025-0>.
- Evangelista, Laura, Fabio Zattoni, Andrea Guttilla, Giorgio Saladini, Filiberto Zattoni, Patrick M. Colletti, and Domenico Rubello. 2013. 'Choline PET or PET/CT and Biochemical Relapse of Prostate Cancer'. *Clinical Nuclear Medicine* 38 (5): 305–14. <https://doi.org/10.1097/rlu.0b013e3182867f3c>.
- Facchini, Gaetano, Orazio Caffo, Cinzia Ortega, Carmine D'Aniello, Marilena Di Napoli, Sabrina C. Cecere, Chiara Della Pepa, et al. 2016. 'Very Early PSA Response to Abiraterone in MCRPC Patients: A Novel Prognostic Factor Predicting Overall Survival'. *Frontiers in Pharmacology* 7 (MAY): 1–8. <https://doi.org/10.3389/fphar.2016.00123>.
- Fanti, Stefano, Karolien Goffin, Boris A. Hadaschik, Ken Herrmann, Tobias Maurer, Steven MacLennan, Daniela E. Oprea-Lager, et al. 2021. 'Consensus Statements on PSMA PET/CT Response Assessment Criteria in Prostate Cancer'. *European Journal of Nuclear Medicine and Molecular Imaging* 48 (2): 469–76. <https://doi.org/10.1007/s00259-020-04934-4>.
- Fanti, Stefano, Boris Hadaschik, and Ken Herrmann. 2020. 'Proposal for Systemic-Therapy Response-Assessment Criteria at the Time of PSMA PET/CT Imaging: The PSMA PET Progression Criteria'. *Journal of Nuclear Medicine* 61 (5): 678–82. <https://doi.org/10.2967/jnumed.119.233817>.
- Fanti, Stefano, Silvia Minozzi, Paolo Castellucci, Sara Balduzzi, Ken Herrmann, Bernd Joachim Krause, Wim Oyen, and Arturo Chiti. 2016. 'PET/CT with 11C-Choline for Evaluation of Prostate Cancer Patients with Biochemical Recurrence: Meta-Analysis and Critical Review of Available Data'. *European Journal of Nuclear Medicine and Molecular Imaging* 43 (1): 55–69. <https://doi.org/10.1007/s00259-015-3202-7>.
- Fanti, Stefano, Silvia Minozzi, Joshua James Morigi, Frederik Giesel, Francesco Ceci, Christian Uprimny, Michael S. Hofman, et al. 2017. 'Development of Standardized Image Interpretation for 68Ga-PSMA PET/CT to Detect Prostate Cancer Recurrent Lesions'. *European Journal of Nuclear Medicine and Molecular Imaging* 44 (10): 1622–35. <https://doi.org/10.1007/s00259-017-3725-1>.
- Fendler, Wolfgang P., Jeremie Calais, Matthias Eiber, Robert R. Flavell, Ashley Mishoe, Felix Y. Feng, Hao G. Nguyen, et al. 2019. 'Assessment of 68Ga-PSMA-11 PET Accuracy in Localizing Recurrent Prostate Cancer: A Prospective Single-Arm Clinical Trial'. *JAMA Oncology* 5 (6): 856–63. <https://doi.org/10.1001/jamaoncol.2019.0096>.
- Ferdinandus, Justin, John Violet, Shahneen Sandhu, Rodney J. Hicks, Aravind S. Ravi Kumar, Amir Iravani, Grace Kong, et al. 2020. 'Prognostic Biomarkers in Men with Metastatic Castration-Resistant Prostate Cancer Receiving [177Lu]-PSMA-617'. *European Journal of Nuclear Medicine and Molecular Imaging* 47 (10): 2322–27. <https://doi.org/10.1007/s00259-020-04723-z>.
- Feria Cardet, Rafael E. de, Michael S. Hofman, Tatiana Segard, Jackie Yim, Scott Williams, Roslyn J. Francis, Mark Frydenberg, Nathan Lawrentschuk, Declan G. Murphy, and Richard De Abreu Lourenco. 2021. 'Is Prostate-Specific Membrane Antigen Positron Emission Tomography/Computed Tomography Imaging Cost-Effective in Prostate Cancer: An Analysis Informed by the ProPSMA Trial'. *European Urology* 79 (3): 413–18. <https://doi.org/10.1016/j.eururo.2020.11.043>.
- Ferraro, Daniela A., Anton S. Becker, Benedikt Kranzbühler, Iliana Mebert, Anka Baltensperger, Konstantinos G. Zeimpekis, Hannes Grünig, et al. 2021. 'Diagnostic Performance of 68Ga-PSMA-11 PET/MRI-Guided Biopsy in Patients with Suspected Prostate Cancer: A Prospective Single-Center Study'. *European Journal of Nuclear Medicine and Molecular Imaging* 48 (10): 3315–24. <https://doi.org/10.1007/s00259-021-05261-y>.

- Feuerecker, Benedikt, Maythinee Chantadisai, Anne Allmann, Robert Tauber, Jakob Allmann, Lisa Steinhelfer, Isabel Rauscher, et al. 2022. 'Pre-Therapeutic Comparative Dosimetry of  $^{177}\text{Lu}$ -RhPSMA-7.3 and  $^{177}\text{Lu}$ -PSMA-I&T in Patients with Metastatic Castration Resistant Prostate Cancer (MCRPC)'. *Journal of Nuclear Medicine* 63 (6): 833–39. <https://doi.org/10.2967/jnumed.121.262671>.
- Fizazi, Karim, NamPhuong Tran, Luis Fein, Nobuaki Matsubara, Alfredo Rodriguez-Antolin, Boris Y. Alekseev, Mustafa Özgüroğlu, et al. 2017. 'Abiraterone plus Prednisone in Metastatic, Castration-Sensitive Prostate Cancer'. *New England Journal of Medicine* 377 (4): 352–60. <https://doi.org/10.1056/nejmoa1704174>.
- Fonager, Randi F, Helle D Zacho, Niels C Langkilde, Joan Fledelius, June A Ejlersen, Christian Haarmark, Helle W Hendel, et al. 2017. 'Diagnostic Test Accuracy Study of  $^{18}\text{F}$ -Sodium Fluoride PET/CT,  $^{99\text{mTc}}$ -Labelled Diphosphonate SPECT/CT, and Planar Bone Scintigraphy for Diagnosis of Bone Metastases in Newly Diagnosed, High-Risk Prostate Cancer.' *American Journal of Nuclear Medicine and Molecular Imaging* 7 (5): 218–27.
- Foss, Catherine A., Ronnie C. Mease, Hong Fan, Yuchuan Wang, Hayden T. Ravert, Robert F. Dannals, Ratal T. Olszewski, Warren D. Heston, Alan P. Kozikowski, and Martin G. Pomper. 2005. 'Radiolabeled Small-Molecule Ligands for Prostate-Specific Membrane Antigen: In Vivo Imaging in Experimental Models of Prostate Cancer'. *Clinical Cancer Research* 11 (11): 4022–28. <https://doi.org/10.1158/1078-0432.CCR-04-2690>.
- Fossati, Nicola, Peter Paul M. Willemse, Thomas Van den Broeck, Roderick C.N. van den Bergh, Cathy Yuhong Yuan, Erik Briers, Joaquim Bellmunt, et al. 2017. 'The Benefits and Harms of Different Extents of Lymph Node Dissection During Radical Prostatectomy for Prostate Cancer: A Systematic Review'. *European Urology* 72 (1): 84–109. <https://doi.org/10.1016/j.eururo.2016.12.003>.
- Gafita, Andrei, Isabel Rauscher, Manuel Weber, Boris Hadaschik, Hui Wang, Wesley Robert Armstrong, Robert Tauber, et al. 2022. 'Novel Framework for Treatment Response Evaluation Using PSMA-PET/CT in Patients with Metastatic Castration-Resistant Prostate Cancer (RECIP 1.0): An International Multicenter Study'. *Journal of Nuclear Medicine*, jnumed.121.263072. <https://doi.org/10.2967/jnumed.121.263072>.
- Galiza Barbosa, Felipe De, Marcelo Araujo Queiroz, Rafael Fernandes Nunes, Larissa Bastos Costa, Elaine Caroline Zaniboni, José Flavio Gomes Marin, Giovanni Guido Cerri, and Carlos Alberto Buchpiguel. 2020. 'Nonprostatic Diseases on PSMA PET Imaging: A Spectrum of Benign and Malignant Findings'. *Cancer Imaging* 20 (1): 1–23. <https://doi.org/10.1186/s40644-020-00300-7>.
- Gandaglia, Giorgio, Firas Abdollah, Jonas Schiffmann, Vincent Trudeau, Shahrokh F. Shariat, Simon P. Kim, Paul Perrotte, et al. 2014. 'Distribution of Metastatic Sites in Patients with Prostate Cancer: A Population-Based Analysis'. *Prostate* 74 (2): 210–16. <https://doi.org/10.1002/pros.22742>.
- Ghosh, Arundhati, and Warren D.W. Heston. 2004. 'Tumor Target Prostate Specific Membrane Antigen (PSMA) and Its Regulation in Prostate Cancer'. *Journal of Cellular Biochemistry* 91 (3): 528–39. <https://doi.org/10.1002/jcb.10661>.
- Giesel, Frederik L., B. Hadaschik, J. Cardinale, J. Radtke, M. Vinsensia, W. Lehnert, C. Kesch, et al. 2017. 'F-18 Labelled PSMA-1007: Biodistribution, Radiation Dosimetry and Histopathological Validation of Tumor Lesions in Prostate Cancer Patients'. *European Journal of Nuclear Medicine and Molecular Imaging* 44 (4): 678–88. <https://doi.org/10.1007/s00259-016-3573-4>.
- Giesel, Frederik L., Karina Knorr, Fabian Spohn, Leon Will, Tobias Maurer, Paul Flechsig, Oliver Neels, et al. 2019. 'Detection Efficacy of  $^{18}\text{F}$ -PSMA-1007 PET/CT in 251 Patients with Biochemical Recurrence of Prostate Cancer after Radical Prostatectomy'. *Journal of Nuclear Medicine* 60 (3): 362–68. <https://doi.org/10.2967/jnumed.118.212233>.
- Giesel, Frederik L., Clemens Kratochwil, Joel Schlittenhardt, Katharina Dendl, Matthias Eiber, Fabian Staudinger, Lukas Kessler, et al. 2021. 'Head-to-Head Intra-Individual Comparison of Biodistribution and Tumor Uptake of  $^{68}\text{Ga}$ -FAPI and  $^{18}\text{F}$ -FDG PET/CT in Cancer Patients'. *European Journal of Nuclear Medicine and Molecular Imaging* 48 (13): 4377–85. <https://doi.org/10.1007/s00259-021-05307-1>.

- Gill, Inderbir S, Abdel-rahmene Azzouzi, Mark Emberton, A Jonathan, Emmanuel Coeytaux, Avigdor Scherz, Peter T Scardino, Los Angeles, Interventional Science, and Urology Service. 2019. 'Randomized Trial of Partial Gland Ablation with Vascular Targeted Phototherapy versus Active Surveillance for Low-Risk Prostate Cancer: Extended Follow-up and Analyses of Effectiveness' 200 (4): 786–93. <https://doi.org/10.1016/j.juro.2018.05.121>. Randomized.
- Giri, Veda N., Sarah E. Hegarty, Colette Hyatt, Erin O'Leary, John Garcia, Karen E. Knudsen, William K. Kelly, and Leonard G. Gomella. 2019. 'Germline Genetic Testing for Inherited Prostate Cancer in Practice: Implications for Genetic Testing, Precision Therapy, and Cascade Testing'. *Prostate* 79 (4): 333–39. <https://doi.org/10.1002/pros.23739>.
- Goffin, Karolien E., Steven Joniau, Peter Tenke, Kevin Slawin, Eric A. Klein, Nancy Stambler, Thomas Strack, John Babich, Thomas Armor, and Vivien Wong. 2017. 'Phase 2 Study of 99m Tc-Trofolostat SPECT/CT to Identify and Localize Prostate Cancer in Intermediate- and High-Risk Patients Undergoing Radical Prostatectomy and Extended Pelvic LN Dissection'. *Journal of Nuclear Medicine* 58 (9): 1408–13. <https://doi.org/10.2967/jnumed.116.187807>.
- Gravis, Gwenaelle, Karim Fizazi, Florence Joly, Stéphane Oudard, Franck Priou, Benjamin Esterni, Igor Latorzeff, et al. 2013. 'Androgen-Deprivation Therapy Alone or with Docetaxel in Non-Castrate Metastatic Prostate Cancer (GETUG-AFU 15): A Randomised, Open-Label, Phase 3 Trial'. *The Lancet Oncology* 14 (2): 149–58. [https://doi.org/10.1016/S1470-2045\(12\)70560-0](https://doi.org/10.1016/S1470-2045(12)70560-0).
- Grubmüller, Bernhard, Sazan Rasul, Pascal Baltzer, Harun Fajkovic, David D'Andrea, Florian Berndl, Agnes Maj-Hes, et al. 2020. 'Response Assessment Using [68Ga]Ga-PSMA Ligand PET in Patients Undergoing Systemic Therapy for Metastatic Castration-Resistant Prostate Cancer'. *Prostate* 80 (1): 74–82. <https://doi.org/10.1002/pros.23919>.
- Gupta, Manoj, Partha Sarathi Choudhury, Sudhir Rawal, Harish Chandra Goel, and Shriram Avinash Rao. 2020. 'Evaluation of Response in Patients of Metastatic Castration Resistant Prostate Cancer Undergoing Systemic Radiotherapy with Lutetium177-Prostate-Specific Membrane Antigen: A Comparison between Response Evaluation Criteria in Solid Tumors, Positron-Emission'. *Urology Annals* 12 (4): 396. <https://doi.org/10.4103/0974-7796.250559>.
- Haas, Gabriel P., Nicolas Delongchamps, Otis W. Brawley, Ching Y. Wang, and Gustavo de la Roza. 2008. 'The Worldwide Epidemiology of Prostate Cancer: Perspectives from Autopsy Studies.' *The Canadian Journal of Urology* 15 (1): 3866–71.
- Habl, Gregor, Katharina Sauter, Kilian Schiller, Sabrina Dewes, Tobias Maurer, Matthias Eiber, and Stephanie E. Combs. 2017. '68 Ga-PSMA-PET for Radiation Treatment Planning in Prostate Cancer Recurrences after Surgery: Individualized Medicine or New Standard in Salvage Treatment'. *The Prostate* 77 (8): 920–27. <https://doi.org/10.1002/pros.23347>.
- Hagens, Marinus Jan, Daniela E Oprea-Lager, Andre N. Vis, Maurits Wondergem, Maarten L. Donswijk, Dennie Meijer, Louise Emmett, Pim J van Leeuwen, and Henk G. van der Poel. 2022. 'Reproducibility of PSMA PET/CT Imaging for Primary Staging of Treatment-Naïve Prostate Cancer Patients Depends on the Applied Radiotracer: A Retrospective Study'. *Journal of Nuclear Medicine* 2548: jnumed.121.263139. <https://doi.org/10.2967/jnumed.121.263139>.
- Hamdy, Freddie C., Jenny L. Donovan, J. Athene Lane, Malcolm Mason, Chris Metcalfe, Peter Holding, Michael Davis, et al. 2016. '10-Year Outcomes after Monitoring, Surgery, or Radiotherapy for Localized Prostate Cancer'. *New England Journal of Medicine* 375 (15): 1415–24. <https://doi.org/10.1056/nejmoa1606220>.
- Harmon, Stephanie A, Ethan Bergvall, Esther Mena, Joanna H Shih, Stephen Adler, Yolanda McKinney, Sherif Mehravivand, et al. 2018. 'A Prospective Comparison of (18)F-Sodium Fluoride PET/CT and PSMA-Targeted (18)F-DCFBC PET/CT in Metastatic Prostate Cancer.' *Journal of Nuclear Medicine: Official Publication, Society of Nuclear Medicine* 59 (11): 1665–71. <https://doi.org/10.2967/jnumed.117.207373>.
- Harris, Paul A., Robert Taylor, Brenda L. Minor, Veida Elliott, Michelle Fernandez, Lindsay O'Neal, Laura McLeod, et al. 2019. 'The REDCap Consortium: Building an International Community of

- Software Platform Partners'. *Journal of Biomedical Informatics* 95 (July): 103208. <https://doi.org/10.1016/J.JBI.2019.103208>.
- Haseebuddin, Mohammed, Farrokh Dehdashti, Barry A. Siegel, Jingxia Liu, Elizabeth B. Roth, Kenneth G. Nepple, Cary L. Siegel, et al. 2013. '11C-Acetate PET/CT before Radical Prostatectomy: Nodal Staging and Treatment Failure Prediction'. *Journal of Nuclear Medicine* 54 (5): 699–706. <https://doi.org/10.2967/jnumed.112.111153>.
- Heemsbergen, Wilma D., Abraham Al-Mamgani, Annerie Slot, Michel F.H. Dielwart, and Joos V. Lebesque. 2014. 'Long-Term Results of the Dutch Randomized Prostate Cancer Trial: Impact of Dose-Escalation on Local, Biochemical, Clinical Failure, and Survival'. *Radiotherapy and Oncology* 110 (1): 104–9. <https://doi.org/10.1016/j.radonc.2013.09.026>.
- Heesakkers, Roel AM, Anke M. Hövels, Gerrit J. Jager, Harrie CM van den Bosch, J. Alfred Witjes, Hein PJ Raat, Johan L. Severens, et al. 2008. 'MRI with a Lymph-Node-Specific Contrast Agent as an Alternative to CT Scan and Lymph-Node Dissection in Patients with Prostate Cancer: A Prospective Multicohort Study'. *The Lancet Oncology* 9 (9): 850–56. [https://doi.org/10.1016/S1470-2045\(08\)70203-1](https://doi.org/10.1016/S1470-2045(08)70203-1).
- Hemminki, Kari. 2012. 'Familial Risk and Familial Survival in Prostate Cancer'. *World Journal of Urology* 30 (2): 143–48. <https://doi.org/10.1007/s00345-011-0801-1>.
- Hicks, Rodney J., Declan G. Murphy, and Scott G. Williams. 2017. 'Seduction by Sensitivity: Reality, Illusion, or Delusion? The Challenge of Assessing Outcomes after PSMA Imaging Selection of Patients for Treatment'. *Journal of Nuclear Medicine* 58 (12): 1969–71. <https://doi.org/10.2967/jnumed.117.198812>.
- Hillier, Shawn M., Kevin P. Maresca, Genliang Lu, Ross D. Merkin, John C. Marquis, Craig N. Zimmerman, William C. Eckelman, John L. Joyal, and John W. Babich. 2013. '99mTc-Labeled Small-Molecule Inhibitors of Prostate-Specific Membrane Antigen for Molecular Imaging of Prostate Cancer'. *Journal of Nuclear Medicine* 54 (8): 1369–76. <https://doi.org/10.2967/jnumed.112.116624>.
- Hirmas, Nader, Catherine Leyh, Miriam Sraieb, Francesco Barbato, Benedikt M. Schaarschmidt, Lale Umutlu, Michael Nader, et al. 2021. '[68Ga]Ga-PSMA-11 PET/CT Improves Tumor Detection and Impacts Management in Patients with Hepatocellular Carcinoma'. *Journal of Nuclear Medicine* 62 (9): 1235–41. <https://doi.org/10.2967/jnumed.120.257915>.
- Hoffman, Richard M., David L. Clanon, Benjamin Littenberg, Joseph J. Frank, and John C. Peirce. 2000. 'Using the Free-to-Total Prostate-Specific Antigen Ratio to Detect Prostate Cancer in Men with Nonspecific Elevations of Prostate-Specific Antigen Levels'. *Journal of General Internal Medicine* 15 (10): 739–48. <https://doi.org/10.1046/j.1525-1497.2000.90907.x>.
- Hofman, Michael S., Louise Emmett, Shahneen Sandhu, Amir Iravani, Anthony M. Joshua, Jeffrey C. Goh, David A. Pattison, et al. 2021. '[177Lu]Lu-PSMA-617 versus Cabazitaxel in Patients with Metastatic Castration-Resistant Prostate Cancer (TheraP): A Randomised, Open-Label, Phase 2 Trial'. *The Lancet* 397 (10276): 797–804. [https://doi.org/10.1016/S0140-6736\(21\)00237-3](https://doi.org/10.1016/S0140-6736(21)00237-3).
- Hofman, Michael S., Nathan Lawrentschuk, Roslyn J. Francis, Colin Tang, Ian Vela, Paul Thomas, Natalie Rutherford, et al. 2020. 'Prostate-Specific Membrane Antigen PET-CT in Patients with High-Risk Prostate Cancer before Curative-Intent Surgery or Radiotherapy (ProPSMA): A Prospective, Randomised, Multicentre Study'. *The Lancet* 395 (10231): 1208–16. [https://doi.org/10.1016/S0140-6736\(20\)30314-7](https://doi.org/10.1016/S0140-6736(20)30314-7).
- Hofman, Michael S., John Violet, Rodney J. Hicks, Justin Ferdinandus, Sue Ping Thang, Tim Akhurst, Amir Iravani, et al. 2018. '[177Lu]-PSMA-617 Radionuclide Treatment in Patients with Metastatic Castration-Resistant Prostate Cancer (LuPSMA Trial): A Single-Centre, Single-Arm, Phase 2 Study'. *The Lancet Oncology* 19 (6): 825–33. [https://doi.org/10.1016/S1470-2045\(18\)30198-0](https://doi.org/10.1016/S1470-2045(18)30198-0).
- Hope, Thomas A., Matthias Eiber, Wesley R. Armstrong, Roxanna Juarez, Vishnu Murthy, Courtney Lawhn-Heath, Spencer C. Behr, et al. 2021. 'Diagnostic Accuracy of 68Ga-PSMA-11 PET for Pelvic Nodal Metastasis Detection Prior to Radical Prostatectomy and Pelvic Lymph Node

- Dissection: A Multicenter Prospective Phase 3 Imaging Trial'. *JAMA Oncology* 7 (11): 1635–42. <https://doi.org/10.1001/jamaoncol.2021.3771>.
- Horger, Marius, Susanne Martina Eschmann, Christina Pfannenber, Reinhard Vonthein, Hariolf Besenfelder, C. D. Claussen, and Roland Bares. 2004. 'Evaluation of Combined Transmission and Emission Tomography for Classification of Skeletal Lesions.' *AJR. American Journal of Roentgenology* 183 (3): 655–61. <https://doi.org/10.2214/ajr.183.3.1830655>.
- Horoszewicz, JS, E. Kawinski, GP Murphy, and D Murphy. 1987. 'Monoclonal Antibodies to a New Antigenic Marker in Epithelial Prostatic Cells and Serum of Prostatic Cancer Patients.' *Anticancer Res.* 7 (5B): 1809–18.
- Hosono, Makoto, Hideharu Ikebuchi, Yoshihide Nakamura, Nobutaka Nakamura, Takahiro Yamada, Sachiko Yanagida, Asami Kitaoka, et al. 2018. 'Manual on the Proper Use of Lutetium-177-Labeled Somatostatin Analogue (Lu-177-DOTA-TATE) Injectable in Radionuclide Therapy (2nd Ed.)'. *Annals of Nuclear Medicine* 32 (3): 217–35. <https://doi.org/10.1007/s12149-018-1230-7>.
- Hövels, A.M., R.A.M. Heesakkers, E.M. Adang, G.J. Jager, S. Strum, Y.L. Hoogeveen, J.L. Severens, and J.O. Barentsz. 2008. 'The Diagnostic Accuracy of CT and MRI in the Staging of Pelvic Lymph Nodes in Patients with Prostate Cancer: A Meta-Analysis'. *Clinical Radiology* 63 (4): 387–95. <https://doi.org/10.1016/J.CRAD.2007.05.022>.
- Ingvar, Jacob, Erland Hvittfeldt, Elin Trägårdh, Athanasios Simoulis, and Anders Bjartell. 2022. 'Assessing the Accuracy of [18F]PSMA-1007 PET/CT for Primary Staging of Lymph Node Metastases in Intermediate- and High-Risk Prostate Cancer Patients'. *EJNMMI Research* 12 (1). <https://doi.org/10.1186/s13550-022-00918-7>.
- Jadvar, Hossein. 2009. 'FDG PET in Prostate Cancer'. *PET Clinics* 23 (1): 1–7. <https://doi.org/10.1016/j.cpet.2009.05.002>.
- Jadvar. 2013. 'Imaging Evaluation of Prostate Cancer with 18Ffluorodeoxyglucose PET/CT: Utility and Limitations'. *Eur J Nucl Med Mol Imaging* 23 (1): 1–7. <https://doi.org/10.1007/s00259-013-2361-7>.
- Jadvar. 2016. 'Is There Utility for FDG PET in Prostate Cancer'. *Semi Nucl Med* 46 (6): 502–6. <https://doi.org/10.1053/j.semnuclmed.2016.07.004>.
- Jambor, Ivan, Ronald Borra, Jukka Kempainen, Virva Lepomäki, Riitta Parkkola, Kirsti Dean, Kalle Alanen, et al. 2012. 'Improved Detection of Localized Prostate Cancer Using Co-Registered MRI and 11C-Acetate PET/CT'. *European Journal of Radiology* 81 (11): 2966–72. <https://doi.org/10.1016/j.ejrad.2011.12.043>.
- Jambor, Ivan, Anna Kuisma, Susan Ramadan, Riikka Huovinen, Minna Sandell, Sami Kajander, Jukka Kempainen, et al. 2016. 'Prospective Evaluation of Planar Bone Scintigraphy, SPECT, SPECT/CT, 18 F-NaF PET/CT and Whole Body 1.5T MRI, Including DWI, for the Detection of Bone Metastases in High Risk Breast and Prostate Cancer Patients: SKELETA Clinical Trial'. *Acta Oncologica* 55 (1): 59–67. <https://doi.org/10.3109/0284186X.2015.1027411>.
- Jambor, Ivan, Janne Verho, Otto Ettala, Juha Knaapila, Pekka Taimen, Kari T. Syvänen, Aida Kiviniemi, et al. 2019. 'Validation of Improd Biparametric Mri in Men with Clinically Suspected Prostate Cancer: A Prospective Multi-Institutional Trial'. *PLoS Medicine* 16 (6). <https://doi.org/10.1371/journal.pmed.1002813>.
- James, Nicholas D., Johann S. de Bono, Melissa R. Spears, Noel W. Clarke, Malcolm D. Mason, David P. Dearnaley, Alastair W.S. Ritchie, et al. 2017. 'Abiraterone for Prostate Cancer Not Previously Treated with Hormone Therapy'. *New England Journal of Medicine* 377 (4): 338–51. <https://doi.org/10.1056/nejmoa1702900>.
- Jansen, B. H.E., Y. J.L. Bodar, G. J.C. Zwezerijnen, D. Meijer, J. P. van der Voorn, J. A. Nieuwenhuijzen, M. Wondergem, et al. 2020. 'Pelvic Lymph-Node Staging with 18F-DCFPyL PET/CT Prior to Extended Pelvic Lymph-Node Dissection in Primary Prostate Cancer - the SALT Trial -'. *European Journal of Nuclear Medicine and Molecular Imaging*. <https://doi.org/10.1007/s00259-020-04974-w>.

- Jensen, R.T., J.F. Battey, E.R. Spindel, and R.V. Benya. 2008. 'International Union of Pharmacology. LXVIII. Mammalian Bombesin Receptors: Nomenclature, Distribution, Pharmacology, Signaling and Functions in Normal and Disease States.' *Pharmacol Rev* 23 (1): 1–7.
- Ji, Guangjie, Gang Song, Cong Huang, Shiming He, and Liqun Zhou. n.d. 'Rapidly Decreasing Level of Prostate-Specific Antigen during Initial Androgen Deprivation Therapy Is a Risk Factor for Early Progression to Castration-Resistant Prostate Cancer: A Retrospective Study', 1–5.
- Johnson, David C., Steven S. Raman, Sohrab A. Mirak, Lorna Kwan, Amirhossein M. Bajgiran, William Hsu, Cleo K. Machara, et al. 2019. 'Detection of Individual Prostate Cancer Foci via Multiparametric Magnetic Resonance Imaging'. *European Urology* 75 (5): 712–20. <https://doi.org/10.1016/j.eururo.2018.11.031>.
- Johnsson, Kerstin, Johan Brynolfsson, Hannicka Sahlstedt, Nicholas G. Nickols, Matthew Rettig, Stephan Probst, Michael J. Morris, Anders Bjartell, Mathias Eiber, and Aseem Anand. 2022. 'Analytical Performance of APROMISE: Automated Anatomic Contextualization, Detection, and Quantification of [18F]DCFPyL (PSMA) Imaging for Standardized Reporting'. *European Journal of Nuclear Medicine and Molecular Imaging* 49 (3): 1041–51. <https://doi.org/10.1007/s00259-021-05497-8>.
- Juzeniene, Asta, Vilde Yuli Stenberg, Øyvind Sverre Bruland, and Roy Hartvig Larsen. 2021. 'Preclinical and Clinical Status of PsmA-Targeted Alpha Therapy for Metastatic Castration-Resistant Prostate Cancer'. *Cancers* 13 (4): 1–25. <https://doi.org/10.3390/cancers13040779>.
- Kahkonen, Esa, Ivan Jambor, Jukka Kempainen, Kaisa Lehtio, Tove J. Gronroos, Anna Kuisma, Pauliina Luoto, et al. 2013. 'In Vivo Imaging of Prostate Cancer Using [68Ga]-Labeled Bombesin Analog BAY86-7548'. *Clinical Cancer Research* 19 (19): 5434–43. <https://doi.org/10.1158/1078-0432.CCR-12-3490>.
- Kalbasi, Anusha, Jiaqi Li, Abigail T. Berman, Samuel Swisher-McClure, Marc Smaldone, Robert G. Uzzo, Dylan S. Small, Nandita Mitra, and Justin E. Bekelman. 2015. 'Dose-Escalated Irradiation and Overall Survival in Men with Nonmetastatic Prostate Cancer'. *JAMA Oncology* 1 (7): 897–906. <https://doi.org/10.1001/jamaoncol.2015.2316>.
- Kalmthout, Ludwike W.M. van, Harm H.E. van Melick, Jules Lavalaye, Richard P. Meijer, Anko Kooistra, John M.H. de Klerk, Arthur J.A.T. Braat, et al. 2020. 'Prospective Validation of Gallium-68 Prostate Specific Membrane Antigen-Positron Emission Tomography/Computerized Tomography for Primary Staging of Prostate Cancer'. *The Journal of Urology* 203 (3): 537–45. <https://doi.org/10.1097/JU.000000000000531>.
- Kasisvisvanathan, Veeru, Antti S. Rannikko, Marcelo Borghi, Valeria Panebianco, Lance A. Mynderse, Markku H. Vaarala, Alberto Briganti, et al. 2018. 'MRI-Targeted or Standard Biopsy for Prostate-Cancer Diagnosis'. *New England Journal of Medicine*, 1767–77. <https://doi.org/10.1056/nejmoa1801993>.
- Kato, Takashi, Eriko Tsukamoto, Yuji Kuge, Toshiaki Takei, Tohru Shiga, Nobuo Shinohara, Chietsugu Katoh, Kunihiko Nakada, and Nagara Tamaki. 2002. 'Accumulation of [11C]Acetate in Normal Prostate and Benign Prostatic Hyperplasia: Comparison with Prostate Cancer'. *European Journal of Nuclear Medicine* 29 (11): 1492–95. <https://doi.org/10.1007/s00259-002-0885-3>.
- Kesler, Mikhail, Charles Levine, Dov Hershkovitz, Eyal Mishani, Yoram Menachem, Hedva Lerman, Yaniv Zohar, Oren Shibolet, and Einat Even-Sapir. 2019. '68 Ga-Labeled Prostate-Specific Membrane Antigen Is a Novel PET/CT Tracer for Imaging of Hepatocellular Carcinoma: A Prospective Pilot Study'. *Journal of Nuclear Medicine* 60 (2): 185–91. <https://doi.org/10.2967/jnumed.118.214833>.
- Khreish, Fadi, Florian Rosar, Clemens Kratochwil, Frederik Lars Giesel, Uwe Haberkorn, and Samer Ezziddin. 2020. 'Positive FAPI-PET/CT in a Metastatic Castration-Resistant Prostate Cancer Patient with PSMA-Negative/FDG-Positive Disease'. *European Journal of Nuclear Medicine and Molecular Imaging* 47 (8): 2040–41. <https://doi.org/10.1007/s00259-019-04623-x>.
- Knaapila, Juha, Ivan Jambor, Otto Ettala, Pekka Taimen, Janne Verho, Ileana Montoya Perez, Aida Kiviniemi, et al. 2021. 'Negative Predictive Value of Biparametric Prostate Magnetic Resonance

- Imaging in Excluding Significant Prostate Cancer: A Pooled Data Analysis Based on Clinical Data from Four Prospective, Registered Studies'. *European Urology Focus* 7 (3): 522–31. <https://doi.org/10.1016/j.euf.2020.04.007>.
- Komori, Tsuyoshi, Isamu Narabayashi, Kaname Matsumura, Mitsuru Matsuki, Hiroyuki Akagi, Yasuharu Ogura, Fumitoshi Aga, and Itaru Adachi. 2007. '2-[Fluorine-18]-Fluoro-2-Deoxy-D-Glucose Positron Emission Tomography/Computed Tomography versus Whole-Body Diffusion-Weighted MRI for Detection of Malignant Lesions: Initial Experience'. *Annals of Nuclear Medicine* 21 (4): 209–15. <https://doi.org/10.1007/s12149-007-0010-6>.
- Kozikowski, A. P., F. Nan, P. Conti, J. Zhang, E. Ramadan, T. Bzdega, B. Wroblewska, J. H. Neale, S. Pshenichkin, and J. T. Wroblewski. 2001. 'Design of Remarkably Simple, yet Potent Urea-Based Inhibitors of Glutamate Carboxypeptidase II (NAALADase) [1]'. *Journal of Medicinal Chemistry* 44 (3): 298–301. <https://doi.org/10.1021/jm000406m>.
- Kratochwil, Clemens, Paul Flechsig, Thomas Lindner, Labidi Abderrahim, Annette Altmann, Walter Mier, Sebastian Adeberg, et al. 2019. '68Ga-FAPI PET/CT: Tracer Uptake in 28 Different Kinds of Cancer'. *Journal of Nuclear Medicine* 60 (6): 801–5. <https://doi.org/10.2967/jnumed.119.227967>.
- Kroenke, Markus, Lilit Mirzoyan, Thomas Horn, Jan C Peecken, Alexander Wurzer, Hans-Juergen Wester, Marcus Makowski, Wolfgang Andreas Weber, Matthias Eiber, and Isabel Rauscher. 2020. 'Matched-Pair Comparison of 68 Ga-PSMA-11 and 18 F-RhPSMA-7 PET/CT in Patients with Primary and Biochemical Recurrence of Prostate Cancer: Frequency of Non-Tumor Related Uptake and Tumor Positivity'. *Journal of Nuclear Medicine*, jnumed.120.251447. <https://doi.org/10.2967/jnumed.120.251447>.
- Kroenke, Markus, Alexander Wurzer, Kristina Schwamborn, Lena Ulbrich, Lena Jooß, Tobias Maurer, Thomas Horn, et al. 2020. 'Histologically Confirmed Diagnostic Efficacy of 18F-RhPSMA-7 PET for N-Staging of Patients with Primary High-Risk Prostate Cancer'. *Journal of Nuclear Medicine: Official Publication, Society of Nuclear Medicine* 61 (5): 710–15. <https://doi.org/10.2967/jnumed.119.234906>.
- Kumar, Arunav, Sreedharan Thankarajan ArunRaj, Khush Bhullar, K. P. Haresh, Subhash Gupta, Sanjana Ballal, Madhav Yadav, et al. 2022. 'Ga-68 PSMA PET/CT in Recurrent High-Grade Gliomas: Evaluating PSMA Expression in Vivo'. *Neuroradiology* 64 (5): 969–79. <https://doi.org/10.1007/s00234-021-02828-2>.
- Kunikowska, Jolanta, Ingeborga Charzyńska, Radosław Kuliński, Dariusz Pawlak, Michał Maurin, and Leszek Królicki. 2020. 'Tumor Uptake in Glioblastoma Multiforme after IV Injection of [177Lu]Lu-PSMA-617'. *European Journal of Nuclear Medicine and Molecular Imaging* 47 (6): 1605–6. <https://doi.org/10.1007/s00259-020-04715-z>.
- Kuyumcu, Serkan, Duygu Has-Simsek, Raim Iliaz, Yasemin Sanli, Fikret Buyukkaya, Filiz Akyuz, and Cuneyt Turkmen. 2019. 'Evidence of Prostate-Specific Membrane Antigen Expression in Hepatocellular Carcinoma Using 68Ga-PSMA PET/CT'. *Clinical Nuclear Medicine* 44 (9): 702–6. <https://doi.org/10.1097/RLU.0000000000002701>.
- Langbein, Thomas, Hui Wang, Isabel Rauscher, Markus Kroenke, Karina Knorr, Alexander Wurzer, Kristina Schwamborn, et al. 2022. 'Utility of 18 F-RhPSMA-7.3 PET for Imaging of Primary Prostate Cancer and Preoperative Efficacy in N-Staging of Unfavorable Intermediate- to Very High-Risk Patients Validated by Histopathology'. *Journal of Nuclear Medicine* 63 (9): 1334–42. <https://doi.org/10.2967/jnumed.121.263440>.
- Lecouvet, Frédéric E., Daphné Geukens, Annabelle Stainier, François Jamar, Jacques Jamart, Bertrand Janne D'Othée, Patrick Therasse, Bruno Vande Berg, and Bertrand Tombal. 2007. 'Magnetic Resonance Imaging of the Axial Skeleton for Detecting Bone Metastases in Patients with High-Risk Prostate Cancer: Diagnostic and Cost-Effectiveness and Comparison with Current Detection Strategies'. *Journal of Clinical Oncology* 25 (22): 3281–87. <https://doi.org/10.1200/JCO.2006.09.2940>.
- Lee, Chul Hee, Ilhan Lim, Sang Keun Woo, Kwang Il Kim, Kyo Chul Lee, Kanghyon Song, Chang Woon Choi, and Sang Moo Lim. 2022. 'The Feasibility of 64Cu-PSMA I&T PET for Prostate

- Cancer'. *Cancer Biotherapy and Radiopharmaceuticals* 37 (6): 417–23. <https://doi.org/10.1089/cbr.2020.4189>.
- Leest, Marloes van der, Erik Cornel, Bas Israël, Rianne Hendriks, Anwar R. Padhani, Martijn Hoogenboom, Patrik Zamecnik, et al. 2019. 'Head-to-Head Comparison of Transrectal Ultrasound-Guided Prostate Biopsy Versus Multiparametric Prostate Resonance Imaging with Subsequent Magnetic Resonance-Guided Biopsy in Biopsy-Naïve Men with Elevated Prostate-Specific Antigen: A Large Prospective Mu'. *European Urology* 75 (4): 570–78. <https://doi.org/10.1016/j.eururo.2018.11.023>.
- Lestingi, Jean F.P., Giuliano B. Guglielmetti, Quoc Dien Trinh, Rafael F. Coelho, Jose Pontes, Diogo A. Bastos, Mauricio D. Cordeiro, et al. 2021. 'Extended Versus Limited Pelvic Lymph Node Dissection During Radical Prostatectomy for Intermediate- and High-Risk Prostate Cancer: Early Oncological Outcomes from a Randomized Phase 3 Trial'. *European Urology* 79 (5): 595–604. <https://doi.org/10.1016/j.eururo.2020.11.040>.
- Liu, He, Ayyoppan K. Rajasekaran, Peggy Moy, Yan Xia, Sae Kim, Vincent Navarro, Rahmatullah Rahmati, and Neil H. Bander. 1998. 'Constitutive and Antibody-Induced Internalization of Prostate-Specific Membrane Antigen'. *Cancer Research* 58 (18): 4055–60.
- Logan, Jean, Joanna S Fowler, Nora D Volkow, Alfred P Wolf, Stephen L Dewey, David J Schlyer, Robert R Macgregor, et al. 2003. 'Graphical Analysis of Reversible Radioligand Binding from Time-Activity Measurements Applied to [N-11C-Methyl]-(-)-Cocaine PET Studies in Human Subjects'. *Journal of Cerebral Blood Flow and Metabolism*, no. 1981: 740–47.
- Luboldt, Wolfgang, Rainer Kufer, and Norbert Blumstein. 2008. 'Prostate Carcinoma: Diffusion-Weighted Imaging as Potential Alternative to Conventional MR and C-Choline PET/CT for Detection of Bone Metastases'. *Radiology*.
- Lütje, Susanne, Benedikt Gomez, Joseph Cohnen, Lale Umutlu, Martin Gotthardt, Thorsten D. Poeppel, Andreas Bockisch, and Sandra Rosenbaum-Krumme. 2017. 'Imaging of Prostate-Specific Membrane Antigen Expression in Metastatic Differentiated Thyroid Cancer Using 68Ga-HBED-CC-PSMA PET/CT'. *Clinical Nuclear Medicine* 42 (1): 20–25. <https://doi.org/10.1097/RLU.0000000000001454>.
- Lütje, Susanne, Sandra Heskamp, Alexander S. Cornelissen, Thorsten D. Poeppel, Sebastiaan A.M.W. van den Broek, Sandra Rosenbaum-Krumme, Andreas Bockisch, Martin Gotthardt, Mark Rijpkema, and Otto C. Boerman. 2015. 'PSMA Ligands for Radionuclide Imaging and Therapy of Prostate Cancer: Clinical Status'. *Theranostics* 5 (12): 1388–1401. <https://doi.org/10.7150/thno.13348>.
- Ma, Jiao, Lanying Li, Taiping Liao, Weidong Gong, and Chunyin Zhang. 2022. 'Efficacy and Safety of 225Ac-PSMA-617-Targeted Alpha Therapy in Metastatic Castration-Resistant Prostate Cancer: A Systematic Review and Meta-Analysis'. *Frontiers in Oncology* 12 (February). <https://doi.org/10.3389/fonc.2022.796657>.
- Maina, Theodosia, Hendrik Bergsma, Harshad R. Kulkarni, Dirk Mueller, David Charalambidis, Eric P. Krenning, Berthold A. Nock, Marion de Jong, and Richard P. Baum. 2016. 'Preclinical and First Clinical Experience with the Gastrin-Releasing Peptide Receptor-Antagonist [68Ga]SB3 and PET/CT'. *European Journal of Nuclear Medicine and Molecular Imaging* 43 (5): 964–73. <https://doi.org/10.1007/s00259-015-3232-1>.
- Malaspina, Simona, Pekka Taimen, Markku Kallajoki, Vesa Oikonen, Anna Kuisma, Otto Ettala, Kalle Mattila, et al. 2022. 'Uptake of 18F-RhPSMA-7.3 in Positron Emission Tomography Imaging of Prostate Cancer: A Phase 1 Proof-of-Concept Study'. *Cancer Biotherapy & Radiopharmaceuticals* 37 (3): 205–13. <https://doi.org/10.1089/cbr.2021.0322>.
- Man, Kathia De, Nick Van Laeken, Vanessa Schelfhout, Wolfgang P. Fendler, Bieke Lambert, Ken Kersemans, Sarah Piron, et al. 2022. '18F-PSMA-11 Versus 68Ga-PSMA-11 Positron Emission Tomography/Computed Tomography for Staging and Biochemical Recurrence of Prostate Cancer: A Prospective Double-Blind Randomised Cross-over Trial'. *European Urology* 82 (68): 501–9. <https://doi.org/10.1016/j.eururo.2022.05.010>.



- Mansi, Rosalba, Achim Fleischmann, Helmut R. Mäcke, and Jean C. Reubi. 2013. 'Targeting GRPR in Urological Cancers - From Basic Research to Clinical Application'. *Nature Reviews Urology* 10 (4): 235–44. <https://doi.org/10.1038/nrurol.2013.42>.
- Maresca, K. P., S. M. Hillier, F. J. Femia, D. Keith, C. Barone, J. L. Joyal, C. N. Zimmerman, et al. 2009. 'A Series of Halogenated Heterodimeric Inhibitors of Prostate Specific Membrane Antigen (PSMA) as Radiolabeled Probes for Targeting Prostate Cancer'. *Journal of Medicinal Chemistry* 52 (2): 347–57. <https://doi.org/10.1021/jm800994j>.
- Maurer, Tobias, Jürgen E. Gschwend, Isabel Rauscher, Michael Souvatzoglou, Bernhard Haller, Gregor Weirich, Hans Jürgen Wester, et al. 2016. 'Diagnostic Efficacy of 68Gallium-PSMA Positron Emission Tomography Compared to Conventional Imaging for Lymph Node Staging of 130 Consecutive Patients with Intermediate to High Risk Prostate Cancer'. *Journal of Urology* 195 (5): 1436–43. <https://doi.org/10.1016/j.juro.2015.12.025>.
- Maurer, Tobias, Stephanie Robu, Margret Schottelius, Kristina Schwamborn, Isabel Rauscher, Nynke S. van den Berg, Fjfs W.B. van Leeuwen, et al. 2019. '99m Technetium-Based Prostate-Specific Membrane Antigen–Radioguided Surgery in Recurrent Prostate Cancer'. *European Urology* 75 (4): 659–66. <https://doi.org/10.1016/j.eururo.2018.03.013>.
- McNeal, Je, Ea Redwine, Fs Freiha, and Ta Stamey. 1988. 'Zonal Distribution of Prostatic Adenocarcinoma. Correlation with Histologic Pattern and Direction of Spread'. *Am J Surg Pathol*.
- Mease, Ronnie C., Crystal L. Dusich, Catherine A. Foss, Hayden T. Ravert, Robert F. Dannals, Jurgen Seidel, Andrew Prideaux, et al. 2008. 'N-[N-[(S)-1,3-Dicarboxypropyl]Carbamoyl]-4-[18F]Fluorobenzyl-L- Cysteine, [18F]DCFCB: A New Imaging Probe for Prostate Cancer'. *Clinical Cancer Research* 14 (10): 3036–43. <https://doi.org/10.1158/1078-0432.CCR-07-1517>.
- Meller, B., F. Bremmer, C. O. Sahlmann, S. Hijazi, C. Bouter, L. Trojan, J. Meller, and P. Thelen. 2015. 'Alterations in Androgen Deprivation Enhanced Prostate-Specific Membrane Antigen (PSMA) Expression in Prostate Cancer Cells as a Target for Diagnostics and Therapy'. *EJNMMI Research* 5 (1): 1–11. <https://doi.org/10.1186/s13550-015-0145-8>.
- Michalski, Kerstin, Juri Ruf, Christian Goetz, Anna Katharina Seitz, Andreas K. Buck, Constantin Lapa, and Philipp E. Hartrampf. 2021. 'Prognostic Implications of Dual Tracer PET/CT: PSMA Ligand and [18F]FDG PET/CT in Patients Undergoing [177Lu]PSMA Radioligand Therapy'. *European Journal of Nuclear Medicine and Molecular Imaging* 48 (6): 2024–30. <https://doi.org/10.1007/s00259-020-05160-8>.
- Minamimoto, Ryogo, Steven Hancock, Bernadette Schneider, Frederick T. Chin, Mehran Jamali, Andreas Loening, Shreyas Vasanawala, Sanjiv Sam Gambhir, and Andrei Iagaru. 2016. 'Pilot Comparison of 68Ga-RM2 PET and 68Ga-PSMA-11 PET in Patients with Biochemically Recurrent Prostate Cancer'. *Journal of Nuclear Medicine* 57 (4): 557–62. <https://doi.org/10.2967/jnumed.115.168393>.
- Minn, H, Kr Zasadny, Le Quint, and Rl Wahl. 1995. 'Lung Cancer: Reproducibility of Quantitative Measurements for Evaluating 2-[F-18]-Fluoro-2-Deoxy-D-Glucose Uptake at PET'. *Radiology*.
- Minner, Sarah, Corinna Wittmer, Markus Graefen, Georg Salomon, Thomas Steuber, Alexander Haese, Hartwig Huland, et al. 2011. 'High Level PSMA Expression Is Associated with Early Psa Recurrence in Surgically Treated Prostate Cancer'. *Prostate* 71 (3): 281–88. <https://doi.org/10.1002/pros.21241>.
- Morigi, Joshua J., Phillip D. Stricker, Pim J. van Leeuwen, Reuben Tang, Bao Ho, Quoc Nguyen, George Hruby, et al. 2015. 'Prospective Comparison of 18F-Fluoromethylcholine Versus 68Ga-PSMA PET/CT in Prostate Cancer Patients Who Have Rising PSA After Curative Treatment and Are Being Considered for Targeted Therapy'. *Journal of Nuclear Medicine* 56 (8): 1185–90. <https://doi.org/10.2967/jnumed.115.160382>.
- Morris, Michael, Timothy Akhurst, Steven Larson, Marisa Ditullio, Elaina Chu, and Karen Siedlecki. 2005. 'Fluorodeoxyglucose Positron Emission Tomography as an Outcome Measure for Castrate

- Metastatic Prostate Cancer Treated with Antimicrotubule Chemotherapy'. *Clin Cancer Res* 23 (1): 1–7. <https://www.ncbi.nlm.nih.gov/pmc/articles/PMC3624763/pdf/nihms412728.pdf>.
- Morris, Michael J., Timothy Akhurst, Iman Osman, Rodolfo Nunez, Homer Macapinlac, Karen Siedlecki, David Verbel, Lawrence Schwartz, Steven M. Larson, and Howard I. Scher. 2002. 'Fluorinated Deoxyglucose Positron Emission Tomography Imaging in Progressive Metastatic Prostate Cancer'. *Urology* 59 (6): 913–18. [https://doi.org/10.1016/S0090-4295\(02\)01509-1](https://doi.org/10.1016/S0090-4295(02)01509-1).
- Morris, Michael J., Steven P. Rowe, Michael A. Gorin, Lawrence Saperstein, Frédéric Pouliot, David Josephson, Jeffrey Y.C. Wong, et al. 2021. 'Diagnostic Performance of 18F-DCFPyL-PET/CT in Men with Biochemically Recurrent Prostate Cancer: Results from the CONDOR Phase III, Multicenter Study'. *Clinical Cancer Research* 27 (13): 3674–82. <https://doi.org/10.1158/1078-0432.CCR-20-4573>.
- Mottet, N, J Bellmunt, E Briers, R.C.N van den Bergh, N.J van Casteren, P Cornford, S Culine, et al. 2022. 'Guidelines on Prostate Cancer. 2022 Update'. *European Association of Urology* 53 (March): 1–137. <https://uroweb.org/guideline/prostate-cancer/#3>.
- Mottet, Nicolas, Roderick C.N. van den Bergh, Erik Briers, Thomas Van den Broeck, Marcus G. Cumberbatch, Maria De Santis, Stefano Fanti, et al. 2021. 'EAU-EANM-ESTRO-ESUR-SIOG Guidelines on Prostate Cancer—2020 Update. Part 1: Screening, Diagnosis, and Local Treatment with Curative Intent'. *European Urology* 79 (2): 243–62. <https://doi.org/10.1016/j.eururo.2020.09.042>.
- Nanni, Cristina, Riccardo Schiavina, Eugenio Brunocilla, Stefano Boschi, Marco Borghesi, Lucia Zanoni, Cinzia Pettinato, Giuseppe Martorana, and Stefano Fanti. 2015. '18F-Fluciclovine PET/CT for the Detection of Prostate Cancer Relapse: A Comparison to 11C-Choline PET/CT'. *Clinical Nuclear Medicine* 40 (8): e386–91. <https://doi.org/10.1097/RLU.0000000000000849>.
- Nitsch, Sascha, Oliver W. Hakenberg, Martin Heuschkel, Desiree Dräger, Guido Hildebrandt, Bernd J. Krause, and Sarah M. Schwarzenböck. 2016. 'Evaluation of Prostate Cancer with 11C- and 18F-Choline PET/CT: Diagnosis and Initial Staging'. *Journal of Nuclear Medicine* 57 (10): 38S-42S. <https://doi.org/10.2967/jnumed.115.169748>.
- Nyberg, Tommy, Debra Frost, Daniel Barrowdale, D. Gareth Evans, Elizabeth Bancroft, Julian Adlard, Munaza Ahmed, et al. 2020. 'Prostate Cancer Risks for Male BRCA1[Formula Presented] and BRCA2 Mutation Carriers: A Prospective Cohort Study'. *European Urology* 77 (1): 24–35. <https://doi.org/10.1016/j.eururo.2019.08.025>.
- O'Keefe, Denise S., Dean J. Bacich, Steve S. Huang, and Warren D.W. Heston. 2018. 'A Perspective on the Evolving Story of PSMA Biology, PSMA-Based Imaging, and Endoradiotherapeutic Strategies'. *Journal of Nuclear Medicine* 59 (7): 1007–13. <https://doi.org/10.2967/jnumed.117.203877>.
- Obata, Atsushi, Shingo Kasamatsu, Deborah W. McCarthy, Michael J. Welch, Hideo Saji, Yoshiharu Yonekura, and Yasuhisa Fujibayashi. 2003. 'Production of Therapeutic Quantities of 64Cu Using a 12 MeV Cyclotron'. *Nuclear Medicine and Biology* 30 (5): 535–39. [https://doi.org/10.1016/S0969-8051\(03\)00024-6](https://doi.org/10.1016/S0969-8051(03)00024-6).
- Oh, So Won, Alexander Wurzer, Eugene J. Teoh, Sohee Oh, Thomas Langbein, Markus Krönke, Michael Herz, et al. 2020. 'Quantitative and Qualitative Analyses of Biodistribution and PET Image Quality of a Novel Radiohybrid PSMA, 18F-RhPSMA-7, in Patients with Prostate Cancer'. *Journal of Nuclear Medicine : Official Publication, Society of Nuclear Medicine* 61 (5): 702–9. <https://doi.org/10.2967/jnumed.119.234609>.
- Omri, Nativ, Malshy Kamil, Kastin Alexander, Kravtsov Alexander, Sabo Edmond, Zisman Ariel, Kakiashvili David, Amiel E. Gilad, and Hoffman Azik. 2020. 'Association between PSA Density and Pathologically Significant Prostate Cancer: The Impact of Prostate Volume'. *Prostate* 80 (16): 1444–49. <https://doi.org/10.1002/pros.24078>.
- Oyama, Nobuyuki, Hironobu Akino, Hiroshi Kanamaru, Yuji Suzuki, Satoshi Muramoto, Yoshiharu Yonekura, Norihiro Sadato, Kazutaka Yamamoto, and Kenichiro Okada. 2002. '11C-Acetate PET Imaging of Prostate Cancer'. *Journal of Nuclear Medicine* 43 (2): 181–86.
- Oyama, Nobuyuki, Hironobu Akino, Yuji Suzuki, Hiroshi Kanamaru, Norihiro Sadato, Yoshiharu Yonekura, and Kenichiro Okada. 1999. 'The Increased Accumulation of [18F]Fluorodeoxyglucose

- in Untreated Prostate Cancer'. *Japanese Journal of Clinical Oncology* 29 (12): 623–29. <https://doi.org/10.1093/jjco/29.12.623>.
- Page, Elizabeth C., Elizabeth K. Bancroft, Mark N. Brook, Melissa Assel, Mona Hassan Al Battat, Sarah Thomas, Natalie Taylor, et al. 2019. 'Interim Results from the IMPACT Study: Evidence for Prostate-Specific Antigen Screening in BRCA2 Mutation Carriers'. *European Urology* 76 (6): 831–42. <https://doi.org/10.1016/j.eururo.2019.08.019>.
- Parker, C, S Nilsson, D Heinrich, S.I. Helle, J.M. O'Sullivan, S.D. Fosså, A Chodacki, et al. 2013. 'Alpha Emitter Radium-223 and Survival in Metastatic Prostate Cancer'. *New England Journal of Medicine* 369 (3): 213–23. <https://doi.org/10.1056/NEJMoa1213755>.
- Parker, Christopher C., Nicholas D. James, Christopher D. Brawley, Noel W. Clarke, Alex P. Hoyle, Adnan Ali, Alastair W.S. Ritchie, et al. 2018. 'Radiotherapy to the Primary Tumour for Newly Diagnosed, Metastatic Prostate Cancer (STAMPEDE): A Randomised Controlled Phase 3 Trial'. *The Lancet* 392 (10162): 2353–66. [https://doi.org/10.1016/S0140-6736\(18\)32486-3](https://doi.org/10.1016/S0140-6736(18)32486-3).
- Pasalic, Dario, Deborah A. Kuban, Pamela K. Allen, Chad Tang, Shane M. Mesko, Stephen R. Grant, Alexander A. Augustyn, et al. 2019. 'Dose Escalation for Prostate Adenocarcinoma: A Long-Term Update on the Outcomes of a Phase 3, Single Institution Randomized Clinical Trial'. *International Journal of Radiation Oncology Biology Physics* 104 (4): 790–97. <https://doi.org/10.1016/j.ijrobp.2019.02.045>.
- Pasoglou, Vasiliki, Ahmed Larbi, Laurence Collette, Laurence Annet, François Jamar, Jean Pascal Machiels, Nicolas Michoux, Bruno C.Vande Berg, Bertrand Tombal, and Frederic E. Lecouvet. 2014. 'One-Step TNM Staging of High-Risk Prostate Cancer Using Magnetic Resonance Imaging (MRI): Toward an Upfront Simplified "All-in-One" Imaging Approach?' *Prostate* 74 (5): 469–77. <https://doi.org/10.1002/pros.22764>.
- Patlak, C. S., and R. G. Blasberg. 1985. 'Graphical Evaluation of Blood-to-Brain Transfer Constants from Multiple-Time Uptake Data. Generalizations'. *Journal of Cerebral Blood Flow and Metabolism* 5 (4): 584–90. <https://doi.org/10.1038/jebfm.1985.87>.
- Pauwels, E. K.J., M. J. Ribeiro, J. H.M.B. Stoot, V. R. McCready, M. Bourguignon, and B. Mazière. 1998. 'FDG Accumulation and Tumor Biology'. *Nuclear Medicine and Biology* 25 (4): 317–22. [https://doi.org/10.1016/S0969-8051\(97\)00226-6](https://doi.org/10.1016/S0969-8051(97)00226-6).
- Perera, Marlon, Nathan Papa, Daniel Christidis, David Wetherell, Michael S. Hofman, Declan G. Murphy, Damien Bolton, and Nathan Lawrentschuk. 2016. 'Sensitivity, Specificity, and Predictors of Positive 68Ga-Prostate-Specific Membrane Antigen Positron Emission Tomography in Advanced Prostate Cancer: A Systematic Review and Meta-Analysis'. *European Urology* 70 (6): 926–37. <https://doi.org/10.1016/J.EURURO.2016.06.021>.
- Petersen, Lars J., Julie B. Nielsen, Niels C. Langkilde, Astrid Petersen, Ali Afshar-Oromieh, Nandita M. De Souza, Katja De Paepe, et al. 2019. '68Ga-PSMA PET/CT Compared with MRI/CT and Diffusion-Weighted MRI for Primary Lymph Node Staging Prior to Definitive Radiotherapy in Prostate Cancer: A Prospective Diagnostic Test Accuracy Study'. *World Journal of Urology*. <https://doi.org/10.1007/s00345-019-02846-z>.
- Phillips, Ryan, William Yue Shi, Matthew Deek, Noura Radwan, Su Jin Lim, Emmanuel S. Antonarakis, Steven P. Rowe, et al. 2020. 'Outcomes of Observation vs Stereotactic Ablative Radiation for Oligometastatic Prostate Cancer: The ORIOLE Phase 2 Randomized Clinical Trial'. *JAMA Oncology* 6 (5): 650–59. <https://doi.org/10.1001/jamaoncol.2020.0147>.
- Pienta, Kenneth J., Michael A. Gorin, Steven P. Rowe, Peter R. Carroll, Frédéric Pouliot, Stephan Probst, Lawrence Saperstein, et al. 2021. 'A Phase 2/3 Prospective Multicenter Study of the Diagnostic Accuracy of Prostate Specific Membrane Antigen PET/CT with 18F-DCFPyL in Prostate Cancer Patients (OSPREY)'. *The Journal of Urology* 206 (1): 52–61. <https://doi.org/10.1097/JU.0000000000001698>.
- Pinker, Katja, Christopher Riedl, and Wolfgang A. Weber. 2017. 'Evaluating Tumor Response with FDG PET: Updates on PERCIST, Comparison with EORTC Criteria and Clues to Future

- Developments'. *European Journal of Nuclear Medicine and Molecular Imaging* 44: 55–66. <https://doi.org/10.1007/s00259-017-3687-3>.
- Plut, Edward M., and George H. Hinkle. 2000. '111In-Capromab Pendetide: The Evolution of Prostate Specific Membrane Antigen and the Nuclear Imaging of Its 111In-Labelled Murine Antibody in the Evaluation of Prostate Cancer'. *BioDrugs* 13 (6): 437–47. <https://doi.org/10.2165/00063030-200013060-00007>.
- Pomper, Martin G., John L. Musachio, Jiazhong Zhang, Ursula Scheffel, Yun Zhou, John Hilton, Atul Maini, Robert F. Dannals, Dean F. Wong, and Alan P. Kozikowski. 2002. '11C-MCG: Synthesis, Uptake Selectivity, and Primate PET of a Probe for Glutamate Carboxypeptidase II (NAALADase)'. *Molecular Imaging* 1 (2): 96–101. <https://doi.org/10.1162/153535002320162750>.
- Pound, Charles R., Alan W. Partin, Mario A. Eisenberger, Daniel W. Chan, Jay D. Pearson, and Patrick C. Walsh. 1999. 'Natural History of Progression after PSA Elevation Following Radical Prostatectomy'. *Journal of the American Medical Association* 281 (17): 1591–97. <https://doi.org/10.1001/jama.281.17.1591>.
- Privé, Bastiaan M., Steffie M.B. Peters, Constantijn H.J. Muselaers, Inge M. van Oort, Marcel J.R. Janssen, J. P. Michiel Sedelaar, Mark W. Konijnenberg, et al. 2021. 'Lutetium-177-PSMA-617 in Low-Volume Hormone-Sensitive Metastatic Prostate Cancer: A Prospective Pilot Study'. *Clinical Cancer Research* 27 (13): 3595–3601. <https://doi.org/10.1158/1078-0432.CCR-20-4298>.
- Puryško, Andrei S., Andrew B. Rosenkrantz, Ismail Baris Turkbey, and Katarzyna J. Macura. 2020. 'PI-RADS Version 2.1—a Pictorial Update'. *Radiographics* 40 (7): E33–37. <https://doi.org/10.1148/rg.2020190207>.
- Rahbar, Kambiz, Ali Afshar-Oromieh, Martin Bögemann, Stefan Wagner, Michael Schäfers, Lars Stegger, and Matthias Weckesser. 2018. '18F-PSMA-1007 PET/CT at 60 and 120 Minutes in Patients with Prostate Cancer: Biodistribution, Tumour Detection and Activity Kinetics'. *European Journal of Nuclear Medicine and Molecular Imaging* 45 (8): 1329–34. <https://doi.org/10.1007/s00259-018-3989-0>.
- Rais-Bahrami, Soroush, Jason A. Efstathiou, Catriona M. Turnbull, Stephen B. Camper, Andy Kenwright, David M. Schuster, and Andrew F. Scarsbrook. 2021. '18F-Fluciclovine PET/CT Performance in Biochemical Recurrence of Prostate Cancer: A Systematic Review'. *Prostate Cancer and Prostatic Diseases* 24 (4): 997–1006. <https://doi.org/10.1038/s41391-021-00382-9>.
- Rauscher, Isabel, Amir Karimzadeh, Kilian Schiller, Thomas Horn, Calogero D'Alessandria, Charlott Franz, Hannah Wörther, et al. 2021. 'Detection Efficacy of 18 F-rhPSMA-7.3 PET/CT and Impact on Management in Patients with Biochemical Recurrence of Prostate Cancer After Radical Prostatectomy and Before Potential Salvage Treatment'. *Journal of Nuclear Medicine* 62 (12): 1719–26. <https://doi.org/10.2967/jnumed.120.260091>.
- Rauscher, Isabel, Markus Krönke, Michael König, Andrei Gafita, Tobias Maurer, Thomas Horn, Kilian Schiller, Wolfgang Weber, and Matthias Eiber. 2020. 'Matched-Pair Comparison of 68Ga-PSMA-11 PET/CT and 18F-PSMA-1007 PET/CT: Frequency of Pitfalls and Detection Efficacy in Biochemical Recurrence after Radical Prostatectomy'. *Journal of Nuclear Medicine* 61 (1): 51–57. <https://doi.org/10.2967/jnumed.119.229187>.
- Raveenthiran, Sheliyan, Rachel Esler, John Yaxley, and Sam Kyle. 2019. 'The Use of 68Ga-PET/CT PSMA in the Staging of Primary and Suspected Recurrent Renal Cell Carcinoma'. *European Journal of Nuclear Medicine and Molecular Imaging* 46 (11): 2280–88. <https://doi.org/10.1007/s00259-019-04432-2>.
- Rawla, Prashanth. 2019. 'Epidemiology of Prostate Cancer'. *World J Oncol* 32 (1): 2–4. <https://doi.org/10.1016/j.mednuc.2007.11.003>.
- Rhee, Handoo, John Blazak, Chui Ming Tham, Keng Lim Ng, Benjamin Shepherd, Malcolm Lawson, John Preston, Ian Vela, Paul Thomas, and Simon Wood. 2016. 'Pilot Study: Use of Gallium-68 PSMA PET for Detection of Metastatic Lesions in Patients with Renal Tumour'. *EJNMMI Research* 6 (1). <https://doi.org/10.1186/s13550-016-0231-6>.
- Roach, Mack, Carol Marquez, Hae Sook Yuo, Perinchery Narayan, Lorie Coleman, Unyime O. Nseyo, Zarrin Navvab, and Peter R. Carroll. 1994. 'Predicting the Risk of Lymph Node Involvement

- Using the Pre-Treatment Prostate Specific Antigen and Gleason Score in Men with Clinically Localized Prostate Cancer'. *International Journal of Radiation Oncology, Biology, Physics* 28 (1): 33–37. [https://doi.org/10.1016/0360-3016\(94\)90138-4](https://doi.org/10.1016/0360-3016(94)90138-4).
- Robu, Stephanie, Alexander Schmidt, Matthias Eiber, Margret Schottelius, Thomas Günther, Behrooz Hooshyar Yousefi, Markus Schwaiger, and Hans Jürgen Wester. 2018. 'Synthesis and Preclinical Evaluation of Novel 18F-Labeled Glu-Urea-Glu-Based PSMA Inhibitors for Prostate Cancer Imaging: A Comparison with 18F-DCFPyl and 18F-PSMA-1007'. *EJNMMI Research* 8. <https://doi.org/10.1186/s13550-018-0382-8>.
- Rooij, Maarten de, Esther H.J. Hamoen, J. Alfred Witjes, Jelle O. Barentsz, and Maroeska M. Rovers. 2016. 'Accuracy of Magnetic Resonance Imaging for Local Staging of Prostate Cancer: A Diagnostic Meta-Analysis'. *European Urology* 70 (2): 233–45. <https://doi.org/10.1016/j.eururo.2015.07.029>.
- Rouvière, Olivier, Philippe Puech, Raphaële Renard-Penna, Michel Claudon, Catherine Roy, Florence Mège-Lechevallier, Myriam Decaussin-Petrucci, et al. 2019. 'Use of Prostate Systematic and Targeted Biopsy on the Basis of Multiparametric MRI in Biopsy-Naive Patients (MRI-FIRST): A Prospective, Multicentre, Paired Diagnostic Study'. *The Lancet Oncology* 20 (1): 100–109. [https://doi.org/10.1016/S1470-2045\(18\)30569-2](https://doi.org/10.1016/S1470-2045(18)30569-2).
- Rowe, Steven P., Michael A. Gorin, Roberto A. Salas Fragomeni, Alexander Drzezga, and Martin G. Pomper. 2017. 'Clinical Experience with 18F-Labeled Small Molecule Inhibitors of Prostate-Specific Membrane Antigen'. *PET Clinics* 12 (2): 235–41. <https://doi.org/10.1016/j.cpet.2016.12.006>.
- Rowe, Steven P., Kenneth L Gage, Sheila F Faraj, Katarzyna J Macura, C Toby, Nilda Gonzalez-roibon, Gunes Guner, et al. 2015. '18F-DCFBC PET/CT for PSMA-Based Detection and Characterization of Primary Prostate Cancer' 56 (7): 1003–10. <https://doi.org/10.2967/jnumed.115.154336.18>.
- Roy, Jyoti, Margaret E. White, Falguni Basuli, Ana Christina L. Opina, Karen Wong, Morgan Riba, Anita T. Ton, et al. 2021. 'Monitoring PSMA Responses to ADT in Prostate Cancer Patient-Derived Xenograft Mouse Models Using [18F]DCFPyL PET Imaging'. *Molecular Imaging and Biology* 23 (5): 745–55. <https://doi.org/10.1007/s11307-021-01605-0>.
- Ryan, Charles J., Matthew R. Smith, Karim Fizazi, Fred Saad, Peter F.A. Mulders, Cora N. Sternberg, Kurt Miller, et al. 2015. 'Abiraterone Acetate plus Prednisone versus Placebo plus Prednisone in Chemotherapy-Naive Men with Metastatic Castration-Resistant Prostate Cancer (COU-AA-302): Final Overall Survival Analysis of a Randomised, Double-Blind, Placebo-Controlled Phase 3 Study'. *The Lancet Oncology* 16 (2): 152–60. [https://doi.org/10.1016/S1470-2045\(14\)71205-7](https://doi.org/10.1016/S1470-2045(14)71205-7).
- Sah, Bert Ram, Irene A. Burger, Roger Schibli, Matthias Friebe, Ludger Dinkelborg, Keith Graham, Sandra Borkowski, et al. 2015. 'Dosimetry and First Clinical Evaluation of the New 18F-Radiolabeled Bombesin Analogue BAY 864367 in Patients with Prostate Cancer'. *Journal of Nuclear Medicine* 56 (3): 372–78. <https://doi.org/10.2967/jnumed.114.147116>.
- Sakata, Takeshi, Golan Ferdous, Tomoko Tsuruta, Takefumi Satoh, Shiro Baba, Tomoko Muto, Akinori Ueno, Yoshikatsu Kanai, Hitoshi Endou, and Isao Okayasu. 2009. 'L-Type Amino-Acid Transporter 1 as a Novel Biomarker for High-Grade Malignancy in Prostate Cancer'. *Pathology International* 59 (1): 7–18. <https://doi.org/10.1111/j.1440-1827.2008.02319.x>.
- Sar, Esmée C.A. van der, Willem R. Keusters, Ludwike W.M. van Kalmthout, Arthur J.A.T. Braat, Bart de Keizer, Geert W.J. Frederix, Anko Kooistra, Jules Lavalaye, Marnix G.E.H. Lam, and Harm H.E. van Melick. 2022. 'Cost-Effectiveness of the Implementation of [68Ga]Ga-PSMA-11 PET/CT at Initial Prostate Cancer Staging'. *Insights into Imaging* 13 (1). <https://doi.org/10.1186/s13244-022-01265-w>.
- Sartor, Oliver, Johann de Bono, Kim N. Chi, Karim Fizazi, Ken Herrmann, Kambiz Rahbar, Scott T. Tagawa, et al. 2021. 'Lutetium-177-PSMA-617 for Metastatic Castration-Resistant Prostate Cancer'. *New England Journal of Medicine* 385 (12): 1091–1103. <https://doi.org/10.1056/nejmoa2107322>.
- Sasaki, T., T. Onishi, and A. Hoshina. 2011. 'Nadir PSA Level and Time to PSA Nadir Following Primary Androgen Deprivation Therapy Are the Early Survival Predictors for Prostate Cancer

- Patients with Bone Metastasis'. *Prostate Cancer and Prostatic Diseases* 14 (3): 248–52. <https://doi.org/10.1038/pcan.2011.14>.
- Satapathy, Swayamjeet, Ashwani Sood, Chandan Krushna Das, and Bhagwant Rai Mittal. 2021. 'Evolving Role of 225Ac-PSMA Radioligand Therapy in Metastatic Castration-Resistant Prostate Cancer—a Systematic Review and Meta-Analysis'. *Prostate Cancer and Prostatic Diseases* 24 (3): 880–90. <https://doi.org/10.1038/s41391-021-00349-w>.
- Scarsbrook, Andrew F., David Bottomley, Eugene J. Teoh, Kevin M. Bradley, Heather Payne, Asim Afaq, Jamshed Bomanji, et al. 2020. 'Effect of 18F-Fluciclovine Positron Emission Tomography on the Management of Patients With Recurrence of Prostate Cancer: Results From the FALCON Trial'. *International Journal of Radiation Oncology Biology Physics* 107 (2): 316–24. <https://doi.org/10.1016/j.ijrobp.2020.01.050>.
- Schmid, Hans-Peter -P, John E. McNeal, and Thomas A. Stamey. 1993. 'Observations on the Doubling Time of Prostate Cancer. The Use of Serial Prostate-specific Antigen in Patients with Untreated Disease as a Measure of Increasing Cancer Volume'. *Cancer* 71 (6): 2031–40. [https://doi.org/10.1002/1097-0142\(19930315\)71:6<2031::AID-CNCR2820710618>3.0.CO;2-Q](https://doi.org/10.1002/1097-0142(19930315)71:6<2031::AID-CNCR2820710618>3.0.CO;2-Q).
- Schmidkonz, Christian, Michael Cordes, Michael Beck, Theresa Ida Goetz, Daniela Schmidt, Olaf Prante, Tobias Bäuerle, et al. 2018. 'SPECT/CT with the PSMA Ligand 99mTc-MIP-1404 for Whole-Body Primary Staging of Patients with Prostate Cancer'. *Clinical Nuclear Medicine* 43 (4): 225–31. <https://doi.org/10.1097/RLU.0000000000001991>.
- Schmidt-Hegemann, Nina Sophie, Wolfgang Peter Fendler, Harun Ilhan, Annika Herlemann, Alexander Buchner, Christian Stief, Chukwuka Eze, et al. 2018. 'Outcome after PSMA PET/CT Based Radiotherapy in Patients with Biochemical Persistence or Recurrence after Radical Prostatectomy'. *Radiation Oncology* 13 (1): 1–9. <https://doi.org/10.1186/s13014-018-0983-4>.
- Schöder, Heiko, Ken Herrmann, Mithat Gönen, Hedvig Hricak, Stephen Eberhard, Peter Scardino, Howard I. Scher, and Steven M. Larson. 2005. '2-[18F]Fluoro-2-Deoxyglucose Positron Emission Tomography for the Detection of Disease in Patients with Prostate-Specific Antigen Relapse after Radical Prostatectomy'. *Clinical Cancer Research* 11 (13): 4761–69. <https://doi.org/10.1158/1078-0432.CCR-05-0249>.
- Seitz, Anna Katharina, Isabel Rauscher, Bernhard Haller, Markus Krönke, Sophia Luther, Matthias M. Heck, Thomas Horn, et al. 2018. 'Preliminary Results on Response Assessment Using 68Ga-HBED-CC-PSMA PET/CT in Patients with Metastatic Prostate Cancer Undergoing Docetaxel Chemotherapy'. *European Journal of Nuclear Medicine and Molecular Imaging* 45 (4): 602–12. <https://doi.org/10.1007/s00259-017-3887-x>.
- Shah, Taimur T., Max Peters, David Eldred-Evans, Saiful Miah, Tet Yap, Nicholas A. Faure-Walker, Feargus Hosking-Jervis, et al. 2019. 'Early-Medium-Term Outcomes of Primary Focal Cryotherapy to Treat Nonmetastatic Clinically Significant Prostate Cancer from a Prospective Multicentre Registry'. *European Urology* 76 (1): 98–105. <https://doi.org/10.1016/j.eururo.2018.12.030>.
- Shen, Guohua, Houfu Deng, Shuang Hu, and Zhiyun Jia. 2014. 'Comparison of Choline-PET/CT, MRI, SPECT, and Bone Scintigraphy in the Diagnosis of Bone Metastases in Patients with Prostate Cancer: A Meta-Analysis'. *Skeletal Radiology* 43 (11): 1503–13. <https://doi.org/10.1007/s00256-014-1903-9>.
- Shore, Neal D. 2013. 'Experience with Degarelix in the Treatment of Prostate Cancer'. *Therapeutic Advances in Urology* 5 (1): 11–24. <https://doi.org/10.1177/1756287212461048>.
- Song, Rachel, Varinder Jeet, Rajan Sharma, Martin Hoyle, and Bonny Parkinson. 2022. 'Cost-Effectiveness Analysis of Prostate-Specific Membrane Antigen (PSMA) Positron Emission Tomography/Computed Tomography (PET/CT) for the Primary Staging of Prostate Cancer in Australia'. *PharmacoEconomics* 40 (8): 807–21. <https://doi.org/10.1007/s40273-022-01156-4>.
- Souvatzoglou, Michael, Gregor Weirich, Sarah Schwarzenboeck, Tobias Maurer, Tibor Schuster, Ralph Alexander Bundschuh, Matthias Eiber, et al. 2011. 'The Sensitivity of [11C]Choline PET/CT to Localize Prostate Cancer Depends on the Tumor Configuration.' *Clinical Cancer*

- Research : An Official Journal of the American Association for Cancer Research* 17 (11): 3751–59. <https://doi.org/10.1158/1078-0432.CCR-10-2093>.
- Sprute, Katharina, Vasko Kramer, Stefan A. Koerber, Manuel Meneses, Rene Fernandez, Cristian Soza-Ried, Mathias Eiber, et al. 2021. ‘Diagnostic Accuracy of 18F-PSMA-1007 PET/CT Imaging for Lymph Node Staging of Prostate Carcinoma in Primary and Biochemical Recurrence’. *Journal of Nuclear Medicine* 62 (2): 208–13. <https://doi.org/10.2967/jnumed.120.246363>.
- Sprute, Katharina, Vasko Kramer, Stefan Koerber, Manuel Meneses, Rene Fernandez, Cristian Soza-Ried, Mathias Eiber, et al. 2020. ‘Diagnostic Accuracy of 18 F-PSMA-1007-PET/CT Imaging for Lymph Node Staging of Prostate Carcinoma in Primary and Biochemical Recurrence’. *Journal of Nuclear Medicine*, jnumed.120.246363. <https://doi.org/10.2967/jnumed.120.246363>.
- Stabile, Armando, Clement Orczyk, Feargus Hosking-Jervis, Francesco Giganti, Mani Arya, Richard G. Hindley, Louise Dickinson, et al. 2019. ‘Medium-Term Oncological Outcomes in a Large Cohort of Men Treated with Either Focal or Hemi-Ablation Using High-Intensity Focused Ultrasonography for Primary Localized Prostate Cancer’. *BJU International* 124 (3): 431–40. <https://doi.org/10.1111/bju.14710>.
- Stamey, Ta, N Yang, Ar Hay, Je McNeal, Fs Freiha, and E Redwine. 1987. ‘Prostate-Specific Antigen as a Serum Marker for Adenocarcinoma of the Prostate’. *New England Journal of Medicine*.
- Stewart, Grant, Kelly Gray, Caroline Pennington, Dylan Edwards, Antony Riddick, and James Ross. 2008. ‘Analysis of Hypoxia-Associated Gene Expression in Prostate Cancer: Lysyl Oxidase and Glucose Transporter-1 Expression Correlate with Gleason Score’. *Oncology Reports* 23 (3): 861–67. <https://doi.org/10.3892/or>.
- Stolzenburg, Jens Uwe, Sigrun Holze, Petra Neuhaus, Iason Kyriazis, Hoang Minh Do, Anja Dietel, Michael C. Truss, et al. 2021. ‘Robotic-Assisted Versus Laparoscopic Surgery: Outcomes from the First Multicentre, Randomised, Patient-Blinded Controlled Trial in Radical Prostatectomy (LAP-01)[Formula Presented]’. *European Urology* 79 (6): 750–59. <https://doi.org/10.1016/j.eururo.2021.01.030>.
- Suh, C. H., A. B. Shinagare, A. M. Westenfield, N. H. Ramaiya, A. D. Van den Abbeele, and K. W. Kim. 2018. ‘Yield of Bone Scintigraphy for the Detection of Metastatic Disease in Treatment-Naive Prostate Cancer: A Systematic Review and Meta-Analysis’. *Clinical Radiology* 73 (2): 158–67. <https://doi.org/10.1016/j.crad.2017.08.004>.
- Sweeney, Christopher J., Yu-Hui Chen, Michael Carducci, Glenn Liu, David F. Jarrard, Mario Eisenberger, Yu-Ning Wong, et al. 2015. ‘Chemohormonal Therapy in Metastatic Hormone-Sensitive Prostate Cancer’. *New England Journal of Medicine* 373 (8): 737–46. <https://doi.org/10.1056/nejmoa1503747>.
- Szabo, Zsolt, Esther Mena, Steven P. Rowe, Donika Plyku, Rosa Nidal, Mario A. Eisenberger, Emmanuel S. Antonarakis, et al. 2015. ‘Initial Evaluation of [18F]JDCFpyL for Prostate-Specific Membrane Antigen (PSMA)-Targeted PET Imaging of Prostate Cancer’. *Molecular Imaging and Biology* 17 (4): 565–74. <https://doi.org/10.1007/s11307-015-0850-8>.
- Tannock, Ian F., Ronald de Wit, Freidele Soban, Ronald De Wit, Mario Eisenberger, and Ian F. Tannock. 2004. ‘Docetaxel plus Prednisone or Mitoxantrone plus Prednisone for Advanced Prostate Cancer: Updated Survival in the TAX 327 Study’. *New England Journal of Medicine* 26 (2): 242–45. <https://doi.org/10.1200/JCO.2007.12.4008>.
- Thie, A. 2004. ‘Understanding the Standardized Uptake Value, Its Methods, and Implications for Usage’, 1431–34.
- Thoeny, Harriet C., Johannes M. Froehlich, Maria Triantafyllou, Juerg Huesler, Lauren J. Bains, Peter Vermathen, Achim Fleischmann, and Urs E. Studer. 2014. ‘Metastases in Normal-Sized Pelvic Lymph Nodes: Detection with Diffusion-Weighted MR Imaging’. *Radiology*. Radiological Society of North America Inc. <https://doi.org/10.1148/radiol.14132921>.
- Thompson, IM, DK Pauler, PJ Goodman, CM Tangen, Lucia MS, and Coltman CA Parnes HL, Minasian LM, Ford LG, Lippman SM, Crawford ED, Crowley JJ. 2004. ‘Prevalence of Prostate

- Cancer among Men with a Prostate-Specific Antigen Level  $\leq 4.0$  Ng per Milliliter'. *N Engl J Med*, 2239–46.
- Tiguert, Rabi, Edward L. Gheiler, Marcos V. Tefilli, Peter Oskanian, Mousumi Banerjee, David J. Grignon, Wael Sakr, J. Edson Pontes, and David P. Wood. 1999. 'Lymph Node Size Does Not Correlate with the Presence of Prostate Cancer Metastasis'. *Urology* 53 (2): 367–71. [https://doi.org/10.1016/S0090-4295\(98\)00518-4](https://doi.org/10.1016/S0090-4295(98)00518-4).
- Tolvanen, Tuula, Kari Kalliokoski, Simona Malaspina, Anna Kuisma, Salla Lahdenpohja, Ernst J. Postema, Matthew P. Miller, and Mika Scheinin. 2021. 'Safety, Biodistribution, and Radiation Dosimetry of 18F-RhPSMA-7.3 in Healthy Adult Volunteers'. *Journal of Nuclear Medicine* 62 (5): 679–84. <https://doi.org/10.2967/jnumed.120.252114>.
- Tomioka, Atsushi, Nobumichi Tanaka, Motokiyo Yoshikawa, Makito Miyake, Satoshi Anai, Yoshitomo Chihara, Eijiro Okajima, Akihide Hirayama, Yoshihiko Hirao, and Kiyohide Fujimoto. 2014. 'Nadir PSA Level and Time to Nadir PSA Are Prognostic Factors in Patients with Metastatic Prostate Cancer'. *BMC Urology* 14 (1): 1–6. <https://doi.org/10.1186/1471-2490-14-33>.
- Toriihara, Akira, Tomomi Nobashi, Lucia Baratto, Heying Duan, Farshad Moradi, Sonya Park, Negin Hatami, Carina Mari Aparici, Guido Davidzon, and Andrei Iagaru. 2020. 'Comparison of 3 Interpretation Criteria for 68Ga-PSMA11 PET Based on Interand Intra-reader Agreement'. *Journal of Nuclear Medicine* 61 (4): 533–39. <https://doi.org/10.2967/jnumed.119.232504>.
- Tseng, Jing Ren, Szu Han Chang, Yao Yu Wu, Kang Hsing Fan, Kai Jie Yu, Lan Yan Yang, Ing Tsung Hsiao, Feng Yuan Liu, and See Tong Pang. 2022. 'Impact of Three-Month Androgen Deprivation Therapy on [68Ga]Ga-PSMA-11 PET/CT Indices in Men with Advanced Prostate Cancer—Results from a Pilot Prospective Study'. *Cancers* 14 (5). <https://doi.org/10.3390/cancers14051329>.
- Tulshyan, Shruti, Chandan J. Das, Madhavi Tripathi, Amlesh Seth, Rajeev Kumar, and Chandrasekhar Bal. 2017. 'Comparison of 68 Ga-PSMA PET/CT and Multiparametric MRI for Staging of High-Risk Prostate Cancer 68 Ga-PSMA PET and MRI in Prostate Cancer'. *Nuclear Medicine Communications* 38 (12): 1094–1102. <https://doi.org/10.1097/MNM.0000000000000749>.
- Turkington, Timothy. 2001. 'Introduction to PET Instrumentation'. *Journal of Nuclear Medicine Technology* 30 (2): 63.
- Uijen, M. J.M., Y. H.W. Derks, R. I.J. Merckx, M. G.M. Schilham, J. Roosen, B. M. Privé, S. A.M. van Lith, et al. 2021. 'PSMA Radioligand Therapy for Solid Tumors Other than Prostate Cancer: Background, Opportunities, Challenges, and First Clinical Reports'. *European Journal of Nuclear Medicine and Molecular Imaging* 48 (13): 4350–68. <https://doi.org/10.1007/s00259-021-05433-w>.
- Uprimny, Christian, Alexander Stephan Kroiss, Clemens Decristoforo, Josef Fritz, Elisabeth von Guggenberg, Dorota Kandler, Lorenza Scarpa, et al. 2017. '68Ga-PSMA-11 PET/CT in Primary Staging of Prostate Cancer: PSA and Gleason Score Predict the Intensity of Tracer Accumulation in the Primary Tumour'. *European Journal of Nuclear Medicine and Molecular Imaging* 44 (6): 941–49. <https://doi.org/10.1007/s00259-017-3631-6>.
- Uprimny, Christian, Anna Sviridenka, Josef Fritz, Alexander Stephan Kroiss, Bernhard Nilica, Clemens Decristoforo, Roland Haubner, et al. 2018. 'Comparison of [(68)Ga]Ga-PSMA-11 PET/CT with [(18)F]NaF PET/CT in the Evaluation of Bone Metastases in Metastatic Prostate Cancer Patients Prior to Radionuclide Therapy.' *European Journal of Nuclear Medicine and Molecular Imaging* 45 (11): 1873–83. <https://doi.org/10.1007/s00259-018-4048-6>.
- Verma, Priyanka, Gaurav Malhotra, Ritesh Agrawal, Sunita Sonavane, Vilas Meshram, and Ramesh V. Asopa. 2018. 'Evidence of Prostate-Specific Membrane Antigen Expression in Metastatic Differentiated Thyroid Cancer Using 68Ga-PSMA-HBED-CC PET/CT'. *Clinical Nuclear Medicine* 43 (8): e265–68. <https://doi.org/10.1097/RLU.00000000000002161>.
- Verma, Priyanka, Gaurav Malhotra, Atul Goel, Sutapa Rakshit, Ashok Chandak, Rupal Chedda, Sharmila Banerjee, and Ramesh V. Asopa. 2019. 'Differential Uptake of 68Ga-PSMA-HBED-CC (PSMA-11) in Low-Grade Versus High-Grade Gliomas in Treatment-Naive Patients'. *Clinical Nuclear Medicine* 44 (5): E318–22. <https://doi.org/10.1097/RLU.00000000000002520>.



- Vidal, Adriana C., Lauren E. Howard, Daniel M. Moreira, Ramiro Castro-Santamaria, Gerald L. Andriole, and Stephen J. Freedland. 2014. 'Obesity Increases the Risk for High-Grade Prostate Cancer: Results from the REDUCE Study'. *Cancer Epidemiology Biomarkers and Prevention* 23 (12): 2936–42. <https://doi.org/10.1158/1055-9965.EPI-14-0795>.
- Vincenza Conteduca, Giulia Poti, Paola Caroli, Sabino Russi, Nicole Brighi, Cristian Lolli, Giovanni Paganelli Giuseppe Schepisi, Antonino Romeo, Federica Matteucci, and Paolo Marchetti and Ugo De Giorgi. 2021. 'Flare Phenomenon in Prostate Cancer: Recent Evidence on New Drugs and next Generation Imaging'. *Therapeutic Advances in Medical Oncology* 9 (6): 259–61. <https://doi.org/10.1177/https>.
- Violet, John, Shahneen Sandhu, Amir Iravani, Justin Ferdinandus, Sue Ping Thang, Grace Kong, Aravind Ravi Kumar, et al. 2020. 'Long-Term Follow-up and Outcomes of Retreatment in an Expanded 50-Patient Single-Center Phase II Prospective Trial of 177Lu-PSMA-617 Theranostics in Metastatic Castration-Resistant Prostate Cancer'. *Journal of Nuclear Medicine* 61 (6): 857–65. <https://doi.org/10.2967/jnumed.119.236414>.
- Vries, Lisa H De, Lutske Lodewijk, Arthur J A T Braat, Gerard C Krijger, Gerlof D Valk, Marnix G E H Lam, Inne H M Borel Rinkes, Menno R Vriens, and Bart De Keizer. 2021. 'Ga-PSMA PET / CT in Radioactive Iodine- Refractory Differentiated Thyroid Cancer and First Treatment Results with 177 Lu-PSMA-617', no. 2020.
- Wahl, R. L., L. E. Quint, R. D. Cieslak, A. M. Aisen, R. A. Koeppe, and C. R. Meyer. 1993. "Anatometabolic" Tumor Imaging: Fusion of FDG PET with CT or MRI to Localize Foci of Increased Activity". *Journal of Nuclear Medicine* 34 (7): 1190–97.
- Wang, Rang, Guohua Shen, Mingxing Huang, and Rong Tian. 2021. 'The Diagnostic Role of 18F-Choline, 18F-Fluciclovine and 18F-PSMA PET/CT in the Detection of Prostate Cancer With Biochemical Recurrence: A Meta-Analysis'. *Frontiers in Oncology* 11 (June). <https://doi.org/10.3389/fonc.2021.684629>.
- Weineisen, M., M. Schottelius, J. Simecek, R. P. Baum, A. Yildiz, S. Beykan, H. R. Kulkarni, et al. 2015. '68Ga- and 177Lu-Labeled PSMA I&T: Optimization of a PSMA-Targeted Theranostic Concept and First Proof-of-Concept Human Studies'. *Journal of Nuclear Medicine* 56 (8): 1169–76. <https://doi.org/10.2967/jnumed.115.158550>.
- Welch, Gilbert, David Gorski, and Peter Albertsen. 2015. 'Trends in Metastatic Breast and Prostate Cancer — Lessons in Cancer Dynamics'. *The New England Journal of Medicine*, 1685–87.
- Werner, P., C. Neumann, M. Eiber, H. J. Wester, and M. Schottelius. 2020. '[99cmTc]Tc-PSMA-I&S-SPECT/CT: Experience in Prostate Cancer Imaging in an Outpatient Center'. *EJNMMI Research* 10 (1). <https://doi.org/10.1186/s13550-020-00635-z>.
- Werner, Rudolf A., Thorsten Derlin, Constantin Lapa, Sara Sheikbahaei, Takahiro Higuchi, Frederik L. Giesel, Spencer Behr, et al. 2020. '18F-Labeled, PSMA-Targeted Radiotracers: Leveraging the Advantages of Radiofluorination for Prostate Cancer Molecular Imaging'. *Theranostics* 10 (1): 1–16. <https://doi.org/10.7150/thno.37894>.
- Werner, Rudolf A., James T. Thackeray, Martin G. Pomper, Frank M. Bengel, Michael A. Gorin, Thorsten Derlin, and Steven P. Rowe. 2019. 'Recent Updates on Molecular Imaging Reporting and Data Systems (MI-RADS) for Theranostic Radiotracers—Navigating Pitfalls of SSTR-and PSMA-Targeted PET/CT'. *Journal of Clinical Medicine* 8 (7). <https://doi.org/10.3390/jcm8071060>.
- Wieser, Gesche, Rosalba Mansi, Anca L. Grosu, Wolfgang Schultze-Seemann, Rebecca A. Dumont-Walter, Philipp T. Meyer, Helmut R. Maecke, Jean Claude Reubi, and Wolfgang A. Weber. 2014. 'Positron Emission Tomography (PET) Imaging of Prostate Cancer with a Gastrin Releasing Peptide Receptor Antagonist - from Mice to Men'. *Theranostics* 4 (4): 412–19. <https://doi.org/10.7150/thno.7324>.
- Wit, Ronald de, Johann de Bono, Cora N. Sternberg, Karim Fizazi, Bertrand Tombal, Christian Wülfing, Gero Kramer, et al. 2019. 'Cabazitaxel versus Abiraterone or Enzalutamide in Metastatic Prostate Cancer'. *New England Journal of Medicine* 381 (26): 2506–18. <https://doi.org/10.1056/nejmoa1911206>.

- Wundergem, Maurits, Friso M. van der Zant, Wouter A.M. Broos, and Remco J.J. Knol. 2021. 'Matched-pair Comparison of 18F-DCFPyL PET/CT and 18F-PSMA-1007 PET/CT in 240 Prostate Cancer Patients; Inter-reader Agreement and Lesion Detection Rate of Suspected Lesions.' *Journal of Nuclear Medicine* 62 (10): 1422–29. <https://doi.org/10.2967/jnumed.120.258574>.
- Wundergem, Maurits, Friso M. van der Zant, Remco J.J. Knol, Anne Marij G. Burgers, Siebe D. Bos, Igle J. de Jong, and Jan Pruim. 2018. '99mTc-HDP Bone Scintigraphy and 18F-Sodiumfluoride PET/CT in Primary Staging of Patients with Prostate Cancer'. *World Journal of Urology* 36 (1): 27–34. <https://doi.org/10.1007/s00345-017-2096-3>.
- Wright, George L., B. Mayer Grob, Cara Haley, Katie Grossman, Kathy Newhall, Daniel Petrylak, John Troyer, Alice Konchuba, Paul F. Schellhammer, and Richard Moriarty. 1996. 'Upregulation of Prostate-Specific Membrane Antigen after Androgen- Deprivation Therapy'. *Urology* 48 (2): 326–34. [https://doi.org/10.1016/S0090-4295\(96\)00184-7](https://doi.org/10.1016/S0090-4295(96)00184-7).
- Wu, Hui, Ting Xu, Xiao Wang, Yong Bo Yu, Zhong Yuan Fan, Dan Xia Li, Lei Luo, Xue Cheng Yang, Wei Jiao, and Hai Tao Niu. 2020. 'Diagnostic Performance of 68gallium Labelled Prostate-Specific Membrane Antigen Positron Emission Tomography/Computed Tomography and Magnetic Resonance Imaging for Staging the Prostate Cancer with Intermediate or High Risk Prior to Radical Prostatectomy: '. *World Journal of Men's Health* 38 (2): 208–19. <https://doi.org/10.5534/wjmh.180124>.
- Wurzer, Alexander, Daniel Di Carlo, Alexander Schmidt, Roswitha Beck, Matthias Eiber, Markus Schwaiger, and Hans Jürgen Wester. 2020. 'Radiohybrid Ligands: A Novel Tracer Concept Exemplified by 18F- or 68Ga-Labeled RhPSMA Inhibitors'. *Journal of Nuclear Medicine* 61 (5): 735–42. <https://doi.org/10.2967/jnumed.119.234922>.
- Wurzer, Alexander, Mara Parzinger, Matthias Konrad, Roswitha Beck, Thomas Günther, Veronika Felber, Stefanie Färber, Daniel Di Carlo, and Hans Jürgen Wester. 2020. 'Preclinical Comparison of Four [18F, NatGa]RhPSMA-7 Isomers: Influence of the Stereoconfiguration on Pharmacokinetics'. *EJNMMI Research* 10 (1). <https://doi.org/10.1186/s13550-020-00740-z>.
- Wynant, Gordon E., Gerald P. Murphy, Julius S. Horoszewicz, Charles E. Neal, B. David Collier, Edith Mitchell, Gary Purnell, et al. 1991. 'Immunoscintigraphy of Prostatic Cancer: Preliminary Results with 111in-labeled Monoclonal Antibody 7E11-C5.3 (CYT-356)'. *The Prostate* 18 (3): 229–41. <https://doi.org/10.1002/pros.2990180305>.
- Yaxley, John W., Sheliyan Raveenthiran, François Xavier Nouhaud, Hemamali Samaratunga, William J. Yaxley, Geoff Coughlin, Anna J. Yaxley, et al. 2019. 'Risk of Metastatic Disease on 68gallium-Prostate-Specific Membrane Antigen Positron Emission Tomography/Computed Tomography Scan for Primary Staging of 1253 Men at the Diagnosis of Prostate Cancer'. *BJU International* 124 (3): 401–7. <https://doi.org/10.1111/bju.14828>.
- Yu, Ting, Qiongwen Zhang, Tianying Zheng, Huashan Shi, Yang Liu, Shijian Feng, Meiqin Hao, Lei Ye, Xueqian Wu, and Cheng Yang. 2016. 'The Effectiveness of Intensity Modulated Radiation Therapy versus Three-Dimensional Radiation Therapy in Prostate Cancer: A Meta-Analysis of the Literatures'. *PLoS ONE* 11 (5): 1–17. <https://doi.org/10.1371/journal.pone.0154499>.
- Zacho, Helle D, Julie B Nielsen, Ali Afshar-Oromieh, Uwe Haberkorn, Nandita DeSouza, Katja De Paepe, Katja Dettmann, et al. 2018. 'Prospective Comparison of (68)Ga-PSMA PET/CT, (18)F-Sodium Fluoride PET/CT and Diffusion Weighted-MRI at for the Detection of Bone Metastases in Biochemically Recurrent Prostate Cancer.' *European Journal of Nuclear Medicine and Molecular Imaging* 45 (11): 1884–97. <https://doi.org/10.1007/s00259-018-4058-4>.
- Zanotti-Fregonara, Paolo, Kewei Chen, Jehi San Liow, Masahiro Fujita, and Robert B. Innis. 2011. 'Image-Derived Input Function for Brain PET Studies: Many Challenges and Few Opportunities'. *Journal of Cerebral Blood Flow and Metabolism* 31 (10): 1986–98. <https://doi.org/10.1038/jcbfm.2011.107>.
- Zechmann, Christian M., Ali Afshar-Oromieh, Tom Armor, James B. Stubbs, Walter Mier, Boris Hadaschik, John Joyal, et al. 2014. 'Radiation Dosimetry and First Therapy Results with a 124I/131I-Labeled Small Molecule (MIP-1095) Targeting PSMA for Prostate Cancer Therapy'.

- European Journal of Nuclear Medicine and Molecular Imaging* 41 (7): 1280–92. <https://doi.org/10.1007/s00259-014-2713-y>.
- Zhao, Gege, and Bin Ji. 2022. ‘Head-To-Head Comparison of 68Ga-PSMA-11 PET/CT and 99mTc-MDP Bone Scintigraphy for the Detection of Bone Metastases in Patients with Prostate Cancer: A Meta-Analysis’. *American Journal of Roentgenology* 219 (3): 386–96. <https://doi.org/10.2214/AJR.21.27323>.
- Zhao, Ruining, Yajie Li, Lihong Nie, Kaiyue Qin, Hang Zhang, and Hongbin Shi. 2021. ‘The Meta-Analysis of the Effect of 68Ga-PSMA-PET/CT Diagnosis of Prostatic Cancer Compared with Bone Scan’. *Medicine* 100 (15): e25417. <https://doi.org/10.1097/MD.0000000000025417>.
- Zhao, Songji, Yuji Kuge, Takafumi Mochizuki, Toshiyuki Takahashi, Kunihiro Nakada, Masayuki Sato, Toshiki Takei, and Nagara Tamaki. 2005. ‘Biologic Correlates of Intratumoral Heterogeneity in 18F-FDG Distribution with Regional Expression of Glucose Transporters and Hexokinase-II in Experimental Tumor’. *Journal of Nuclear Medicine* 46 (4): 675–82.
- Zhou, Jing, Zhengxing Gou, Renhui Wu, Yuan Yuan, Guiquan Yu, and Yigang Zhao. 2019. ‘Comparison of PSMA-PET/CT, Choline-PET/CT, NaF-PET/CT, MRI, and Bone Scintigraphy in the Diagnosis of Bone Metastases in Patients with Prostate Cancer: A Systematic Review and Meta-Analysis’. *Skeletal Radiology* 48 (12): 1915–24. <https://doi.org/10.1007/s00256-019-03230-z>.
- Zukotynski, Katherine A., Urban Emmenegger, Sebastien Hotte, Anil Kapoor, Wei Fu, Amanda L. Blackford, John Valliant, et al. 2021. ‘Prospective, Single-Arm Trial Evaluating Changes in Uptake Patterns on Prostate-Specific Membrane Antigen (PSMA)-Targeted 18F-DCFPyL PET/CT in Patients with Castration-Resistant Prostate Cancer Starting Abiraterone or Enzalutamide’. *Journal of Nuclear Medicine* 62 (10). <https://doi.org/10.2967/jnumed.120.259069>.



## Original Publications

**Malaspina S, Oikonen V, Kuisma A, Ettala O, Mattila K, Boström PJ, Minn H, Kalliokoski K, Postema EJ, Miller MP, Scheinin M. (2021) Kinetic analysis and optimisation of  $^{18}\text{F}$ -rhPSMA-7.3 PET imaging of prostate cancer**  
European Journal of Nuclear Medicine and Molecular Imaging





# Kinetic analysis and optimisation of $^{18}\text{F}$ -rhPSMA-7.3 PET imaging of prostate cancer

Simona Malaspina<sup>1</sup> · Vesa Oikonen<sup>1</sup> · Anna Kuisma<sup>2</sup> · Otto Ettala<sup>3</sup> · Kalle Mattila<sup>2</sup> · Peter J. Boström<sup>3</sup> · Heikki Minn<sup>2</sup> · Kari Kalliokoski<sup>1</sup> · Ernst J. Postema<sup>4</sup> · Matthew P. Miller<sup>4</sup> · Mika Scheinin<sup>5</sup> ·

Received: 15 January 2021 / Accepted: 29 March 2021 / Published online: 12 April 2021  
© The Author(s) 2021

## Abstract

**Purpose** This phase 1 open-label study evaluated the uptake kinetics of a novel theranostic PET radiopharmaceutical,  $^{18}\text{F}$ -rhPSMA-7.3, to optimise its use for imaging of prostate cancer.

**Methods** Nine men, three with high-risk localised prostate cancer, three with treatment-naïve hormone-sensitive metastatic disease and three with castration-resistant metastatic disease, underwent dynamic 45-min PET scanning of a target area immediately post-injection of 300 MBq  $^{18}\text{F}$ -rhPSMA-7.3, followed by two whole-body PET/CT scans acquired from 60 and 90 min post-injection. Volumes of interest (VoIs) corresponding to prostate cancer lesions and reference tissues were recorded. Standardised uptake values (SUV) and lesion-to-reference ratios were calculated for 3 time frames: 35–45, 60–88 and 90–118 min. Net influx rates ( $K_i$ ) were calculated using Patlak plots.

**Results** Altogether, 44 lesions from the target area were identified. Optimal visual lesion detection started 60 min post-injection. The  $^{18}\text{F}$ -rhPSMA-7.3 signal from prostate cancer lesions increased over time, while reference tissue signals remained stable or decreased. The mean (SD) SUV (g/mL) at the 3 time frames were 8.4 (5.6), 10.1 (7) and 10.6 (7.5), respectively, for prostate lesions, 11.2 (4.3), 13 (4.8) and 14 (5.2) for lymph node metastases, and 4.6 (2.6), 5.7 (3.1) and 6.4 (3.5) for bone metastases. The mean (SD) lesion-to-reference ratio increases from the earliest to the 2 later time frames were 40% (10) and 59% (9), respectively, for the prostate, 65% (27) and 125% (47) for metastatic lymph nodes and 25% (19) and 32% (30) for bone lesions. Patlak plots from lesion VoIs signified almost irreversible uptake kinetics.  $K_i$ , SUV and lesion-to-reference ratio estimates showed good agreement.

**Conclusion**  $^{18}\text{F}$ -rhPSMA-7.3 uptake in prostate cancer lesions was high. Lesion-to-background ratios increased over time, with optimal visual detection starting from 60 min post-injection. Thus,  $^{18}\text{F}$ -rhPSMA-7.3 emerges as a very promising PET radiopharmaceutical for diagnostic imaging of prostate cancer.

**Trial Registration** NCT03995888 (24 June 2019).

**Keywords**  $^{18}\text{F}$  · Kinetics · PET/CT · PSMA · rhPSMA

This article is part of the Topical Collection on Oncology - Genitourinary.

Simona Malaspina and Vesa Oikonen are joint first authors.

✉ Simona Malaspina  
simona.malaspina@tyks.fi

<sup>1</sup> Turku PET Centre University of Turku and Turku University Hospital Turku Finland

<sup>2</sup> Department of Oncology, University of Turku and Turku University Hospital, Turku, Finland

<sup>3</sup> Department of Urology, University of Turku and Turku University Hospital, Turku, Finland

<sup>4</sup> Blue Earth Diagnostics Ltd, Oxford, UK

<sup>5</sup> Clinical Research Services Turku – CRST Ltd, Turku, Finland

## Introduction

$^{18}\text{F}$ -rhPSMA-7.3 is a prostate specific membrane antigen (PSMA)-targeted radiopharmaceutical in development for the imaging of patients with prostate cancer.  $^{18}\text{F}$ -labelled PSMA PET radiopharmaceuticals are increasingly used in preference to their  $^{68}\text{Ga}$ -labelled counterparts due to their favourable features, which include a longer half-life, lower positron range and larger batch production [1].  $^{18}\text{F}$ -rhPSMA-7.3 is the lead compound of a novel series of radiohybrid PSMA (rhPSMA) radiopharmaceuticals. Further to labelling with  $^{18}\text{F}$  for imaging purposes, the agent can be labelled with radiometals for use as a therapeutic agent for patients with prostate cancer [2].  $^{18}\text{F}$ -rhPSMA-7.3 was

selected as the lead rhPSMA compound for clinical development based on preclinical assessments [3].  $^{18}\text{F}$ -rhPSMA-7.3 is a single diastereoisomer form of  $^{18}\text{F}$ -rhPSMA-7, which has been shown to have good diagnostic efficacy in patients with primary and recurrent prostate cancer [4–6].

Prior to the start of this investigation,  $^{18}\text{F}$ -rhPSMA-7.3 was administered to six healthy volunteers to evaluate its safety, biodistribution in healthy organs and radiation dosimetry [7]. In the present phase 1 open-label study, we report the results of an evaluation of the uptake kinetics of this novel radiopharmaceutical in primary prostate tumours, local recurrence, lymph node metastases and bone metastases in patients with newly diagnosed high-risk localised prostate cancer, in treatment-naïve patients with hormone-sensitive metastatic disease and in patients with castration-resistant metastatic disease. The safety and lesion detectability results from the current study will be presented separately.

## Material and methods

### Subjects

Participants were recruited from three distinct patient populations (referred to as Cohorts A–C). All participants had histologically confirmed adenocarcinoma of the prostate without neuroendocrine differentiation or small cell features.

Cohort A comprised patients with newly diagnosed, high-risk prostate cancer as defined by the NCCN Guidelines [8] who were scheduled for radical prostatectomy. Cohort B consisted of patients who had newly diagnosed, treatment-naïve hormone-sensitive metastatic prostate cancer. Patients in Cohort C had castration-resistant metastatic prostate cancer [9], defined as a level of serum testosterone  $<1.7$  nmol/L plus biochemical progression (three consecutive rises in PSA 1 week apart) or radiological progression (appearance of new lesions using RECIST criteria [10]), while receiving androgen-deprivation therapy. The metastatic status in both Cohort B and C patients was defined as a quantifiable number or a high likelihood of metastases documented by standard-of-care imaging (computed tomography [CT] and/or bone scintigraphy) performed in the 12-week period preceding enrolment into this trial.

Between October 18, 2019 and March 17, 2020, 10 patients were assigned to these groups. One Cohort C patient's PET scan was deemed not to be evaluable for the purposes of this kinetic analysis according to the predetermined study evaluability criteria as the target region with documented disease was outside of the region scanned for kinetic evaluation. The remaining nine evaluable subjects were assigned to Cohorts A–C, with three patients in each.

### Radiopharmaceutical preparation

$^{18}\text{F}$ -rhPSMA-7.3 was produced on site at Turku PET Centre using a single-use cassette-based proprietary automated synthesis platform for radiolabelling, purification and formulation (Scintomics GRP, Scintomics GmbH, Fürstfeldbruck, Germany), and using an in-house remotely operated sterile filtration device for aseptic filling, in accordance with GMP and Turku PET Centre's standard procedures.

### Imaging procedures

Patients were requested not to eat for at least 4 h before the administration of  $^{18}\text{F}$ -rhPSMA-7.3 but drinking of water was allowed and encouraged. Patients were encouraged to void just before  $^{18}\text{F}$ -rhPSMA-7.3 was administered and between Scans 1 and 2 (detailed below). Two i.v. cannulae were positioned, one in each arm. Diuretics were not administered for the purposes of imaging.

Scans were conducted using a GE Discovery MI PET/CT scanner (GE Healthcare, Milwaukee, WI, USA). Patients underwent a 45-min dynamic scan (Scan 1) starting at the time of  $^{18}\text{F}$ -rhPSMA-7.3 administration and two whole-body 28-min PET scans from mid-thigh to vertex (7 bed positions at 4 min/bed), starting at 60 min (Scan 2) and 90 min (Scan 3) post-injection. The first scan was performed in list mode and the target region was based on the target lesion for each patient: for Cohort A patients this was the prostate gland and for Cohort B and C patients it was the most relevant lesion identified on standard-of-care imaging. In case of multiple metastases, the target area that included the largest number of lesions was selected. Care was taken to include at least one bone lesion and one lymph node metastasis, when both present. Moreover, when possible, the area that included the thoracic or abdominal aorta was chosen.

A vacuum mattress was used to position the subjects on the PET imaging bed and to ensure the same positioning after the break between dynamic and whole-body scans. Low-dose CT scans (one of the target area and one from vertex to mid-thigh) were acquired for attenuation correction and anatomic correlation. The CT acquisition parameters were: tube potential 120 kV, tube current 10–120 mA, noise index 30, resulting in an effective dose of 1.4 mSv for the target area and 5.3 mSv for the scan from vertex to mid-thigh. The CT scan was followed by a bolus injection of  $^{18}\text{F}$ -rhPSMA-7.3.

The patients received a target radioactivity of 300 MBq ( $\pm 10\%$ ) of  $^{18}\text{F}$ -rhPSMA-7.3, as informed by dosimetry data from healthy volunteers [7]. An administered activity of 300 MBq would result in a total effective dose of 4.2 mSv which was considered acceptable for the purposes of this investigation. All results were corrected for radiochemical decay from the time of administration. Scans were read according to the current interpretation guidelines for PSMA PET/CT [11]



by one nuclear medicine physician (S.M) with 3 years of experience reading PSMA PET scans.

### In vitro radioactivity concentrations

Non-arterialised venous blood samples (2 mL) were collected starting after the administration of <sup>18</sup>F-rhPSMA-7.3 and according to the following approximate sampling schedule: 20 s, 40 s, 60 s, 80 s, 100 s, 120 s, 140 s, 160 s, 180 s, 4 min, 5 min, 7.5 min, 10 min, 15 min, 20 min, 30 min, 40 min, 50 min, 59 min and 120 min post-injection. Blood samples were collected into heparinised tubes, mixed and chilled on ice. They were promptly divided into two aliquots, and one aliquot was centrifuged in a cooled (+4 °C) centrifuge at 2118 g for 5 min. Next, 700 µl of plasma was separated into another tube. Both plasma and whole blood radioactivity was measured.

### In vivo radioactivity concentrations from imaging data

Experienced PET researchers (K.K. and S.M.) manually drew volume of interest (VoI) regions on as many lesions and healthy reference tissues as were identified in the images of the target area. Blood pool VoI regions were drawn on large arteries, usually the abdominal aorta. If allowed by reference tissue size, VoIs were drawn over at least four mid-tissue PET planes with the help of the correlating anatomic CT image. Care was taken to avoid the surfaces of the reference tissues to prevent partial volume effects in the measurement of radioactivity. The positions of the VoIs were checked against all three PET scan sets and if any movement was observed, the VoI position was adjusted accordingly. Finally, the mean VoI radioactivity values of each lesion/reference tissue, each scan set and each subject were extracted and individual time–activity concentration curves (TACs) for each lesion/reference tissue were generated for each subject. The VoI radioactivity concentrations from the two static PET scans were corrected for the decay of <sup>18</sup>F to the administration time, and the corrected radioactivity concentrations were added to the TACs of the dynamic scan to construct full 0–118 min regional TACs.

Regional TACs and venous plasma and blood TACs were converted from radioactivity concentration units (Bq/mL and kBq/mL, respectively) into standardised uptake value (SUV) units (g/mL) to enable direct comparisons of TACs between subjects.

SUV was calculated using Eq. 1:

$$\text{SUV} = \text{Radioactivity concentration (kBq/ml)} \times \frac{\text{Weight of the subject (Kg)}}{\text{Administered activity (MBq)}} \tag{1}$$

### Calculations based on the time–activity concentration curves

#### Plasma and blood TACs

To explore the relationship between the radioactivity concentrations in blood and plasma, the plasma-to-blood ratio as a function of time was calculated using the collected blood and plasma samples. The plasma-to-blood ratio remained constant (see the “Results” section) suggesting that <sup>18</sup>F-rhPSMA-7.3 and any potential radioactive metabolites remain in blood plasma and do not enter the red blood cells. Thus, the blood TACs can be converted to plasma TACs using Eq. 2:

$$\text{Plasma radioactivity} = \frac{\text{Blood radioactivity}}{1 - \text{Haematocrit}} \tag{2}$$

Haematocrit (i.e. the volume proportion of red blood cells in blood) was measured at screening, at baseline (–120 to –5 min, relative to injection), at 45 min, 3 h, 4 h and at 24 h post-injection (as part of the study safety laboratory evaluations). The average haematocrit value from the baseline, 45-min, and 3-h samples was used to convert PET image-based blood TACs to plasma TACs. Plasma-to-blood ratios averaged over time were calculated for each subject from the actual plasma and whole blood data, excluding the first 2 min, and these individual ratios were compared to the estimated plasma-to-blood ratios based on the haematocrit values.

The plasma and blood TACs were constructed as combinations of image-derived arterial TACs and manually sampled venous blood TACs to correct the expected discrepancies between the individual TACs that occur as a result of the time taken to reach transient equilibrium between arterial and venous plasma [12, 13]. Image-derived arterial blood pool TACs were utilised from the time of administration until the peak of each TAC, and manual sample venous TACs were utilised starting from their peak value. Because of the sparse sampling [14], the function in Eq. 3 was fitted to the combined plasma and blood TACs:

$$f(t) = \begin{cases} 0 & , \text{if } t \leq T_{ap} \\ [A_1(t - T_{ap}) - A_2 - A_3]e^{-\lambda_1(t - T_{ap})} + A_2e^{-\lambda_2(t - T_{ap})} + A_3e^{-\lambda_3(t - T_{ap})} & , \text{if } t > T_{ap} \end{cases} \tag{3}$$

The fitted function parameters (coefficients A<sub>1-3</sub>, eigenvalues of the system λ<sub>1-3</sub>, and appearance time of

radioactivity T<sub>ap</sub>) were used to construct smooth plasma and blood TACs.

## Lesion-to-background ratios

Relative radioactivity uptake in possible cancer-associated lesions and in healthy reference tissues was analysed. For bone metastases, healthy bone marrow was used as the reference tissue. For lymph node metastases, combined initial imaging blood pool and venous blood was used as the reference tissue. For primary prostate tumours, skeletal muscle was used as the reference region. Lesion-to-reference ratios (SUV ratios) were calculated and plotted as a function of time, and ratios at the end of the dynamic scan (35–45 min) and during Scans 2 and 3 (60–88 min and 90–118 min, respectively) were calculated. During the dynamic scan, reference tissues were measured at the same time points as the lesions. In the late static scans with multiple bed positions, the measurement time points may have been somewhat different, but insignificantly so because of the relatively constant radioactivity uptake values, especially in the reference tissues.

## Multiple-time graphical analysis

Multiple-time graphical analysis (MTGA) was performed for the target lesion and reference tissue data, using plasma TAC as an input function [15]. Compartmental models for the radiopharmaceutical and tissues of interest [16] have not been defined at this stage of development, and MTGAs (Patlak plot for irreversible and Logan plot for reversible uptake kinetics) are independent of the number of tissue compartments. We constructed Patlak and Logan plots from the data and fitted a line to the linearly increasing phase of the plot to determine the net influx rate ( $K_i$ ) in the case of a Patlak plot or the volume of distribution ( $V_T$ ) in the case of a Logan plot. Fractional uptake rates (FUR), related to the Patlak plot  $K_i$  [17], were calculated at different time points by dividing the VoI concentration by the area under the curve of the plasma TAC.

## Software

The Carimas image analysis tool (version 2.10, Turku PET Centre, Turku, Finland) was used to measure radioactivity concentrations in target lesions and reference tissues at different time points post-injection. Data were processed using a spreadsheet program (Excel, Microsoft Corporation) and in-house software (tpcplib 0.7.6, Turku PET Centre, Turku, Finland).

## Statistical analysis

Descriptive data are presented as mean values and their standard deviations from the mean.

## Results

### Patients

Nine caucasian males with prostate cancer were included in this analysis. The participants had a mean age of 66 years (range 55 to 80 years) and a mean body mass index of 26.9 kg/m<sup>2</sup> (range 21.9 to 30.6 kg/m<sup>2</sup>). PSA levels at the screening visit had ranges of 6.1–21 ng/mL for Cohort A, 3.9–35 ng/mL for Cohort B and 17–170 ng/mL for Cohort C. Testosterone levels for Cohort C patients before the PET scan were 0.05, 0.58 and 0.61 nmol/L, respectively. The mean administered activity of <sup>18</sup>F-rhPSMA-7.3 was 301 MBq (range 284 to 322 MBq). The molar activity (GBq/μmol) for each patient at the time of injection is presented in Online Resource Table 1. The variation in injected mass is thought to have no significant effect on <sup>18</sup>F-rhPSMA-7.3 biodistribution and tumour uptake [18].

A total of 44 lesions were identified and analysed in the selected target regions: 6 prostate/prostate bed lesions (4 primary and 2 recurrent tumours), 26 lymph node metastases and 12 bone metastases. In detail, within the target area, <sup>18</sup>F-rhPSMA-7.3 identified lesions in the prostate gland in all Cohort A patients. One patient in Cohort C was found to have two sites of disease in the prostate bed. Lymph node lesions were found in two patients in Cohort B and in all three patients in Cohort C. Bone metastases were found in two patients in Cohort B and in one patient in Cohort C. No visceral metastases were identified. The great majority of lesions (36/44) were already confirmed by standard-of-care imaging. In patient B-03 and C-03, <sup>18</sup>F-rhPSMA 7.3 PET/CT detected additional pelvic lymph nodes (1 and 3, respectively) that were smaller than the anatomical cut-off value used in CT (short axis of 8 mm), but that showed clearly pathological PSMA-uptake. Moreover, patient C-04, who already had confirmed nodal metastases, presented with four strong bone uptakes in the target area that were not clearly visualised by conventional imaging. Given also the already known metastatic status of the patients, these lesions were considered as metastatic. The lesions that were found in whole-body static scans outside of the target area of the dynamic scan will be reported in a separate publication.

### Blood and plasma data

Plasma and blood TACs were well fitted with the function specified in the “Material and methods” section. Blood radioactivity concentrations decreased rapidly after administration, as <sup>18</sup>F-rhPSMA-7.3 was distributed in the blood pool and in the reference tissues, but radioactivity concentrations in blood remained above the average whole-body radioactivity concentration (SUV >1 g/ml). The average (SD) haematocrit during the PET investigations was 0.41 (0.04). The plasma-to-blood

ratio was stable during the scans, with an average of 1.66 when calculated from samples collected starting from 2 min after radiopharmaceutical administration (Online Resource Fig. 1). Assuming that all radioactivity present in blood remains in the plasma compartment (Eq. 2), this plasma-to-blood ratio amounts to a haematocrit level of 0.40.

### Volume of interest time activity concentration curves

Radioactivity concentrations, scaled for administered dose and subject weight (SUV, g/mL), as a function of time, are shown in Fig. 1 for the dynamic and static scan data combined. Target lesion uptake increased during the scanning sessions, although in less active lesions the increases were modest during the whole-body PET sessions. The mean (SD) SUVs at 35–45, 60–88 and 90–118 min were 8.4 (5.6), 10.1 (7) and 10.6 (7.5) g/ml, respectively, for prostate lesions, 11.2 (4.3), 13 (4.8) and 14 (5.2) g/ml for lymph node metastases, and 4.6 (2.6), 5.7 (3.1) and 6.4 (3.5) g/ml for bone metastases.

The mean (SD) percentage of SUV increases from the earliest (35–45 min) to the later (60–88 and 90–118 min) scan time frames were 17% (8) and 23% (7), respectively, for the prostate, 19% (17) and 29% (20) for lymph node metastases, and 23% (12) and 40% (18) for bone lesions. Between the two later scans, the mean (SD) SUV increase in prostate, lymph node and bone lesions were 5% (3), 8% (7) and 14% (8), respectively. The absolute values of SUV for each lesion and reference tissue are shown in Online Resource Table 2.

### Lesion-to-background ratios

The lesion-to-reference tissue ratio curves are shown in Figs. 2, 3, and 4, with healthy bone marrow, combined initial imaging blood pool and venous blood, and muscle as reference tissues, respectively. Tissue-to-blood ratios generally increased with time, suggesting a significant irreversible uptake component. The mean (SD) lesion-to-reference ratios at 35–

45, 60–88 and 90–118 min were 14.5 (9.6), 20.8 (14.6) and 23.6 (16.4) for the prostate, 7 (3.5), 8.7 (4.2) and 9.1 (4.5) for lymph node metastases and 3.4 (1.4), 5.4 (2) and 7.3 (2.5) for bone lesions, respectively.

The mean (SD) lesion-to-reference ratio percentages of increases from the earliest (35–45 min) to the later (60–88 and 90–118 min) time frames were 40% (10) and 59% (9) for the prostate, 65% (27) and 125% (47) for lymph node metastases and 25% (19) and 32% (30) for bone lesions, respectively. Between the later scans, ratios increased by a mean (SD) of 14% (5), 35% (12) and 5% (10) for prostate, lymph node and bone lesions, respectively. The absolute values of ratios for each lesion/reference tissue are presented in Online Resource Table 3.

### Uptake kinetics

Tissue radioactivity concentrations and lesion-to-reference ratios increased at least until the end of the PET scanning period (118 min post-injection). The increases were not substantial after the first static scan, and optimal visual detection of primary tumours and/or metastases was achieved in the first whole-body scan, starting 60 min post-injection.

MTGA for irreversible uptake kinetics (Patlak plot) reached linearity about 10 min post-injection (Online Resource Fig. 2). The  $K_i$  values of  $^{18}\text{F}$ -rhPSMA-7.3 (calculated as the slope of the linear part of the plot) were clearly higher in suspected disease lesions than in reference tissues (Online Resource Table 4). The Patlak data suggest that  $^{18}\text{F}$ -rhPSMA-7.3 uptake kinetics in lesions and relevant reference tissues is dominated by irreversible components, but reversible components were also apparent. Since the lesion uptake kinetics of  $^{18}\text{F}$ -rhPSMA-7.3 were found to be mainly irreversible, and as all patient scans could be reliably analysed using Patlak plots, but most patient scans could not be analysed using Logan plots, the Logan plot  $V_T$  results are not reported here. SUVs that were calculated from the final time frame of the dynamic

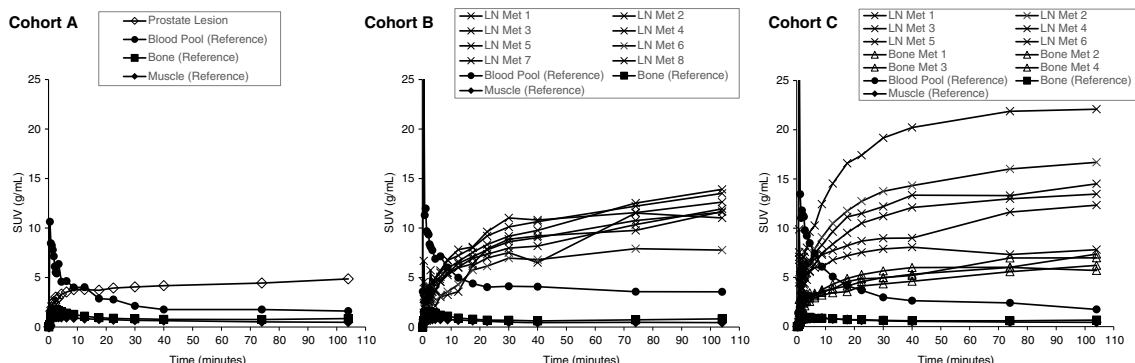


**Fig. 1** Representative SUV (g/mL) results as a function of time (min) using both the dynamic and static scan data. Left panel presents data from a patient in Cohort A, middle panel from a patient in Cohort B and right panel from a patient in Cohort C

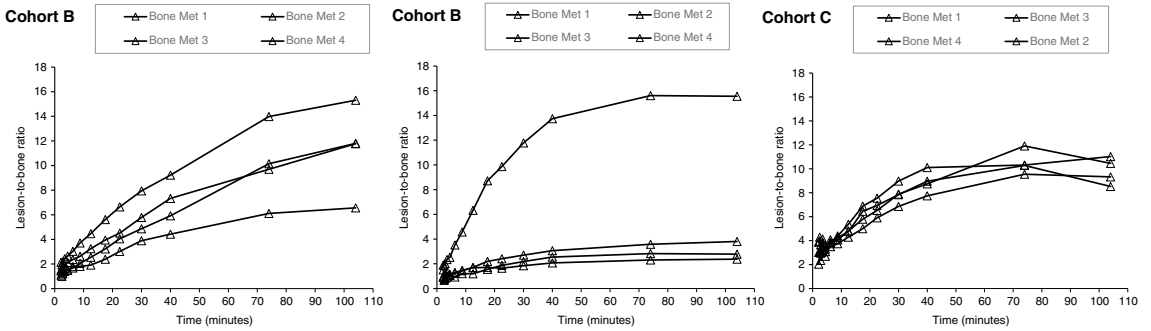


**Fig. 2** Representative lesion-to-bone marrow ratios as a function of time. Plots displayed from patients with bone metastases (Cohort B left and middle panels, and Cohort C, right panel)

scan (35–45 min post-injection) and the two static scans were in good agreement with Patlak  $K_i$  values (Fig. 5, left panel), considering that the measured plasma input function was not used in the calculation of SUV and the usage of SUV in interindividual comparisons is based on the assumption of similar total plasma clearance. Tissue-to-blood ratios (obtained using venous blood sampling) also appeared to agree well with the Patlak  $K_i$  results (Fig. 5 middle panel).

FUR provides an estimate of the Patlak  $K_i$ , using the static PET scan data and the measurement of plasma TAC from the time of  $^{18}\text{F}$ -rhPSMA-7.3 administration. FUR values also matched well with the Patlak  $K_i$  values (Fig. 5, right panel).

**Discussion**

This phase 1 open-label study evaluated the uptake kinetics of  $^{18}\text{F}$ -rhPSMA-7.3 in nine patients with prostate cancer in order to optimise its use for PET/CT imaging.

Following administration,  $^{18}\text{F}$ -rhPSMA-7.3 uptake in the reference tissues was of a similar level to that noted in healthy volunteers [7]. We observed high uptake in prostate cancer lesions within the first hour and both the tissue radioactivity concentration and lesion-to-reference ratios increased at least until the end of the scanning sessions (118 min post-injection).

This might suggest that later time points could provide more optimal imaging, as has been previously demonstrated for other PSMA-tracers [19–22]. However, according to the results of our study, the increases were not substantial after the first whole-body scan (Scan 2). Therefore, considering logistical reasons for diagnostic use in clinical practice, the optimal time for  $^{18}\text{F}$ -rhPSMA-7.3 PET for the assessment of both primary prostate tumours and metastatic lesions is between 60 and 90 min post-injection and the optimal timing to commence scanning is 60 min post-injection. In contrast with the studies mentioned above with other tracers, we have not evaluated later time points (> 2 h post-injection) in the present study. This might be a limitation, considering that this information could be useful in a radiometabolic treatment setting. However, this study was designed to investigate the uptake kinetics of rhPSMA 7.3 specifically to optimise its diagnostic use.

Radioactivity concentrations in the blood decreased rapidly after  $^{18}\text{F}$ -rhPSMA-7.3 administration as  $^{18}\text{F}$ -rhPSMA-7.3 was distributed in the blood pool and in the reference tissues. Our data show that the plasma-to-blood ratio remained constant over the scanning period and at a level implying that  $^{18}\text{F}$ -rhPSMA-7.3 remains in blood plasma and does not enter the red blood cells during the relevant time period from injection. As demonstrated by our previous studies with  $^{18}\text{F}$ -FDG [23,

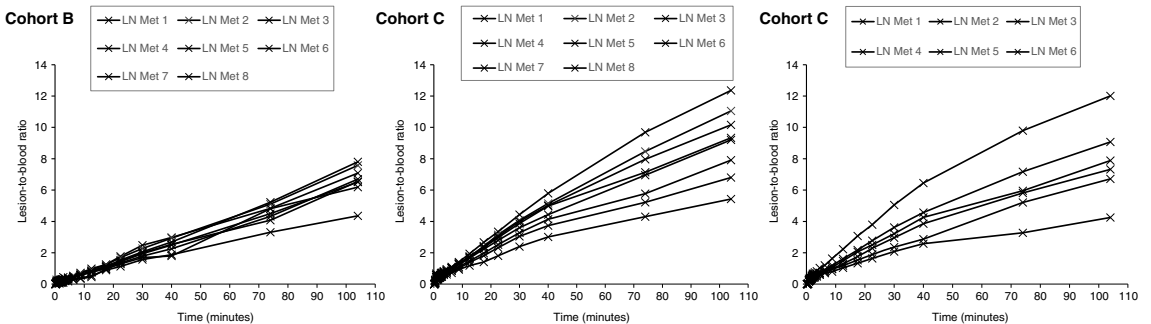


**Fig. 3** Representative lesion-to-blood (combined initial image blood pool and venous blood) ratios as a function of time. Plots displayed from patients in Cohort B (left panel) and Cohort C (middle and right panels)

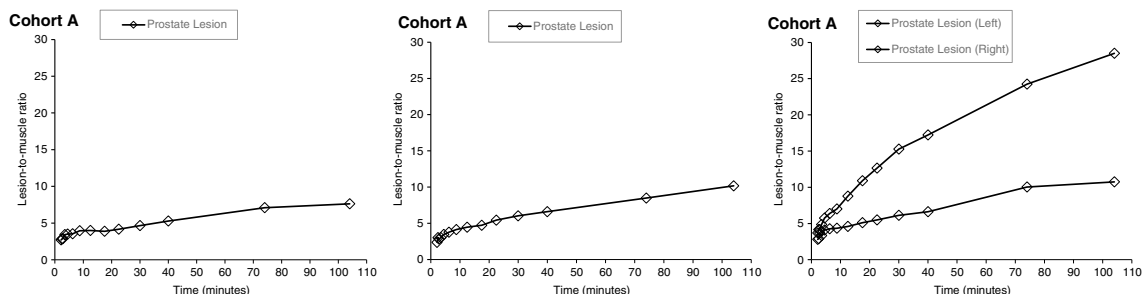


**Fig. 4** Representative lesion-to-muscle ratios as a function of time. Data shown for prostate lesions from three individual patients in Cohort A; two distinct lesions were identified in one of the patients (right panel)

24], combining venous sampling and image-based arterial/venous estimates as input functions for the TACs is a useful technique in kinetic studies. Here, combining venous blood sampling data with initial arterial data from a blood pool in the PET images improved the otherwise underestimated initial phase of the plasma TACs. Generally, if a blood pool of high enough quality can be identified from PET images, then venous sampling can be replaced with a blood pool-derived estimation from the PET image, thus removing the need for blood sampling for radioactivity analyses.

The general increase in tissue-to-blood ratios with time suggests a significant irreversible uptake component. The MTGA data further confirm this; the Patlak plots suggest that <sup>18</sup>F-rhPSMA-7.3 uptake kinetics in lesions and relevant reference tissues is dominated by irreversible components, but some reversible components were also apparent. This is as expected for a radiopharmaceutical that can bind reversibly to its specific target molecule residing on cell membranes but can also be internalised into cells when bound to its receptor, and possibly slowly recirculated back to the cell surface. Downward curvature of the Patlak plot leads to  $K_i$  estimates that are dependent on the scan duration and on the selection of the time range used for the slope estimation from the plot. If the uptake kinetics were fully irreversible during the PET scan, the Patlak slope would be time-independent after an initial equilibration period; this would be a considerable advantage over SUV and ratio methods which can only provide time-dependent measures. The curvature of the plots prevents a bias-free, scan duration-

independent assessment of the slope (net influx rate  $K_i$  in the case of Patlak plots). Thus, a dynamic PET protocol with blood sampling may not offer such quantitative advantages over the simpler SUV and ratio methods that would support the use of a longer and more laborious imaging protocol.

Since Patlak  $K_i$  estimates are dependent on the selected line fit time range, and FUR estimates on the PET time frame used for the calculations, the results are here reported from different time frames. The decreases over time suggest that extending the PET scan duration beyond 90 min may not improve the detectability of lesions, possibly even the opposite, if Patlak or FUR analyses are employed.

Taken together, the different analyses presented here provided concordant results. The findings indicate that neither dynamic PET scans nor blood sampling should be required in clinical applications of <sup>18</sup>F-rhPSMA-7.3 imaging of patients with prostate cancer.

The present study is not without limitations. Although not uncommon for studies of this nature, the small number of study participants limits the conclusions that can be drawn from these data. Nevertheless, the present results have already been used to determine the optimal time window for PET imaging following administration of <sup>18</sup>F-rhPSMA-7.3 in the ongoing pivotal phase 3 trials of <sup>18</sup>F-rhPSMA-7.3 in newly diagnosed patients [LIGHTHOUSE; NCT04186819] and in patients with biochemical recurrence of prostate cancer [SPOTLIGHT; NCT04186845], and the results of these trials are eagerly awaited.

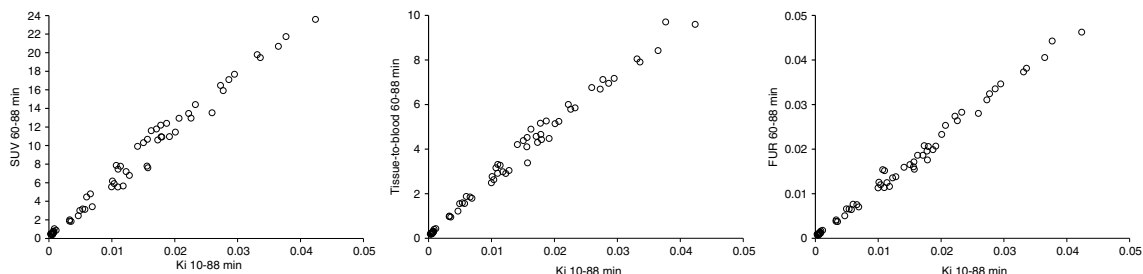


**Fig. 5** Comparison of Patlak  $K_i$  results with SUV, tissue-to-blood ratios and with FUR values. Left panel shows comparison with SUV. Middle panel shows comparison with tissue-to-blood ratio. Right plot shows comparison with FUR values

## Conclusions

$^{18}\text{F}$ -rhPSMA-7.3 uptake kinetics in prostate cancer lesions and relevant reference tissues are dominated by irreversible components. Uptake in prostate cancer lesions and lesion-to-background ratios increased over time, with the optimal timing for  $^{18}\text{F}$ -rhPSMA-7.3 PET imaging for the assessment of both primary prostate tumours and metastatic lesions appearing to be between 60 and 90 min post-injection. The optimal timing to commence scanning is therefore 60 min post-injection. In the clinical setting, simplified measures of  $^{18}\text{F}$ -rhPSMA-7.3 uptake are sufficient for optimal detection of prostate cancer lesions, removing the need for dynamic PET scans and/or blood sampling. Thus,  $^{18}\text{F}$ -rhPSMA-7.3 emerges as a very promising radiopharmaceutical for diagnostic imaging of prostate cancer, with possible further applications in theranostics.

**Supplementary Information** The online version contains supplementary material available at <https://doi.org/10.1007/s00259-021-05346-8>.

**Acknowledgements** Medical writing support was provided by Dr. Catriona Turnbull (BED).

**Authors' contributions** Study conception and design: Mika Scheinin, Vesa Oikonen, Peter J. Boström, Kari Kalliokoski, Simona Malaspina, Ernst J. Postema and Matthew P. Miller. Material preparation and data collection: Simona Malaspina, Vesa Oikonen, Kari Kalliokoski, Anna Kuisma, Otto Ettala, Kalle Mattila, Peter J. Boström and Heikki Minn. Data analysis: Simona Malaspina, Vesa Oikonen and Kari Kalliokoski. Drafting of the manuscript: Simona Malaspina, Vesa Oikonen, Kari Kalliokoski, Matthew Miller and Ernst J. Postema. All authors commented on previous versions of the manuscript and read and approved the final manuscript.

**Funding** Open access funding provided by University of Turku (UTU) including Turku University Central Hospital. This study was funded by Blue Earth Diagnostics Ltd., Oxford, UK (BED).

**Data availability** Anonymised data are available from the Corresponding author on reasonable request.

## Declarations

**Ethics approval** Ethical approval was received from the Ethics Committee of the Hospital District of Southwest Finland.

**Consent to participate** All subjects provided written, informed consent.

**Consent for publication** All subjects provided written, informed consent regarding the publishing of study data.

**Conflict of interest** Clinical Research Services Turku (CRST Ltd) and Turku University Hospital were contracted by BED to carry out the research and received funding from BED for this work. Mika Scheinin is an employee, shareholder and board member of CRST Ltd. Simona Malaspina, Vesa Oikonen, Anna Kuisma, Otto Ettala, Kalle Mattila, Peter J. Boström, Heikki Minn and Kari Kalliokoski are employees of

Turku University Hospital and/or University of Turku. Matthew P. Miller is an employee and shareholder of BED. Ernst J. Postema received personal fees from BED during the conduct of this study. No other potential conflicts of interest relevant to this article exist.

**Open Access** This article is licensed under a Creative Commons Attribution 4.0 International License, which permits use, sharing, adaptation, distribution and reproduction in any medium or format, as long as you give appropriate credit to the original author(s) and the source, provide a link to the Creative Commons licence, and indicate if changes were made. The images or other third party material in this article are included in the article's Creative Commons licence, unless indicated otherwise in a credit line to the material. If material is not included in the article's Creative Commons licence and your intended use is not permitted by statutory regulation or exceeds the permitted use, you will need to obtain permission directly from the copyright holder. To view a copy of this licence, visit <http://creativecommons.org/licenses/by/4.0/>.

## References

1. Werner RA, Derlin T, Lapa C, Sheikbahaei S, Higuchi T, Giesel FL, et al.  $^{18}\text{F}$ -Labeled, PSMA-targeted radiotracers: leveraging the advantages of radiofluorination for prostate cancer molecular imaging. *Theranostics*. 2020;10:1–16.
2. Wurzer A, DiCarlo D, Schmidt A, Beck R, Eiber M, Schwaiger M, et al. Radiohybrid ligands: a novel tracer concept exemplified by  $^{18}\text{F}$ - or  $^{68}\text{Ga}$ -labeled rhPSMA-inhibitors. *J Nucl Med*. 2019;61:735–42.
3. Wurzer A, Parzinger M, Konrad M, Beck R, Günther T, Felber V, et al. Preclinical comparison of four [ $^{18}\text{F}$ ,  $^{nat}\text{Ga}$ ]rhPSMA-7 isomers: influence of the stereoconfiguration on pharmacokinetics. *EJNMMI Res*. 10(1):149.
4. Oh SW, Wurzer A, Teoh EJ, Oh S, Langbein T, Kronke M, et al. Quantitative and qualitative analyses of biodistribution and PET image quality of novel radiohybrid PSMA,  $^{18}\text{F}$ -rhPSMA-7, in patients with prostate cancer. *J Nucl Med*. 2019;61:702–9.
5. Eiber M, Kronke M, Wurzer A, Ulbrich L, Jooss L, Maurer T, et al.  $^{18}\text{F}$ -rhPSMA-7 positron emission tomography for the detection of biochemical recurrence of prostate cancer following radical prostatectomy. *J Nucl Med*. 2019;61:696–701.
6. Kronke M, Wurzer A, Schwamborn K, Ulbrich L, Jooss L, Maurer T, et al. Histologically-confirmed diagnostic efficacy of  $^{18}\text{F}$ -rhPSMA-7 positron emission tomography for N-staging of patients with primary high risk prostate cancer. *J Nucl Med*. 2019;61:710–5.
7. Tolvanen T, Kalliokoski K, Malaspina S, Kuisma A, Lahdenpohja S, Postema EJ, et al. (2020) Safety, biodistribution and radiation dosimetry of  $^{18}\text{F}$ -rhPSMA-7.3 in healthy adult volunteers. *J Nucl Med*. [jnumed.120.252114](https://doi.org/10.1007/s00259-021-05346-8).
8. NCCN. NCCN clinical practice guidelines in oncology: prostate cancer. Version 4.2019. <https://www2.tri-kobe.org/nccn/guideline/urological/english/prostate.pdf> 2019. Accessed December 2020.
9. Cornford P, Bellmunt J, Bolla M, Briers E, De Santis M, Gross T, et al. EAU-ESTRO-SIOG guidelines on prostate cancer. Part II: treatment of relapsing, metastatic, and castration-resistant prostate cancer. *Eur Urol*. 2017;71(4):630–42.
10. Eisenhauer EA, Therasse P, Bogaerts J, Schwartz LH, Sargent D, Ford R, et al. New response evaluation criteria in solid tumours: revised RECIST guideline (version 1.1). *Eur J Cancer*. 2009;45(2):228–47.
11. Eiber M, Herrmann K, Calais J, Hadaschik B, Giesel FL, Hartenbach M, et al. Prostate cancer molecular imaging standardized evaluation (PROMISE): proposed miTNM classification for

- the interpretation of PSMA-ligand PET/CT. *J Nucl Med.* 2018;59(3):469–78.
12. Zanolini-Fregonara P, Chen K, Liow JS, Fujita M, Innis RB. Image-derived input function for brain PET studies: many challenges and few opportunities. *J Cereb Blood Flow Metab.* 2011;31:1986–98.
  13. Eary JF, Mankoff DA. Tumor metabolic rates in sarcoma using FDG PET. *J Nucl Med.* 1998;39:250–4.
  14. Wang X, Feng D (1992) A study on physiological parameter estimation accuracy for tracer kinetic modelling with positron emission tomography (PET). American Control Conference. Chicago, IL, USA. p. 1632–3.
  15. Logan J. Graphical analysis of PET data applied to reversible and irreversible tracers. *Nucl Med Biol.* 2000;27:661–70.
  16. Huang SC, Phelps ME. Principles of tracer kinetic modeling in positron emission tomography and autoradiography. In: Phelps M, Mazziotta J, Schelbert H, editors. *Positron emission tomography and autoradiography: principles and applications for the brain and heart.* New York: Raven Press; 1966. p. 287–346.
  17. Thie JA. Clarification of a fractional uptake concept. *J Nuc Med.* 1995;36:711–2.
  18. Langbein A, Wurzer A, Gafita A, Robertson H, Wang A, Arçay M, et al. Does the injected mass influence the biodistribution of F-18-rhPSMA-7.3 on positron emission tomography in prostate cancer patients? *Eur J Nucl Med Mol Imaging.* 2020;47:S375.
  19. Afshar-Oromieh A, Malcher A, Eder M, Eisenhut M, Linhart HG, Hadaschik BA, et al. PET imaging with a [68Ga]gallium-labelled PSMA ligand for the diagnosis of prostate cancer: biodistribution in humans and first evaluation of tumour lesions. *Eur J Nucl Med Mol Imaging.* 2013;40:486–95.
  20. Afshar-Oromieh A, Hetzheim H, Kratochwil C, Benesova M, Eder M, Neels OC, et al. The theranostic PSMA ligand PSMA-617 in the diagnosis of prostate cancer by PET/CT: biodistribution in humans, radiation dosimetry, and first evaluation of tumor lesions. *J Nucl Med.* 2015;56:1697–705.
  21. Rahbar K, Afshar-Oromieh A, Bogemann M, Wagner S, Schafers M, Stegger L, et al. <sup>18</sup>F-PSMA-1007 PET/CT at 60 and 120 minutes in patients with prostate cancer: biodistribution, tumour detection and activity kinetics. *Eur J Nucl Med Mol Imaging.* 2018;45:1329–34.
  22. Giesel FL, Hadaschik B, Cardinale J, Radtke J, Vinsensia M, Lehnert W, et al. F-18 labelled PSMA-1007: biodistribution, radiation dosimetry and histopathological validation of tumor lesions in prostate cancer patients. *Eur J Nucl Med Mol Imaging.* 2017;44(4): 678–88.
  23. Minn H, Zasadny KR, Quint LE, Wahl RL. Lung cancer: reproducibility of quantitative measurements for evaluating 2-[F-18]-fluoro-2-deoxy-D-glucose uptake at PET. *Radiology.* 1995;196:167–73.
  24. Eskelinen JJ, Heinonen I, Loyttyniemi E, Saunavaara V, Kirjavainen A, Virtanen KA, et al. Muscle-specific glucose and free fatty acid uptake after sprint interval and moderate-intensity training in healthy middle-aged men. *J Appl Physiol (1985).* 2015;118:1172–80.
- Publisher's note** Springer Nature remains neutral with regard to jurisdictional claims in published maps and institutional affiliations.





**Ettala O, Malaspina S, Tuokkola T, Luoto P, Löyttyniemi E,  
Boström PJ, Kemppainen J. (2020)  
Prospective study on the effect of short-term androgen deprivation  
therapy on PSMA uptake evaluated with <sup>68</sup>Ga-PSMA-11 PET/MRI in  
men with treatment-naïve prostate cancer.  
European Journal of Nuclear Medicine and Molecular Imaging**





# Prospective study on the effect of short-term androgen deprivation therapy on PSMA uptake evaluated with $^{68}\text{Ga}$ -PSMA-11 PET/MRI in men with treatment-naïve prostate cancer

Otto Ettala<sup>1</sup> · Simona Malaspina<sup>2,3</sup> · Terhi Tuokkola<sup>3</sup> · Pauliina Luoto<sup>3</sup> · Eliisa Löyttyniemi<sup>4</sup> · Peter J. Boström<sup>1</sup> · Jukka Kempainen<sup>2,3</sup>

Received: 22 June 2019 / Accepted: 22 November 2019 / Published online: 26 December 2019  
© The Author(s) 2019

## Abstract

**Purpose** Based on in vitro studies, it is known that androgen deprivation therapy (ADT) increases prostate-specific membrane antigen (PSMA) expression. Therefore, we hypothesised that ADT improves the performance of PSMA-PET imaging in primary staging of prostate cancer. The purpose of the study was to demonstrate the time course effect of ADT on PSMA uptake in different types of metastatic lesions evaluated with  $^{68}\text{Ga}$ -PSMA-11 PET/MRI.

**Methods** Nine men with treatment-naïve prostate cancer were enrolled to a prospective, registered (NCT03313726) clinical trial. A  $^{68}\text{Ga}$ -PSMA-11 PET/MRI was performed once before and 3 times post-ADT (degarelix, Firmagon). Change of maximum standardised uptake values (SUVmax) in prostate, lymph nodes, bone metastases, and physiologically PSMA-avid organs were evaluated in a time frame of 1–8 weeks.

**Results** All patients reached castration levels within 10 days, and 50% decrease in prostate-specific antigen (PSA) concentration was observed 14 days post-ADT. A heterogeneous increase in PSMA uptake was observed 3 to 4 weeks post-ADT. This phenomenon was definitively more evident in bone metastases: 13 (57%) of the metastasis, with a mean (range) SUVmax increase of 77% (8–238%). In one patient, already having bone metastases at baseline, three new bone metastases were observed post-ADT. Of lesions with reduced SUVmax, none disappeared.

**Conclusions** Both in patient and region level, increase in PSMA uptake post-ADT is heterogenous and is seen most evidently in bone metastases. Preliminary results on a small cohort of patients suggest the clinical impact of ADT on improving the performance of  $^{68}\text{Ga}$ -PSMA PET in staging seems to be minor. However, the optimal imaging time point might be 3 to 4 weeks post-ADT. Since none of the metastases with decreasing SUVmax disappeared, it seems that short-term usage of ADT does not interfere with the interpretation of  $^{68}\text{Ga}$ -PSMA PET.

**Trial registration** NCT03313726, registered 18 October 2017; EUDRA-CT, 2017-002345-29.

**Keywords** Prostate cancer · PSMA · PET · androgen deprivation therapy · ADT

## Introduction

Currently, small-molecule imaging with gallium- or fluoride-labelled prostate-specific membrane antigen ( $^{68}\text{Ga}/^{18}\text{F}$ -

PSMA) has been rapidly taken into clinical use in many European countries [1–3], although its utility in primary staging of prostate cancer still needs further validation [4–6]. At present, according to the majority of published data, the main indication of  $^{68}\text{Ga}$ -PSMA PET imaging is re-staging in presence of biochemical recurrence, especially at low prostate-specific antigen (PSA) values [7]. However, in recent years, there has been also a growing evidence on the promising role of  $^{68}\text{Ga}$ -PSMA PET imaging in nodal and distant staging in patients with high-risk disease [8].

Based on in vitro studies and animal models, it is known that administration of androgen deprivation therapy (ADT) increases PSMA expression [9, 10]. Although this notion

Otto Ettala and Simona Malaspina contributed equally to this work.

**Electronic supplementary material** The online version of this article (<https://doi.org/10.1007/s00259-019-04635-7>) contains supplementary material, which is available to authorized users.

✉ Otto Ettala  
otto.ettala@tyks.fi

Extended author information available on the last page of the article

was primarily published more than 20 years ago [9], first clinical case report was published only 2 years ago. Hope et al. demonstrated a 7-fold increase in maximum standardised uptake value (SUV<sub>max</sub>) of PSMA uptake after the initiation of ADT [10]. However, in two recent series, the effect of ADT on PSMA-PET findings was deemed as heterogeneous [11, 12]. However, in both of these series, all the metastases were analysed as whole and no region-based analysis was performed. In addition, no data is present if increase is also seen in physiologically avid organs. According to previous published data, we hypothesised that ADT might improve the performance of PSMA-PET imaging in primary staging of prostate cancer. In addition, the hypothesis was that different regions of prostate cancer (primary tumour in prostate and metastases in lymph nodes, bone, viscera) and physiologically avid organs as well (salivary glands, kidneys, liver, and spleen) respond differently to ADT.

The purpose of the current study is to demonstrate in patient and region-based analysis of the time course effect of ADT on PSMA uptake observed in repeated <sup>68</sup>Ga-PSMA-11 PET/MRI scans in men with newly diagnosed, treatment-naïve prostate cancer patients.

## Materials and methods

### Study population and design

In this prospective, registered (NCT03313726) clinical trial, men with newly diagnosed, treatment-naïve, high-risk prostate cancer with high risk for metastases were enrolled. In seven patients, 12-core TRUS-guided biopsies were performed, while in two patients suffering from urinary retention, the diagnosis was made from specimens obtained from transurethral resection of the prostate (TURP). The inclusion criteria were (1) histologically confirmed adenocarcinoma of the prostate and (2) no previous surgical, radiation, or endocrine treatment of the prostate cancer. Exclusion criteria were (1) presence of uncontrolled serious infection and (2) contraindications for MRI imaging. Also, since 5- $\alpha$ -reductase inhibitors, namely finasterid and dutasterid, affect the steroid pathway and possibly the PSMA uptake, men with prior usage of 5- $\alpha$ -reductase inhibitor medication in the past 12 months were excluded.

A <sup>68</sup>Ga-PSMA-11 PET/MRI was performed before and 3 times after the subcutaneous administration of ADT (degarelix). The post-ADT PSMA-PET/MRI scans were performed at a mean (range) of 1.5 (0.8–2.5) weeks, 2.9 (1.9–4.5) weeks, and 6.2 (3.5–8.7), respectively.

PSA and testosterone blood samples were collected before every scan. After the study, all patients were treated based on current institutional guidelines.

### Ethical issues

The study was conducted in compliance with the current revision of Declaration of Helsinki guiding physicians and medical research involving human subjects (64th World Medical Association General Assembly, Fortaleza, Brazil, 2013). All patients signed a written informed consent, and the study received the approval of Finnish Medicines Agency (FIMEA; EUDRA-CT, 2017-002345-29) and the Ethical Committee of the Hospital District of Southwest Finland.

### PSMA-PET/MRI imaging protocol

PSMA-PET/MRI scans were performed using a sequential Philips Ingenuity time-of-flight (TF) PET/MR scanner (Philips Healthcare, Cleveland, OH). All patient received an intravenous injection of <sup>68</sup>Ga-PSMA-11 (mean  $\pm$  SD administered activity, 153  $\pm$  10 MBq). After 20 min from radiotracer injection, MRI scanning protocol started with T2-weighted turbo-spin-eco sequences in transaxial, coronal, and sagittal direction, and diffusion-weighted sequence using a dedicated external coil for the lower abdomen (SENSE-TORSOXL). Subsequently, whole-body T2-weighted and an MRI-based attenuation correction sequence were obtained. PET whole-body acquisition from the orbital region to the mid-thighs (approximately 10 table positions, 4 min/table) started 64  $\pm$  3 min (mean  $\pm$  SD) from radiotracer injection. PET imaging reconstructions were performed using the default reconstruction algorithm “Blob-OS-TF”, a 3D ordered subset iterative TOF reconstruction technique. The reconstruction used 3 iterations and 33 subsets in 144  $\times$  144 matrix with an isotropic voxel size of 4 mm. All reconstructions included the necessary corrections for image quantification: attenuation, random, scatter, dead-time, decay, and detector normalisation.

### Image analysis

Image analysis was performed using an AW 4.5 workstation by General Electrics (GE) Healthcare. Two experienced nuclear medicine physicians analysed the images blinded for the results of the other reader but unblinded for other imaging modalities and clinical data available. In case of equivocal findings, a consensus between the two readers was reached in a multidisciplinary board meeting.

Volumes of interest (VOIs) were drawn on PSMA positive prostate lesions, lymph nodes, and bone metastases. Similar VOIs were drawn in salivary glands (parotid, submandibular, and sublingual), liver, spleen, and kidneys (avoiding the renal pelvis). PSMA uptake was measured using the standardised uptake value maximum (SUV<sub>max</sub>) values and  $\Delta$ SUV<sub>max</sub> at different time points was calculated compared to the pre-ADT scan.

**Table 1** Patient characteristics. *PSA*, prostate-specific antigen; *S-Testo*, serum testosterone; *cT*, clinical T stage; *cN*, clinical N stage; *cM*, clinical M stage according to PSMA-PET

	Age (years)	PSA (µg/l)	S-Testo (nmol/L)	Gleason score	cT	cN	cM
Patient 1	64	21	26	4 + 5	2c	1	1
Patient 2	69	25	13	4 + 5	3a	0	0
Patient 3	69	7	19	5 + 5	3a	0	0
Patient 4	77	7	7	4 + 5	1b	1	1
Patient 5	66	280	10	4 + 5	2a	0	1
Patient 6	71	52	9	5 + 4	3a	1	1
Patient 7	78	54	23	5 + 4	4	1	0
Patient 8	70	26	18	5 + 4	1b	1	1
Patient 9	70	9	12	5 + 3	2a	0	0

Findings on PSMA-PET scans were interpreted according to the current suggested procedure guideline on <sup>68</sup>Ga-PSMA PET imaging, taking into consideration normal biodistribution of the tracer and possible pitfalls [13]. PSMA-positivity was defined as a focal tracer uptake higher than adjacent background on prostate, suspicious bone, and lymph node lesions, without using a strict cut-off value of SUVmax to indicate or confirm malignancy. Moreover, any anatomical or functional correspondence on MRI imaging, such as altered signal on T2w and/or diffusion restriction on DWI or LN diameter and morphology, was also used in guiding the interpretation.

in two groups: “decrease”, lesions in which, when comparing to baseline, change in SUVmax was constantly negative in every time point; “increase”, all other lesions. In Table 3, the two groups were further analysed by evaluating the maximum increase and maximum decrease in SUVmax from each lesion by selecting a time point at which the highest or the lowest SUVmax occurred. At this specific time point, the change in SUVmax was described as mean proportion (range) and the time point as mean weeks (range). To evaluate inter-reader agreement, Cohen’s Kappa (95% CI) was calculated.

**Statistical methods**

In order to differentiate the effect of ADT in region level in Figs. 2 and 3, and Table 3, lesions were divided and analysed

**Results**

Nine patients were included in the study. Patients’ characteristics are shown in Table 1. At baseline, five had metastatic

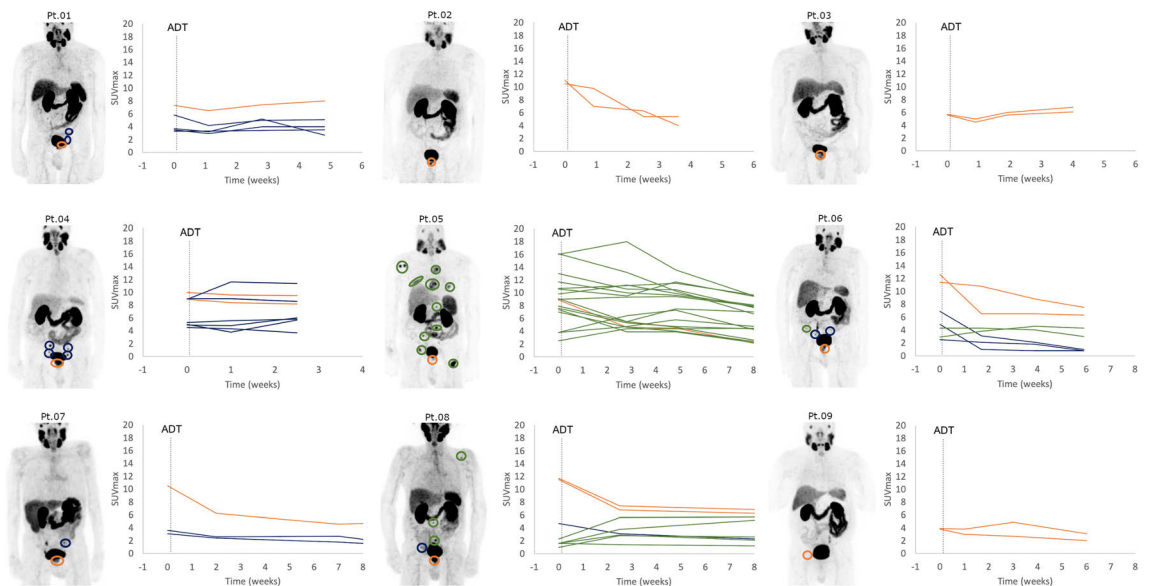


**Fig. 1** Patient-based changes in SUVmax after the administration of ADT (degarelix). Orange line, prostate lesions; blue line, lymph node metastases; green lines, bone metastases; dotted vertical line, initiation of androgen deprivation therapy (ADT)

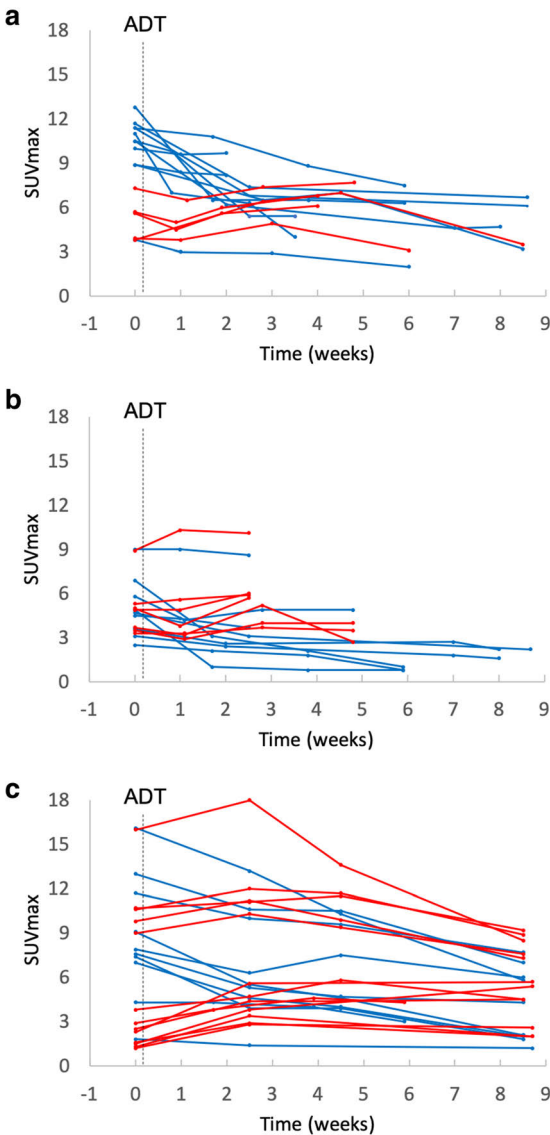


**Fig. 2** Lesion-based SUVmax trend in prostate lesions (a), lymph nodes (b), and bone metastases (c). Blue lines, lesions with decreasing SUVmax trend compared with baseline; red lines, lesions with increasing SUVmax trend compared with baseline; dotted vertical line, initiation of androgen deprivation therapy (ADT)

prostate cancer (other than regional lymph nodes and/or bone), while four patients presented with local or locally advanced disease. Visceral metastases were not present in any of the patients. All patients reached castration levels (serum testosterone < 1.7 nmol/L) within a period of 10 days after the initiation of ADT. Eight patients completed all the four PET/MRI scans, while one patient performed only three scans due to study withdrawal.

Patient-based observations are depicted in Fig. 1. In two patients (patients no. 2 and no. 7), no increase in SUVmax was observed, whereas in 7 (78%) patients, a heterogeneous change in PSMA uptake occurred. In patient no. 8, who had two bone metastases already at baseline, three new bone metastases were observed post-ADT.

A region-based analysis of the primary tumour in prostate, metastatic lesions, and the uptake pattern in physiologically avid organs is depicted in Figs. 2 and 3, and in Table 2. Also, the specific locations of the metastases are presented in Table 3. All the lesions in baseline and in follow-up, except for a discordance in two parailiac lymph node metastases, were detected by the two readers, Cohen's Kappa 0.89 (95% CI, 0.79–0.99). After a consensus reading, in total, 16 prostate, 16 lymph node, and 23 bone lesions were detected and analysed.

There was a marked increase in SUVmax (maximum increase in SUVmax of 76%) in more than half of the bone metastasis and a less pronounced and not so frequent increase in lesions in prostate (29%), and lymph nodes (19%). The increase was observed within the first 3 to 4 weeks post-ADT. In all lesions, which were considered “decrease”, the maximum SUVmax decrease was 50% or less. Despite the decrease, none of the lesions disappeared during the follow-up.

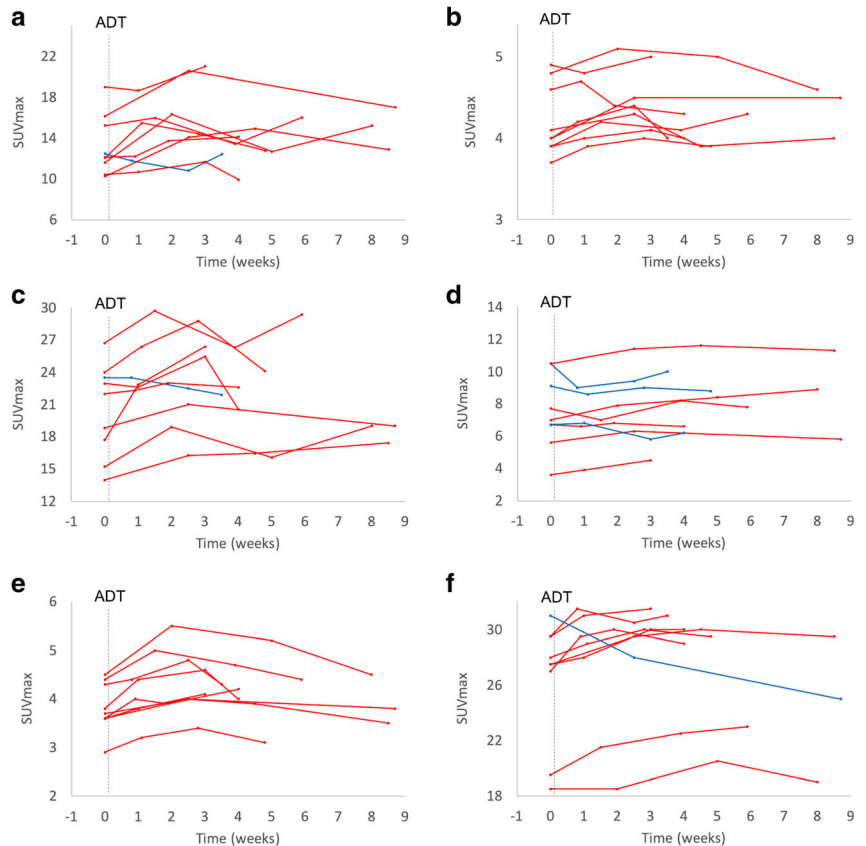
The most pronounced increase in physiologically avid organs was observed in parotid glands (23%), and submandibular glands (22%). In other physiologically avid organs, the increase was less than 20%. The decrease was seen very seldom or not at all, and the mean decrease was less than 20% (Fig. 4).

## Discussion

In this prospective registered study, a heterogeneous increase of PSMA uptake was observed after ADT in treatment-naïve prostate cancer patients in repeated  $^{68}\text{Ga}$ -PSMA PET/MRI scans. The most evident increase in SUVmax was observed 3 to 4 weeks post-ADT especially in bone metastasis. In one patient, with bone metastases already at baseline, three new bone metastases, which were already visible anatomically on MRI images, were observed. Of those lesions with decreasing SUVmax, none disappeared.

It has already been demonstrated that in both androgen-sensitive and androgen-resistant human prostate adenocarcinoma cells (LNCaP), the expression of PSMA is upregulated post-ADT and downregulated in the presence of testosterone or DHT [14–16]. Although a case report published by Hope et al. corroborated these preclinical studies, demonstrating a 7-fold increase in PSMA SUVmax values after the initiation of ADT, our results are in line with the two very recently published studies [10–12]. Aggarwal et al. performed a study in

**Fig. 3** SUVmax trend in parotid glands (a), liver (b), submandibular glands (c), spleen (d), sublingual glands (e), and kidneys (f) after initiation of ADT (degarelix): blue lines, lesions with decreasing SUVmax; red lines, lesions with increasing SUVmax trend compared with baseline; dotted vertical line, initiation of androgen deprivation therapy (ADT)



eight patients, scanned with <sup>68</sup>Ga-PSMA-11 PET before and after the initiation of ADT within a variable period of 2–4 weeks. The study demonstrated a heterogeneous increase in SUVmax, in 68% and in 41% of lesions in castration-

sensitive men (*n* = 4) and in castration-resistant men (*n* = 4), respectively. The other study, conducted by Emmet et al., studied also both castration-sensitive (*n* = 8) and castration-resistant men (*n* = 7). Although they showed that the increase was more evidently seen in castration-resistant men, in the light of our data and the study by Aggarwal, it seems that the increase occurs also in castration-sensitive men. In fact, in the study by Emmet et al., of those eight men with castration-sensitive disease, half of them had Gleason score 7 prostate cancer. It might well be that the increase is more evidently seen in poorly differentiated tumours. Also, our study clearly demonstrates the biological difference between testosterone flare and PSMA flare. Since degarelix directly inhibits the action of GnRH, no PSA flare occurs, and serum testosterone decreases rapidly. Despite the rapid decrease in testosterone levels, the increase in PSMA uptake was still observed.

ADT is the gold standard treatment in patients with metastatic prostate cancer. The effect of continuous long-term ADT on reducing the visibility of castration-sensitive prostate cancer lesions on PSMA-PET has already been investigated; however, it is still uncertain if initiation of ADT could interfere

**Table 2** Location of metastases

Lymph nodes	<i>n</i> (%)
Parailiacal	13 (33)
Mesorectal	1 (3)
Para-aortic	2 (5)
Bone	<i>n</i> (%)
Humerus	1 (3)
Sternum	2 (5)
Scapula	1 (3)
Ribs	2 (5)
Cervical vertebra	1 (3)
Thoracic vertebra	3 (7)
Lumbar vertebra	4 (10)
Iliac bone	7 (17)
Sacrum	1 (3)
Femur	1 (3)

**Table 3** Maximum increase and maximum decrease of maximum standardised uptake values. (SUVmax) in prostate, lymph node, bone lesions, and normal PSMA-avid organs. SUVmax is presented in proportional change and the time point at which the maximum SUVmax occurred is presented in weeks. Paired organs are analysed as a mean of right and left

Lesion/normal organ	Maximum increase			Maximum decrease		
	<i>n</i>	SUVmax (%); mean (range)	Time point (weeks); mean (range)	<i>n</i>	SUVmax (%); mean (range)	Time point (weeks); mean (range)
Primary tumour (prostate)	5	29 (6–84)	4.3 (3.0–4.8)	11	–46 (–64(–4))	5.8 (1.0–8.6)
Lymph node metastases	7	19 (11–41)	2.7 (1.0–4.8)	9	–48 (–86(–4))	5.2 (1.1–8.7)
Bone lesions	13	76 (8–238)	4.3 (2.5–8.7)	10	–50 (–77(–20))	7.7 (2.5–8.7)
Parotid glands	8	23 (5–45)	3.3 (1.1–5.9)	1	–8	3.5
Submandibular glands	8	22 (5–49)	4.1 (1.7–8.5)	1	–14	2.5
Sublingual glands	9	15 (8–22)	2.7 (1.7–4.0)	–	–	–
Liver	9	7 (2–13)	2.8 (0.9–5.9)	–	–	–
Spleen	6	16 (2–36)	4.0 (1.9–8.0)	3	–19 (–6(–14))	1.6 (0.8–3.0)
Kidneys	8	10 (7–18)	3.6 (0.8.7.0)	1	–19	8.7

with the staging results [17]. According to our preliminary findings, as none of the lesions disappeared during the observational period, ongoing short-term ADT does not represent a

contraindication on performing a staging PSMA-PET. Although ADT did not significantly increase PSMA-PET staging performance as only in one patient new metastases

**Fig. 4** T2W-MRI (a), PET (b), and fused PET/MRI (c) images of patient no. 8 at baseline and 2.5 weeks after ADT (degarelix). A new bone metastasis in L2 vertebra was detected. The lesion was already visible at baseline T2W-MRI images but PSMA uptake occurred 2.5 weeks after the initiation of ADT





were found, PSMA activity in the majority metastatic lesion reached the highest uptake 3 to 4 weeks post-ADT. Therefore, this time window might improve the detection rate, providing better lesion to background ratio. This aspect might be interesting especially in an oligometastatic disease, where bone metastases detected could then be selectively treated with radiotherapy. However, further studies are warranted to investigate the possible clinical impact of the phenomenon.

Since this is the first study where changes in PSMA SUVmax values were analysed on a region-based analysis, the fact that we observed the increase most evidently in bone metastasis is also interesting. This notion is supported also by two case reports demonstrating a similar increase of PSMA uptake in bone metastasis [18, 19]. Although the biology of the phenomenon is not known, authors hypothesised that increase of PSMA uptake in bone might be caused by osteoblastic turn over or bone reparation processes. However, most probably, this is not the case, since we observed the increase also in lymph nodes, in primary tumours, and in some of the physiologically avid organs suggesting a more general rather than organ-specific mechanism. This is, in fact, the first study to report that changes in PSMA-PET findings post-ADT are not restricted only to tumour tissue.

One might also question whether this flare phenomenon is dependent on the different mechanisms of action of ADT treatments. However, our results with GnRH antagonist therapy are similar with previous studies, in which LhRH agonist, antiandrogens, or new androgen signalling pathway modulators were administered [10–12, 16]. Given these facts, it seems rather evident that PSMA is connected to the androgen pathway [10–12, 16]. More recently, also mTOR pathway with mTOR inhibitor, rapamycin has shown to be linked to increase in PSMA uptake [16, 20]. Taken this all together, one might hypothesise that the observed effects of ADT on PSMA uptake in lesion level depict the androgen sensitivity of the specific lesions and also potentially the heterogeneity in aggressiveness of the lesions. Therefore, could it be possible to select those lesions that are prone to progress or are insensitive to ADT and selectively treat only those lesions? To understand this phenomenon, further studies with larger number of patients and longer follow-up are warranted.

Moreover, understanding what lies behind this phenomenon might raise a great interest from a theragnostic perspective. A preclinical study on a mouse model of castration-resistant prostate cancer (CRPC) demonstrated that pre-treatment with enzalutamide for 21 days followed by  $^{177}\text{Lu}$ -PSMA radioligand therapy (RLT) resulted in a significantly enhanced RLT-induced DNA-damage. However, pre-treatment with androgen receptor blockade did not show any additive effect on tumour growth reduction, suggesting that ADT might not necessarily guarantee an increased efficacy of

RLT [21]. Nevertheless, considering the heterogeneity of PSMA expression and the lack of clinical studies about this specific theragnostic aspect, the possible synergistic effect of ADT + RLT still needs to be defined.

Moreover, although  $^{177}\text{Lu}$ -PSMA radionuclide therapy is at the present moment used in castration-resistant prostate cancer patients, there are ongoing clinical trials to study its use also in castration-sensitive patients [22]. If proven to be effective in castration-sensitive men, according to our data, it would be reasonable to hypothesise that the timing between administration of ADT and of  $^{177}\text{Lu}$ -PSMA radionuclide therapy is crucial. ADT could increase the tumour targeting and therefore increase the efficacy of  $^{177}\text{Lu}$ -PSMA treatment during the time window of maximum PSMA uptake.

Also, our finding of increased PSMA uptake in normal salivary glands post-ADT needs to be taken into account as a possible increased therapy-related risk factor for significant xerostomia in patient candidates for  $^{177}\text{Lu}$ -PSMA therapy.

The study has some limitations. First, the cohort is small and underpowered to infer firm conclusions. In addition, there is variability in time intervals of the scans between the different patients. Therefore, the results should be considered preliminary and the study as a proof of concept. However, all the patients were thoroughly examined, and eight of the nine patients completed the study by undergoing four sequential PSMA-PET/MRI scans. In addition, the strength of the study is its truly prospective and registered nature. Second, the cohort is heterogenous. However, this can also be seen as an advantage since with this cohort, we are able to demonstrate that, although the increase is minor, PSMA flare is not merely seen in metastatic patients.

## Conclusions

Both in patient and region level, a heterogeneous increase of PSMA uptake was observed post-ADT, observed most evidently in bone metastases. The highest response on PSMA uptake was observed 3 to 4 weeks after ADT. Although the impact of ADT on  $^{68}\text{Ga}$ -PSMA PET staging performance was minor in this small patient cohort, more research is needed to investigate whether ADT could significantly improve detection rate and have clinical impact in patients with oligometastatic disease. Moreover, results were encouraging that short-term usage of ADT does not seem to represent a contraindication to perform  $^{68}\text{Ga}$ -PSMA PET for staging purpose, since none of the lesions disappeared.

**Funding information** Open access funding provided by University of Turku (UTU) including Turku University Central Hospital. This study was funded by academic grants from Finnish Cancer Society and Hospital District of Southwest Finland.

## Compliance with ethical standards

**Conflict of interest** The authors declare that they have no conflict of interest.

**Ethical approval** All procedures performed in studies involving human participants were in accordance with the ethical standards of the institutional and/or national research committee and with the 1964 Helsinki declaration and its later amendments or comparable ethical standards.

**Informed consent** Informed consent was obtained from all individual participants included in the study.


**Open Access** This article is licensed under a Creative Commons Attribution 4.0 International License, which permits use, sharing, adaptation, distribution and reproduction in any medium or format, as long as you give appropriate credit to the original author(s) and the source, provide a link to the Creative Commons licence, and indicate if changes were made. The images or other third party material in this article are included in the article's Creative Commons licence, unless indicated otherwise in a credit line to the material. If material is not included in the article's Creative Commons licence and your intended use is not permitted by statutory regulation or exceeds the permitted use, you will need to obtain permission directly from the copyright holder. To view a copy of this licence, visit <http://creativecommons.org/licenses/by/4.0/>.

## References

- Afshar-Oromieh A, Malcher A, Eder M, et al. PET imaging with a [68Ga]gallium-labelled PSMA ligand for the diagnosis of prostate cancer: biodistribution in humans and first evaluation of tumour lesions. *Eur J Nucl Med Mol Imaging*. 2013;40(4):486–95.
- Maurer T, Gschwend JE, Rauscher I, et al. Diagnostic efficacy of (68)gallium-PSMA positron emission tomography compared to conventional imaging for lymph node staging of 130 consecutive patients with intermediate to high risk prostate cancer. *J Urol*. 2016;195:1436–43.
- Bailey J, Piert M. Performance of 68Ga-PSMA PET/CT for prostate cancer management at initial staging and time of biochemical recurrence. *Curr Urol Rep*. 2017;18(11):84.
- Hofman MS, Hicks RJ, Maurer T, Eiber M. Prostate-specific membrane antigen PET: clinical utility in prostate cancer, normal patterns, pearls, and pitfalls. *Radiographics*. 2018;38(1):200–17.
- Von Eyben FE, Picchio M, von Eyben R, et al. 68Ga-labeled prostate-specific membrane antigen ligand positron emission tomography/computed tomography for prostate cancer: a systematic review and meta-analysis. *Eur Urol Focus*. 2018;4(5):686–93.
- Fanti S, Minozzi S, Antoch G, et al. Consensus on molecular imaging and theranostics in prostate cancer. *Lancet Oncol*. 2018;19(12):e696–708.
- Perera M, Papa N, Christidis, et al. Sensitivity, specificity and predictors of positive <sup>68</sup>Ga-prostate specific membrane antigen positron emission tomography in advanced prostate cancer: a systematic review and meta-analysis. *Eur Urol*. 2016;70(6):926–37.
- Corfield J, Perera M, Bolton D, et al. <sup>68</sup>Ga-prostate specific membrane antigen (PSMA) positron emission tomography (PET) for primary staging of high-risk prostate cancer: a systematic review. *World J Urol*. 2018;36(4):519–27.
- Wright GL Jr, Grob BM, Haley C, et al. Upregulation of prostate-specific membrane antigen after androgen-deprivation therapy. *Urology*. 1996;48(2):326–34.
- Hope TA, Truillet C, Ehman EC, et al. 68Ga-PSMA-11 PET imaging of response to androgen receptor inhibition: first human experience. *J Nucl Med*. 2017;58:81–4.
- Aggarwal R, Wei X, Kim W, et al. Heterogeneous flare in prostate-specific membrane antigen positron emission tomography tracer uptake with initiation of androgen pathway blockade in metastatic prostate cancer. *Eur Urol Oncol*. 2018;1(1):78–82.
- Emmett LM, Yin C, Crumbaker M, et al. Rapid modulation of PSMA expression by androgen deprivation: serial 68Ga PSMA-11 PET in men with hormone sensitive and castrate resistant prostate cancer commencing androgen blockade. *J Nucl Med*. 2019;60(7):950–4.
- Fendler WP, Eiber M, Beheshti M, et al. 68Ga-PSMA PET/CT joint EANM and SNMMI procedure guideline for prostate cancer imaging: version 1.0. *Eur J Nucl Med Mol Imaging*. 2017;44(6):1014–24.
- Bakht MK, Oh SW, Youn H, et al. Influence of androgen deprivation therapy on the uptake of PSMA-targeted agents: emerging opportunities and challenges. *Nucl Med Mol Imaging*. 2017;51:202–11.
- Meller B, Bremmer F, Sahlmann CO, et al. Alterations in androgen deprivation enhanced prostate-specific membrane antigen (PSMA) expression in prostate cancer cells as a target for diagnostics and therapy. *EJNMMI Res*. 2015;5:66.
- Kranzbühler B, Salemi S, Umbricht CA, et al. Pharmacological upregulation of prostate-specific membrane antigen (PSMA) expression in prostate cancer cells. *Prostate*. 2018;78(10):758–65.
- Afshar-Oromieh A, Debus N, Uhrig M, et al. Impact of long-term androgen deprivation therapy on PSMA ligand PET/CT in patients with castration-sensitive prostate cancer. *Eur J Nucl Med Mol Imaging*. 2018;45(12):2045–54.
- Zacho HD, Petersen LJ. Bone flare to androgen deprivation therapy in metastatic, hormone-sensitive prostate cancer on 68Ga-prostate-specific membrane antigen PET/CT. *Clin Nucl Med*. 2018;43(11):e404–6.
- Zukotynski KA, Valliant J, Bénard F, et al. Flare on serial prostate-specific membrane antigen-targeted 18F-DCFPyL PET/CT examinations in castration-resistant prostate cancer: first observations. *Clin Nucl Med*. 2018;43(3):213–6.
- Cinar B, De Benedetti A, Freeman MR. Post-transcriptional regulation of the androgen receptor by mammalian target of rapamycin. *Cancer Res*. 2005;65:2547–53.
- Lückerath K, Wei L, Fendler WP, et al. Preclinical evaluation of PSMA expression in response to androgen receptor blockade for theranostics in prostate cancer. *EJNMMI Res*. 2018;8(1):96.
- Privé B, Nagarajah J Lutetium-177-PSMA-617 in low volume metastatic prostate cancer. Available from: <https://clinicaltrials.gov/ct2/show/NCT03828838>. NLM identifier: NCT03828838. Accessed June 15, 2019.

**Publisher's note** Springer Nature remains neutral with regard to jurisdictional claims in published maps and institutional affiliations.

## Affiliations

Otto Ettala<sup>1</sup>  · Simona Malaspina<sup>2,3</sup> · Terhi Tuokkola<sup>3</sup> · Pauliina Luoto<sup>3</sup> · Eliisa Löyttyniemi<sup>4</sup> · Peter J. Boström<sup>1</sup> · Jukka Kemppainen<sup>2,3</sup>

<sup>1</sup> Department of Urology, University of Turku and Turku University Hospital, Turku, Finland

<sup>2</sup> Department of Clinical Physiology and Nuclear Medicine, University of Turku and Turku University Hospital, Turku, Finland

<sup>3</sup> Turku PET Centre, University of Turku and Turku University Hospital, Turku, Finland

<sup>4</sup> Department of Biostatistics, University of Turku, Turku, Finland



**Malaspina S, Ettala O, Tolvanen T, Rajander J, Eskola O, Boström PJ,  
Kemppainen J. (2023)**

**Flare on [<sup>18</sup>F]PSMA-1007 PET/CT after short-term androgen  
deprivation therapy and its correlation to FDG uptake: possible  
marker of tumor aggressiveness in treatment-naïve metastatic  
prostate cancer patients.**

European Journal of Nuclear Medicine and Molecular Imaging







# Flare on [<sup>18</sup>F]PSMA-1007 PET/CT after short-term androgen deprivation therapy and its correlation to FDG uptake: possible marker of tumor aggressiveness in treatment-naïve metastatic prostate cancer patients

Simona Malaspina<sup>1,2</sup> · Otto Ettala<sup>3</sup> · Tuula Tolvanen<sup>1,4</sup> · Johan Rajander<sup>5</sup> · Olli Eskola<sup>1</sup> · Peter. J. Boström<sup>3</sup> · Jukka Kempainen<sup>1,2</sup>

Received: 15 June 2022 / Accepted: 15 September 2022 / Published online: 26 September 2022  
© The Author(s) 2022

## Abstract

**Purpose** Short-term androgen deprivation therapy (ADT) is known to increase heterogeneously prostate-specific membrane antigen (PSMA) expression. This phenomenon might indicate the potential of cancer lesions to respond to ADT. In this prospective study, we evaluated the flare on [<sup>18</sup>F]PSMA-1007 PET/CT after ADT in metastatic prostate cancer (PCa). Given that aggressive PCa tends to display FDG uptake, we particularly investigated whether the changes in PSMA uptake might correlate with glucose metabolism.

**Methods** Twenty-five men with newly diagnosed treatment-naïve metastatic PCa were enrolled in this prospective registered clinical trial. All the patients underwent [<sup>18</sup>F]PSMA-1007 PET/CT immediately before and 3–4 weeks after ADT initiation (degarelix). Before ADT, [<sup>18</sup>F]FDG PET/CT was also performed. Standardized uptake values (SUV)max of primary and metastatic lesions were calculated in all PET scans. Serum PSA and testosterone blood samples were collected before the two PSMA PET scans. The changes in PSMA uptake after ADT were represented as  $\Delta$ SUVmax.

**Results** All the patients reached castration levels of testosterone at the time of the second [<sup>18</sup>F]PSMA-1007 PET/CT. Overall, 57 prostate, 314 lymph nodes (LN), and 406 bone lesions were analyzed. After ADT, 104 (26%) bone, 33 (11%) LN, and 6 (11%) prostate lesions showed an increase ( $\geq 20\%$ ) in PSMA uptake, with a median  $\Delta$ SUVmax of +50%, +60%, and +45%, respectively. Among the lesions detected at the baseline [<sup>18</sup>F]PSMA-1007 PET/CT, 63% bone and 46% LN were FDG-positive. In these metastases, a negative correlation was observed between the PSMA  $\Delta$ SUVmax and FDG SUVmax ( $p < 0.0001$ ). Moreover, a negative correlation between the  $\Delta$ SUVmax and the decrease in serum PSA after ADT was noted ( $p < 0.0001$ ).

**Conclusions** A heterogeneous increase in PSMA uptake after ADT was detected, most evidently in bone metastases. We observed a negative correlation between the PSMA flare and the intensity of glucose uptake as well as the decrease of serum PSA, suggesting that lesions presenting with such flare might potentially be less aggressive.

**Trial registration** NCT03876912, registered 15 March 2019.

**Keywords** Prostate cancer · PSMA · PET · [<sup>18</sup>F]PSMA-1007 PET/CT · ADT · Androgen deprivation therapy

This article is part of the Topical Collection on Oncology - Genitourinary.

✉ Simona Malaspina  
simona.malaspina@tyks.fi

<sup>1</sup> Turku PET Centre, University of Turku and Turku University Hospital, Turku, Finland

<sup>2</sup> Department of Clinical Physiology and Nuclear Medicine, University of Turku and Turku University Hospital, Turku, Finland

<sup>3</sup> Department of Urology, University of Turku and Turku University Hospital, Turku, Finland

<sup>4</sup> Department of Medical Physics and Turku PET Centre, University of Turku and Turku University Hospital, Turku, Finland

<sup>5</sup> Turku PET Centre, Accelerator Laboratory, Åbo Akademi University, Turku, Finland

## Introduction

Androgen deprivation therapy (ADT) by surgical castration or administration of luteinising-hormone-releasing-hormone (LHRH) analogues is considered the first-line treatment in metastatic hormone-sensitive prostate cancer (PCa) [1, 2]. Despite favorable response rates, the onset of castration-resistance (CRPC) in patients with metastases is typical and could occur even within 1–2 years from the initiation of ADT [3, 4].

Therefore, defining the extent of the disease and the best treatment approach in metastatic PCa is paramount, in order to delay its progression towards CRPC and, possibly, prolong patients' survival. Prostate-specific membrane antigen (PSMA) PET has gained increasing acceptance in the imaging of PCa, including its recent usage in primary staging setting [5–7]. PSMA is a type II membrane glycoprotein that is overexpressed in the prostate compared to other tissues, and its expression is tenfold higher in PCa cells compared to healthy prostate [8].

Preclinical studies on cell lines and animal models have demonstrated that short-term ADT upregulates the expression of PSMA in PCa cells in both hormone-sensitive and castration-resistant states [9, 10]. This phenomenon has been successively investigated in a few prospective clinical studies using PSMA PET imaging on PCa patients [11–13]. A heterogeneous increase in PSMA uptake, known as the PSMA flare, was observed in PCa lesions after short-term ADT, with considerable inter- and inpatient variability.

In our previous prospective clinical trial on a cohort of 9 treatment-naïve PCa patients, we demonstrated a heterogeneous increase in PSMA uptake after 3–4 weeks of ADT, most evidently seen in bone lesions, followed mainly by a decrease of the uptake at 6–8 weeks after the initiation of the treatment [13]. Based on these preliminary results, we hypothesized that lesions exhibiting the flare in PSMA uptake might have a distinctive potential to response to ADT. However, research on this phenomenon is still limited, and the underlying biology of the PSMA flare remains uncertain and needs further clarification. Moreover, there is no consensus on the interpretation and the possible clinical significance of the flare on PSMA PET imaging.

The current prospective clinical trial represents a continuation of our previous study [13], and its aim is to assess the PSMA flare phenomenon after short-term ADT in a larger cohort of treatment-naïve metastatic PCa patients. In particular, since aggressive PCa tends to display FDG uptake [14], we investigated whether the changes in PSMA uptake after ADT might correlate with glucose metabolism.

## Materials and methods

### Subjects and study design

Men with newly diagnosed treatment-naïve metastatic PCa were enrolled in this prospective registered clinical trial. The inclusion criteria were (1) histologically confirmed adenocarcinoma of the prostate without neuroendocrine differentiation, small cell, or ductal features; (2) absence of previous surgical, radiation, or hormonal treatment of PCa; and (3) clinical stage Tany Nany M1. The exclusion criteria included (1) presence of uncontrolled serious infection and (2) presence or history of malignances other than PCa.

The metastatic status of the patients was defined as a quantifiable number of metastases documented by standard-of-care imaging (CT and/or bone scintigraphy) performed within 2 weeks from enrolment. All the patients underwent [<sup>18</sup>F]PSMA-1007 PET/CT immediately before and 3–4 weeks after the subcutaneous administration of ADT (degarelix, 240 mg). This time point was chosen as the most suitable to assess the flare in PSMA uptake according to the results of our previous study [13]. Before the initiation of ADT, a [<sup>18</sup>F]FDG PET/CT scan was performed during the same week of the baseline [<sup>18</sup>F]PSMA-1007 PET/CT to evaluate the aggressiveness of the PSMA-positive lesions. In addition, serum PSA and testosterone blood samples were collected before the two [<sup>18</sup>F]PSMA-1007 PET/CT scans. The change in serum PSA levels between these two time points was defined as  $\Delta$ PSA.

### Imaging protocol

All PET/CT scans were carried out using a GE Discovery MI PET/CT scanner (GE Healthcare, Milwaukee, WI, USA). Fasting for 6 h was required before administration of [<sup>18</sup>F]FDG. The patients underwent whole-body PET/CT scans from mid-thigh to the vertex starting at 60 min and 50 min after receiving intravenous injection of [<sup>18</sup>F]PSMA-1007 and [<sup>18</sup>F]FDG, respectively. Low-dose CT scans were acquired for attenuation correction and anatomic correlation. The CT acquisition parameters were as follows: tube potential of 120 kV, tube current modulated between 10 and 120 mA, and noise index of 30. The PET scans were acquired in 3-dimensional mode with 2 min/bed positions. The sinogram data were corrected for deadtime, decay, and photon attenuation and, then, reconstructed on a 256 × 256 matrix. Image reconstruction utilized a Bayesian penalized-likelihood iterative reconstruction algorithm (QClear) with a  $\beta$  value of 500 for [<sup>18</sup>F]PSMA-1007 and 350 for [<sup>18</sup>F]FDG, incorporating random and scatter corrections.



## Radiopharmaceutical preparation

The synthesis of [ $^{18}\text{F}$ ]PSMA-1007 and [ $^{18}\text{F}$ ]FDG solutions for injection was conducted on-site at the Radiopharmaceutical Chemistry Laboratory of Turku PET Centre. [ $^{18}\text{F}$ ]FDG was synthesized following an analogous procedure as described previously [15]. A FASTLab® synthesizer (GE Healthcare, Waukesha, WI, USA) and FDG-phosphate cassettes were used for the production. The radiochemical purity exceeded 98%. [ $^{18}\text{F}$ ]PSMA-1007 was synthesized with TRASIS AllInOne synthesizer (TRASIS Radiopharma, Ans, Belgium) using the single-use cassettes supplied by TRASIS and reagents supplied by ABX (ABX advanced biochemical compounds Gmb, Radeberg, Germany). The radiochemical purity exceeded 93%.

## Imaging analysis and interpretation

Image analysis was performed using an AW 4.5 workstation (General Electrics (GE) Healthcare). An experienced nuclear medicine physician (S.M.) reviewed all the PET scans.

The PSMA PET findings were reported according to the current suggested procedure guidelines, taking the normal biodistribution and the possible pitfalls of the tracers into consideration [16]. All the metastases documented on conventional imaging (CT and bone scintigraphy) that showed PSMA-uptake at the baseline [ $^{18}\text{F}$ ]PSMA-1007 PET/CT were included in the analysis. Moreover, lesions were considered malignant on PSMA PET imaging if the following criteria were met: [ $^{18}\text{F}$ ]PSMA-1007 focal uptake above the local background in the prostate for T-staging; [ $^{18}\text{F}$ ]PSMA-1007 uptake above the blood pool with corresponding CT finding (also normally sized lymph nodes) in a site typical for prostate cancer for N-staging; [ $^{18}\text{F}$ ]PSMA-1007 uptake above the blood pool with corresponding CT finding (e.g., sclerotic or lytic bone lesion) in a site typical for prostate cancer for M-staging.

All the PSMA-positive lesions were then carefully matched with [ $^{18}\text{F}$ ]FDG PET/CT. Lesions with tracer uptake above the blood pool were considered FDG-positive.

The standardized uptake value (SUV)max of the PSMA-avid lesions in the prostate and in PCa metastases was calculated. The changes in PSMA uptake after ADT were represented as  $\Delta\text{SUVmax}$ . The PSMA-positive lesions were then divided into two groups. The first group included all the lesions with a  $\Delta\text{SUVmax} \geq +20\%$  (PSMA flare) while the second group consisted of the remaining lesions exhibiting either a decrease or no change ( $<20\%$ ) of SUVmax. The FDG SUVmax was further divided into three categories:  $\leq$  blood pool (FDG-negative),  $>$  blood pool up to 10 (mild to moderate uptake), and  $> 10$  (strong uptake). All data were collected using a RedCap database [17].

## Statistical analysis

The descriptive data are presented as a median value, interquartile range (IQR), and range. Pearson's coefficient was used to assess the correlation between PSMA SUVmax and FDG SUVmax as well as the correlation between PSMA  $\Delta\text{SUVmax}$ , FDG SUVmax, and  $\Delta\text{PSA}$ . Welch's analysis of variance (Anova) was used to compare PSMA  $\Delta\text{SUVmax}$  to different classes of FDG SUVmax.  $p$  values  $< 0.05$  were considered statistically significant. Statistical analysis was carried out using JMP® pro 16 software.

## Results

Twenty-five patients were prospectively enrolled in the study and completed all the three PET scans. The patients' characteristics are presented in Table 1. Their median age was 74 years old (IQR 70–78; range 63–84), and the median PSA before the initiation of ADT was 49 ng/ml (IQR 33–140; range 15–5000). The median time interval from the baseline [ $^{18}\text{F}$ ]PSMA-1007 PET/CT scan to the administration of ADT was 2 days (IQR 1–3; range 0–8). The median time interval between the baseline [ $^{18}\text{F}$ ]PSMA-1007 PET/CT and the [ $^{18}\text{F}$ ]FDG scan was 1 day (IQR 1–2; range 1–6). The second [ $^{18}\text{F}$ ]PSMA-1007 PET/CT scan was performed after a median of 27 days (IQR 21–30; range 20–33) from ADT initiation. The median administered activity of [ $^{18}\text{F}$ ]PSMA-1007 and [ $^{18}\text{F}$ ]FDG were 255 MBq (IQR 251–259; range 241–278) and 368 MBq (IQR 333–381; range 278–398), respectively. Scanning time after the radiotracer injection

**Table 1** Patients' demographics

Age	Median (IQR; range)
Years	74 (70–78; 63–84)
PSA at baseline ng/ml	Median (IQR; range) 49 (33–140; 15–5000)
S-testo at baseline nmol/L	Median (IQR; range) 12 (7–17; 2–27)
Biopsy GGG <sup>a</sup>	$n$ (%)
1	0 (0)
2	0 (0)
3	3 (12)
4	4 (16)
5	18 (72)
Clinical T-category	$n$ (%)
cT1	0 (0)
cT2	2 (8)
cT3	19 (76)
cT4	4 (16)

<sup>a</sup>Gleason grade group

was 60 min (median, IQR 59–60) for [ $^{18}\text{F}$ ]PSMA-1007 and 50 min (median, IQR 50–50) for [ $^{18}\text{F}$ ]FDG. All the patients reached castration levels (testo < 1.7 nmol/L) within the time of the second [ $^{18}\text{F}$ ]PSMA-1007 PET/CT scan. Serum PSA decreased in all the patients at 3–4 weeks after ADT, with a median decrease of 87% (IQR 81–92; range 32–99).

All the patients presented with strong PSMA uptake in the prostate gland at the baseline, 10 of whom presented uptakes that extended to the seminal vesicles. All the patients had PSMA-avid lymph node (LN) metastases in the pelvis, while 12 of them also had pathological uptakes in retroperitoneal and/or mediastinal LNs. Twenty-three patients presented with PSMA-positive bone lesions. Finally, two patients had PSMA-avid lung nodules. An overview of the positive lesions detected at the baseline [ $^{18}\text{F}$ ]PSMA-1007 PET/CT for each patient is depicted in Supplemental Fig. 1.

In all the men, an increase of PSMA uptake after ADT was observed in at least one bone and/or lymph node metastasis (Supplemental Fig. 2). In particular, except for one man, all patients with bone metastases ( $n=22$ ) exhibited flare of PSMA uptake in the bone at the second PSMA PET scan, despite significant inter-patient variability (Supplemental Fig. 2). A total of 57 prostate/seminal vesicle, 314 LN (250 regional and 64 extra-regional), 406 bone and 5 lung lesions that were positive on the baseline [ $^{18}\text{F}$ ]PSMA-1007 PET/CT were included in the analysis. The changes observed in the PSMA uptake after ADT at the lesion level are represented in Table 2. An increase in PSMA uptake was observed in 26% of the bone lesions, with a median  $\Delta\text{SUVmax}$  of +50% (IQR 32–72; range 20–161). This flare in PSMA uptake was more evident in the bone metastases compared to the LN or prostate, where 11% and 11% of the lesions showed a median PSMA increase ( $\Delta\text{SUVmax}$ ) of +60% (IQR 32–114; range 20–222) and +45% (IQR 20–106; range 23–134), respectively. The lung nodules did not show any flare in PSMA uptake. The remaining lesions showed either a decrease or no change in PSMA uptake (Table 2). No lesion became PSMA-negative (uptake below the blood pool) at the second PSMA PET scan.

At the baseline, among the PSMA-positive lesions, 27 (47%) prostate, 144 (46%) LN, 254 (63%) bone, and 3 (60%) lung lesions were positive on the [ $^{18}\text{F}$ ]FDG PET/CT. On comparing the intensity of baseline PSMA SUVmax and FDG SUVmax in the bone metastases, a positive correlation was observed ( $p < 0.001$ ) (Fig. 1). Moreover, the comparison of the changes in PSMA uptake after ADT ( $\Delta\text{SUVmax}$ ) and the FDG SUVmax showed a negative correlation ( $p < 0.001$ ), indicating that lesions presenting the PSMA flare had less intense FDG uptake (Fig. 2). Similar correlations were observed in the lymph nodes (Supplemental Figs. 3–4), while correlations in the prostate lesions were not significant (Supplemental Figs. 5–6). The comparison between PSMA  $\Delta\text{SUVmax}$  and FDG uptake, including the FDG-negative lesions (SUVmax < blood pool), is depicted in Fig. 3. A significant difference in the PSMA  $\Delta\text{SUVmax}$  was observed between the bone metastases with strong FDG uptake (SUVmax > 10) and those having either a moderate FDG uptake or uptake  $\leq$  blood pool ( $p < 0.001$ ). Similar results were observed in the lymph nodes, but not in the prostate lesions (Supplemental Figs. 7–8). The correlation between PSMA  $\Delta\text{SUVmax}$  and changes in serum PSA ( $\Delta\text{PSA}$ ) is depicted in Fig. 4. The results showed a negative correlation ( $p < 0.001$ ), indicating that the PSMA flare phenomenon was less evident in patients experiencing a rapid decrease in serum PSA (Fig. 4).

Ten patients with known bone lesions presented with new PSMA bone uptakes at the second [ $^{18}\text{F}$ ]PSMA-1007 PET/CT scan (median SUVmax 5; IQR 5–10; range 4–18). An example is illustrated in Fig. 5. None of these uptakes was positive on the [ $^{18}\text{F}$ ]FDG PET/CT scan.

## Discussion

In this prospective trial, we demonstrated that short-term ADT increased PSMA uptake in metastatic treatment-naïve hormone-sensitive PCa. This PSMA flare was observed in all the patients, most evidently in bone metastases. According

**Table 2** Changes in PSMA uptake after ADT

Lesion type	Lesions ( $n$ ) at baseline PSMA PET	Increase ( $\geq 20\%$ ) of PSMA uptake, $n$ (%)	$\Delta\text{SUVmax}\%$ , median (IQR; range)	No change/decrease ( $< 20\%$ ) of PSMA uptake, $n$ (%)	$\Delta\text{SUVmax}\%$ median (IQR; range)
Prostate	57	6 (11%)	+45% (20–106; 23–134)	49 (89%)	–28% (–45 to –7; –78 to 14)
Lymph nodes	314	33 (11%)	+60% (32–114; 20–222)	281 (89%)	–51% (–74 to –21; –99 to 9)
Bone	406	104 (26%)	+50% (32–72; 20–161)	302 (74%)	–33% (–53 to –15; –90 to 14)
Visceral (lung)	5	-	-	5 (100%)	–40% (–49 to –22; –53 to –16)

**Fig. 1** Correlation between baseline PSMA SUVmax and FDG SUVmax in bone lesions

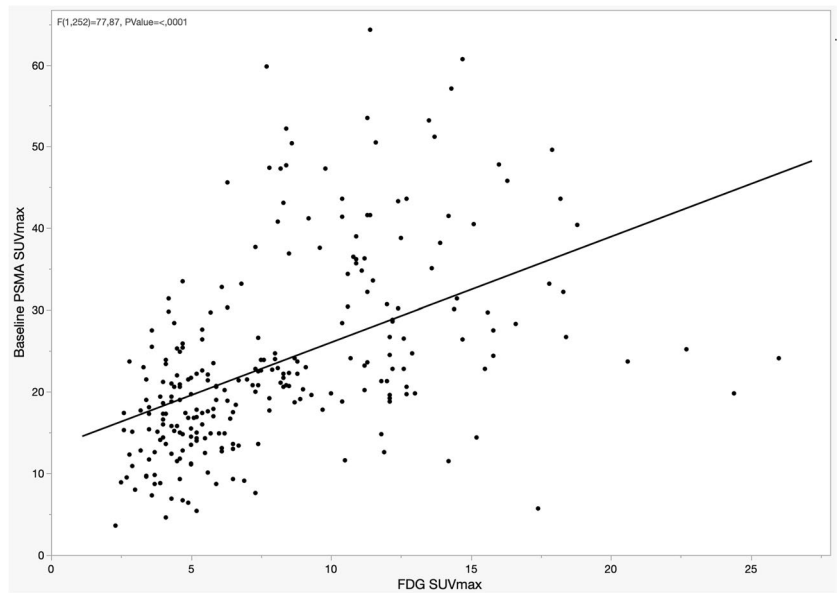
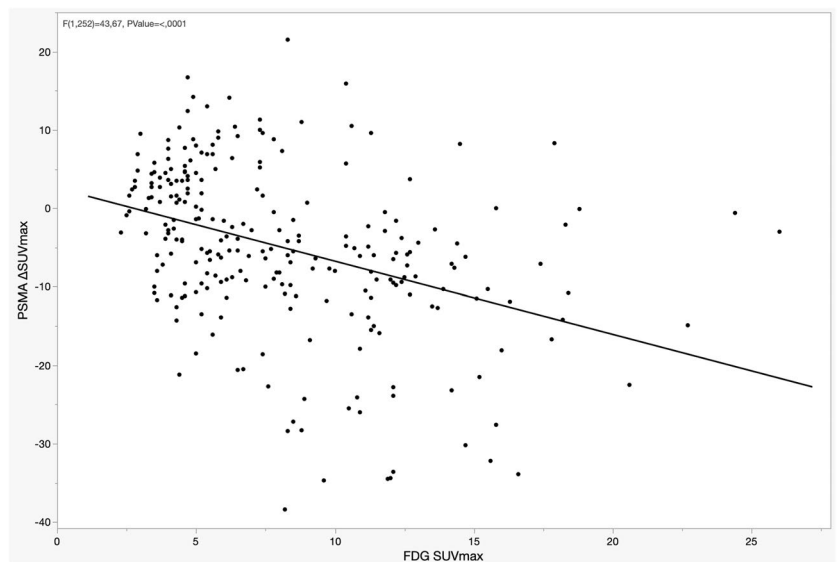


**Fig. 2** Correlation between PSMA ΔSUVmax and FDG SUVmax in bone lesions



to the negative correlation between FDG uptake and changes of PSMA uptake after ADT, the flare phenomenon seems to be linked to less aggressive behavior of the lesions.

The possible association between the flare in PSMA uptake and glucose metabolism had not been investigated so far. It is well known that FDG uptake and its intensity is associated with more aggressive PCa [14, 18, 19]. Given the metastatic status of our patient cohort, the presence

of FDG-positive lesions was expected. Interestingly, we observed a negative correlation between the flare in PSMA uptake and the intensity of FDG uptake in bone metastases and, to less extent, in lymph node metastases. This suggests that lesions presenting with the flare and milder FDG uptake might be less aggressive compared to lesions without the flare and with stronger FDG uptake. Therefore, this flare phenomenon might be able to identify more aggressive

**Fig. 3** Box plot for PSMA  $\Delta$ SUVmax according to FDG SUVmax in bone lesions

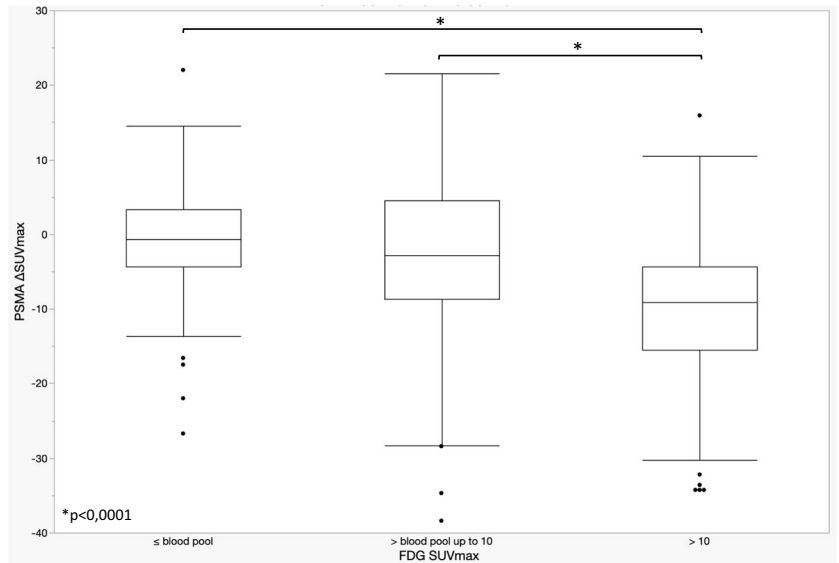
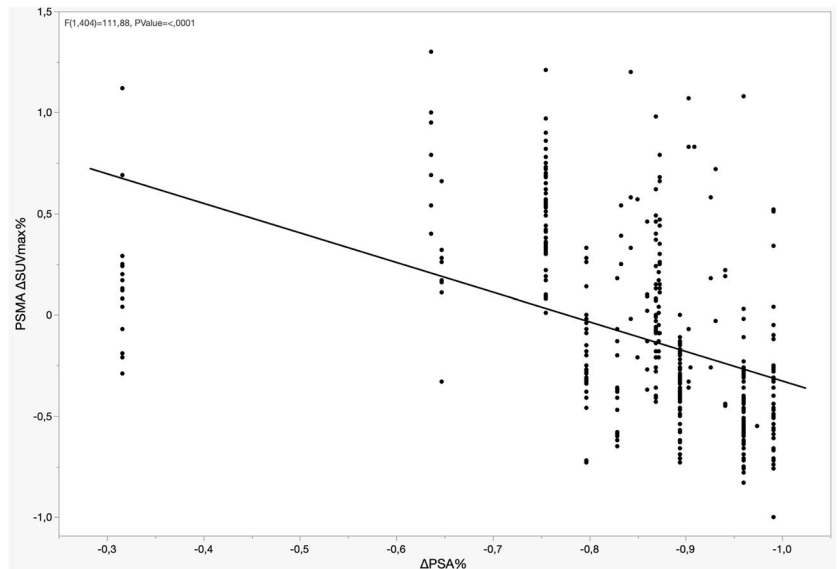


**Fig. 4** Correlation between PSMA  $\Delta$ SUVmax and  $\Delta$ PSA in bone lesions



metastases, and potentially predict the response to ADT and the progression to CRPC.

Bone flare is a phenomenon that has already been observed in bone scintigraphy as either an increase in metabolic activity or the presence of new lesions within few weeks to few months of oncological treatments in PCa as well as other malignances. This phenomenon has been considered as a sign of favorable response to treatment [20]. In our study, 22/23 patients with bone metastases presented

with flare of PSMA uptake after ADT in the bone. Moreover, ten of them exhibited new PSMA bone uptakes without anatomical correspondence at the second PSMA PET scan. Whether these new PSMA uptakes are true metastases or hormone-sensitive tissue reaction as part of the flare remains to be confirmed by longer follow-up. Nevertheless, these uptakes were negative also in the baseline FDG PET scan. This finding is consistent with our observation of the presence of PSMA flare in lesions with mild or no FDG-uptake,

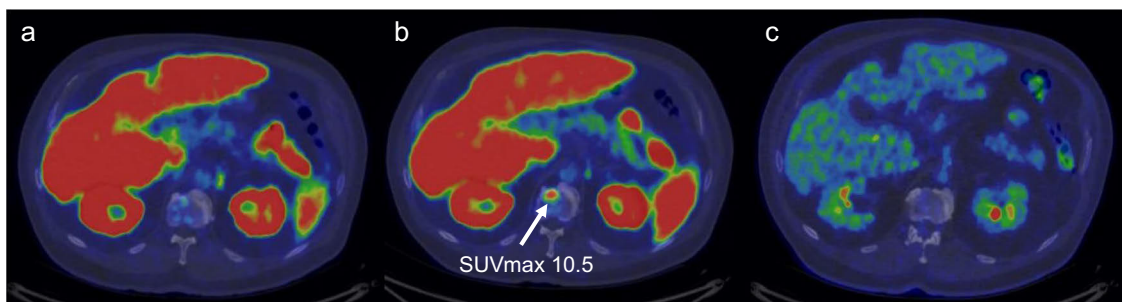


**Fig. 5** New PSMA bone uptake on L1 vertebra detected in the [ $^{18}\text{F}$ ] PSMA-1007 PET/CT after ADT. The uptake was not seen in the [ $^{18}\text{F}$ ]FDG PET/CT scan. **a** Baseline [ $^{18}\text{F}$ ] PSMA-1007 PET/CT. **b** [ $^{18}\text{F}$ ] PSMA-1007 PET/CT after ADT. **c** Baseline [ $^{18}\text{F}$ ]FDG PET/CT

suggesting a less aggressive behavior. In view of this, the PSMA flare might resemble the flare observed in bone scintigraphy. The possible pathogenesis of the flare in bone tissue might be caused by the healing processes of new bone formation after short-term treatment. In addition, an immune response, specifically a T-cell reaction accompanied by the release of pro-inflammatory cytokines might possibly be involved in the flare phenomenon [20].

However, we demonstrated that the phenomenon is not bone-specific, as the increase in PSMA uptake was also observed in the lymph nodes and prostate lesions. It is possible that a similar immune response might be occurring in those tissues as well. Nevertheless, it is unlikely that this would be the only mechanism involved in the increase in PSMA uptake. A recent study on genomically characterized patient-derived xenografts (PDX) observed increases in PSMA and androgen receptor (AR) mRNA as well as tumor microdensity after ADT in castration-sensitive models [21]. Moreover, this study observed that the model exhibiting increased PSMA and AR mRNA had an intact PTEN gene, while the model with PTEN loss exhibited repressed AR transcriptional signaling. Given that the loss of PTEN gene is usually associated with more aggressive disease, these findings might corroborate our hypothesis of the PSMA flare as a marker of less aggressive disease. In view of this, understanding the possible molecular mechanisms and genetic phenotypes that modulate the heterogeneous PSMA responses to ADT might help to better understand the flare phenomenon.

The possible clinical significance of the PSMA flare still requires further clarification. Given the heterogeneity of the phenomenon, increase in the diagnostic performances is most likely limited, as no changes in staging were observed in our cohort of patients. On the other hand, identifying patients at risk of rapid progression would allow the implementation of appropriate follow-up strategies or further therapies. In particular, knowing that certain metastases are potentially more prone to progress might help in selectively treat those with stereotactic radiotherapy. However, this might not always be feasible in

high-volume disease. Moreover, the impact of targeted radiotherapy of metastatic lesions on patient outcome is still under debate. Another aspect to consider is whether the PSMA flare might have an impact on the planning of radionuclide therapies. A recent prospective pilot study demonstrated the safety and the feasibility of [ $^{177}\text{Lu}$ ]PSMA treatment in hormone-sensitive metastatic PCa [22]. In this scenario, hormone-sensitive patients who exhibit more evident PSMA flare after ADT could have increased binding sites for radionuclide therapy. Further prospective trials are needed to confirm whether ADT-related PSMA flare could improve the outcome of [ $^{177}\text{Lu}$ ]PSMA therapy.

In this study, FDG PET has been used to select potentially aggressive PCa lesions and, through that, to investigate the possible correlation between FDG uptake and the PSMA flare phenomenon. Based on the results of our study, we would not recommend the use of FDG PET in the clinical practice for primary staging of PCa. However, it would be scientifically interesting to observe whether FDG-positivity could have a predictive value in the development of castration resistance. Moreover, as we hypothesize about the PSMA-flare, FDG-positivity could also have a potential role in selecting aggressive lesions for metastases-targeted therapies. Longer follow-up will hopefully give insight into these aspects.

We observed that the decrease in serum PSA is correlated negatively with the presence of the PSMA flare; in other words, PSA decreased more rapidly in patients whose majority of lesions did not present with the PSMA flare. Serum PSA and several other PSA-related parameters, such as PSA at diagnosis, PSA nadir, time to nadir, and percentage of decrease, have been widely accepted as prognostic factors to predict response to therapy [23, 24]. One might expect that a rapid decrease in serum PSA after ADT would be the result of rapid PCa cell death and therefore would predict better response to therapy [23, 25]. However, interestingly, some studies have observed that a slower decrease in serum PSA, particularly meaning a longer time to nadir, is associated with better response and longer survival [26–29]. The mechanisms responsible for the association between a rapid decline in PSA

and a worsening prognosis are still not clear. One explanation might be that the rapid fall of PSA is related to a transcriptional effect on PSA production rather than cell death. Another possibility is that a rapid removal of hormone-sensitive cells can initiate the growth of castration-resistant cells [27, 28]. Our results seem to be consistent with this concept, since the serum PSA decreased more rapidly in patients with potentially more aggressive lesions. If proven right, this might corroborate the hypothesis of the PSMA flare as a favorable prognostic factor. However, the follow-up time for serum PSA in our cohort is too short to draw conclusions and longer follow-up is needed to confirm this hypothesis.

Our results regarding the PSMA flare in hormone-sensitive patients are consistent with the previous prospective studies that investigated the effect of short-term ADT on PSMA uptake [10, 11, 13]. Emmet et al. reported a reduction of PSMA uptake after short-term ADT in 8 hormone-sensitive PCa patients, according to a patient-based analysis and a single median SUV<sub>max</sub> value [12]. However, despite similar patient characteristics and imaging time-points, our study was performed on a larger cohort of patients and the image analysis was lesion-based. These considerations are likely to explain the differences in the reported findings.

The use of SUV<sub>max</sub> as the only parameter for tracer uptake might be a limitation of this study. However, we used a 20% as a cut-off to define the increase in PSMA uptake in order to avoid any possible variation in the SUV<sub>max</sub> due to technical reproducibility aspects. Moreover, all the patients were scanned with the same camera in order to minimize possible technical variation and no differences in injected activities or scanning times were observed. The presence of only one PET reader might also be considered as a limitation. However, the aim of this study was not to assess the diagnostic performance of [<sup>18</sup>F]PSMA-1007 PSMA PET, but rather to investigate the phenomenon of the flare in PSMA uptake in patients with already known distant metastases. Moreover, we had already assessed the inter-reader agreement in our previous trial [13] that did not demonstrate significant differences between the readers. Finally, the absence of histological verification of potential metastases, especially in the bone, might be another limitation, considering that non-specific bone uptakes might be encountered in [<sup>18</sup>F]PSMA-1007 PET imaging [6]. However, the presence of bone metastases was confirmed on conventional imaging performed within 2 weeks from enrollment. Moreover, to avoid the risk of possible false-positive bone uptakes, only those PSMA uptakes with corresponding findings on CT (sclerotic or lytic lesion) were included in our analysis.

## Conclusion

A heterogeneous flare in PSMA uptake after short-term ADT was observed in metastatic treatment-naïve PCa patients, most evidently in bone lesions. There seems to

be a negative correlation between the PSMA flare and the intensity of FDG uptake, suggesting that lesions presenting with the flare might potentially be less aggressive. Moreover, serum PSA decreased less rapidly in patients with a higher number of lesions exhibiting the PSMA flare, which might also potentially be a sign of less aggressiveness. It is still unclear whether the flare phenomenon could predict a better response to ADT. Longer follow-up is needed to confirm these hypotheses. All the patients in the current trial will receive follow-up and will be scanned with [<sup>18</sup>F]PSMA-1007 PET/CT at an interval of 1 year and at onset of CRPC. The future results will hopefully provide further insight into this matter.

**Supplementary Information** The online version contains supplementary material available at <https://doi.org/10.1007/s00259-022-05970-y>.

**Author contribution** Study design: Malaspina, Ettala, Boström, Kempainen

Analysis of the data: Malaspina

Statistical analysis: Malaspina, Ettala

Drafting of the manuscript: Malaspina, Ettala, Kempainen

Critical revision of the manuscript: Ettala, Kempainen, Boström, Tolvanen, Eskola, Rajander

**Funding** Open Access funding provided by University of Turku (UTU) including Turku University Central Hospital.

**Data availability** Data are available on reasonable request to the corresponding author.

## Declarations

**Ethics approval** The study was conducted in compliance with the current revision of the Declaration of Helsinki that guides physicians and medical research involving human subjects (64th World Medical Association General Assembly, Fortaleza, Brazil, 2013). The study received the approval of the Finnish Medicines Agency (FIMEA; EUDRA-CT, 2018–004853-26) and the Ethical Committee of the Hospital District of Southwest Finland (ETMK Dnro: 6/1800/2019).

**Consent to participate** Written informed consent was obtained from all the patients in the study.

**Conflict of interest** The authors declare no competing interests.

**Open Access** This article is licensed under a Creative Commons Attribution 4.0 International License, which permits use, sharing, adaptation, distribution and reproduction in any medium or format, as long as you give appropriate credit to the original author(s) and the source, provide a link to the Creative Commons licence, and indicate if changes were made. The images or other third party material in this article are included in the article's Creative Commons licence, unless indicated otherwise in a credit line to the material. If material is not included in the article's Creative Commons licence and your intended use is not permitted by statutory regulation or exceeds the permitted use, you will need to obtain permission directly from the copyright holder. To view a copy of this licence, visit <http://creativecommons.org/licenses/by/4.0/>.

## References

- Pagliarulo V. Contemporary role of androgen deprivation therapy for prostate cancer. *Eur Urol* [Internet]. 2012;61(1):11–25. <https://doi.org/10.1016/j.eururo.2011.08.026>.
- Sharifi N. Androgen deprivation therapy for prostate cancer. *JAMA*. 2005;1126:1–30.
- Taplin ME. Drug insight: role of the androgen receptor in the development and progression of prostate cancer. *Nat Clin Pract Oncol*. 2007;4:236–44.
- Tamada S, Iguchi T, Kato M, Asakawa J, Kita K, Yasuda S, et al. Time to progression to castration-resistant prostate cancer after commencing combined androgen blockade for advanced hormone-sensitive prostate cancer. *Oncotarget*. 2018;9:36966–74.
- Hofman MS, Lawrentschuk N, Francis RJ, Tang C, Vela I, Thomas P, et al. Prostate-specific membrane antigen PET-CT in patients with high-risk prostate cancer before curative-intent surgery or radiotherapy (proPSMA): a prospective, randomised, multicentre study. *Lancet*. 2020;395:1208–16. [https://doi.org/10.1016/S0140-6736\(20\)30314-7](https://doi.org/10.1016/S0140-6736(20)30314-7).
- Anttinen M, Ettala O, Malaspina S, Jambor I, Sandell M, Kajander S, et al. A prospective comparison of 18F-prostate-specific membrane antigen-1007 positron emission tomography computed tomography, whole-body 1.5 T magnetic resonance imaging with diffusion-weighted imaging, and single-photon emission computed tomography/computed Tomography with traditional imaging in primary distant metastasis staging of prostate cancer (PROSTAGE). *Eur Urol Oncol*. 2021;4(4):635–44. <https://doi.org/10.1016/j.euo.2020.06.012>.
- Malaspina S, Anttinen M, Taimen P, Löyttyniemi E, Kempainen J, Seppänen M, et al. Prospective comparison of <sup>18</sup>F-PSMA-1007 PET/CT, whole-body MRI and CT in primary nodal staging of unfavourable intermediate- and high-risk prostate cancer. *Eur J Nucl Med Mol Imaging*. 2021;48:2672–3.
- Ghosh A, Heston WDW. Tumor target prostate specific membrane antigen (PSMA) and its regulation in prostate cancer. *J Cell Biochem*. 2004;91:528–39.
- Meller B, Bremmer F, Sahlmann CO, Hijazi S, Bouter C, Trojan L, et al. Alterations in androgen deprivation enhanced prostate-specific membrane antigen (PSMA) expression in prostate cancer cells as a target for diagnostics and therapy. *EJNMMI Res*. 2015;5:1–11. <https://doi.org/10.1186/s13550-015-0145-8>.
- Hope TA, Truillet C, Ehman EC, Afshar-Oromieh A, Aggarwal R, Ryan CJ, et al. 68Ga-PSMA-11 PET imaging of response to androgen receptor inhibition: first human experience. *J Nucl Med Soc Nucl Med Molec Imaging*. 2017;58:81–4.
- Aggarwal R, Wei X, Kim W, Small EJ, Ryan CJ, Carroll P, et al. Heterogeneous flare in prostate-specific membrane antigen positron emission tomography tracer uptake with initiation of androgen pathway blockade in metastatic prostate cancer. *Eur Urol Oncol*. 2018;1:78–82. <https://doi.org/10.1016/j.euo.2018.03.010>.
- Emmett L, Yin C, Crumbaker M, Hruby G, Kneebone A, Epstein R, et al. Rapid modulation of PSMA expression by androgen deprivation: serial 68Ga-PSMA-11 PET in men with hormone-sensitive and castrate-resistant prostate cancer commencing androgen blockade. *J Nucl Med*. 2019;60:950–4.
- Ettala O, Malaspina S, Tuokkola T, Luoto P, Löyttyniemi E, Boström PJ, et al. Prospective study on the effect of short-term androgen deprivation therapy on PSMA uptake evaluated with 68Ga-PSMA-11 PET/MRI in men with treatment-naïve prostate cancer. *Eur J Nucl Med Mol Imaging*. 2020;47:665–73.
- Jadvar H. Is there utility for FDG PET in prostate cancer. *Semi Nucl Med*. 2016;46:502–6.
- Long JZ, Jacobson MS, Hung JC. Comparison of FASTlab [<sup>18</sup>F] FDG production using phosphate and citrate buffer cassettes. *J Nucl Med Technol*. 2013;41:32–4.
- Ceci F, Oprea-Lager DE, Emmett L, Adam JA, Bomanji J, Czernin J, et al. E-PSMA: the EANM standardized reporting guidelines v1.0 for PSMA-PET. *Eur J Nucl Med Mol Imaging*. 2021;48(5):1626–38. <https://doi.org/10.1007/s00259-021-05245-y>.
- Harris PA, Taylor R, Minor BL, Elliott V, Fernandez M, O'Neal L, et al. The REDCap consortium: building an international community of software platform partners. *J Biomed Inform*. 2019;95:103208 <https://www.sciencedirect.com/science/article/pii/S1532046419301261?via%3Dihub>. Accessed 27 Aug 2022.
- Jadvar Hossein. Imaging evaluation of prostate cancer with 18Ffluorodeoxyglucose PET/CT: utility and limitations. *Eur J Nucl Med Mol Imaging*. 2013;40 Suppl 1(1):S5–10. <https://doi.org/10.1007/s00259-013-2361-7>.
- Oyama N, Akino H, Suzuki Y, Kanamaru H, Sadato N, Yonekura Y, et al. The increased accumulation of [<sup>18</sup>F]fluorodeoxyglucose in untreated prostate cancer. *Jpn J Clin Oncol*. 1999;29:623–9.
- Conteduca V, Poti G, Caroli P, Russi S, Brighi N, Lolli C, Schepisi G, Romeo A, Matteucci F, Paganelli G, Marchetti P, Giorgi UD. Flare phenomenon in prostate cancer: recent evidence on new drugs and next generation imaging. *Ther Adv Med Oncol*. 2021;9:259–61.
- Roy J, White ME, Basuli F, Opina ACL, Wong K, Riba M, et al. Monitoring PSMA responses to ADT in prostate cancer patient-derived xenograft mouse models using [<sup>18</sup>F]DCFPyL PET imaging. *Mol Imaging Biol*. 2021;23:745–55.
- Privé BM, Peters SMB, Muselaers CHJ, van Oort IM, Janssen MJR, Michiel Sedelaar JP, et al. Lutetium-177-PSMA-617 in low-volume hormone-sensitive metastatic prostate cancer: a prospective pilot study. *Clin Cancer Res*. 2021;27:3595–601.
- Arai Y, Yoshiki TYO. Prognostic significance of prostate specific antigen in endocrine treatment for prostatic cancer. 1990;144(6):1415–9. [https://doi.org/10.1016/s0022-5347\(17\)39757-4](https://doi.org/10.1016/s0022-5347(17)39757-4).
- Miller JJ, Ahmann FR, Drach GW, Emerson SS, Bottaccini MR. The clinical usefulness of serum prostate specific antigen after hormonal therapy of metastatic prostate cancer. *J Urol*. 1992;147:956–61. [https://doi.org/10.1016/S0022-5347\(17\)37432-3](https://doi.org/10.1016/S0022-5347(17)37432-3).
- Facchini G, Caffo O, Ortega C, D'Aniello C, Di Napoli M, Cecere SC, et al. Very early PSA response to abiraterone in mCRPC patients: a novel prognostic factor predicting overall survival. *Front Pharmacol*. 2016;7:1–8.
- Ji G, Song G, Huang C, He S, Zhou L. Rapidly decreasing level of prostate-specific antigen during initial androgen deprivation therapy is a risk factor for early progression to castration-resistant prostate cancer: a retrospective study. *Medicine (Baltimore)*. 2017;96(36):e7823. <https://doi.org/10.1097/MD.00000000000007823>.
- Tomioka A, Tanaka N, Yoshikawa M, Miyake M, Anai S, Chihara Y, et al. Nadir PSA level and time to nadir PSA are prognostic factors in patients with metastatic prostate cancer. *BMC Urol*. 2014;14:1–6.
- Sasaki T, Onishi T, Hoshina A. Nadir PSA level and time to PSA nadir following primary androgen deprivation therapy are the early survival predictors for prostate cancer patients with bone metastasis. *Prostate Cancer Prostatic Dis*. 2011;14:248–52.
- Choueiri TK, Xie W, Amico AVD, Ross RW, Hu JC, Regan MM, et al. Time to prostate-specific antigen nadir independently predicts overall survival in patients who have metastatic hormone-sensitive prostate cancer treated with androgen-deprivation therapy. *Cancer*. 2009;115(5):981–7. <https://doi.org/10.1002/cncr.24064>.

**Publisher's note** Springer Nature remains neutral with regard to jurisdictional claims in published maps and institutional affiliations.





**Malaspina S, Anttinen M, Taimen P, Jambor I, Sandell M, Rinta-Kiikka I, Kajander S, Schildt J, Saukko E, Nojonen T, Saunavaara J, Dean PB, Sequeiros RB, Aronen HJ, Kemppainen J, Seppänen M, Boström PJ, Ettala O. (2021)**

**Prospective comparison of  $^{18}\text{F}$ -PSMA-1007 PET/CT, whole-body MRI and CT in primary nodal staging of unfavourable intermediate- and high-risk prostate cancer.**

European Journal of Nuclear Medicine and Molecular Imaging





# Prospective comparison of <sup>18</sup>F-PSMA-1007 PET/CT, whole-body MRI and CT in primary nodal staging of unfavourable intermediate- and high-risk prostate cancer

Simona Malaspina<sup>1</sup> · Mikael Anttinen<sup>2</sup> · Pekka Taimen<sup>3</sup> · Ivan Jambor<sup>4,5</sup> · Minna Sandell<sup>5</sup> · Irina Rinta-Kiikka<sup>6</sup> · Sami Kajander<sup>1</sup> · Jukka Schildt<sup>7</sup> · Ekaterina Saukko<sup>5</sup> · Tommi Noponen<sup>8</sup> · Jani Saunavaara<sup>8</sup> · Peter B. Dean<sup>5</sup> · Roberto Blanco Sequeiros<sup>5</sup> · Hannu J. Aronen<sup>5</sup> · Jukka Kempainen<sup>1</sup> · Marko Seppänen<sup>9</sup> · Peter J. Boström<sup>2</sup> · Otto Ettala<sup>2</sup>

Received: 3 December 2020 / Accepted: 28 February 2021 / Published online: 13 March 2021

© The Author(s) 2021

## Abstract

**Purpose** To prospectively compare <sup>18</sup>F-prostate-specific membrane antigen (PSMA)-1007 positron emission tomography (PET)/CT, whole-body magnetic resonance imaging (WBMRI) including diffusion-weighted imaging (DWI) and standard computed tomography (CT), in primary nodal staging of prostate cancer (PCa).

**Methods** Men with newly diagnosed unfavourable intermediate- or high-risk PCa prospectively underwent <sup>18</sup>F-PSMA-1007 PET/CT, WBMRI with DWI and contrast-enhanced CT within a median of 8 days. Six readers (two for each modality) independently reported pelvic lymph nodes as malignant, equivocal or benign while blinded to the other imaging modalities. Sensitivity, specificity and accuracy were reported according to optimistic (equivocal lesions interpreted as benign) and pessimistic (equivocal lesions interpreted as malignant) analyses. The reference standard diagnosis was based on multidisciplinary consensus meetings where available histopathology, clinical and follow-up data were used.

**Results** Seventy-nine patients completed all the imaging modalities, except for one case of interrupted WBMRI. Thirty-one (39%) patients had pelvic lymph node metastases, which were detected in 27/31 (87%), 14/31 (45%) and 8/31 (26%) patients by <sup>18</sup>F-PSMA-1007 PET/CT, WBMRI with DWI and CT, respectively (optimistic analysis). In 8/31 (26%) patients, only <sup>18</sup>F-PSMA-1007 PET/CT detected malignant lymph nodes, while the other two imaging modalities were reported as negative. At the patient level, sensitivity and specificity values for <sup>18</sup>F-PSMA-1007 PET/CT, WBMRI with DWI and CT in optimistic analysis were 0.87 (95%CI 0.71–0.95) and 0.98 (95%CI 0.89–1.00), 0.37 (95%CI 0.22–0.55) and 0.98 (95%CI 0.89–1.00) and 0.26 (95%CI 0.14–0.43) and 1.00 (95%CI 0.93–1.00), respectively.

**Conclusion** <sup>18</sup>F-PSMA-1007 PET/CT showed significantly greater sensitivity in nodal staging of primary PCa than did WBMRI with DWI or CT, while maintaining high specificity.

**Clinical trial registration** Clinicaltrials.gov ID: NCT03537391

**Keywords** Prostate cancer · Primary staging · Lymph node metastasis · <sup>18</sup>F-PSMA-1007 PET/CT · WBMRI · CT

This article is part of the Topical Collection on Oncology - Genitourinary

✉ Simona Malaspina  
simona.malaspina@tyks.fi

<sup>1</sup> Turku PET Centre, University of Turku and Turku University Hospital, Turku, Finland

<sup>2</sup> Department of Urology, University of Turku and Turku University Hospital, Turku, Finland

<sup>3</sup> Institute of Biomedicine and Department of Pathology, University of Turku and Turku University Hospital, Turku, Finland

<sup>4</sup> Department of Radiology, Icahn School of Medicine at Mount Sinai, New York, NY, USA

<sup>5</sup> Department of Diagnostic Radiology, University of Turku and Turku University Hospital, Turku, Finland

<sup>6</sup> Department of Radiology, Tampere University Hospital, Tampere, Finland

<sup>7</sup> Department of Clinical Physiology and Nuclear Medicine, Helsinki University Central Hospital, Helsinki, Finland

<sup>8</sup> Department of Medical Physics and Nuclear Medicine, University of Turku and Turku University Hospital, Turku, Finland

<sup>9</sup> Department of Clinical Physiology, Nuclear Medicine and Turku PET Centre, University of Turku and Turku University Hospital, Turku, Finland

## Introduction

The presence of pelvic lymph node metastases at initial staging is an important prognostic factor in primary prostate cancer (PCa) [1]. Following radical treatment of localized PCa, such as prostatectomy or external beam radiotherapy, some men are diagnosed with nodal recurrence [2]. This can be partly attributed to the inability of conventional imaging methods to correctly stage patients at the time of initial diagnosis. A more accurate determination of the initial extent of the disease using next-generation imaging modalities could improve therapeutic planning and possibly treatment outcome [3].

Abdominopelvic imaging with conventional computed tomography (CT) is still recommended in primary nodal staging of PCa, although the sensitivity of CT in detecting lymph node metastases is modest [4]. Pelvic magnetic resonance imaging (MRI) with diffusion-weighted imaging (DWI) is the method of choice for assessing local tumour extent, and it plays an important role in the detection of regional lymph node metastases [5]. Moreover, determining the overall extent of PCa with whole-body MRI (WBMRI) has gained increasing interest [6].

Prostate-specific membrane antigen (PSMA) positron emission tomography (PET) imaging has recently been introduced in PCa imaging [7]. Accumulating evidence supports the use of PSMA PET/CT for the restaging of PCa after biochemical recurrence. However, there is less evidence supporting its use in primary staging, and yet the data are mainly limited to  $^{68}\text{Ga}$ -labelled PSMA tracers. Alternatively, novel  $^{18}\text{F}$ -labelled PSMA ligands, such as  $^{18}\text{F}$ -PSMA-1007 [8], are able to offer longer half-life, superior energy characteristics and higher image resolution compared with  $^{68}\text{Ga}$ -labelled tracers. In addition,  $^{18}\text{F}$ -PSMA-1007 is only minimally excreted by the urinary tract, an advantage in pelvic imaging. There is preliminary evidence that  $^{18}\text{F}$ -labelled PSMA tracers might have a higher incidence of benign uptake in bone tissue and unspecific lymph nodes [9, 10], although no prospective comparative studies with  $^{68}\text{Ga}$ -labelled tracer are available.

To date, only a limited number of studies evaluating  $^{18}\text{F}$ -labelled PSMA tracers in the detection of PCa regional lymph node metastases have been published [11–13].

We have previously prospectively compared the diagnostic performance of next-generation ( $^{18}\text{F}$ -PSMA-1007 PET/CT, WBMRI with DWI and SPECT/CT) and conventional imaging modalities (CT and bone scintigraphy) in primary distant metastasis staging of PCa [10].

Using the same patient cohort, the aim of the current study was to prospectively compare  $^{18}\text{F}$ -PSMA-1007 PET/CT, WBMRI using DWI and CT in primary nodal staging of men with unfavourable intermediate- and high-risk PCa.

## Material and methods

### Study design and patient population

This is a prospective non-randomized registered (NCT03537391) single-centre trial that included patients with newly diagnosed histologically confirmed unfavourable intermediate- or high-risk PCa (International Society of Urological Pathology grade group  $\geq 3$  and/or prostate-specific antigen [PSA]  $\geq 20$  and/or cT  $\geq \text{T3}$ ). Exclusion criteria included any previous PCa imaging for metastasis staging, PCa treatment before enrolment and contraindications for MRI. Administration of androgen deprivation therapy (ADT) at enrolment was permitted if necessary for symptomatic very high-risk PCa patients. All participants underwent  $^{99\text{m}}\text{Tc}$ -HMDP planar bone scintigraphy,  $^{99\text{m}}\text{Tc}$ -HMDP SPECT/CT, contrast-enhanced abdominopelvic and thoracic CT, WBMRI with DWI and  $^{18}\text{F}$ -PSMA-1007 PET/CT within 2 weeks of enrolment and without a prespecified sequence. Since the current study solely focused on regional nodal staging, the following imaging modalities were evaluated:

1. Standard imaging: contrast-enhanced CT
2. Imaging under evaluation: WBMRI with DWI and  $^{18}\text{F}$ -PSMA-1007 PET/CT

### Imaging modalities

**Contrast-enhanced CT** Abdominopelvic and thoracic CT was performed with a Discovery NM/CT 670 CZT, a digital SPECT/CT imaging system, including Optima CT540 subsystem (GE Healthcare, Tirat, Hacarmel, Israel). A helical CT tomogram with a modulated mAs (noise index  $\sim 30$ ), a rotation time of 0.5 s, 120 kVp, a pitch of 0.938 and 1.25-mm slice thickness was acquired. Soft tissue, bone and lung kernels were employed with a 40% dose reduction in the Adaptive Statistical Iterative Reconstruction (ASIR, GE Healthcare, USA) algorithm. A biphasic contrast-enhanced CT protocol (arterial phase of 10 s, followed by venous phase at 30 s) was performed. Contrast agent (Omnipaque (iohexol)<sup>TM</sup> GE Healthcare, iodine concentration of 350 mg/ml) was used unless clinical contraindications were present.

**Whole-body MRI** WBMRI imaging was performed using a Siemens Magnetom Avanto fit 1.5 T MR system (Siemens Healthcare GmbH, Erlangen, Germany). WBMRI acquisition protocol consisted of axial T2-weighted fat suppressed (FS) half-Fourier single shot turbo-spin echo images (HASTE), axial short-tau inversion recovery (STIR) DWI,  $b$ -values 0, 50, 900  $\text{s}/\text{mm}^2$  and coronal 3D T1-weighted volumetric interpolated breath-hold examination (VIBE) Dixon sequences. In

addition, whole spine sagittal T1- and T2-weighted STIR turbo spin-echo (TSE) sequences and axial STIR DWI images from the level of the pelvis, b values 0, 1500 s/mm<sup>2</sup>, were acquired.

**<sup>18</sup>F-PSMA 1007 tracer synthesis and PET/CT** <sup>18</sup>F-PSMA-1007 tracer was manufactured by MAP Medical Technologies Oy, Curium Pharma (Helsinki, Finland), as previously described [14].

The PET/CT study was carried out with Discovery MI digital PET/CT system (GE Healthcare, Milwaukee, WI, USA), with a 128 slice CT and a 3D PET imaging capability. The PET imaging field of view (FOV) was 70 cm in diameter and 20 cm in axial length. Transmission scan for attenuation correction was performed using a low-dose (noise index 30, automatic 3D current modulation, 10–120 mAs and 120 kVp) CT protocol. A static emission scan was acquired from vertex to mid-thigh (6 bed positions, 2 min/bed). The sinogram data were corrected for deadtime, decay and photon attenuation and reconstructed in a 256 × 256 matrix. Image reconstruction utilized a Q. Clear method (a Bayesian penalized likelihood reconstruction algorithm for PET) with  $\beta$  value of 500 incorporating random and scatter corrections. The final in-plane FWHM (full-width half-maximum) of the systems is <5 mm.

### Imaging interpretation and reference standard

There were a total of six readers (4 radiologists and 2 nuclear medicine physicians), two for each of the three imaging modalities. Each imaging modality was independently reviewed by the same pair of experienced modality-based experts, blinded for the other modalities.

The pelvic lymph nodes were reported as malignant, equivocal or benign, and these data were collected on an electronic database [15]. Both optimistic (equivocal lesions interpreted as benign) and pessimistic (equivocal lesions interpreted as malignant) analyses were performed to resolve equivocal lesion status. Lesions were interpreted in all modalities according to clinical expertise and following current guidelines [3, 16]. In CT and WBMRI, lymph node diameter (short diameter > 8 mm) and morphology (rounded) were used to determine malignancy. In MRI, diffusion restriction was also used to assess nodal invasion, especially in normal-sized lymph nodes. In <sup>18</sup>F-PSMA-1007 PET/CT, lymph nodes in a typical site of PCa metastasis and with tracer uptake (expressed as standardized uptake value [SUV<sub>max</sub>]) above the blood pool were considered malignant. Imaging studies were interpreted using Advantage Workstation (version 4.7, GE Healthcare, Buc, France), Weasis Medical Viewer (version 3.5.3, University Hospital of Geneva, Switzerland) and Vue PACS (version 12.2.0.1007, Carestream Health Inc., Rochester, USA).

For the validation of all reported lesions, the reference standard diagnosis was utilized, which included histopathological specimens (when available), information from all primary imaging modalities, follow-up imaging and clinical follow-up data. When histopathology was not available, lymph nodes were considered malignant when at least three of the following criteria were met: (1) concordance between primary imaging modalities, (2) increase in size or number of lymph nodes during follow-up imaging, (3) decrease in size or number of lymph nodes during follow-up imaging in response to treatment, (4) increase in serum PSA suggesting progression, (5) decrease in serum PSA in response to treatment, (6) increase in PSMA uptake during follow-up imaging (when available), and (7) decrease in PSMA uptake during follow-up imaging (when available) in response to treatment.

The reference standard diagnosis was determined at the lesion level in a regularly organized consensus meeting by a multidisciplinary team including two urologists, one uropathologist, two radiologists (CT and MRI specialists) and two nuclear medicine physicians.

### Histopathological analysis

Surgical tissue specimens from pelvic lymph node dissection (PLND, i.e., removal of lymphatic tissue around external and internal iliac vessels and obturator nerve starting from the ureter crossing and extending to the pelvic wall) were fixed in 10% buffered formalin for minimum of 24 h. The number of palpable lymph nodes identified on each side was determined, and the lymph nodes were cut in 3–4 mm sections before routine tissue processing. Consecutive histological sections of 4  $\mu$ m thickness were used for haematoxylin and eosin (H&E) staining and for immunohistochemistry. Epitope unmasking was done by microwaving the slides in Tris-EDTA buffer. PSMA staining was carried out with a Lab Vision autostainer (Thermo Fisher Scientific) using a mouse monoclonal PSMA antibody (Dako, clone M3620, 1:100) and Envision detection kit (EP192). Pan-cytokeratin staining was carried out using BenchMark ULTRA automated slide stainer (Ventana Medical Systems, Tucson, Arizona, USA) and anti-pan-cytokeratin antibody (clone AE1/AE3/PCK26, 46.3  $\mu$ g/ml). All the histological slides were reviewed by one board-certified experienced uropathologist blinded to the imaging modality results.

### Statistical analysis

The sample size estimation for this clinical trial has been previously described [10]. Descriptive statistics including median, interquartile range (IQR) and range were used. Sensitivity, specificity and accuracy were reported with 95% confidence interval (CI) and compared between modalities with Fisher's exact test. For both patient- and lesion-based statistical

analysis, correct side of the pelvis (right or left) was considered to achieve correct agreement with the reference standard diagnosis. The inter-reader agreement was assessed using Cohen's Kappa (95% CI). Pearson's  $r$  was used to study correlation between PSMA SUVmax and lesion's size.  $p$ -values less than 0.05 were considered statistically significant. Statistical analyses were performed with JMP® System, version 14.2.0 for MacOS (SAS Institute Inc., Cary, NC, USA).

## Results

Seventy-nine patients were included in this study. All patients underwent all imaging modalities except for one case of interrupted WBMRI due to unexpected claustrophobia. Patient characteristics are summarized in Table 1. The median age was 72 years (interquartile range [IQR] 66–77; range 52–87), and median PSA was 12 (IQR 7–23; range 3–2000). The median interval between the first and last imaging was 8 days (IQR 6–12; range 1–44). The median administered activity of  $^{18}\text{F}$ -PSMA-1007 was 250 MBq (IQR 246–256; range 206–279), and PET/CT scan was acquired at a median of 60 min (IQR 60–60; range 59–63) from tracer injection. The median follow-up period was 21 months (IQR 19–25; range 16–29). Five patients received ADT therapy at enrolment due to symptomatic very high-risk PCa. In all of these patients, metastatic disease was detected, and all imaging modalities were performed within 3 weeks from enrolment. In particular, the median interval between the initiation of ADT and  $^{18}\text{F}$ -PSMA PET/CT was 7 days (IQR 3–17; range 2–22).

According to EAU risk group classification, 17/79 (22%) patients belonged to unfavourable intermediate- and the rest to high-risk group (62/79, 78%). Consensus staging results after all imaging reports were as follows: 41 patients had localized disease, 18 had locally advanced disease, and 20 had distant metastatic disease.

Thirty-one (39%) patients were deemed to have pelvic lymph node metastatic disease, which, in optimistic analysis, was detected in 27/31 (87%), 14/31 (45%) and 8/31 (26%) patients by  $^{18}\text{F}$ -PSMA-1007 PET/CT, WBMRI with DWI and CT, respectively. In 8/31 (26%) patients, only  $^{18}\text{F}$ -PSMA-1007 PET/CT was able to detect metastatic lymph nodes, while the other two imaging modalities were reported as negative. Sensitivity, specificity and accuracy values at the patient-level are given in Table 2.  $^{18}\text{F}$ -PSMA-1007 PET/CT significantly outperformed WBMRI with DWI and CT in sensitivity and accuracy. Inter-reader agreement for  $^{18}\text{F}$ -PSMA-1007 PET/CT at the patient-level was superior compared to WBMRI with DWI and CT, with Kappa values of 0.89, 0.47 and 0.69, respectively, in optimistic analysis (Supplementary Table S1).

**Table 1** Patient demographics

Age	Median ([IQR] range)
Years	72 ([66–77] 52–87)
PSA	Median ([IQR] range)
ng/ml	12 ([7–23] 3–2000)
Clinical T-category <sup>a</sup>	$n$ (%)
cT1	7 (11)
cT2	37 (46)
cT3	27 (33)
cT4	8 (10)
Biopsy GGG	$n$ (%)
1 <sup>b</sup>	3 (4)
2	1 (1)
3	29 (37)
4	13 (16)
5	33 (42)
Primary treatment <sup>c</sup>	$n$ (%)
RALP	5 (6)
RALP + PLND	17 (22)
EBRT	37 (47)
TULSA	2 (3)
ADT	17 (21)
Watchful waiting	1 (1)

PSA prostate-specific antigen, GGG Gleason grade group, RALP robot-assisted laparoscopic prostatectomy, PLND pelvic lymph node dissection, EBRT external beam radiotherapy with ( $n = 36$ ) or without ( $n = 1$ ) ADT androgen deprivation therapy, TULSA transurethral ultrasound ablation of prostate; ADT with ( $n = 4$ ) or without ( $n = 13$ ) early chemotherapy with docetaxel

<sup>a</sup> Clinical T-category was determined based on transrectal ultrasound and digital rectal examination before any imaging

<sup>b</sup> All patients with GGG 1 had PSA >20 ng/ml

<sup>c</sup> All treatments were performed and/or initiated after the imaging studies, except for 5 patients, who began ADT at enrolment due to symptomatic very high-risk PCa. In two cases, palliative transurethral resection of the prostate was performed due to bladder outlet obstruction prior to EBRT, and one case underwent palliative TULSA combined with ADT

At the lesion level, 206 lymph nodes were interpreted as malignant (the reference standard diagnosis). The number of true positive, false positive and false negative lesions for each imaging modality and reader is shown in Table 3. The detection rate of lymph node metastases for  $^{18}\text{F}$ -PSMA-1007 PET/CT was 83%, compared to 58% for WBMRI with DWI and 52% for CT. Out of all the metastatic lesions detected by  $^{18}\text{F}$ -PSMA 1007 PET/CT, 126/170 (74%) were smaller than the anatomical cutoff value of 8 mm, of which 90 lymph nodes had the short diameter between 5 and 8 mm and 36 lymph nodes <5 mm (Supplementary Fig. S1). SUVmax intensity did not show correlation with lymph node's dimensions ( $r^2 = 0.010$ ;  $p = 0.33$ ).

**Table 2** Sensitivity, specificity and accuracy of both readers of each imaging modality in pessimistic and optimistic analysis at the patient level

Imaging modality	Reader	Pessimistic analysis			Optimistic analysis		
		Sensitivity (95%CI)	Specificity (95%CI)	Accuracy (95%CI)	Sensitivity (95%CI)	Specificity (95%CI)	Accuracy (95%CI)
CT	1	0.39 (0.24–0.56) <sup>a,b</sup>	0.94 (0.83–0.98)	0.72 (0.61–0.80) <sup>a,b</sup>	0.16 (0.07–0.32) <sup>a,b</sup>	1.00 (0.93–1.00)	0.67 (0.56–0.76) <sup>a,b</sup>
	2	0.32 (0.19–0.50) <sup>a,b</sup>	0.94 (0.83–0.98)	0.70 (0.59–0.79) <sup>a,b</sup>	0.26 (0.14–0.43) <sup>a,b</sup>	0.98 (0.89–0.99)	0.70 (0.59–0.79) <sup>a,b</sup>
WBMRI with DWI	1	0.40 (0.25–0.58) <sup>a,b</sup>	0.96 (0.86–0.99)	0.74 (0.63–0.83) <sup>a,b</sup>	0.37 (0.22–0.55) <sup>a,b</sup>	0.98 (0.89–1.00)	0.74 (0.63–0.83) <sup>a,b</sup>
	2	0.50 (0.33–0.67) <sup>a,b</sup>	0.91 (0.80–0.97)	0.75 (0.65–0.84) <sup>a,b</sup>	0.37 (0.22–0.55) <sup>a,b</sup>	0.98 (0.89–1.00)	0.74 (0.63–0.83) <sup>a,b</sup>
<sup>18</sup> F-PSMA-1007 PET/CT	1	0.84 (0.67–0.93)	0.96 (0.86–0.99)	0.91 (0.83–0.96)	0.77 (0.60–0.89)	0.98 (0.89–1.00)	0.90 (0.81–0.95)
	2	0.90 (0.75–0.97)	0.94 (0.83–0.98)	0.93 (0.85–0.96)	0.87 (0.71–0.95)	0.96 (0.86–0.99)	0.92 (0.84–0.96)

CT computed tomography, WBMRI whole-body magnetic resonance imaging, DWI diffusion-weighted imaging, <sup>18</sup>F-PSMA-1007 PET/CT prostate-specific membrane antigen positron emission tomography-CT, CI confidence interval

<sup>a</sup>Statistically significant difference ( $p < 0.05$ ) compared to <sup>18</sup>F-PSMA-1007 PET/CT reader 1

<sup>b</sup>Statistically significant difference ( $p < 0.05$ ) compared to <sup>18</sup>F-PSMA-1007 PET/CT reader 2

Seventeen patients (22%) were treated with robot-assisted laparoscopic prostatectomy (RALP) and PLND, and five of these patients showed lymph node metastases in histopathological examination. The results of the patient- and lesion-based analyses from all the operated patients are shown in Supplementary Table S2 and S3. Compared to the other two imaging modalities, <sup>18</sup>F-PSMA-1007 PET/CT demonstrated superior sensitivity and accuracy at the patient level (0.67 and 0.82 in optimistic analysis) and the highest detection rate at the lesion level (27%). <sup>18</sup>F-PSMA-1007 PET/CT was concordant with histopathology in 14/17 (82%) patients, while the corresponding numbers for WBMRI with DWI and CT were 12/17 (71%) and 11/17 (65%), respectively. The number of metastases detected by histopathology and <sup>18</sup>F-PSMA-1007 PET/CT are presented in Supplementary Table S4. Of the five patients with histologically confirmed lymph node metastases, three were detected by

<sup>18</sup>F-PSMA-1007 PET/CT, while both CT and WBMRI were negative in all five cases. In each of these three patients, additional histologically confirmed lymph nodes metastases were also found, which were not detected by <sup>18</sup>F-PSMA-1007 PET/CT (Fig. 1). Supplementary Fig. S2 demonstrates one of the two histologically confirmed <sup>18</sup>F-PSMA-1007 PET/CT false negative cases. The only false positive <sup>18</sup>F-PSMA-1007 PET/CT case is shown in Supplementary Fig. S3. All the lymph node metastases detected by H&E staining ( $n = 11$ ) were also positive in the immunohistochemical pan-cytokeratin and PSMA staining. Immunohistochemical staining alone revealed additional lymph node micrometastases ( $n = 3$ ) in three patients, each of whom was already diagnosed with other histologically confirmed metastases, thus not affecting the overall nodal status.

Pelvic follow-up imaging was available for 56/62 (90%) of patients not treated with surgery ( $n = 62$ ), including CT ( $n =$

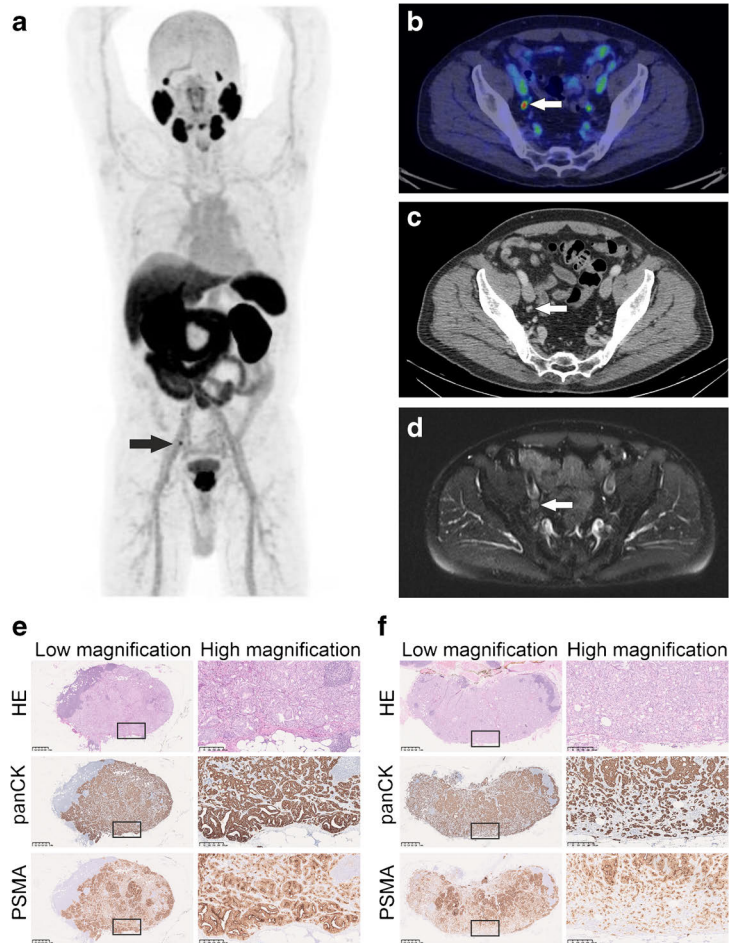
**Table 3** The total number of reported lesions by both readers of each imaging modality and their concordance with the reference standard diagnosis at the lesion level

Imaging modality	Reader	Number of positive lesions reported	Number of true positive lesions	Detection rate of true positive lesions	Number of false positive lesions	Number of false negative lesions	Number of equivocal lesions reported
CT	1	52	52	25%	0	154	36
	2	146	107	52%	39	99	12
WBMRI with DWI	1	93	91	44%	2	110	1
	2	179	120	58%	59	81	9
<sup>18</sup> F-PSMA-1007 PET/CT	1	178	170	83%	8	36	4
	2	156	144	70%	12	62	1

CT computed tomography, WBMRI whole-body magnetic resonance imaging, DWI diffusion-weighted imaging, <sup>18</sup>F-PSMA-1007 PET/CT prostate-specific membrane antigen positron emission tomography-CT

There were 206 lymph node metastases according to reference standard diagnosis

**Fig. 1** Imaging and histopathological findings of patient 48.  $^{18}\text{F}$ -PSMA-1007 PET/CT clearly identified one pelvic lymph node metastasis (short diameter: 6 mm) on the right (a–b) which was retrospectively identified by CT (c) and WBMRI (d). Histopathological examination confirmed one lymph node metastasis on the right (maximum diameter 7 mm) with intense PSMA and pan-cytokeratin staining in immunohistochemistry (E). On the other hand,  $^{18}\text{F}$ -PSMA-1007 PET/CT did not detect another lymph node metastasis found in histopathological examination on the left (maximum diameter: 8,5 mm, f). This lymph node showed less intense immunohistochemical PSMA staining when compared to one on the right. Boxed areas in low magnification images are shown in high magnification images



15), MRI with DWI ( $n = 31$ ) or  $^{18}\text{F}$ -PSMA-1007 PET/CT ( $n = 10$ ).

## Discussion

This prospective clinical trial compared standard (CT) and next-generation imaging modalities (PSMA PET/CT using the novel tracer  $^{18}\text{F}$ -PSMA-1007 and WBMRI with DWI) in primary nodal staging of men with unfavourable intermediate- and high-risk prostate cancer. Thirty-one patients had pelvic lymph node metastases, of which  $^{18}\text{F}$ -PSMA 1007 PET/CT detected 87%, while the detection rates for WBMRI and CT were 45% and 26%, respectively.  $^{18}\text{F}$ -PSMA-1007 PET/CT showed the highest sensitivity, accuracy and inter-reader agreement.

Many prospective studies that have used histopathology as a validation have already demonstrated adequate diagnostic

performance of PSMA PET/CT in primary nodal staging [12, 13, 17–19]. However, only a small number of prospective multimodality comparative studies are available [20–22], and none conducted using  $^{18}\text{F}$ -PSMA-1007 tracer. Recently, Hofman et al. [20] demonstrated superior diagnostic accuracy of  $^{68}\text{Ga}$ -PSMA-11 PET/CT in primary staging of men with high-risk PCa in a randomized study setting, showing significantly higher sensitivity (0.85 vs 0.38) and better specificity (0.98 vs 0.91) compared to conventional imaging. In line with the results of our study, the superiority of  $^{68}\text{Ga}$ -PSMA PET/CT was also confirmed in the subgroup of patients with pelvic nodal metastases. Similarly, the other two non-randomized prospective comparative studies on smaller patient cohorts [21, 22] showed higher performance, especially in terms of sensitivity, of  $^{68}\text{Ga}$ -PSMA PET/CT compared to MRI and/or CT.

The higher sensitivity of  $^{18}\text{F}$ -PSMA-1007 PET/CT is most probably based on the fact that lymph node metastases in PCa



are not necessarily present only in enlarged lymph nodes [23, 24]. Our data is consistent with this concept since it demonstrated that 74% of all lymph node metastases detected by  $^{18}\text{F}$ -PSMA-1007 PET/CT were smaller than the anatomical cutoff value of 8 mm (short diameter) used in CT and MRI.

Recent prospective studies that used histopathology as a reference standard showed results similar to our subgroup analysis of operated patients, especially in terms of specificity of PSMA PET/CT in primary nodal staging (Supplementary Table S5). The sensitivity in our subanalysis was only partially in concordance with the results of those studies, which showed heterogeneous values (0.39–0.64). This could be explained to some extent by differences in patient population or in study methodology.

In our subgroup analysis of patients undergoing pelvic lymph node dissection,  $^{18}\text{F}$ -PSMA-1007 PET/CT was concordant with histology in 82% of the cases. However, there were histologically confirmed nodal metastases ( $n=9$ ) with longest diameter of  $\leq 4$  mm that were not detected by  $^{18}\text{F}$ -PSMA-1007 PET/CT (Fig. 1, S2). Given the limits of PET/CT resolution, limited accuracy in detecting very small or micrometastases was expected.

Factors other than anatomical size should also affect the detection rate of lymph node metastases. In this patient cohort, lower SUVmax values were observed in smaller lymph nodes with short diameter  $< 5$  mm (Fig. S1). However, PSMA SUVmax values did not correlate with the anatomical size of the lymph nodes. The varying detectability in PSMA PET might be also due to heterogeneity in PSMA expression, as we observed variable intensity in immunohistochemical PSMA staining between positive metastatic lymph nodes (Fig. 1, Supplementary Fig. S2, S4). Nevertheless, none of the lymph node metastases detected by H&E was negative on PSMA immunostaining, in line with recently published data [22]. Weak PSMA expression was occasionally detected also in non-metastatic tissues, as in the germinal centres of lymphoid follicles as well as in the endothelial cells of medullary sinuses (Supplementary Fig. S4). The former may represent tumour cell-derived PSMA phagocytosed by antigen presenting cells as this finding was more frequently observed among patients with metastatic lymph nodes. Further research is needed in this respect.

We might tentatively speculate that another challenge in  $^{18}\text{F}$ -PSMA-1007 PET/CT interpretation is the risk of false positive cases in possibly reactive lymph nodes located in the very distal iliac region. We observed only one histologically confirmed PSMA false-positive case (Supplementary Fig. S3), where PSA values dropped  $< 0.006$  ng/ml during follow-up after surgery.

The main limitation of this study is the relatively small percentage of patients (22%) with histopathologically verified lymph node status, of whom only 5 patients had lymph node metastases. This could have led to a sub-optimal reference

standard and a possible underestimation of the true prevalence of lymph node metastases in the majority of participants.

Since this prospective clinical trial was designed to find the most appropriate imaging modality for the overall (local, nodal and distant) staging of men with newly diagnosed unfavourable intermediate- and high-risk PCa, treatment management followed current clinical practice and surgical treatment was not performed in all patients.

Furthermore, a strength of this study is that all patients were examined within a very short time window by three different imaging modalities ( $^{18}\text{F}$ -PSMA-1007 PET/CT WBMRI with DWI and CT) to support the standard reference diagnosis. Another strength of the study is that all patients had long follow-up times supporting the image-based validation of reference standard diagnosis in lesions lacking histopathological evidence.

A small number of the study patients ( $n=5$ ) with symptomatic very high-risk PCa began ADT therapy at enrolment, which could be considered a minor limitation. However, despite it has been reported that ADT therapy might influence heterogeneously PSMA uptake [25, 26], short-term treatment is unlikely to have affected the lesion detectability. Moreover, all five patients had metastatic disease detected using each of the imaging modalities.

Another limitation of the study is that the effect of the next-generation modalities on treatment decision-making was not prospectively collected and investigated. Nevertheless, additional randomized evidence is needed to support the oncological benefit of detecting earlier metastatic disease with next-generation imaging.

## Conclusion

This prospective comparative clinical trial showed significantly improved sensitivity and accuracy of  $^{18}\text{F}$ -PSMA-1007 PET/CT over WBMRI with DWI and CT in the detection of pelvic lymph node metastases in primary unfavourable intermediate- and high-risk PCa, while maintaining high specificity. Additional evidence is needed to confirm the possible clinical benefit of the early detection of lymph node metastases by  $^{18}\text{F}$ -PSMA-1007 PET/CT.

**Supplementary Information** The online version contains supplementary material available at <https://doi.org/10.1007/s00259-021-05296-1>.

**Authors' contribution** Study concept and design: Malaspina, Anttinen, Seppänen, Saunavaara, Noponen, Aronen, Boström, Ettala

Acquisition of data: Malaspina, Sandell, Jambor, Rinta-Kiikka, Schildt, Kajander

Analysis and interpretation of data: Malaspina, Anttinen, Ettala, Seppänen, Sandell, Taimen, Boström

Drafting of the manuscript: Malaspina, Anttinen, Taimen, Ettala  
 Critical revision of the manuscript for important intellectual content: Seppänen, Boström, Dean, Kempainen  
 Statistical analysis: Malaspina, Ettala  
 Obtaining funding: Boström, Aronen, Seppänen, Blanco Sequeiros  
 Administrative, technical or material support: Saukko, Saunavaara, Noponen, Aronen, Blanco Sequeiros, Seppänen

**Funding** Open access funding provided by University of Turku (UTU) including Turku University Central Hospital. Financial support was provided by the Finnish Government Research and Development Funds for Medical Research, Turku University Hospital, and TYKS-SAPA Research Fund.

**Data availability** Data are available on request to the corresponding author.

## Declarations

**Ethics approval** The study received approval from the Ethical Committee of South West Finland (Dnro:26/1801/2018).

**Consent to participate and for publication** All patients signed written consent prior to the initiation of the study.

**Competing interests** The authors declare no competing interests.

**Open Access** This article is licensed under a Creative Commons Attribution 4.0 International License, which permits use, sharing, adaptation, distribution and reproduction in any medium or format, as long as you give appropriate credit to the original author(s) and the source, provide a link to the Creative Commons licence, and indicate if changes were made. The images or other third party material in this article are included in the article's Creative Commons licence, unless indicated otherwise in a credit line to the material. If material is not included in the article's Creative Commons licence and your intended use is not permitted by statutory regulation or exceeds the permitted use, you will need to obtain permission directly from the copyright holder. To view a copy of this licence, visit <http://creativecommons.org/licenses/by/4.0/>.

## References

- Daneshmand S, Quek ML, Stein JP, Lieskovsky G, Cai J, Pinski J, et al. Prognosis of patients with lymph node positive prostate cancer following radical prostatectomy: long-term results. *J Urol*. 2004;172:2252–5.
- Bernstein AN, Shoag JE, Golan R, Halpern JA, Schaeffer EM, Hsu WC, et al. Contemporary incidence and outcomes of prostate cancer lymph node metastases. *J Urol*. 2018;199:1510–7.
- Mottet N, Bellmunt J, Bolla M, Briers E, Cumberbatch MG, De Santis M, et al. EAU-ESTRO-SIOG guidelines on prostate cancer. Part 1: screening, diagnosis, and local treatment with curative intent. *Eur Urol*. 2017;71:618–29.
- Hövels AM, Heesakkers RAM, Adang EM, Jager GJ, Strum S, Hoogeveen YL, et al. The diagnostic accuracy of CT and MRI in the staging of pelvic lymph nodes in patients with prostate cancer: a meta-analysis. *Clin Radiol*. 2008;63:387–95 [cited 2020 Jan 11]. Available from: <https://www.sciencedirect.com/science/article/pii/S0009926007003340?via%3Dihub>.
- Ahmed HU, El-Shater Bosaily A, Brown LC, Gabe R, Kaplan R, Parmar MK, et al. Diagnostic accuracy of multi-parametric MRI and TRUS biopsy in prostate cancer (PROMIS): a paired validating confirmatory study. *www.thelancet.com* [Internet]. 2017 [cited 2017 Dec 19];389. Available from: [https://ac.els-cdn.com/S0140673616324011/1-s2.0-S0140673616324011-main.pdf?\\_tid=b9cd608e-e4c5-11e7-9ee7-00000aab0f6b&acdnat=1513692533\\_a34dba27c3144cdee43c911f1def4c4a](https://ac.els-cdn.com/S0140673616324011/1-s2.0-S0140673616324011-main.pdf?_tid=b9cd608e-e4c5-11e7-9ee7-00000aab0f6b&acdnat=1513692533_a34dba27c3144cdee43c911f1def4c4a).
- Johnston EW, Latifoltojar A, Sidhu HS, Ramachandran N, Sokolska M, Bainbridge A, et al. Multiparametric whole-body 3.0-T MRI in newly diagnosed intermediate- and high-risk prostate cancer: diagnostic accuracy and interobserver agreement for nodal and metastatic staging. *Eur Radiol*. 2019;29:3159–69.
- Bouchelouche K, Choyke PL, Capala J. Prostate specific membrane antigen- a target for imaging and therapy with radionuclides. *Discov Med*. 2010;9:55–61.
- Giesel FL, Hadaschik B, Cardinale J, Radtke J, Vinsensia M, Lehnert W, et al. F-18 labelled PSMA-1007: biodistribution, radiation dosimetry and histopathological validation of tumor lesions in prostate cancer patients. *Eur J Nucl Med Mol Imaging*. 2017;44:678–88.
- Kroenke M, Mirzoyan L, Horn T, Peeken JC, Wurzer A, Wester H-J, et al. Matched-pair comparison of 68 Ga-PSMA-11 and 18 F-rhPSMA-7 PET/CT in patients with primary and biochemical recurrence of prostate cancer: frequency of non-tumor related uptake and tumor positivity. *J Nucl Med*. 2020;jnumed.120.251447.
- Anttinen M, Ettala O, Malaspina S, Jambor I, Sandell M, Kajander S, et al. A prospective comparison of 18F-prostate-specific membrane antigen-1007 positron emission tomography computed tomography, whole-body 1.5 t magnetic resonance imaging with diffusion-weighted imaging, and single-photon emission computed tomography/computed. *Eur Urol Oncol*. 2020;1–10.
- Sprute K, Kramer V, Koerber S, Meneses M, Fernandez R, Soza-Ried C, et al. Diagnostic accuracy of 18 F-PSMA-1007-PET/CT imaging for lymph node staging of prostate carcinoma in primary and biochemical recurrence. *J Nucl Med*. 2020;jnumed.120.246363.
- Jansen BHE, Bodar YJL, Zwezerijnen GJC, Meijer D, van der Voorn JP, Nieuwenhuijzen JA, et al. Pelvic lymph-node staging with 18F-DCFPyL PET/CT prior to extended pelvic lymph-node dissection in primary prostate cancer - the SALT trial. *Eur J Nucl Med Mol Imaging*. 2020.
- Krönke M, Wurzer A, Schwamborn K, Ulbrich L, Jooß L, Maurer T, et al. Histologically-confirmed diagnostic efficacy of <sup>18</sup>F-rhPSMA-7 positron emission tomography for N-staging of patients with primary high risk prostate cancer. *J Nucl Med* [Internet]. 2019;jnumed.119.234906. Available from: <http://jnm.snmjournals.org/lookup/doi/10.2967/jnumed.119.234906>.
- Cardinale J, Martin R, Remde Y, Schäfer M, Hienzsch A, Hübner S, et al. Procedures for the GMP-compliant production and quality control of [18F]PSMA-1007: a next generation radiofluorinated tracer for the detection of prostate cancer. *Pharmaceuticals*. 2017;10.
- Harris PA, Taylor R, Minor BL, Elliott V, Fernandez M, O'Neal L, et al. The REDCap consortium: Building an international community of software platform partners. *J Biomed Inform*. 2019;95:103208 [cited 2020 Jan 11]. Available from: <https://www.sciencedirect.com/science/article/pii/S1532046419301261?via%3Dihub>.
- Fendler WP, Eiber M, Beheshti M, Bomanji J, Ceci F, Cho S, et al. 68Ga-PSMA PET/CT: Joint EANM and SNMMI procedure guideline for prostate cancer imaging: version 1.0. *Eur J Nucl Med Mol Imaging*. 2017;44:1014–24.
- van Leeuwen PJ, Emmett L, Ho B, Delprado W, Ting F, Nguyen Q, et al. Prospective evaluation of 68Gallium-prostate-specific membrane antigen positron emission tomography/computed tomography for preoperative lymph node staging in prostate cancer. *BJU Int*. 2017;119:209–15.

18. Öbek C, Doğanca T, Demirci E, Ocak M, Kural AR, Yıldırım A, et al. The accuracy of 68Ga-PSMA PET/CT in primary lymph node staging in high-risk prostate cancer. *Eur J Nucl Med Mol Imaging*. 2017;44:1806–12.
19. van Kalmthout LWM, van Melick HHE, Lavalaye J, Meijer RP, Kooistra A, de Klerk JMH, et al. Prospective validation of Gallium-68 prostate specific membrane antigen-positron emission tomography/computerized tomography for primary staging of prostate cancer. *J Urol*. 2020;203:537–45.
20. Hofman MS, Lawrentschuk N, Francis RJ, Tang C, Vela I, Thomas P, et al. Prostate-specific membrane antigen PET-CT in patients with high-risk prostate cancer before curative-intent surgery or radiotherapy (proPSMA): a prospective, randomised, multicentre study. *Lancet*. 2020;395:1208–16. [https://doi.org/10.1016/S0140-6736\(20\)30314-7](https://doi.org/10.1016/S0140-6736(20)30314-7).
21. Tulsyan S, Das CJ, Tripathi M, Seth A, Kumar R, Bal C. Comparison of 68 Ga-PSMA PET/CT and multiparametric MRI for staging of high-risk prostate cancer 68 Ga-PSMA PET and MRI in prostate cancer. *Nucl Med Commun*. 2017;38:1094–102.
22. Petersen LJ, Nielsen JB, Langkilde NC, Petersen A, Afshar-Oromieh A, De Souza NM, et al. 68Ga-PSMA PET/CT compared with MRI/CT and diffusion-weighted MRI for primary lymph node staging prior to definitive radiotherapy in prostate cancer: a prospective diagnostic test accuracy study. *World J Urol*. 2019.
23. Tiguert R, Gheiler EL, Tefilli MV, Oskanian P, Banerjee M, Grignon DJ, et al. Lymph node size does not correlate with the presence of prostate cancer metastasis. *Urology*. 1999;53:367–71.
24. Heesakkers RA, Hövels AM, Jager GJ, van den Bosch HC, Witjes JA, Raat HP, et al. MRI with a lymph-node-specific contrast agent as an alternative to CT scan and lymph-node dissection in patients with prostate cancer: a prospective multicohort study. *Lancet Oncol*. 2008;9:850–6.
25. Ettala O, Malaspina S, Tuokkola T, Luoto P, Löytyniemi E, Boström PJ, et al. Prospective study on the effect of short-term androgen deprivation therapy on PSMA uptake evaluated with 68Ga-PSMA-11 PET/MRI in men with treatment-naïve prostate cancer. *Eur J Nucl Med Mol Imaging*. 2020;47:665–73.
26. Emmett L, Yin C, Crumbaker M, Hruby G, Kneebone A, Epstein R, et al. Rapid modulation of PSMA expression by androgen deprivation: serial 68Ga-PSMA-11 PET in men with hormone-sensitive and castrate-resistant prostate cancer commencing androgen blockade. *J Nucl Med*. 2019;60:950–4.

**Publisher's note** Springer Nature remains neutral with regard to jurisdictional claims in published maps and institutional affiliations.



**TURUN  
YLIOPISTO**  
UNIVERSITY  
OF TURKU

ISBN 978-951-29-9184-6 (PRINT)  
ISBN 978-951-29-9185-3 (PDF)  
ISSN 0355-9483 (Print)  
ISSN 2343-3213 (Online)